Identification of Novel Fission Yeast Cell Polarity Regulators by Mass Spectrometry of Detergent-Resistant Membranes

Dissertation

zur

Erlangung der naturwissenschaftlichen Doktorwürde

(Dr. sc. nat.)

vorgelegt der

Mathematisch-naturwissenschaftlichen Fakultät

der

Universität Zürich

von

Michèle Gemünden

aus

Deutschland

Promotionskommission

Prof. Dr. Damian Brunner (Vorsitz, Leitung der Dissertation)

Prof. Dr. Rudolf Aebersold

Prof. Dr. Bernd Bodenmiller

Prof. Dr. Carsten Schultz

Zürich, 2019

Abstract

Cell shape and function are closely linked. In order to adopt a certain shape, the ability of cells to polarise is essential. During my PhD project, I used the fission yeast *Schizosaccharomyces pombe* as a model organism to study cell polarisation. Fission yeast is a unicellular, rod-shaped organism that grows in a polarised manner by cell-end extension, switching from mono- to bipolar growth followed by fission in the cell middle.

Besides the microtubule and actin cytoskeleton, sterol-rich membrane (SRM) domains - in mammalian cells often called «*lipid rafts*» - are important for cell polarisation in fission yeast. They are essential for growth in fission yeast and correlate with sites of growth. Glucose-starved fission yeast cells do not have detectable SRM domains in the plasma membrane. SRM formation and subsequent polarisation are the essential first steps in the re-establishment of cell polarity and growth upon nutrient addition. The molecules participating in these processes are not known and do not involve known polarity factors except for the microtubule-associated cell end marker Tea1. The deletion mutant *tea1Δ* grows strictly monopolar in a bent or branched fashion. How Tea1 acts to stabilise SRM domains at the cell poles as the future growth sites is unknown. The working hypothesis is that Tea1 interacts with so far unknown protein factors associated with the SRMs.

During my PhD project, I developed a method to isolate detergent-resistant membranes (DRMs) as a biochemical approximation of SRM domains from fission yeast. By comparing the protein composition of DRMs from exponentially growing wild-type and *tea1Δ* cells with mass spectrometry (MS), I identified novel regulators of cell polarisation. For example, deletion mutants lacking the protein Lub1 are severely delayed in polarisation and initiate growth at ectopic SRM domains before they successfully polarise. This WD40 domain containing protein is known to be involved in ubiquitin homeostasis. I demonstrated that overexpression of polyubiquitin fully rescues the polarisation defect in *lub1Δ* cells. Their delayed polarisation might also depend on Tea1.

In this thesis, I demonstrated that a comparative MS approach allowed the identification of new players in the cell polarisation process. The MS results can be used as a resource to potentially uncover more relevant factors. Furthermore, the method developed can be applied to isolate and compare DRMs from different mutants and cell polarisation states.

Zusammenfassung

Die Form einer Zelle und ihre Funktion sind eng miteinander verbunden. Um eine bestimmte Form anzunehmen, ist die Fähigkeit von Zellen zu polarisieren essentiell. In meinem Doktorat habe ich die Spalthefe *Schizisaccharomyces pombe* als Modellorganismus, zur Untersuchung von Zellpolarisation genutzt. Spalthefe ist ein einzelliger, stäbchenförmiger Organismus, der auf polare Art und Weise durch Verlängerung der Zellenden wächst und dabei von mono- zu bipolarem Wachstum hin- und herschaltet bevor sie sich in der Zellmitte spaltet.

Neben dem Mikrotubuli- und Aktin-Zytoskelett sind sterolreiche Membran (SRM) Domänen – in Säugerzellen häufig als «*lipid rafts*» bezeichnet – wichtig für Zellpolarisation in Spalthefe. Sie sind für deren Wachstum essentiell und korrelieren mit Wachstumsregionen. Durch Glukosemangel hungernde Spalthefe-Zellen haben keine detektierbaren SRM-Domänen in der Plasmamembran. Die Bildung und anschliessende Polarisation von SRM-Domänen sind die essentiellen ersten Schritte im Wiederaufbau der Zellpolarisation und des Wachstums bei erneuter Zugabe von Nährstoffen. Die Moleküle, die an diesen Prozessen beteiligt sind, sind unbekannt und auch bekannte Polaritätsfaktoren sind nicht involviert, mit Ausnahme des mikrotubuliassoziierten Zellendmarkers Tea1. Die Deletionsmutante *tea1Δ* wächst strikt monopolar in gebogener oder verzweigter Form. Wie Tea1 agiert, um SRM-Domänen an den Zellpolen als zukünftige Wachstumszonen zu stabilisieren, ist unbekannt. Die Arbeitshypothese lautet, dass Tea1 mit bisher unbekannten Proteinfaktoren interagiert, die mit sterolreichen Membranen assoziiert sind.

In meinem Doktorat habe ich eine Methode entwickelt, um detergenzresistente Membranen (DRMs) als biochemische Näherung für SRM-Domänen aus Spalthefe zu isolieren. Durch den Vergleich der Proteinzusammensetzung von DRMs aus exponentiell wachsenden Wildtyp- und *tea1Δ*-Zellen mit Massenspektrometrie (MS) habe ich neuartige Regulatoren der Zellpolarisation identifiziert. Deletionsmutanten beispielsweise, denen das Protein Lub1 fehlt, polarisieren stark verzögert und beginnen an fehlplatzierten SRM-Domänen zu wachsen, bevor sie erfolgreich polarisieren. Dieses Protein mit einer WD40-Domäne ist an der Ubiquitinhomöostase beteiligt. Ich habe gezeigt, dass Überexpression

von Polyubiquitin den Polarisierungsdefekt von *lub1Δ*-Zellen komplett aufhebt. Deren verspätete Polarisation hängt möglicherweise von Tea1 ab.

In dieser Dissertation habe ich demonstriert, dass ein vergleichender MS-Ansatz die Identifikation neuer Mitspieler im Zellpolarisationsprozess erlaubt. Die MS-Resultate können als Ressource genutzt werden, um möglicherweise weitere relevante Faktoren zu entdecken. Ausserdem kann die entwickelte Methode dazu angewendet werden, um DRMs aus anderen Mutanten und Zellpolarisationsstadien zu isolieren und zu vergleichen.

Acknowledgements

First of all, I want to thank my supervisor Damian Brunner for the possibility to work on this inspiring project of which we did't know, where it will lead us. Thank you, for your openness to me as someone grown up somewhere between the disciplines. I am grateful for the possibilities you gave me to explore the fission yeast field that was first new to me. It was great to know that you always believed in the project. Even when I had my doubts sometimes, you spread your positive excitement to overcome the research-inherent slow-moving periods.

Next, I would like to thank the members of my PhD committee: Prof. Dr. Ruedi Aebersold, Prof. Dr. Bernd Bodenmiller, Prof. Dr. Carsten Schultz and Dr. Robin Klemm. I am grateful for the inspiring discussions we had, your valuable advice and thoughts and the right questions you asked. Special thanks to you, Carsten, I felt very honored that you made quite an effort to meet and discuss.

Thank you, Robin, for sharing your excitement and vast knowledge also in various other discussions. Thank you, for your invaluable help by practically introducing me to ultracentrifugation and gradient preparation, letting me use your great ultracentrifuge and sharing necessary materials. Without your help, this project would not have been possible.

Erich Brunner, thank you for your willingness to discuss MS results, your great experimental advice and sharing of precious materials.

I would like to thank all current and former lab members for the great atmosphere we always had. I think it was a huge luck, to have such a positive, never competitive, real team spirit in the group. Laurynas, Fiona, David, Arne, Francesco, Thom, Lara, Adam, Steve, Arina, Erich, Nadia, Werner, Eliane, Wolfgang, Daniel, Dominika, **M**aria, **M**eret, **M**arisa, **M**artina, **M**irjam, **M**andy and **M**agda, it was great working with you all! Among you, I would like to point out my dear Yeasties, for your support and the willingness to discuss the problems we encountered. Adam Kijowski, it was fun to join your exciting project and I am happy that I had the possibility to collaborate with you. I always enjoyed our scientific and also our personal discussions. Thank you, Maria Heimlicher, for sharing a bench with me, later even the desk and in general, many thoughts. Your open, direct

personality and your clarity of thinking always inspired me. Thank you, Stephen Huisman for introducing me to fission yeast, for always having an open ear when problems occurred. Werner Boll, without you, we all would not have any data. Thank you so much for all your help and support regarding working with the microscopes.

Thanks goes to all the good souls from the institute that were often around when lab days became longer than planned or that just spread their good mood everyday.

I want to thank my family and friends. You were always there, always supportive, always interested in what I am doing, although you maybe sometimes wondered.

Last but not least, I want to thank you, Patrick, for your incredible patience, love and support, for your curiosity and for the adventure of having our wonderful Elin joining our live.

Table of Contents

List of Figures

List of Tables

Abbreviations

ATP	adenosine triphosphate
DRM	detergent-resistant membrane
ER	endoplasmic reticulum
FGCZ	Functional Genomics Center Zurich
GFP	green fluorescent protein
MLR	membrane lipid raft
MS	mass spectrometry
PCR	polymerase chain reaction
P1	random SRM domain formation during SE
P2	SRM polarisation to the cell poles during SE
P3	growth initiation from one cell end during SE
P4	growth initiation from the second cell end (bipolar growth) during SE
SDS	sodium dodecyl sulfate
SE	starvation exit
SRM	sterol-rich membrane
SUMEB	SDS, Urea, MOPS, EDTA, Bromophenol blue solution
Tea1	"tip elongation aberant" protein, all proteins in this work are labelled with their name and the three-letter code in normal writing
tea1	Tea1-encoding gene – all genes are written italic
tea1Δ	*tea1*-deletion mutant, deletion mutants are labelled this way
HL-tagRFP	tagRFP (red fluorescent protein) attached with the "happy linker"
cdc42-3	temperature-sensitive *cdc42* allele
TNE	Tris-NaCl-EDTA buffer

1 Introduction

It needs a single cell to create organisms as complex as a human being. From this first cell, a fertilised egg, many different cell types of various functions arise. They arrange in a composition that makes us able to sense and interact with the environment, eat, listen to music, and gives us the ability to be curious about the wonder of life and the unique opportunity to study ourselves.

To achieve this high complexity level, this first, single cell needs to divide, and its progeny undergo various transitions to specialise into various cell types, like neurons or epithelial cells. The ability to polarise, i.e. to actively break the symmetry of the cells, is core to these processes and leads to cells of different shape and function.

With this thesis, I aim to provide a new piece of the puzzle to the question of how cells are able to generate polarity and which mechanisms they use. I have used the fission yeast *Schizosaccharomyces pombe* as model system to study *de novo* cell polarisation. As a theoretical background, examples for polarised cells will be given and the yeast model system will be introduced. Specifically, the mechanisms underlying cell polarisation in this system will be described and compared to other cell types. Sterol-rich membrane (SRM) domains will be introduced, as they were recently described to be essential for *de novo* polarisation of fission yeast. From there, the rationale behind the method developed in this thesis to isolate and compare these membrane domains from wild type and mutant cells will be explained. Additionally, a method to quantitatively describe and analyse this process is going to be introduced.

1.1 Cell polarisation

Cell polarisation describes the asymmetric spatial distribution of cellular components. This asymmetry is necessary for directed growth of a cell to obtain a certain shape. The shape of a cell is closely linked to its function. Human neurons, for example, receives signals at their dendrites and are able to transport the information over distances as long as 1 m in humans to communicate via their synapses with other nerve cells. In order to grow to this special, long cell shape, the growth cone advances along external signals (Dickson 2002; Head, Patel, and Insel 2014). The ability of cells to migrate, which is

essential for embryonic morphogenesis, also relies on polarisation processes. Instead of growing along morphogenic gradients, migrating cells physically move along them by growing cellular protrusions in the front, adhering to the extracellular matrix and retracting them at the back of the cell (reviewed by Ridley et al. 2003). Another prominent example of polarised cells are epithelial cells. By forming a layer of cells, the apical side is exposed to an environment very different from the basal and lateral sides. This is reflected on the cytoskeletal, protein and membrane level in order for the different regions to fulfil their specific tasks (Yeaman, Grindstaff, and Nelson 1999; Schuck and Simons 2004; Head, Patel, and Insel 2014).

1.2 Fission yeast as a model system to study cell polarisation

Schizosaccharomyces pombe or fission yeast is a unicellular eukaryotic rod-shaped organism with a length of about 7.5-15 µm and a width of 3-4 µm (J. M. Mitchison and Nurse 1985; Hayles and Nurse 2001; Drake and Vavylonis 2013). *S. pombe* cells are enclosed by a rigid cell wall mainly composed of α- and β-glucans and galactomannan (Ishiguro 1998). They grow by cell-end extension driven by turgor pressure (Slaughter and Li 2006). As indicated by its name, fission yeast divides by medial fission. It was first discovered in 1893 by P. Lindner in and isolated from African millet beer called "Pombe" in Swahili which led to its scientific name (V. Wood et al. 2002; Wixon 2002; Martin and Arkowitz 2014). *S. pombe* was introduced as a model organism by Urs Leupold and Murdoch Mitchison in the middle of the last century. The strains they created form the basis of all laboratory strains in use today (Yanagida 2002). The ease of the maintenance of fission yeast and the straightforward accessibility to genetic modifications play a role for its popularity and an increasing scientific community worldwide. Fission yeast is only distantly related to the baker's and brewer's yeast *Saccharomyces cerevisiae* also called budding yeast and appears to be similarly related to humans (V. Wood et al. 2002; Wixon 2002; Dujon and Louis 2017). The Nobel prize in Physiology or Medicine in 2001 awarded to Sir Paul M. Nurse, who worked with fission yeast, together with Tim Hunt and Leland H. Hartwell for their discoveries of key regulators of the cell cycle, demonstrates the relevance of this single celled organism for meaningful basic research.

Since the awarding of the Nobel prize, the 14 Mbp genome localised on three chromosomes has been sequenced, which made the genetic manipulation of fission yeast even

easier (V. Wood et al. 2002). 73.9% of the 4836 protein coding genes are non-essential (Kim et al. 2010). Thus, full deletion mutants of these genes can be analysed to study the role of these proteins. A strain library, with 3420 deletion mutants containing the majority of non-essential genes, provides easy access to the deletion mutants (Kim et al. 2010, Bioneer deletion library version 5). Fission yeast normally stays haploid in contrast to baker's yeast cells that are diploid by default. Nitrogen limitation induces fusion of cells with opposing mating types and form a diploid zygote that subsequently creates four haploid spores to generate progeny. Alternatively, diploid cells can be cultured under appropriate conditions (Moreno, Klar, and Nurse 1991).

S. pombe has a very characteristic, regular growth pattern that correlates with the cell cycle. The cells grow by cell end extension and divide by medial fission when the cells reach the appropriate size. When a new cell is born after cell division, it first grows at the old end inherited from the original cell. During G2, it switches to bipolar growth. This process is referred to as NETO – new end take-off. The cell then grows bipolar until the next cell division (J. M. Mitchison and Nurse 1985). This constant switching of growth sites makes fission yeast an excellent and widely used tool to study cell polarisation (Hayles and Nurse 2001).

A range of mutants exhibiting growth and polarity defects have been described. Although many components are known to play a role during polarised growth, the process is not fully understood. An assay to study the *de novo* cell polarisation in fission yeast after glucose starvation was recently established in the Damian Brunner group. In order to understand how cell polarity is established and maintained to allow polar growth, the system allows to dissect the functions of different factors at different times during cell polarisation (Makushok et al. 2016). The latter points will be discussed in more detail in the next sections.

1.2.1 The role of the Cdc42-system

The conserved, essential Rho-type GTPase Cdc42 plays a central role in polarised growth (Johnson 1999; Etienne-Manneville 2004). It is active in the GTP- and inactive in its GDP-bound form (Etienne-Manneville and Hall 2002; Perez and Rincón 2010). In fission yeast, Cdc42 localises to the cell outline, and is enriched at the cell poles and the division site. It

attaches to the membrane with a prenylation anchor (Bendezú et al. 2015). Its activity is spatially regulated by the guanine exchange factors (GEFs) Gef1 and Scd1 that activate Cdc42 and the GTPase-activating proteins (GAPs) Rga4 and Rga6 that act as inhibitors (Perez and Rincón 2010; Revilla-Guarinos et al. 2016). Scd1, Gef1 and the scaffold protein Scd2 localise to the cell poles and the site of cytokinesis while GAPs localise to the cell sides, restricting the activity to the cell poles and the division site (Perez and Rincón 2010; Coll et al. 2003).

Interestingly, Cdc42 activity shows an oscillatory behaviour between the cell ends, which was suggested to be involved in defining growth site dimensions and the initiation of bipolar growth (M. Das et al. 2012; Bendezú and Martin 2012; Martin and Arkowitz 2014). Although Cdc42 was reported to be able to establish cell polarity on unpolarised spores, probably via positive feedback loops, it is dispensable for *de novo* cell polarisation of fission yeast upon glucose starvation (J. M. Johnson, Jin, and Lew 2011; Bonazzi et al. 2014; Makushok et al. 2016).

It is believed that polarised growth depends on Cdc42-mediated activation of the formin For3 and the exocyst complex, leading to polarised exocytosis of cell wall-remodelling factors (Bendezu and Martin 2011; Kokkoris, Gallo Castro, and Martin 2014). For this, it integrates signals from the activators acting upstream (Efc25, Ras1, Scd1, Nak1/Orb3, Orb6, Gef1) and also acts on the downstream effector Shk1, a p21-activated kinase (summarised in Huisman and Brunner 2011). Although the exact link between the Cdc42-system and the polarity factors remains unclear, the local growth activation by ectopic localisation of the landmark protein Tea4, normally localising to the cell ends (compare section 1.2.3), suggests that it works via its connection with the catalytic subunit Dis2 or Scs21 of the type I phosphatase (PP1) (Kokkoris, Gallo Castro, and Martin 2014).

The connection of the Cdc42 pathway to the Ras1 GTPase and the fact that also other Rho GTPases are involved in polarised growth in fission yeast, suggest that redundant pathways exist and that all six Rho GTPases probably work together in a complex network in order to control polarised growth. For example, mutants of Rho1, one of the Rho GTPases in fission yeast described to play a role in cell wall integrity, have a round morphology (Nakano, Arai, and Mabuchi 1997; Santos et al. 2003; Pérez, Portales, and Santos 2015).

1.2.2 The role of the cytoskeleton

1.2.2.1 Microtubules

Microtubules are composed of heterodimers of α- and β-tubulin that polymerise into straight, highly ordered tubes of 25 nm in diameter and are made of 13 protofilaments (Downing and Nogales 1998). Due to the head-to-tail alignment of the α/β-tubulin dimers, leading to an asymmetric composition, the two ends are referred to as plus- and minus-ends. Growth (polymerisation or rescue) and shrinkage (catastrophe) happen at the highly dynamic plus-end, while the minus ends are thought of as capped and less dynamic (T. Mitchison and Kirschner 1984; Downing and Nogales 1998; Keating and Borisy 2000). In interphase fission yeast cells, 3-6 antiparallel microtubule (MT) bundles are oriented along the long cell axis (Höög et al. 2007). They are attached at the nucleus with their overlapping minus ends and grow towards the cell ends where they touch the cortex, bend and eventually undergo catastrophe (Sawin and Nurse 1998; Höög et al. 2007; Höög et al. 2013). This pushing force serves to centre the nucleus in the geometric middle of the cell (Tran et al. 2001). As the position of the nucleus defines the division site, MTs thereby play a role in cytokinesis (Daga and Chang 2005). Thus, in contrast to budding yeast where MTs are dispensable for polarised growth, they play an important role for cell polarisation in fission yeast (Huffaker, Thomas, and Botstein 1988; Martin and Arkowitz 2014). During mitosis, microtubules rearrange to form the mitotic spindle and, as in all eukaryotes, separate the duplicated chromosomes (Höög et al. 2007).

Additionally, interphase MTs are important for delivering polarity landmark proteins to the cell ends for growth site positioning (Mata and Nurse 1997, compare also chapter 1.2.3). Another function is the distribution of mitochondria, the cellular power plants, that also dynamically grow and shrink in the cell, independent of motor proteins (Yaffe, Stuurman, and Vale 2003; Höög et al. 2007).

During glucose starvation, microtubules reorganise. In prolonged starvation, only a single stable, antiparallel bundle of reduced length remains. This bundle is associated with the spindle pole body (Laporte et al. 2015).

1.2.2.2 Actin

Actin monomers (G-actin) polymerise to polarised helical filaments (F-actin) made of two actin strands. The filaments are oriented. The asymmetric structure of G-actin leads to a pointed and a barbed end (Holmes et al. 1990). It is a complex of actin and myosin that enables various organisms from yeast to humans to exert forces due to the movement of myosin molecules along actin polymers leading to a relative displacement of these structures (Berg, Tymoczko, and Stryer 2007).

In fission yeast, actin is present in different forms. Actin cables, composed of parallel actin bundles, serve as tracks for polarised Myosin V mediated vesicle trafficking, which is important for cell growth (Presti, Chang, and Martin 2012). Vesicles and organelles are transported to growing cell ends (Kovar, Sirotkin, and Lord 2011). Actin patches, an Arp2/3-mediated network of branching F-actin, also localise to the growing cell ends (Marks, Hagan, and Hyams 1986; Kovar, Sirotkin, and Lord 2011). They are important for endocytosis as actin is providing both the scaffold and the force for the clathrin-mediated internalisation of endocytic vesicles (Sirotkin et al. 2010; Kovar, Sirotkin, and Lord 2011; Mooren, Galletta, and Cooper 2012; Chen and Pollard 2013). Additionally, antiparallel actin bundles form the contractile ring at the division site that divides the cell in two during cytokinesis (Pelham and Chang 2002).

During glucose starvation, actin structures delocalise (Makushok et al. 2016). Upon prolonged starvation, actin has been reported recently to form actin bodies (Laporte et al. 2015).

1.2.3 The role of polarity factors

Polarity factors localise to the growing cell ends and the site of cytokinesis. Microtubules are important for the transport of these landmark proteins to the cell poles. A critical one is the ezrin-like factor Tea1 (Mata and Nurse 1997; Vega and Solomon 1997; Huisman and Brunner 2011). It accumulates at the plus ends of growing MTs and is deposited at the cell ends when they reach the cortex and undergo catastrophe (Mata and Nurse 1997). To ensure proper delivery of Tea1, the microtubule dynamics are controlled by so-called +TIPs, proteins interacting with growing MT plus ends. The EB1 family member Mal3, the CLIP-170 protein family member Tip1 and the kinesin motor Tea2 provide spatial

control over the MT dynamics (Beinhauer et al. 1997; Brunner and Nurse 2000; Busch et al. 2004). The Tea2/Tip1/Mal3 complex stabilises microtubules to effectively ensure that they reach the cell ends, at least partially due to an altered microtubule lattice by incorporation of Mal3 (Karl E. Busch and Brunner 2004; Sandblad et al. 2006; Von Loeffelholz et al. 2017). Tea2 transports the MT stabilising Tip1 to the MT plus end, preventing premature MT catastrophe and thereby ensuring the precise localisation of Tea1 at the cell poles. There, the interaction with Mod5 connects Tea1 to the plasma membrane. Mod5 is tethered to the plasma membrane via a prenylation anchor (Snaith and Sawin 2003). The interaction of Tea1 and Mod5 leads to a self-focussed localisation to the cell tip of both. If either one is missing, the localisation of the other is less confined (Bicho et al. 2010).

The SH3 domain protein Tea4 directly binds Tea1. It is transported together with Tea1 and links to the actin cable nucleating formin For3 (Tatebe et al. 2005; Martin et al. 2005). Deletions of either Tea1, Tea4 or Tip1 lead to bent or branched cells due to growth site positioning defects (Mata and Nurse 1997). Disruption of the microtubule dynamics have the same effect (Umesono et al. 1983). Additionally, these mutants have a NETO defect and are unable to switch to bipolar growth (Mata and Nurse 1997; Martin et al. 2005). In case of *tip1Δ*, this is most likely caused by the destabilised MTs that fail to deliver Tea1 to the cell poles (Huisman and Brunner 2011). Another factor that leads to these phenotypes when deleted, is the DYRK kinase Pom1 (Jürg Bähler and Nurse 2001). In this case, however, this is not due to altered MT dynamics. Pom1 is rather thought to act in general growth control downstream of Tea1/Tea4 (Bähler and Nurse 2001). Pom1 negatively regulates the Cdc42 GAP Rga4. Its role as sizer, forming a gradient from the poles in order to serve for cell division at a certain cell length, has however been questioned (Martin and Berthelot-Grosjean 2009; Wood and Nurse 2013; Bhatia et al. 2014; Rincon et al. 2014).

In interaction with Mod5, Tea4 and the Tea1 homologue Tea3 at the new cell end, Tea1 forms clusters at the cell poles. They are about 50-100 nm in size. Strikingly, Tea1 and Tea3 have to localise into distinct clusters with increasing co-localisation during mitosis, leading to a spatio-temporal regulation of polarity (Arellano, Niccoli and Nurse 2002; Dodgson et al. 2013).

Although many factors playing a role in this complex system were identified, the picture is not yet complete. It is for example not understood how the polarity machinery

ultimately links to growth. Although a link of Tea1-Tea4 via For3 was proposed to lead to actin cable formation and growth as the interaction of these factors was shown biochemically, more is yet to be discovered (Martin et al. 2005). While *tea1Δ* and *tea4Δ* cells are NETO defective, *for3Δ* cells are able to grow bipolar, even mutants with deletions of all three fission yeast formin genes *for3, fus1* and *cdc12* are able to grow in a polarised manner (Huisman and Brunner 2011; Bendezu and Martin 2011).

Taken together, the polarity markers are the critical factors for polarised cell growth by selecting the growth site. The actin and microtubule cytoskeleton only play a secondary role by supporting the system. During glucose starvation, the polarity factors are delocalised. However, Tea1 still localises to the cell ends until 2-3 days in starvation after which it is mostly found on the remaining MTs (Laporte et al. 2015; Makushok et al. 2016).

Complications in studying the polarisation machinery arise from the inheritance system in fission yeast and the close interplay between shape and polarity (Terenna et al. 2008; Abenza et al. 2014). During exponential growth, the polarity factors mark the growth sites at the poles and at the midzone during cytokinesis. After cell division the growth machinery can go back to the marked, previous growth sites. Thus, this "memory" makes this self-sustained system very robust against perturbations. The connection between cell shape and growth site selection underlines this. If a straight wild-type cell is mechanically bent, the altered MT localisation and thus altered delivery of landmark proteins leads to mis-positioned growth sites. In contrast, round shape mutants with a mis-localised MT cytoskeleton can retain bipolar growth when squeezed into a normal elongated cell shape.

To overcome these problems and the redundancy between different systems acting in this complex process (Huisman and Brunner 2011), an assay to analyse *de novo* cell polarisation was developed previously in the Damian Brunner group by Paulo Alves and Tatyana Makushok (Makushok et al. 2016). It will be introduced in more detail in section 1.5.

1.2.4 The role of sterol-rich membranes

It has been known for a while that sterol-rich membrane (SRM) domains, in mammalians often called "lipid rafts", co-localise with growth sites in fission yeast: the cell ends and the site of cytokinesis. Many fission yeast mutants with aberrant growth polarity and with defects in SRM formation or maintenance are described (Wachtler 2003; Huisman and

Brunner 2011; Makushok et al. 2016). Thus, many mutants with growth defect also show aberrant SRM localisation (Wachtler 2003). For example, SRMs localise to the growing end of *tea1Δ* mutant cells, growing bent or in a T-shape.

However, their localisation has been regarded rather as a consequence of growth rather than SRMs being actively involved in the polarisation process (V. Wachtler 2003; Wachtler and Balasubramanian 2006). SRMs are dynamic microdomains enriched in sterols and sphingolipids (Klose et al. 2010). In yeast, ergosterol is the main sterol (Harmouch, Coulon, and Bonlay 1995). They can be visualised with the specific dye filipin that binds to free 3-β-hydroxysterols (V. Wachtler 2003).

In contrast to the previous view, it has been shown recently that SRMs have an instructive role and are on top of the hierarchy of the cell polarisation process (Makushok et al. 2016). During glucose starvation, no SRMs in the plasma membrane stain with filipin.

As SRMs are an important core component of this thesis, the following section will provide a closer look on these special membrane domains, their role and how they were studied. A more detailed description of the developed *de novo* polarisation assay and the role of SRMs during cell polarisation of fission yeast will be presented in section 1.5.

1.3 The role of lipid rafts in other systems

In other organisms, membrane/lipid rafts (MLR) are closely connected with cell polarisation. They serve as platforms for structural and signalling molecules, integrating the cytoskeleton with morphological remodelling processes and for structural functions (reviewed in Head, Patel, and Insel 2014).

MLR at the leading edge of neuronal growth cones are essential for their advancement during axon guidance (Grider et al. 2009). Also, in this system microtubules coordinate polarity and actin dynamics (Siegrist and Doe 2007). Proteins that localise to MLR in focal adhesion sites of migrating cells and the cytoskeleton play a role during the detachment of cancer cells from the extracellular matrix when they become invasive, leading to metastasis (Su et al. 2013). Epithelial cells, having an apical and a basolateral domain, act as a barrier against the environment. The environment-facing apical side contains MLR. The proteins localising there serve as platforms for signalling and interaction with the actin cytoskeleton (Cao, Surma, and Simons 2012; Head, Patel, and Insel 2014). At the

immunologic synapse, the interaction between an antigen-presenting cell and a T-cell leads to an immune response. The T-cell receptors are localised to MLR and upon interaction with the presented antigen, MLR rearrange to supramolecular activation cluster and the actin cytoskeleton is remodelled (Carrie Miceli et al. 2001; Tomassian et al. 2011; Molnár et al. 2012). During the maturation of mammalian sperm, necessary for fertilisation, MLR reorganise (Cross 2004). Besides these examples, also in endothelial cells, striated and smooth muscle cells, erythrocytes and platelets MLRs are important for mediating various cell functions including mechanotransduction and the already mentioned adherence and migration (reviewed in Head, Patel, and Insel 2014).

This brief overview demonstrates that the connection of MLR with the cytoskeleton is a common and conserved feature in cell polarisation (Head, Patel, and Insel 2014). Of course, the exact players and their way of orchestration vary over different cell types and organisms. It is not surprising, that defects in the complex system of membrane-protein-cytoskeleton interactions are for example linked to cancer and Alzheimers's disease (Head et al. 2010; Thompson et al. 2010).

1.4 Lipid rafts and how they were studied so far

The fluid mosaic model of the plasma membrane was first presented by Singer and Nicolson in the year 1972 (Singer and Nicolson 1972). Hundreds of different lipid species of different types - sphingolipids, glycerophospholipids and sterols (ergosterol in yeasts) – form the plasma membrane as a lipid bilayer that separates the cellular contents from the outside (Simons and Sampaio 2011). The incorporation of sterols into the membrane modifies the membrane fluidity (van Meer, Voelker, and Feigenson 2008). Proteins are associated with the membrane, either by spanning a transmembrane domain through the lipid bilayer or by inserting lipid anchors into the membrane (peripheral membrane proteins) (Berg, Tymoczko, and Stryer 2007). The fluid mosaic model, proposed more than 45 years ago, states that the interacting lipids and proteins in the membrane can laterally diffuse. Within this matrix, proteins and lipids can phase separate into aggregates (Singer and Nicolson 1972). Until now, this view appears to be generally valid, although it has been refined with the research done in the last decades (Nicolson 2014; Goñi 2014). For example, it is now known that membranes are more crowded with proteins, and the lateral heterogeneity is higher than first anticipated before (Goñi 2014).

Membrane/lipid rafts (MLR) were first identified because of their resistance to cold non-ionic detergents as glycolipids-rich complexes. These detergent-resistant membranes were enriched in sphingolipids and sterols (Brown and Rose 1992; Simons and Ikonen 1997). Due to the presence of a higher proportion of saturated lipids in MLR, the membrane is stiffer and slightly thicker. Therefore, MLR are also referred to as liquid-ordered (L_o) in contrast to liquid disordered (L_d) domains that are coexisting (Swamy et al. 2006; van Meer, Voelker, and Feigenson 2008).

Many proteins have been identified that localise depending on MLR, a prominent example is caveolin, a transmembrane protein forming the caveolae, nanoscale invaginations in the plasma membrane. Nevertheless, the existence and relevance of MLR in biological systems has been under debate (Swamy et al. 2006; A. Das et al. 2014). The problem arises from the fact that their appearance depends on the way of investigation and can be even influenced by the applied method (reviewed by Klotzsch and Schütz 2013). Some examples will be presented here.

It was argued that the detergent treatment during isolation changes their composition (Kurzchalia, Hartmann, and Dupree 1995). Additionally, the low temperature during the extraction has been criticised because the lipid-lipid interactions at these temperatures are altered and therefore influence the extractability (London and Brown 2000; Heerklotz 2002). However, it still is the method of choice to gain inside into the differential protein composition of membranes based on their solubility. Thus, detergent-resistant membrane (DRMs) localisation of a protein is distinct from MLR, as it reflects a physicochemical property (Klotzsch and Schütz 2013).

Atomic-force microscopy was used as a method that provides topological information. A probe is physically scanning over a surface and the deflection of a cantilever is detected. This method allowed to dynamically visualise different membrane domains and was used to study transmembrane proteins and their lipid environment (Henderson et al. 2004).

When trying to visualise them with antibodies against raft-localised proteins, the membrane domains coalesce to larger patches due to crosslinking. Proteins that would localise to different sub-domains appear to colocalise (Harder et al. 1998). As the size range of rafts and the space in-between them appears to be in the same range, their direct

visualisation has been challenging (Grossmann et al. 2006; Simons and Gerl 2010). Fluorescence microscopy both of living cells and model membranes requires fluorescent probes that either segregate specifically to the ordered or the disordered domain or that change fluorescence in the different environments. However, also their application in living cells is not trivial (Klymchenko and Kreder 2014). Nevertheless, superresolution imaging for example with STED (stimulated emission depletion) expands the experimental possibilities and shows the transient trapping of GPI-anchored proteins and sphingolipids in complexes in a cholesterol-dependent manner (Eggeling et al. 2009; Owen and Gaus 2013).

Already in the earlier days of MLR research, mass spectrometry was used to identify DRM-localised proteins, for example in yeast (Bagnat et al. 2000). Secondary ion mass spectrometry more recently provided the "first direct, molecule specific, visual evidence for the colocalisation of cholesterol and (the ganglioside) G_{M1}" (Lozano et al. 2013). Furthermore, the growing field of lipidomics and theoretical simulations provided their part in further understanding of MLR (Cooke, Kremer, and Deserno 2005; Simons and Gerl 2010; Meinhardt, Vink, and Schmid 2013).

Today, it is commonly accepted that they exist. However, the concept has evolved with the information gained over time (Simons and Gerl 2010). In 2006, a Keystone Symposium finally defined them as: *"small (10–200 nm), heterogeneous, highly dynamic, sterol- and sphingolipid-enriched domains that compartmentalize cellular processes. Small rafts can sometimes be stabilized to form larger platforms through protein-protein and protein-lipid interactions"* (Pike 2006). Thus, also in living systems, MLR are highly dynamic and exist in different length and time scales. For example, epithelial apical membranes can be seen as stable "super-rafts" (Danielsen and Hansen 2003).

1.5 Fission yeast cell polarisation depends on sterol-rich membranes

The main findings of the publication "Sterol-Rich Membrane Domains Define Fission Yeast Cell Polarity" (Makushok et al. 2016) relevant for this thesis will be summarised.

1.5.1 Sterol-rich membranes are essential for cell polarisation

Glucose starved fission yeast cells lose their polarity. This includes rearrangement of the MT and actin cytoskeleton and the polarity factors and the loss of filipin staining (see also, for example, V. Wachtler 2003; Laporte et al. 2015). Addition of nutrients leads to re-establishment of cell polarity. An example of recovering wild-type cells stained with filipin is presented in Figure 1a. Initially, random SRM domains form before they are stabilised at the cell poles.

Makushok et al. demonstrated that the polarisation process depends on newly synthesised sterols. By blocking the sterol synthesis with ketoconazole, repolarisation failed. They established a starvation exit assay to dissect timing of the different events and components of the system. Starvation exit (SE) of cells starved for 2 or 5 days in low glucose medium was triggered by the addition of fresh medium. First, microtubules reappeared and Tea1 was again transported to the cell ends. Filipin staining of SRMs in recovering cells demonstrated that the formation of randomly distributed SRM domains happens within 5-10 min. Makushok et al. tested the localisation of the polarity marker Bud6, the actin patch-visualizing Crn1 during SE. Strikingly, both markers localised already to these early SRM domains although no growth was detected there. The lateral SRM domains were shown to be removed in an actin-dependent manner and the polar caps were stabilised. Once they reached a critical size after ca. 60 min of SE, the polarised cells started growing.

In order to analyse the SRM dynamics also of various polarisation mutants by live-cell imaging, GFP-Tna1 was introduced as a marker protein co-localising with filipin staining in the plasma membrane.

For a clearer description and comparison, Makushok et al. divided the polarisation process into four phases. The initial phase with randomly distributed SRM domains (P1), the polarisation phase during which slow growth occurred (P2), the initiation of fast growth (P3) and the initiation of bipolar growth (P4) in a subset of cells.

It was demonstrated, that SRM domains are required but not sufficient for growth. Although only one cell end grows after SRM polarisation is complete, both poles are covered with SRM caps. Thus, SRMs mark potential growth sites, explaining why *myo1Δ* mutant cells with SRMs covering the whole plasma membrane still grow polarised. In contrast, *tea1Δ* mutant cells fail to stabilise SRMs at the cell pole, have a prolonged P1 and

eventually select a random domain as growth site, leading to mainly branched cells. Exponentially growing *tea1Δ* cells in contrast, grow mainly bent. In general, mutants show more severe phenotypes during SE than during exponential growth because the inheritance system does not work as efficiently.

Strikingly, the polarisation process was shown to be independent of Cdc42 and rather depends on Tea1 as key factor. How Tea1 is able to stabilise SRMs at the non-growing end remains to be discovered.

1.6 Method to quantify the cell polarisation process during starvation exit

In this thesis, SE of glucose starved cells is going to be a central assay to analyse a protein's/gene's function in cell polarisation. To visualise the SRMs during SE, they are mainly labelled with filipin. To be able to describe the cell polarisation process in a more quantitative and comparable way, the concept of the *polarisation ratio* (*rP*) was designed and developed in collaboration with Adam Kijowski and David Dreher (Kijowski et al., unpublished, in preparation). It classifies the polarity of cells, or of cell populations, of fission yeast based on filipin staining by assigning a value between 0 (non-polar) and 1 (polar) (Figure 1). Experimental details of the procedure and the calculations can be found in section 6.2.3 in the materials and methods part.

Briefly, the filipin signal is detected and classified based on its position on the cell membrane as either polar or side localised (Figure 1c). The *rP* is a simple ratio of polar to total filipin signal of a cell. In this thesis, it is going to be used to illustrate the polarisation process by analysing samples at several points in time during SE. Figure 1 summarises the analysis pipeline from imaging to the final boxplots of *rP* for each timepoint. In order to be able to calculate the *rP* from the imaging data, the cells have to be segmented. In this thesis, the cells were therefore labelled with an outline marker (Rhodamine Lectin). This allows the cell segmentation with ilastik and Cell profiler (Sommer et al. 2011; Dimopoulos et al. 2014). The filipin signal on the cell outlines is subsequently analysed with a MATLAB script written by David Dreher (unpublished, in preparation). The quantification of the imaging data from a wild-type cell culture illustrates the polarisation process during SE based on the *rP*. The boxplots summarise the distribution of *rP* of the

culture at a certain time in SE. The notches around the median value represent the 95% confidence interval, the box the interquartile range (25 to 75 percentile). For normal distributions, the whiskers should include 99.3% of the data, assumed outliers are represented as dots. There is strong evidence that two medians are different if the notches of two boxes do not overlap (Chambers et al. 1983). For all boxplots presented in this thesis, the number of cells (n) is depicted on top of the boxplot.

The example recovery in Figure 1e shows the transition of *rP* from 0 to 1 within 60 minutes.

Additionally, the *bipolarity ratio* (*rB*) was calculated for polar cells. It is only meaningful for cells having one or two polar SRM signals, therefore it is only computed for those. Its value gives an idea if the cells are monopolar (0) having only one filipin stained polar cap or bipolar (1) with two equal polar caps by comparing the polar signals. The quantification in Figure 1f shows an initial increase of *rB* to 0.7, indicating almost equal staining with one pole slightly stronger than the other. The following decrease in *rB* illustrates the stronger filipin staining of the growing cell end. As soon as also bipolar growth occurs, the values increase again, due to the more equal staining.

Furthermore, the analysis procedure simultaneously provided information about the cell dimensions based on the segmentations. The computed long and short axis dimensions served as a measure of cell length and width, respectively.

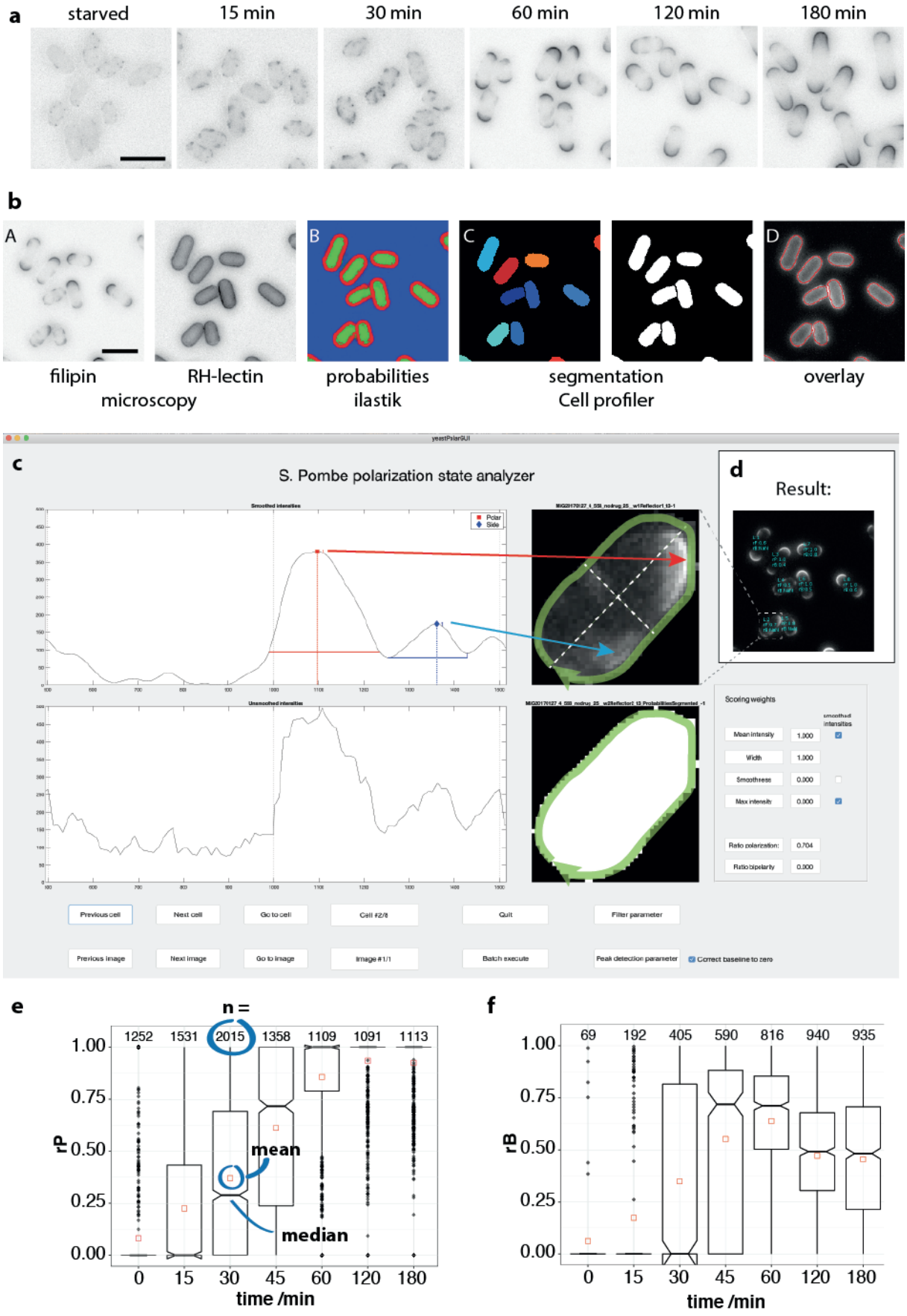

Figure 1: Analysis pipeline to compute the *polarisation ratio* (*rP*).

(a) Filipin stained wild-type cells during SE. (b) Image processing steps to read out the filipin signal on the plasma membrane. A: filipin and Rhodamine-lectin stained cells (60 min in SE), B: Probabilities for cell seeds (green), cell outline (red) and background (blue) extracted from ilastik, C: Identification of single cells based on the probabilities from ilastik (coloured) and final segmentation (black and white), D: Segmentation outlines overlaid with the original cell outline (Rhodamine lectin stained cells from A). (c) Graphical user interface of the MATLAB analysis tool. Detection of polar (red) and side SRMs (blue). (d) Original filipin stained cells with calculated *rP* values. (e) Example analysis (data extracted from wild-type in Figure 21), notched boxplots summarising the *rP* of a population of cells. Red square: mean *rP* value; n= number of analysed cells for each time point, above box plot, in this and all following figures. All notched boxplots in this thesis are presented the same way (f) Example quantification of the bipolarity ratio *rB* (data extracted from wild-type in Figure 21). Scale bars: 10 μm.

1.7 Hypothesis

Although many factors of the polarisation machinery in fission yeast are identified and well characterised, the picture is not complete. Although a physical interaction of Tea1/Tea4 with For3, based on biochemical evidence, was proposed to lead to actin formation and growth, something must be missing in this view. Mutants of *tea1* or *tea4* grow monopolar, in a bent or branched cell shape, while *for3* mutants are able to grow bipolar, having difficulties to stabilise the growing ends. Even when all three formin genes are deleted, the cells are able to grow in a polar fashion (Bendezu and Martin 2011; Huisman and Brunner 2011).

Additional evidence for a missing factor comes from results of the semi-lethal *myo1Δ tea1Δ* double mutant cells. Myo1 restricts the SRM dimensions, Tea1 serves for their confinement to the cell poles. While *myo1Δ* cells still grow polar although they have SRMs all over the plasma membrane and *tea1Δ* cells grow monopolar, *myo1Δ tea1Δ* cells are misshapen. However, the fact that a proportion of even these cells is able to polarise to some extent, suggests that there is an additional, redundant pathway (Makushok et al. 2016).

Still, Tea1 is the central player in the cell polarisation process. During SE, it directs SRMs to the cell poles and stabilises them also at the non-growing end. The other polarity factors turn out to be involved in the maintenance of polarity rather than its setting up. However, it is unknown how Tea1 manages this task. *Tea1Δ* mutant cells not only grow strictly monopolar, they are also delayed in polarisation and growth initiation, indicating an additional function of Tea1.

We hypothesise that there is a sterol-rich membrane-associated factor, linking to Tea1 and facilitating its function in stabilising SRMs at the cell poles independent of growth.

1.8 Aim of the thesis

The aim of the thesis is to identify and characterise the missing link between Tea1 and sterol-rich membranes, potentially also connecting to the growth machinery. In order to identify this factor, a protocol to isolate proteins localising to detergent-resistant membranes (DRMs) is established and the proteins residing in DRMs from wild-type and *tea1Δ* mutant cells are compared by mass spectrometry analysis. To study the function for cell polarisation of proteins that vary in their presence between the compared strains, mutants of the according genes are analysed during starvation exit.

Besides first results indicating that the method is able to identify novel factors to have a role in the cell polarisation process, this thesis provides a resource for following studies. Further analysis of the obtained mass spectrometry results is expected to allow the selection of additional factors to be analysed *in vivo*.

2 Comparative mass spectrometry of fission yeast detergent-resistant membranes

2.1 General method development and validation

The following chapter describes the development of a method to isolate detergent resistant membranes (DRMs) from fission yeast cells for subsequent mass spectrometry analysis. Further details can also be found in the methods section. The final protocol developed is shown schematically in Figure 11. My aim was to identify differences between the protein composition of the detergent-resistant membranes that are present at the fission yeast cell poles of wild-type cells versus *tea1Δ* mutant cells.

As described in detail in the previous chapter, wild-type cells show a characteristic growth pattern. Wild-type cells frequently change growth sides, switching from mono- to bipolar growth in a highly regulated manner. Both the growing and the non-growing end have filipin stainable sterol-rich membranes (SRMs). *Tea1Δ* cells, in contrast, only grow monopolar and are unable to stabilise sterol-rich membranes at the non-growing end. To identify new factors important for the stabilisation of SRMs at the non-growing end and to understand how Tea1 potentially interacts with them to stabilise these SRMs, I developed a method to isolate DRMs. Mass spectrometry analysis was then used to compare the proteins present in DRMs from wild-type and *tea1Δ* mutant cells.

2.1.1 Collection of cellular material for detergent-resistant membrane isolation

Although phenotypic differences between wild-type and *tea1Δ* mutant cells are most pronounced during starvation exit, in which most *tea1Δ* mutant cells start to grow in a T-shape, exponentially growing cultures were used to isolate DRMs. It is expected that the factors that play a role in stabilising the SRMs at the non-growing end are the same during SE and exponential growth.

In order to get substantial amounts of cellular material from exponentially growing cultures that have a low optical density, large liquid cultures were grown over night. The cells were then isolated by centrifugation in large conical centrifuge tubes. This step is critical, as the centrifugation should not be too harsh in order to minimize stress for the cells and to avoid the risk that the SRMs might become rearranged during the sample preparation.

Unfortunately, the resulting cell pellet is very soft and easily gets lost when the supernatant is removed, so the use of conical tubes with a high volume was necessary to avoid material loss. Filtration of the cultures as an alternative worked in principle but was tedious and did not result in more cellular material. Also, it is not clear whether filtration might increase the stress for the cells due to drying.

I aimed to preserve the membrane composition as close as possible to the membranes of cells in exponentially growing conditions. Therefore, the cell pellet was transferred to a syringe with a needle and shock frozen by dropping the cell slurry into liquid nitrogen. The samples were stored at -80° C and could be kept for a minimum of several months.

To break the cells and to get access to the SRMs, the frozen yeast droplets were ground up in liquid nitrogen using a motorized mortar grinder. This method has been described, for example, in Givens et al. (2011) as a means to isolate intact nuclei from a range of fission yeast strains, and has been shown to be the most efficient way to extract lipids from *Chlorella vulgaris* (Zheng et al. 2011). It was expected to be beneficial, also for my purposes, to just break the cells open and to have the possibility to easily remove the other cellular components and isolate the DRM fraction. Therefore, grinding in liquid nitrogen allowed a mechanical lysis, again to preserve the membrane composition as close to the native state as possible. Cellular fractionation of yeast cells has been described after digestion of the cell wall with zymolyase before rupturing the cells by nitrogen cavitation (Wang, Lilley, and Oliver 2014). However, it was shown that the resulting spheroplasts lose their polarity, which cells have to re-establish when the cell wall grows back (Kelly and Nurse 2011; Drake and Vavylonis 2013). The mechanical lysis I used circumvented this problem and allowed transferring the cell powder from the ground cells directly into lysis buffer (Lingwood and Simons 2007). This avoided the use of glass beads in the procedure. These are commonly used as an effective tool to break yeast cells (Bagnat et al. 2000; Insenser et al. 2006) but locally produce temperature maxima, which may lead to degradation or aggregation of the proteins (Papanayotou et al. 2010; Islam, Aryasomayajula, and Selvaganapathy 2017) and interfere with protein and membrane interactions (Rieder and Emr 2001).

The process of cell isolation, freezing and grinding, was monitored by microscopy. Figure 2 shows that the filipin and the GFP-Tna1 life-marker signals could still be recognized even in the ground yeast cell samples, providing good evidence that the membrane

composition stayed intact throughout the procedure. It also showed that besides empty cell walls stained with Rhodamine-Lectin and cellular material that came out of the cells showing some remaining filipin and GFP signal, the cell powder still contained intact cells.

2.1.2 Isolation of the plasma membrane fraction and testing its solubility in detergents

Following cell grinding, protease inhibitors were added to all solutions to prevent protein degradation during the sample preparation. Further lysis of the cells by simply transferring the powder into the lysis buffer followed by vortexing at 4° C was sufficient to extract enough cellular material out of the broken cells. In the following centrifugation procedure, supernatant (S) and pellet (P) fractions are abbreviated with the centrifugation speed in 1000x*g*. For example, S3 is the supernatant after a 3000x*g* centrifugation step.

Centrifugation at 3000x*g* was used to pellet nuclei, cell wall and intact cells from the lysate (P3). According to Takeda, Kawate, and Chang (2004), mitochondria are also pelleted. However, others state that they fractionate only with higher centrifugation speed (12 000x*g*) and thus should stay in the supernatant (Harner et al. 2016). The supernatant (S3) was then spun in an ultracentrifuge at 100 000x*g* for one hour to separate the total membrane fraction, which may also contain mitochondria, in a high-speed pellet fraction (P100) and a supernatant fraction (S100) containing the cytoplasmic components (Takeda, Kawate, and Chang 2004; Vögtle et al. 2017).

In initial control experiments, I verified that the SRM life-marker GFP-Tna1 used in our lab localises to the membrane pellet (P100) together with Pma1, a commonly used marker for DRMs. If the pellet was further treated with Triton X-100 for 30 min on ice, GFP-Tna1 and Pma1 stayed in the pellet while they could be dissolved from the membranes by SDS treatment. Notably, considerable amounts of tubulin were always detected in the insoluble fraction. In contrast, the ER marker Ost1-mCherry substantially localises to the soluble fraction also upon Triton-X 100 treatment. These tests showed that the available markers appeared to be valid and could be used to follow and evaluate the isolation and purification of DRMs.

2.1.3 Isolation of detergent-resistant membranes

Optiprep (Iodoxanol) is a commonly used medium used for density gradient centrifugation. Stable gradients can be made by layering solutions of different Optiprep concentrations resp. densities on top of each other, the densest one on the bottom of the gradient. Solutions of components to be separated by density can either be placed on top or at the bottom. During ultracentrifugation, the components move to the density of the gradient that corresponds to their own density. Undissolved membranes, like DRMs, have a lower density compared to the dissolved components.

According to literature, 35% Optiprep appeared to work for fission yeast DRMs to float on top and was chosen also to be comparable with Takeda, Kawate, and Chang (2004). The initial trials to isolate DRMs on top of a 30% Optiprep solution, the standard for budding yeast and *Candida albicans* (Bagnat et al. 2000; Insenser et al. 2006; Lingwood and Simons 2007) as well as to fission yeast according to Iwaki et al. (2008), were not successful. No floating DRM band was visible under these conditions.

To isolate the DRMs, the membrane pellet P100 was resuspended in TNE buffer and treated for 30 min with 1% Triton X-100 on ice. The solution was then mixed with Optiprep to a final concentration of 40% Optiprep and placed at the bottom of a step gradient (Figure 3). It was overlaid with 35% Optiprep in TNE covered with plain buffer. Two hours of ultracentrifugation at 200 000 x*g* allowed isolating detergent resistant membranes, floating as a band on top of the 35% Optiprep layer.

The DRMs were isolated by fractionating the gradient. The top TNE layer (no Optiprep) (100-120 µl) including the easily visible floating band on top of the 35% Optiprep layer was taken as floating fraction (F). The 35% Optiprep layer was isolated as intermediate (I) fraction (approx. 300 µl). At the interface between 35% and 40% Optiprep, one or two bands were visible and isolated as dense fraction (D) (100-120 µl). In general, it appeared as two fuzzy bands very close to each other, sometimes fusing into one. The remaining bottom fraction (B) was usually around 200 µl.

To further purify the DRMs and remove as much unspecific material as possible, the floating fraction was treated with 1% Triton for a second time and re-isolated by ultracentrifugation on the same kind of an Optiprep gradient. The material visible at the interface

between 35% and 40% Optiprep after the first extraction disappeared after the second round. The floating band on top of the 35% Optiprep layer was usually thinner than after the first round of extraction.

The fractionation process and isolation quality were monitored by Western blotting (Figure 4). The SRM life-marker GFP-Tna1 and the commonly used raft-marker Pma1 consistently co-purify with the floating DRM fraction and are detected less in the denser fractions. In contrast, the ER marker Ost1-mCherry appeared mostly in the dense fractions of the first gradient, showing that the ER could be successfully removed by detergent treatment in the cold and gradient centrifugation. The floating fraction obtained from the second extraction and gradient (F2) was then treated further in preparation for the mass spectrometry analysis.

It has to be noted that the bands visible on the Western blots in Figure 4 cannot be used for direct quantitative comparisons. Only small amounts of the remaining material from the floating fractions could be analysed as the material was mainly used for the second extractions (F1) and the following mass spectrometry analysis (F2), respectively. In contrast, the denser fractions could be transferred to the Western gel completely.

Although the Western blots cannot exactly represent a quantification, they still show that the floating fractions are highly enriched in the marker proteins Tna1 and Pma1, while the concentration of these markers is significantly lower in the denser fractions of the gradient. For each sample sent for MS analysis, the fractionation was controlled by Western blotting (Figure 4b). As mentioned before, tubulin was mainly enriched in the soluble fractions S3 and S100. However, a considerable proportion separated with the membrane fraction and specifically co-purified with the DRM fraction. In the first gradient, tubulin was still detected in the denser fractions and mainly in the floating fraction F2 on the second gradient. Amidoblack staining demonstrates the low protein concentration in the dense fractions after the second gradient. Throughout several experiments, the overall behaviour of the markers used was consistent for wild-type as well as for fission yeast mutants.

2.1.4 Sample preparation for Western blots and mass spectrometry analysis

In the following, the sample preparation that was used for the first screen will be described. The modifications that were applied for the second screen will be discussed in the next section.

The main part of the floating fraction from the second Optiprep gradient was prepared for mass spectrometry except for a small sample that was kept to control the sample preparation process by Western blotting. The intermediate, dense and bottom fractions were exclusively used for Western blot analysis. Two volumes of 15% TCA were added to all isolated fractions to precipitate the proteins. In general, the samples mixed with TCA were stored at -20° C for at least 16 hours. However, the sample preparation can, in principle, also be continued after shorter precipitation with TCA in the cold (≥1 hour on ice). Centrifugation of the thawed samples at 5° C at the maximum speed of a cooled table-top centrifuge (16000 x*g*) pelleted the proteins that were subsequently washed twice with ice cold ethanol by rinsing and slurring the pellet followed by centrifugation and drying in an Eppendorf tube on a clean paper cloth. The washing is needed to remove the protease inhibitors. These would interfere with the tryptic digest for mass spectrometry. Washing also removes residual Triton X-100 and Optiprep that might otherwise both interfere with the mass spectrometry measurements. Acetone was tried but cannot be used for the washing steps as it precipitated Optiprep.

The dried F2 samples were sent to the Functional Genomics Centre Zurich (FGCZ) for mass spectrometry analysis. For Western blot analysis, a small aliquot of F2 and all other samples from the precipitated fractions were dissolved in SUMEB and directly transferred to a poly-acrylamide gel (Figure 4).

2.1.5 Discussion of the sample preparation

It has to be noted that the purification of DRMs cannot be done in a perfectly clean manner, and variation between experiments on the Western blots was both expected and observed. To start with, the amount of cell material used for the extraction varies. It is not trivial to transfer and exactly weigh a certain amount of the prepared cell powder into the buffer for the following lysis. To avoid any thawing and potential damage to the samples, the cell powder was stored at -80° C and kept in liquid nitrogen when material was

removed from the stock. Whatever was then taken with the cooled spatula was weighed and used for the lysis, but varied by weight. Additionally, I did not analyse systematically how much of the cell powder is actually accessible for lysis or how many of the cells were broken. I also did not know the minimal amount of Triton X-100 needed to dissolve all detergent-sensitive membranes under the conditions used. Nevertheless, the tests done and the results described above suggest that the amount of material used was in a reasonable range and the control experiments show the robustness of the method. We were then confident enough to use the purification protocol for mass spectrometry analysis of the isolated F2 fraction containing DRMs and comparison of the contents between wild-type and mutant cells.

2.2 Results: mass spectrometry screen 1

During several experimental rounds, DRMs were isolated from wild-type and *tea1Δ* mutant cells. Additionally, *myo1Δ* mutant cells that have SRMs all around the cell membrane and the temperature sensitive mutants *cdc25-22* and *cdc10-129* that, at restrictive temperature, grow only bipolar and monopolar, respectively, were used for the DRM preparation and analysis.

I hypothesised that in the strictly monopolar growing *tea1Δ* mutant, a potential factor localising to SRMs linked to Tea1 is missing. By including more mutants with a distinct growth pattern, I expected to gain a better insight into which proteins might be critical. As *cdc25-22* cells grow bipolar at restrictive temperature, it was expected that a factor that links to growing ends is present at increased concentrations compared to wild-type cells that also grow monopolar. In contrast, *cdc10-129* mutants grow exclusively monopolar. Thus, in this case the factor should be present at reduced levels compared to wild-type, potentially half of the amount detected in *cdc25-22* cells at restrictive temperature. *Myo1Δ* mutant cells have SRMs all around the plasma membrane and still grow at the cell poles. I expected to find the SRM localising factor at potentially lower concentrations in these cells because of the increased amount of DRMs, however the reduced turnover of the persisting SRMs in this strain might facilitate its co-purification and detection. By comparing the different mutants, I expected to get access to proteins that are present in all strains, but at different levels depending on the growth mode. Complementary, in starved cells the DRMs were expected to be composed differently, and the factor of interest might be

absent completely. However, I cannot exclude that the factor only serves as a linker always present and that its function depends on the additional presence of Tea1. Thus, it is possible that it is already present in starved cells.

The following section describes the resulting mass spectrometry data and how it was used to select candidate proteins/genes for further *in vivo* studies. The first results of the *in vivo* experiments to test these candidates will be shown. Finally, a discussion will lead into the further refinement of the method that will be the content of the next chapter.

2.2.1 Summary of the mass spectrometry results

In total, 16 samples were analysed in four independent mass spectrometry experiments. From these, six samples were prepared from wild-type, five samples from *tea1Δ* and two from *myo1Δ* mutant cells growing exponentially. An additional sample analysed was taken from wild-type cells starved for 3 days. Of the temperature-sensitive mutants *cdc25-22* and *cdc10-129* one sample each was prepared.

In total, 1576 proteins were identified by mass-spectrometry, with at least two exclusive unique peptide counts in at least one sample. Exclusive unique peptide counts are the number of peptides identified that are associated with a single protein. The number of identified proteins varied between 344 and 1098 in the different experiments and samples. On average, 635 ± 294 proteins were identified with at least two exclusive unique peptide counts. Table 1 provides an overview of the number of identified proteins in the different samples and experiments. The sample IDs also provide information about the experiment, meaning which samples were analysed in each individual experiment (sample ID: yymmdd_sample).

strain	**sample ID**	**≥ 2 exclusive unique peptide counts**	**≥ 1 exclusive unique peptide counts 100% conf.**
wild-type	141113_1	1098	1326
wild-type	141113_2	1094	1341

wild-type 3 days starved	141113_3	1090	1289
tea1Δ	141113_4	1047	1314
wild-type	141203_1	640	872
tea1Δ	141203_2	814	1058
tea1Δ	141203_3	788	1046
wild-type	141217_1	344	509
wild-type	141217_2	391	533
tea1Δ	141217_3	352	538
tea1Δ	141217_4	399	605
myo1Δ	150115_1	459	608
cdc10-129	150115_2	433	593
cdc25-22	150115_3	468	619
myo1Δ	150115_4	365	506
wild-type	150115_5	376	488

Table 1: Number of proteins identified by mass spectrometry in different DRM samples and on different experimental days.

In general, the samples of any individual experiment were comparable regarding the number of proteins identified and the identity of the detected proteins. But as illustrated in the table above, the number of proteins identified varied greatly between the different experiments. This will be discussed in more detail at the end of the chapter. Unfortunately, no protein was identified that was present in all wild-type samples and absent in all *tea1Δ* samples or vice versa. All clear-cut differences between wild-type and *tea1Δ* cells found in one of the independent mass-spectrometry experiments were absent in the others. Additionally, such differences only appeared in the less abundant proteins that were represented with a lower spectrum count in the mass spectrometry data. Accordingly, if a protein was detected or not varied greatly, also between the different samples of the same strain. Also, neither the results from the strictly bipolar and monopolar growing temperature sensitive mutants *cdc25-22* and *cdc10-129* respectively, nor the *myo1Δ*

mutant provided any hint towards a protein present in DRMs and potentially important for the specific SRM localisations present in these strains.

However, I still wanted to test if proteins functionally linked to Tea1 and cell polarisation were identified with the method. Notably, the applied mass spectrometry method did not necessarily allow the detection of quantitative differences between samples. Despite this, in the sample from a 3 day-starved wild-type cell culture, a few proteins were identified with a clearly higher abundance than in the other samples. Some proteins were even absent in all other samples, suggesting that quantitative differences at least in a certain range should be detectable. Consistently, the Lanosterol 14 alpha-demethylase Erg11 was detected in all other samples from growing cells, but not from the starved cells. The result that an enzyme from the ergosterol synthesis pathway could not be detected in the sample from starved cells fits well with the fact that these cells do not stain with the sterol-binding dye filipin and that the new sterols need to be synthesised for *de novo* cell polarisation (Makushok et al. 2016). That this might consequently change the protein composition of the DRM fraction can therefore be expected.

2.2.2 Candidate selection for *in vivo* screen

Initially, I hypothesised that the protein content in DRMs from *tea1Δ* mutant and wild-type cells may differ. However, I also considered the possibility that the factor of interest is always present and needs interaction with Tea1 for functionality. Regarding this, despite the lack of obvious differences between the strains of interest, the overall method appeared to work and it was decided to select candidate genes for further *in vivo* experiments based on the MS results. The list of proteins resulting from the mass spectrometry was analysed manually, considering proteins belonging to certain categories as candidates. To test a putative role of these proteins of interest in cell polarisation, I used the fission yeast deletion library ((Kim et al. 2010), version 5). This library holds all viable deletion strains of the fission yeast *S. pombe*. The deletion mutants of the respective genes were tested for a phenotype during starvation exit as previously reported (Makushok et al. 2016).

In the *S. pombe* post-genome database, the localisations of many over-expressed proteins can be found from a systematic protein-tagging screen (Matsuyama et al. 2006). The localisation as it is visible there was considered when deciding if a protein is included in the list of candidates. Proteins showing a polar localisation were deemed potentially more relevant than those localising to the nucleus, for example. As I was looking for some factor potentially localising to the plasma membrane, any protein containing a transmembrane domain was considered to be of interest. Also, proteins described to have interactions with Tea1, or functions at least potentially connected to polarisation, were considered. All uncharacterised proteins were added to that initial list of candidates. It was expected that among those, some might offer new insights into the cell polarisation process. Regarding the vast amount of proteins identified in the samples, the inferred function of a protein as well as a portion of "gut feeling" played a role in the selection process. The fission yeast database "Pombase" was used as a resource to get first descriptive information of the proteins (www.pombase.org). Also, factors having "(ergo)sterol" in the descriptive name or those involved in transport were added to the initial list of potential candidates.

To narrow down the number of candidate mutants to an amount that can be analysed manually, all essential genes were removed from the list. Out of initially 415 candidate genes selected, 89 were essential and therefore removed. Further literature and database research provided additional information about the proteins selected in order to further restrict the list to keep only the most promising candidates.

Finally, 166 candidates were selected for a first *in vivo* analysis. Of these, 13 were not present in the fission yeast deletion library, leading to a reduced list of 153 candidate proteins/genes chosen for further analysis. These are listed in Table 6 in the supplements.

2.2.3 Experimental setup and analysis of the starvation exit screen

The experimental setup of the mass spectrometry analysis of DRMs, which compared wild-type to *tea1Δ* mutant cells was designed to identify an unknown Tea1-interacting factor that provides information about how Tea1 is able to stabilise SRMs at the cell poles. To find such a factor within the selected candidates, a starvation exit experiment was chosen as assay to screen for deletion mutants potentially phenocopying *tea1Δ* or showing a defect in any other aspect of *de novo* cell polarisation. As described in detail in the

introduction, *tea1Δ* cells fail to stabilise SRM domains at the cell poles during SE and cells eventually initiate growth at any of the randomly distributed SRM domains, often leading to a T-shaped cell. It is expected that any factor acting downstream of Tea1 should also show this behaviour. T-shaped cells are easily and clearly identifiable by eye.

The deletion mutants were taken from the fission yeast deletion library and were grown to exponential phase in 96-well plates in rich medium. The standard growth medium was then exchanged with low glucose medium and incubated for 2 days during which cells entered starvation. Some of the starved cell culture was transferred to fresh high glucose medium to start starvation exit (SE). 90 min after initiating SE, the cells were stained with filipin and imaged with an epifluorescence microscope. This timepoint was chosen because wild-type cells were usually already clearly bipolar by then and had started to grow. *Tea1Δ* mutant cells are still either in P1, showing their known delay in SE, or have just started to grow in a T-shape.

From the 153 candidates selected and prepared for the experiment, 130 could be analysed during SE. The remaining 23 strains either could not be woken up from the library, or they did not grow sufficiently or not at all after being transferred to the 96-well plates. For some, the cell number might also just have been too low to be found on the microscopy slide.

Both parental deletion library strains were used as wild-type controls. In addition, a *tea1Δ* deletion strain from the laboratory collection was used together with the *tea1Δ* mutant from the deletion library as reference for the phenotype of interest. For logistic reasons, the experiment had to be done on two different days in two individual 96-well plates. Thus, half of the candidates were prepared for one day, the other half for the next day. On both days, all controls were tested with the strains of interest. The wild-type cells showed the expected normal polarisation in both controls and on both experimental days. The *tea1Δ* control samples were more variable. They contained mainly growing T-shaped cells in P3 on one day (day 1), and mainly non-polarised cells in P1 on the other experimental day (day 2) (Figure 6a).

None of the imaged candidate deletion mutants showed T-shapes at 90 min of SE. Various phenotypes were observed in different mutants. Those included cells still in P1, meaning that among the selected candidates, some are delayed in SE like *tea1Δ* mutant cells are. A different phenotype identified was characterised by dotty filipin staining.

To identify the candidate mutants that were worth further investigating, they were classified based on the filipin staining patterns of the cells. Mutants were classified into different categories following manual screening of the images. The categories were as follows: cells were either *mono-* or *bipolar* like the wild-type. Additional, among bipolar cells, the ones also having a *weak second pole* were classified. This could be the case in a polar cell that grows monopolar, with a strong and a weak pole, which is also a possible phenotype in a proportion of wild-type cells. A mutant having difficulties to stabilise the second pole might only show this phenotype. Cells were classified as *patchy*, with the typical P1 phenotype observed when cell polarisation was delayed. Surprisingly, a few mutants had a rather *dotty* filipin staining pattern and some showed filipin staining *all around* the cell. Some samples contained *septated* cells. Rarely, *no SRMs* were stained with filipin or the staining was *not clear*. Figure 5 illustrates the experimental workflow and the classification process. Examples of the different phenotypes observed are given.

The classifications were compared to the wild-type and to the *tea1Δ* control samples. Because the *tea1Δ* cells behaved slightly different on the two different days, the overall phenotypes of the candidate mutants were compared to the control samples of the same experimental day (Figure 6 and Figure 7).

The main phenotype of *tea1Δ* mutant cells is a polarisation delay. Thus, it is possible that mutants with a polarisation delay start T-shaped cell growth later and were included as potential candidates. On day 1, the mutants analysed rarely showed signs of a delay, while eight of them were classified as mainly monopolar like *tea1Δ* mutant cells (Figure 6c). As the cells appeared to be more delayed on day 2, ten mutants were classified to have cells mainly in the patchy phase (P1), comparable to the *tea1Δ* mutant cells on that day (Figure 6d). Eight strains showed a dotty staining pattern of filipin; two of them, *ccr1Δ* and *erm1Δ*, showed the dots overlaying another pattern like the patchy stain (Figure 7a). All mutants with dots were identified on day 2. In total, three strains were analysed that showed filipin straining all around the cell (Figure 7b). As this initial secondary *in vivo* screen only served to filter the candidate mutants chosen for some that show a polarisation phenotype, it was not tested further why the experimental results varied between the two days.

The variability was expected to be enhanced by the use of 96-well plates that provide only a small volume for cell culturing. In addition, the breathable lid probably allowed a

different level of gas exchange compared to the well-controlled standard growth and SE conditions in larger Erlenmeyer flasks. Furthermore, the use of a pin tool to inoculate cells and to transfer them to low glucose medium for starvation added another level of variability that was visible in the phenotypic variation of the strains. Before inoculation, cells were grown on agar plates in the required 96-well format to allow the use of a pin tool to transfer the cells into 96-well culture plates. The number of transferred cells probably varied greatly, depending on how many cells initially grew on the plate and how many cells on the plate stick to the metal pins. In general, the differences should level out to some extent if the cells were able to grow properly in the small volume of the plate. The mutant cells were first grown to a high density before they were transferred to fresh medium for reaching the exponential growth phase. The mini-cultures were expected to reach a similar cell density and to transfer more equally from one liquid medium to the next with the pin tool. However, some mutants probably grew less efficiently than the majority and thus the cell density probably was lower such that too little cells were transferred for exponential growth and the subsequent starvation cultures. This might be the reason why some mutants could not be analysed in this experiment. Another expected experimental problem is the possibility that some mutant strains might not have been properly starved at the beginning of the SE experiment. It is possible that the variable amounts of cells that were transferred to low glucose starvation medium with the pin tool led to differently starved cells on the two experimental days, reflected in different polarisation speeds on the different days.

Still, the results described above demonstrate that the experimental setup allowed the identification of candidate mutants that are worth further investigation. To begin with, three deletion mutants were selected for validation and further phenotypic analysis (Figure 7c). *Cfr1Δ* and *fzo1Δ* mutant cells were characterised as mainly *patchy*, having a delay in polarisation, similar to the *tea1Δ* mutant cells. The *mfs3Δ* mutant showed a mainly *dotty* phenotype. Among the other mutants identified in these categories, the three were chosen based on their described biological role.

2.2.4 Characterisation of three selected candidate mutants

For the three mutants chosen for further experiments – *cfr1Δ, fzo1Δ* and *mfs3Δ* - the deletion in the strain taken from the fission yeast deletion library was verified by PCR. In

the library, all strains depend on the presence of Adenine, Leucin and Uracil. They have the gene deletion genotype and the auxotrophic marker genes *ade6-M210* (or *ade6-M216*) *leu1-32 ura4-D18.* All strains were crossed to wild-type cells to remove all of these auxotrophic markers from the genetic background. Crossing to the wild-type strain containing GFP-Tna1 simultaneously allowed introducing the life marker to follow the formation and polarisation of SRMs in the candidate mutant strains.

The strains were starved for two days at 30° C and the polarisation process was followed based on the localisation of GFP-Tna1 during live-imaging (Figure 8a). As previously shown, starved wild-type cells only showed intracellular GFP signal and no signal at the plasma membrane (Makushok et al. 2016). Upon glucose addition, SE started and GFP-Tna1 patches became visible at the cell periphery at random positions during P1. Eventually, the side patches were removed and the cells polarised in P2. In this experiment, polar wild-type cells were visible after 2 hours and more prominent ones with strong polar caps after 3 hours. In general, the polarisation process is slowed down here because the cells are recovering on a microscopy dish and due to phototoxicity when they are imaged over time. In contrast, wild-type cells recovering in liquid culture usually polarise within one hour (Makushok et al. 2016).

2.2.4.1 Cfr1 – a Golgi protein

The Golgi protein Cfr1 was described to play a role during mating. *Cfr1Δ* mutant cells fail to digest the cell wall at the contact site of two mating cells (Cartagena-Lirola, Durán, and Valdivieso 2006; Curto et al. 2014). Cfr1 is a homolog of the Chs5p protein from the budding yeast *S. cerevisiae* that is involved in the exit of Fus1 from the Golgi (Proszynski et al. 2005). It also contains a fibronectin type III (FN3) and a BRCA1 (BRCT) domain, required for its localisation to the Golgi apparatus and its role in the transport of the chitin synthase III (Chs3) to the plasma membrane (Martín-García et al. 2011). Recently, the protein has been found to form an exomer-like complex with Bch1 that is involved in vesicle-trafficking from the *trans*-Golgi or early endosomes to the plasma membrane in fission yeast (Hoya et al. 2017).

In *cfr1Δ* mutant cells, GFP-Tna1 signal was only intracellular during starvation, like in wild-type cells. *Cfr1Δ* mutant cells normally entered P1 and were able to polarise within 3-5 hours, having a slight delay in P2 compared to the wild-type but showing the normal, sequential polarisation process.

2.2.4.2 Fzo1 – a mitofusin

The mitofusin or fuzzy onion Fzo1, a transmembrane ATPase, is needed for mitochondria fusion, namely the fusion of the outer mitochondrial membrane and is conserved from yeast to mammals (Mozdy and Shaw 2003). It was originally described in the fruit fly *Drosophila melanogaster* and named after the characteristic onion like mitochondria aggregates that fail to form during spermatogenesis in the mutant (Mozdy and Shaw 2003). Due to the dynamics of mitochondria and their constant rearrangement by fission and fusion, budding yeast *fzo1Δ* deletion mutant cells have fragmented mitochondria (Sesaki and Jensen 1999). Fragmented mitochondria lose their mtDNA and the cells become defective in respiration (Hermann et al. 1998). So far, there has been no study concerning the exact role of Fzo1 in fission yeast, although it is expected to function the same way as in the other organisms. The protein was included in the further studies as its description as a transmembrane GTPase involved in membrane fusion makes it an interesting candidate and it cannot be excluded that it plays a different or additional role in fission yeast.

Like wild-type, *fzo1Δ* mutant cells showed intracellular GFP-Tna1 signal. During SE, SRM domains formed in P1 and polarised in P2. The timing of both phases was comparable to wild-type cells, although the mutant shows more variability between individual cells. It was noted that some *fzo1Δ* cells polarised already within one hour. Some started to divide after 5 hours SE, even earlier than wild-type cells, although the majority of the cells becomes polar after 5-7 hours, or do not polarise at all during that time frame. Many cells appeared to produce SRM patches and repositioned these during SE but had difficulties to stably polarise.

2.2.4.3 Mfs3 – a multi-spanning transmembrane protein

The candidate protein Mfs3 contains 11 transmembrane domains and is a member of the major facilitator superfamily. It was found to be involved in the multi-drug resistance of fission yeast and is regulated by the transcription factor Prt1 (Kawashima et al. 2012).

In case of *mfs3Δ*, GFP-Tna1 localised internally in starvation like in wild-type cells. P1 and P2 were also comparable to the control. Some cells were almost bipolar already after two hours, but still had remaining SRMs at the cell sides. These were, however, removed before three hours in SE when the first polar cells became visible.

2.2.4.4 Summary of cfr1Δ, fzo1Δ and mfs3Δ results and further analysis

In summary, besides the described slight delays, the polarisation processes in *cfr1Δ*, *fzo1Δ* and *mfs3Δ* mutant cells were mainly comparable to wild-type cells under these conditions. In order to test if the observed delay in polarisation was due to mis-localisation of the polarisation factors, the localisation of microtubules and Tea1 was analysed during SE. In all mutants, the localisation of microtubules labelled with GFP-atb2 and the positioning of Tea1-HL-tagRFP was the same as in wild-type cells (data not shown). Microtubules formed quickly after glucose addition and Tea1-HL-tagRFP was visible as spots at the cell end. This showed that the cells were delayed although the polarisation factor Tea1 was transported to and present at the cell poles. I conclude from this that the candidates tested should then not be directly involved in the localisation of Tea1 but might still work together with Tea1 to stabilise SRMs at the cell poles.

2.2.5 SE of candidate *tea1Δ* double mutants

None of the mutants showed the formation of T-shaped cells in the SE experiments. As this does not fully exclude a functional connection between the candidate proteins and Tea1, cells were sensitised by additionally introducing a *tea1*-deletion into the mutant strains via mating. Additionally, GFP-Tna1 was present in the cells to follow the polarisation process. Again, cells were starved for 2 days at 30° C, recovered by addition of fresh medium and imaged throughout the recovery process (Figure 8b). *Tea1Δ* mutant cells

started patch formation after glucose addition. After 2 hours, large patches were formed and growth was initiated at one large patch per cell, leading to T-shaped cells after four hours in SE. The cells grew and divided within 10 hours.

The double mutants *cfr1Δ tea1*, *fzo1Δ tea1Δ* and *mfs3Δ tea1Δ* behaved similar to the tea1Δ single mutant. They formed large patches and started monopolar growth leading to T-shaped cells.

It appears that the growth is not strictly limited to one pole anymore in the *mfs3Δ tea1Δ* double mutant cells. An asterisk marks a cell growing from two patches in a bipolar fashion into a C-shape. Still, this is an exception in these double mutants.

2.2.5.1 Fzo1Δ tea1Δ cells struggle in growth patch selection

Fzo1Δ tea1Δ double mutant cells showed a more complex behaviour. Some also grew in the typical T-shape, but most cells are not able to select an SRM domain for growth. They formed patches in P1 that change positions around the cell, in some cases throughout the whole experiment, like the cell marked with an arrowhead. Some other cells like the one marked with an arrow fail to polarise the SRMs and still eventually divide without much growth in length. It is noted though, that the *fzo1Δ tea1Δ* cells appeared to grow into a rather round shape. They were probably able to sequentially initiate growth at any patch during the observed extensively prolonged SRM remodelling phase.

2.2.6 Fzo1 as potential candidate for future investigations

Strikingly, *fzo1Δtea1Δ* cells and *fzo1Δ* cells to a lesser extent always showed a characteristic behaviour: when woken from the frozen stock at -80° C, they needed much more time to grow up on agar plates and in liquid medium compared to other strains. After some time, the cells grew comparable to other strains. Interestingly, the cells and liquid cultures had an unpleasant smell. Based on these findings, the *fzo1Δ* mutant was considered to be of interest and some further experiments were done (data not shown). As expected, mitochondria were mainly fragmented in the mutant as visualized by fluorescently labelled Cox4 in *fzo1Δ* mutant cells. Trials to tag Fzo1 at the C-terminus failed and cells overexpressing tagRFP-HL-Fzo1 or GFP-HL-Fzo1 showed a mitochondrial localisation of the protein. The cultures had the same smell as the deletion mutant. To exclude the possibility

that some factor in the background from the deletion library was responsible for the inconsistent growth behaviour, a new deletion mutant was generated. It showed the same behaviour, suggesting that the strain probably quickly adjusts. Finally, it was decided to leave these mutants for some possible more comprehensive investigations in the future, as they are not trivial to handle and the experiments at this stage did not lead to conclusive results.

2.2.7 Re-visiting the dotty candidates from screen 1

During the work on this project, another project in the lab identified oxysterol-binding proteins as essential factors for patch formation during P1, the initial phase of cell polarisation in fission yeast. More details can be found in chapter 4. The deletion mutants kes1Δ and osh7Δ have a characteristic, dotty filipin staining pattern in starved cells and throughout SE. The single mutants were delayed compared to wild-type cells, the kes1Δ osh7Δ double mutant needs even more time to polarise. The observed dotty filipin signal was reminiscent of the dotty candidates identified in the screen presented above and it was obvious to have them tested again if any of these have a similar role.

The deletion mutants to be re-tested were crossed to wild-type cells to remove the auxotrophic markers from the genetic background. Some of the analysed strains were expressing GFP-Tna1 in the background and were then compared to wild-type cells that also expressed the life marker. The others were tested against plain wild-type cells. In this experiment, the cells were starved for 3 days and recovered by addition of fresh medium at 25° C. Cell samples from liquid culture were stained with filipin and imaged in imaging dishes at several points in time during SE for a total of three hours (Figure 9). The polarisation process was then quantified with the analysis pipeline developed in the group in the meantime. If not stated differently, this is the standard method used in all following experiments.

Under these conditions, none of the tested strains initially described to have a dotty filipin staining pattern showed this phenotype again. All mutants showed a normal patchy phase (P1) until they entered P2 and finally polarised within the same time range as wild-type cells. In summary, all strains analysed showed wild-type behaviour in this experiment. The quantifications summarised in Figure 10 show the same picture. All strains show a

nice transition from non-polar cells with an *rP* value of 0 to polar cells with an *rP* of 1 within 1-2 hours. The quantifications of the mutants are displayed in comparison to the according wild-type control sample from the same experiment. In none of the quantifications a delay compared to the control sample was visible.

For the initial *in vivo* screen, the cells were imaged on simple glass slides, covered with a glass cover slip that is needed to stick the cells to the lectin-coated glass slide. Is it possible that the simple setup introduced artefacts to the filipin signal due to the pressure the cells experienced under the glass cover slip. All later experiments were carried out on imaging dishes that leave space and medium surrounding the cells. Because the result was clear for all tested strains, the two remaining candidates initially classified as dotty have not been tested again as it is likely that they also only showed the dotty phenotype because of the experimental setup.

2.2.8 Discussion of screen 1 – analysis of the problems led to further improvements

To summarise this initial attempt to identify factors that differ in their presence in DRMs from wild-type and *tea1Δ* fission yeast cells, it can be stated that the method developed to isolate DRMs from exponentially growing and starved cells works in principle. Over a range of experiments and mutants, the raft markers were enriched in the fractions prepared for mass spectrometry analysis. This enrichment is a big advantage of the method. Within the same experiment, the MS results were comparable regarding protein number and identity. Proteins that were much more abundant in one sample compared to the others were detectable. High protein abundance was necessary to identify proteins missing in one condition compared to the other because the detection was less reliable in the low abundance range, especially across different experiments.

The difficulty to detect differences between the strains was probably partly due to the fact that it is likely that the factor of interest is only present at low abundance and can thus be expected to be hard to detect. Additionally, if the factor is small, only a few of its peptides might be detectable and thus the protein will be harder to be identified. Another possibility is that the protein looked for is in general hard to detect because it does not fly well in the MS instrument or because it is only poorly solubilized from the DRMs before MS

analysis. The latter complication will be tackled in an optimised sample preparation described in the following chapter.

Based on the MS results, candidate genes were selected and their behaviour during SE was tested *in vivo,* in mutants of that gene, to find possible connections to Tea1. Because no clear differences were detected in the mass spectrometry results, all mutants tested later in the SE experiments were selected manually. Although many mutants were identified that were delayed in polarisation during SE or showed other specific mutant phenotypes, no obvious *tea1Δ* phenocopy was found with the experimental setup.

It is likely that among the proteins identified by MS, some novel factors critical for cell polarisation in fission yeast were detected but were not included in the further tests due to the selection conditions. Furthermore, it is possible that factors were identified and still lacked a clear phenotype.

Importantly, the overall setup comparing data from different MS experiments was not ideal. To make sound conclusions, comparisons should only be made based on data from the same experiment. Because there were no clear differences even within one experiment, different experiments were compared as a compromise to make use of the generated data. This was not optimal.

As discussed in the section above, the imaging conditions probably introduced some artefacts as well. The strains from the library all contain the three auxotrophic marker genes *ade6-M210* or *-M216*, *leu1-32* and *ura4-D18*. For starvation exit experiments they should all be crossed out as they alone already cause a delay in SE and might lead to additional complications in combination with a deletion of a gene important for polarisation. Additionally, the genetic background of some strains of the deletion library contains additional unknown factors that we recognized in our group to also lead to complications. For example, an additional temperature sensitivity factor in the *osh7Δ* strain taken from the deletion library caused a polarisation delay. *Osh7Δ* mutant cells without the temperature sensitivity have a milder polarisation defect (found and tested by Adam Kijowski). The temperature sensitivity was present in the strain although according to Kim et al. (2010), it should be removed from the deletion library and *osh7Δ* was not listed as a strain that contained it in the initial version of the library. Summing this all up, the factor looked for is probably hidden in the noise.

Based on all these considerations, I decided to invest more time in further improving the method as it appeared more promising to work on results from an optimised MS experiment to be able to find differences between DRMs from different samples than to intensively work on factors identified with the suboptimal experimental method. The fact that the isolation of DRMs works reliably and that within an MS experiment the results were very similar provided hope that it should be possible to detect differences between the protein composition of DRMs of wild type and mutant strains in case the protocol would be improved sufficiently. The modifications introduced to the method and the reasoning will be described in detail in the next chapter.

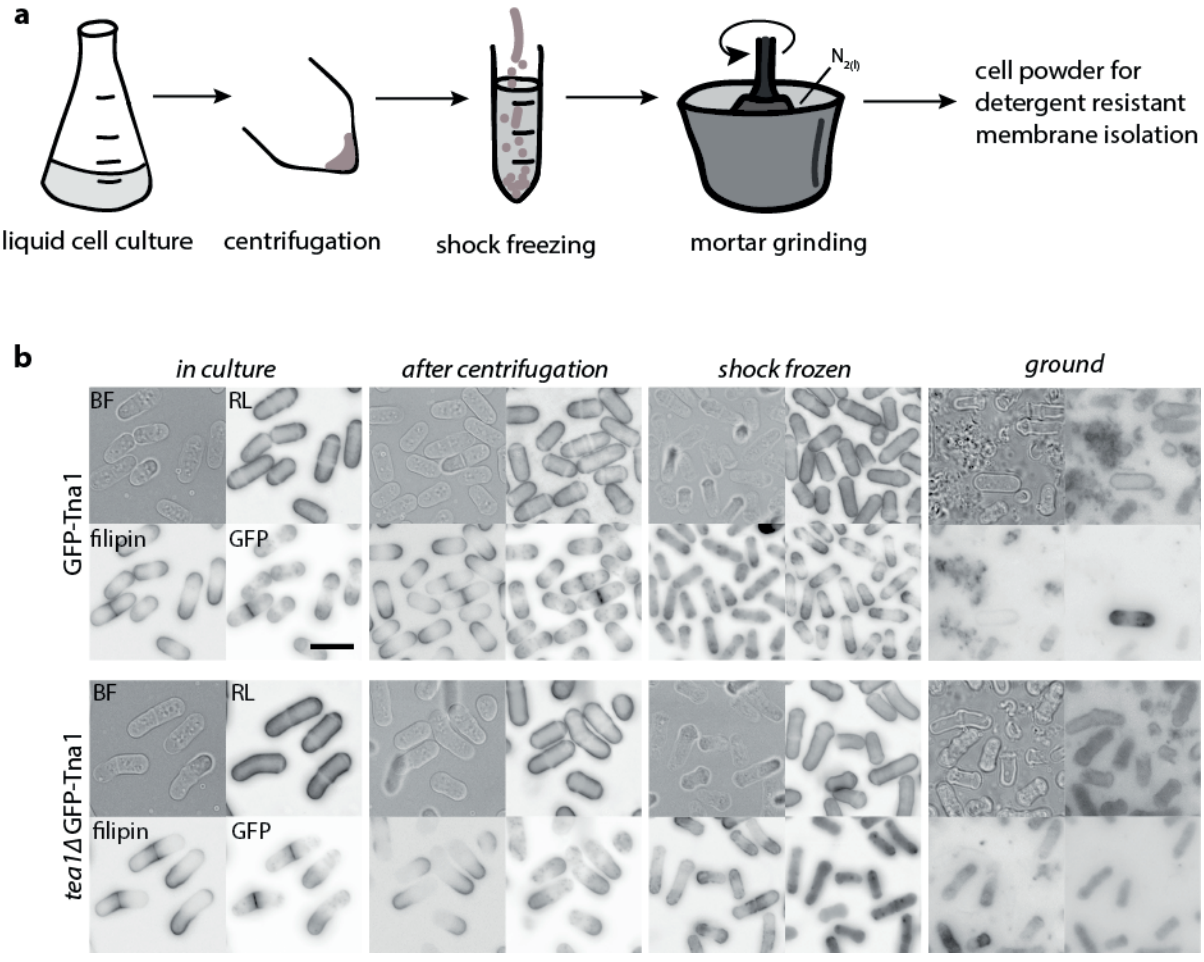

Figure 2: Controlling the collection of cell material.

(a) Experimental steps to prepare cell powder: Centrifugation of liquid cell culture, shock freezing of cell slurry in liquid nitrogen, mortar grinding of frozen yeast cells in liquid nitrogen. (b) Controlling the sample preparation steps. Exponentially growing cells in liquid culture before and after centrifugation, after shock freezing in liquid nitrogen and after mortar grinding in liquid nitrogen (from left to right). BF: Brightfield, RL: Rhodamine-Lectin, GFP: GFP-Tna1. Scale bar: 10 µm.

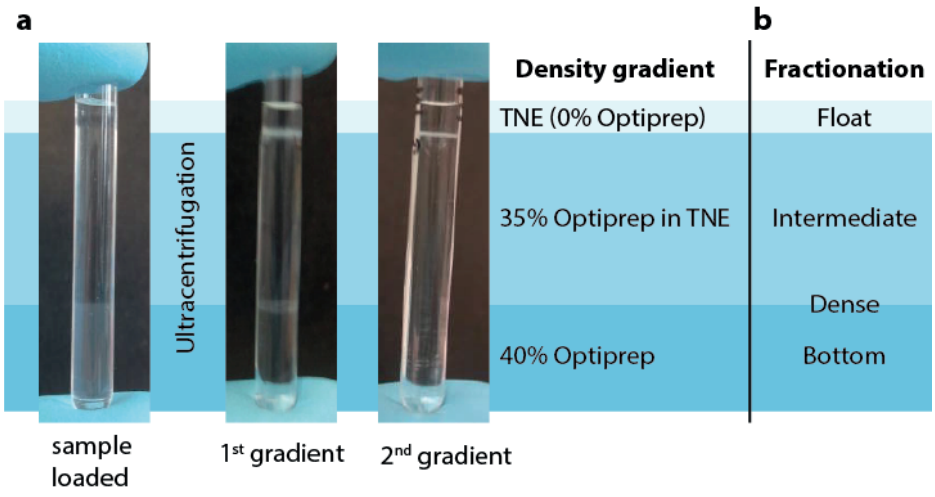

Figure 3: Preparation of Optiprep gradient and fractionation.

(a) Example gradient before (left) and after ultracentrifugation (middle and right) of first (middle) and second (right) extraction with Triton X-100. (b) Fractionation of the gradients.

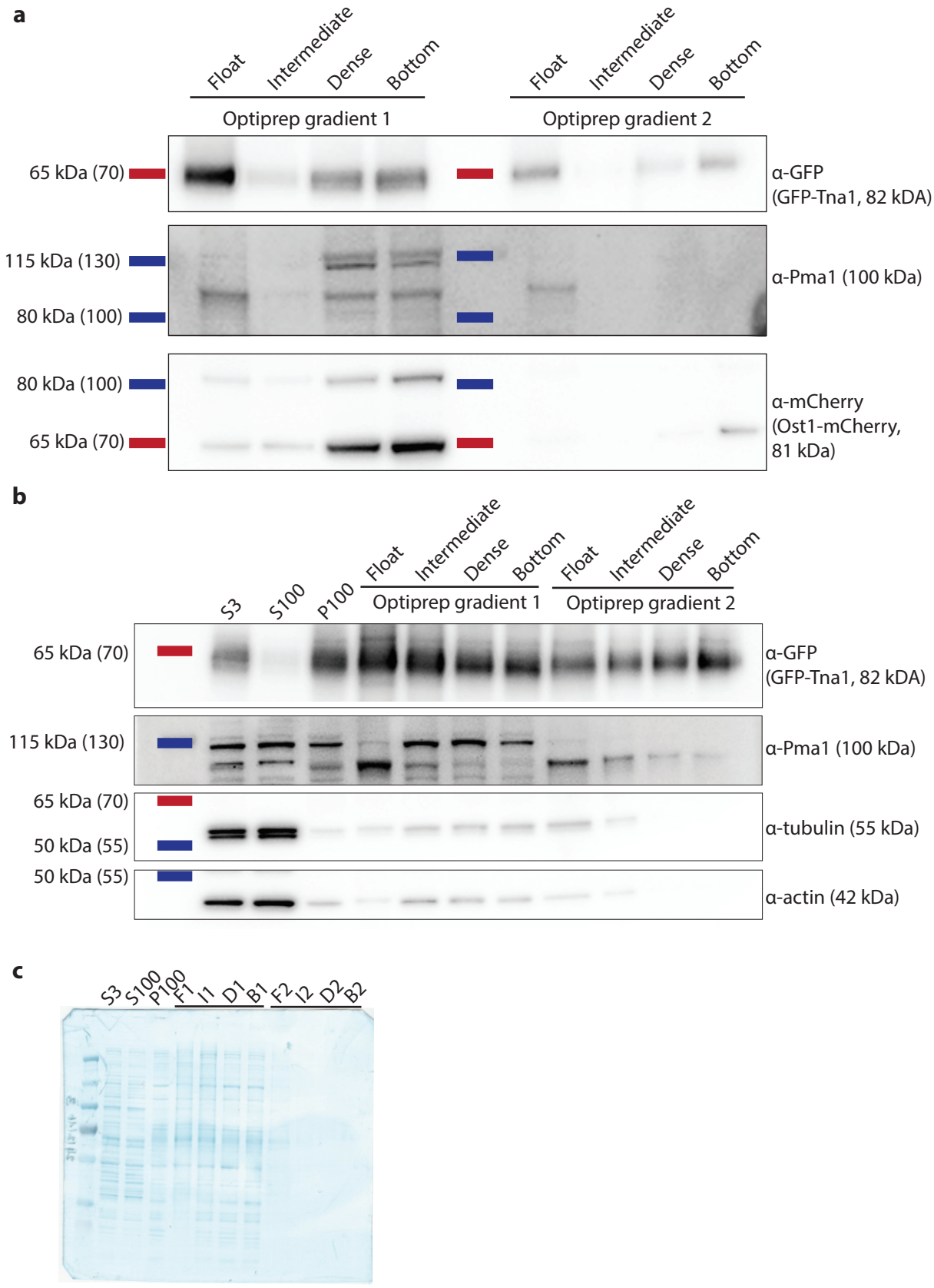

Figure 4: Controlling the fractionation protocol.

(a) Western blot analysis showing the localisation of GFP-Tna1 and Pma1 to the floating (DRM) fraction. (b) Western blot analysis controlling the fractionation process. (c) Amidoblack stained Western blot.

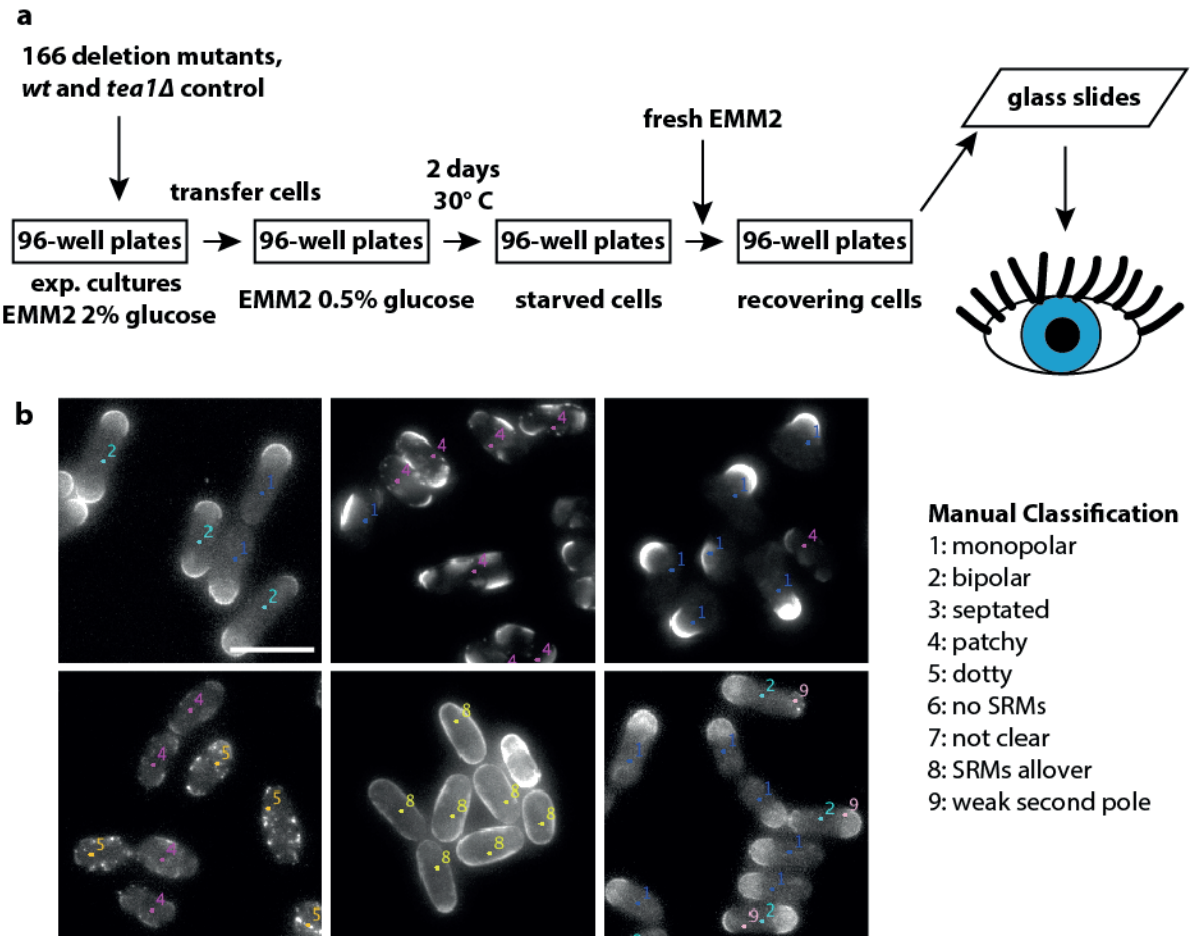

Figure 5: Workflow of *in vivo* screen.

(a) Workflow of *in vivo* screen. (b) Examples of filipin-stained cells of different categories (90 min in SE, 30° C). Scale bar: 10 µm.

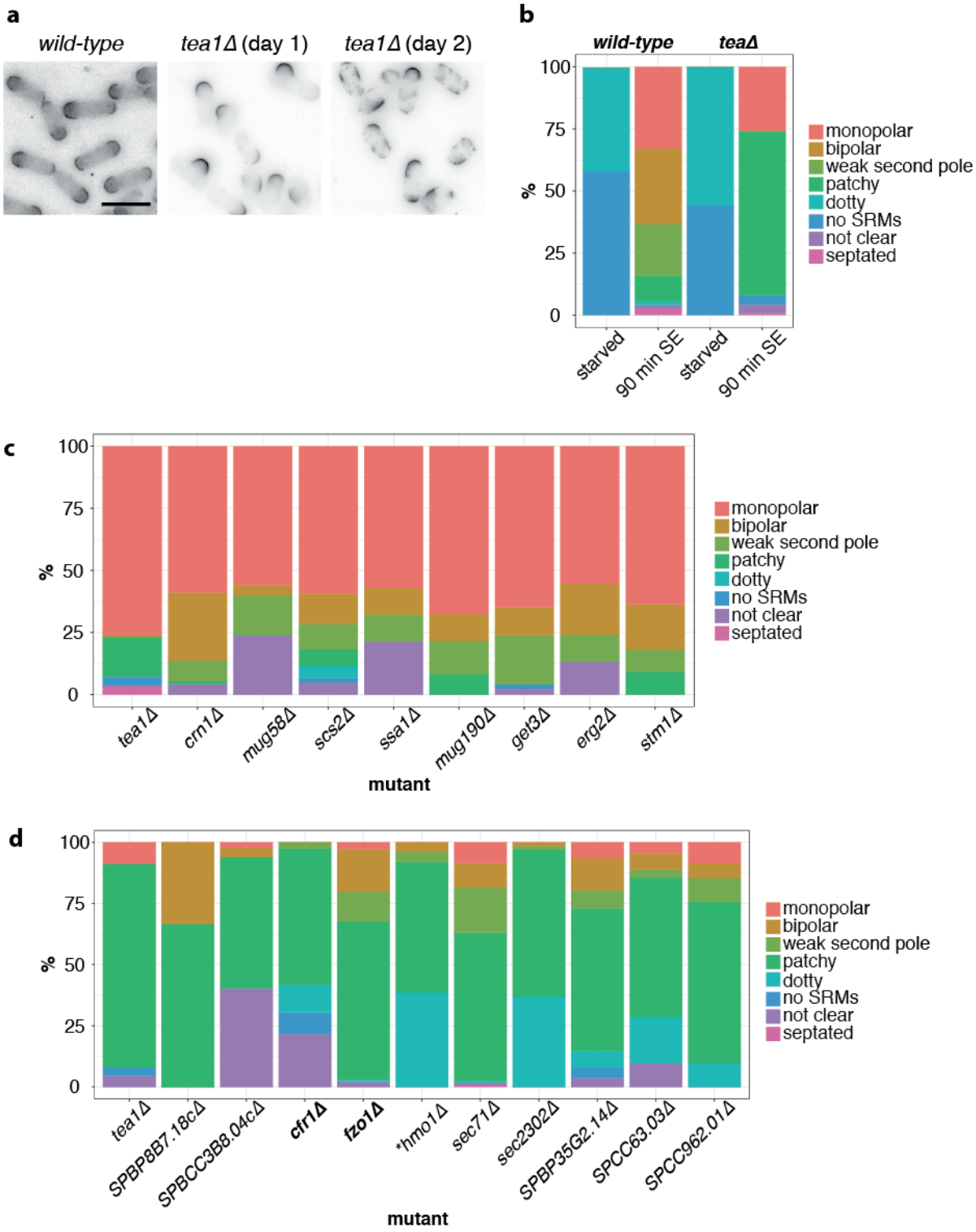

Figure 6: Characterisation of candidates from *in vivo* screen 1.

(a) Filipin stained cells (90 min SE, 30° C). (b)-(d) Summary of observed categories (Figure 5b) in deletion mutants. (b) Comparing wild-type and *tea1Δ* cells, average of both experimental days. (c) Deletion mutants similar to *tea1Δ* (monopolar), day 1. (d) Deletion mutants similar to *tea1Δ* (delayed), day 2.

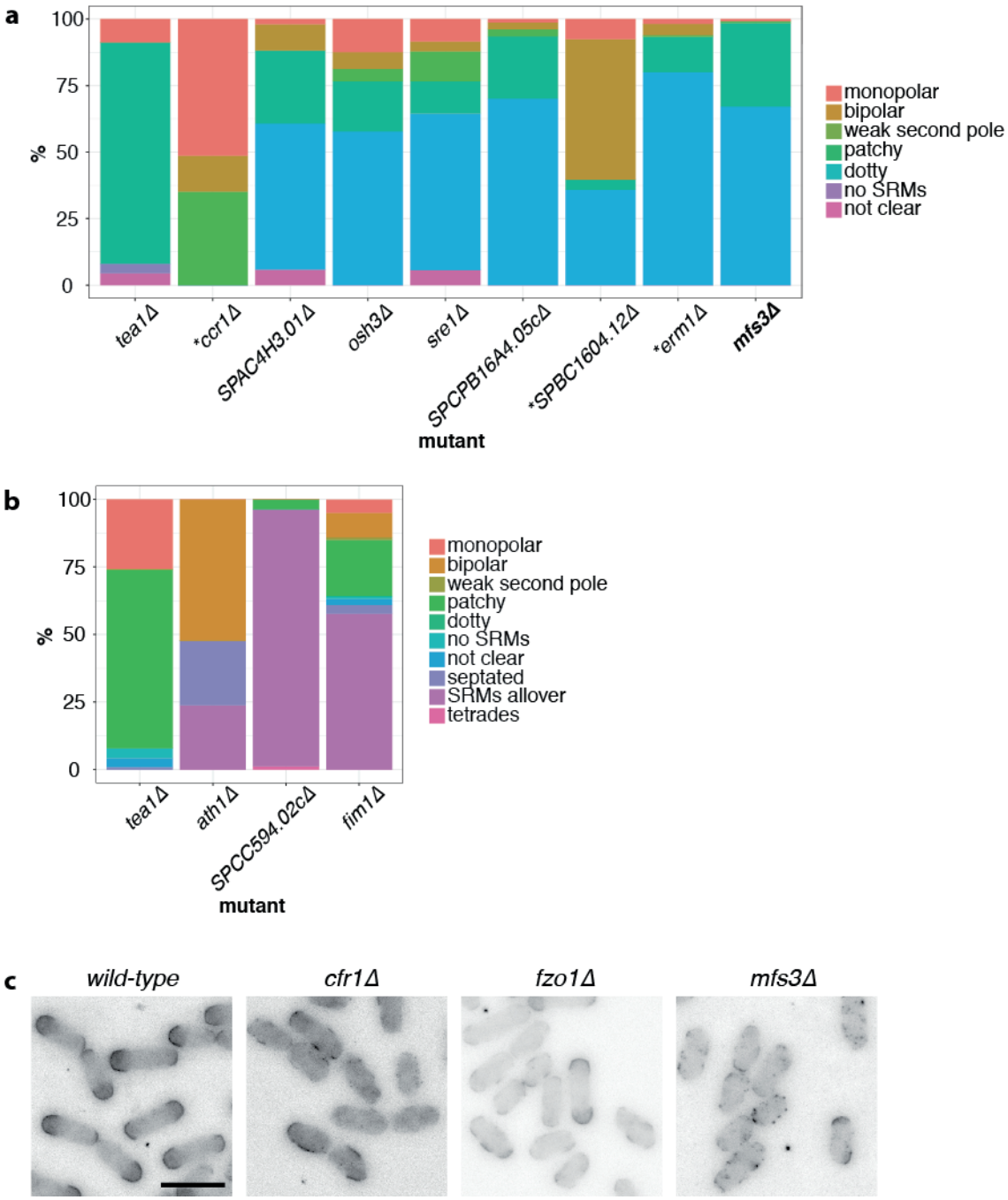

Figure 7: Characterisation of candidates from in vivo screen 1 (continued).

(a) Deletion mutants showing a dotty filipin staining pattern. (b) Deletion mutants with filipin staining all over the plasma membrane. (c) Examples of deletion mutants with polarisation defect in the experiment, stained with filipin.

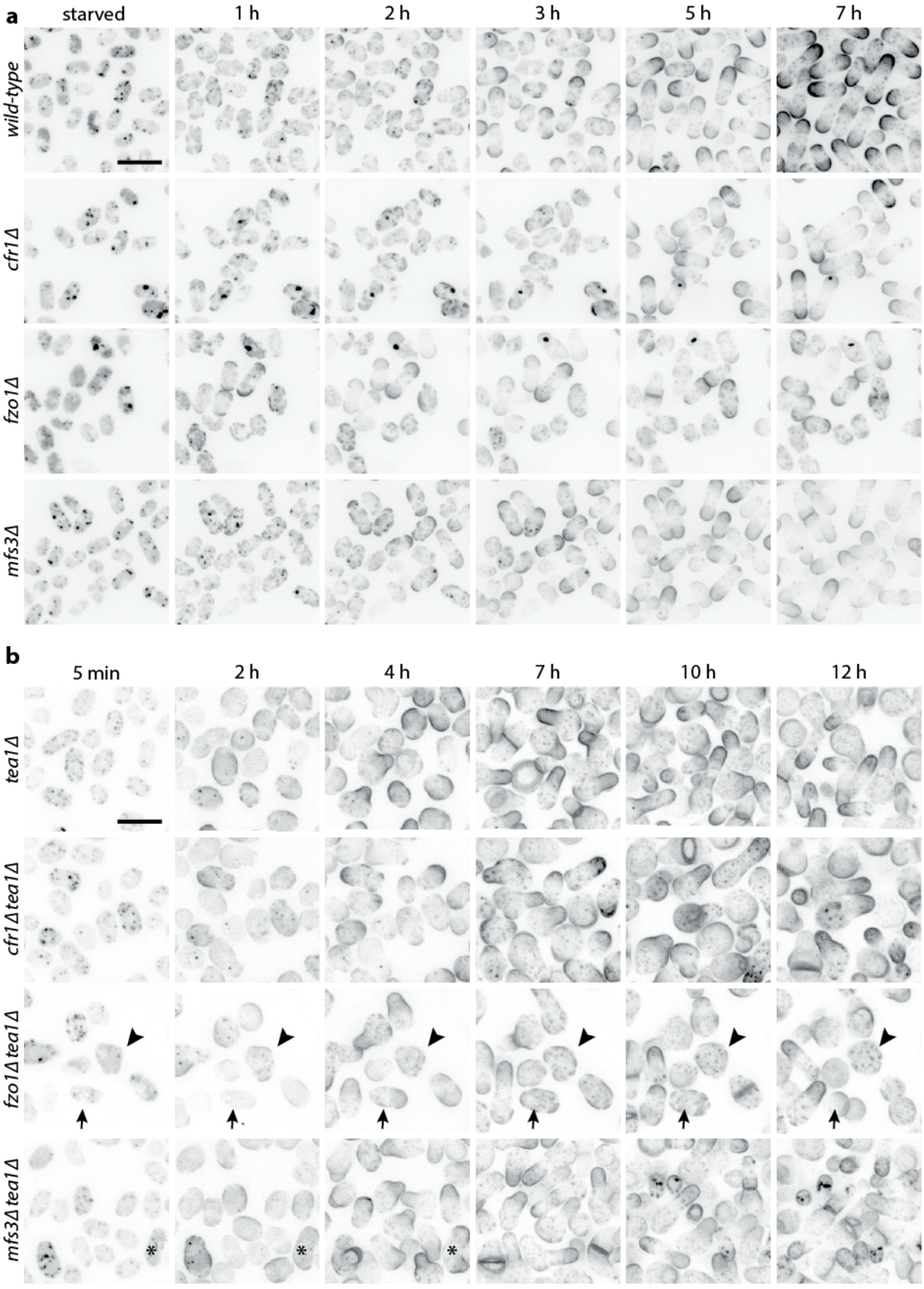

Figure 8: Starvation exit of candidate mutants.

(a) GFP-Tna1 expressing wild-type, *cfr1Δ*, *fzo1Δ* and *mfs3Δ* cells, cultured and starved for 2 days at 30° C, during SE. (b) GFP-Tna1 expressing *tea1Δ*, *tea1Δ cfr1Δ, tea1Δ fzo1Δ* and

tea1Δ mfs3Δ cells, cultured and starved for 2 days at 30° C, during SE. Arrow: example cell not polarising, arrowhead: example cell dividing without polarising. Scale bar: 10 µm.

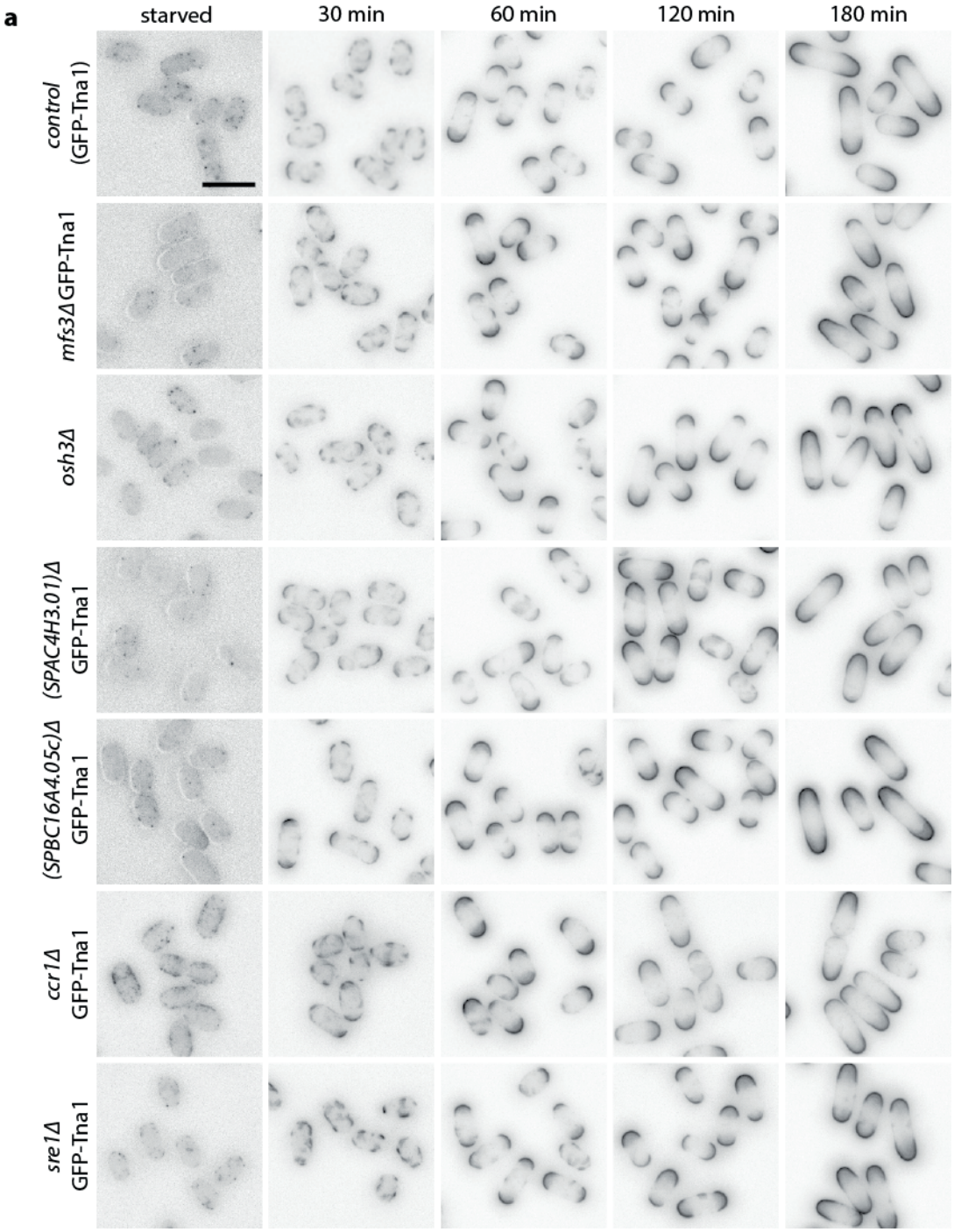

Figure 9: Starvation exit of candidate mutants initially characterised as "dotty".

(a) Filipin-stained GFP-Tna1 (wild-type control), *mfs3Δ* GFP-Tna1, *osh3Δ*, *(SPAC4H3.01)Δ* GFP-Tna1, *(SPBC16A4.05c)Δ* GFP-Tna1, *ccr1Δ* GFP-Tna1 and *sre1Δ* GFP-Tna1 cells during SE, cultured at 25° C and starved for 3 days.

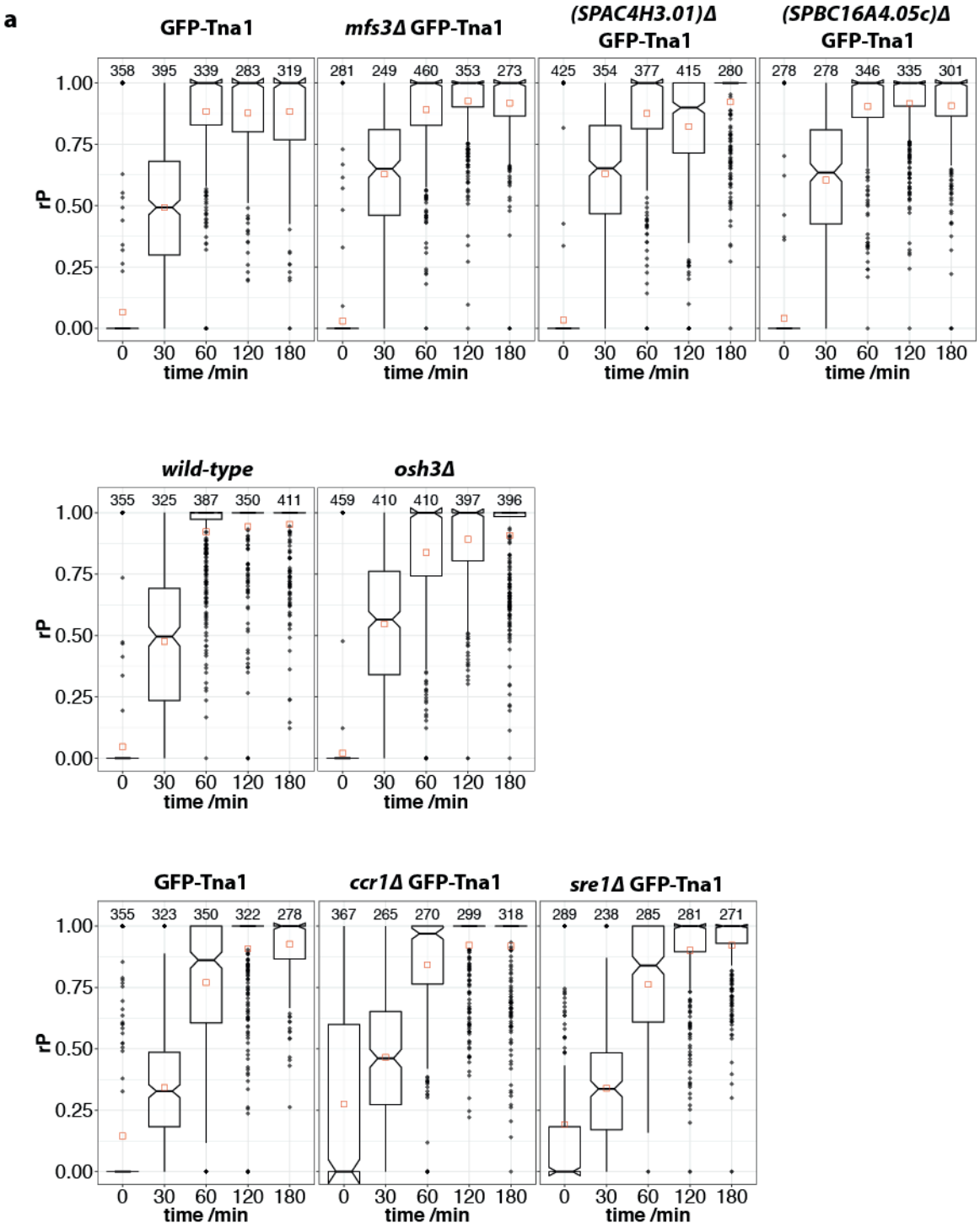

Figure 10: Quantification of starvation exit of re-tested "dotty" candidate mutants.

(a) Notched boxplots showing the polarisation ratio (*rP*) at different time points during SE corresponding to *mfs3Δ* GFP-Tna1, *osh3Δ*, *(SPAC4H3.01)Δ* GFP-Tna1, *(SPBC16A4.05c)Δ* GFP-Tna1, *ccr1Δ* GFP-Tna1 and *sre1Δ* GFP-Tna1 cells shown in Figure 10 with their according wild-type control.

2.3 Improvement of the isolation protocol

This section describes the modifications introduced to the sample preparation for mass spectrometry analysis, aiming to optimise the detection of differences in DRM protein content of different fission yeast strains. The resulting mass spectrometry data will be discussed in the context of the first trial. Also, the selection of new candidate proteins for *in vivo* studies will be described.

2.3.1 Improved sample preparation

To improve the sample preparation such that so far unidentified differences could be detected, I aimed at optimising all critical steps of the protocol. First, I investigated the possible cause of the problems in the previous trial and how this could be circumvented or how the process could be improved. The resulting, final sample preparation is shown as a schematic in Figure 11.

From the initial MS experiments, it appeared that with the previous method, transmembrane proteins were hard to be detected with MS. Although this can generally be expected, I aimed at having them as accessible for MS as possible to reduce the risk of missing any factor in the analysis because of poor solubility after TCA precipitation. The surfactant RapiGest was chosen to resuspend the proteins after DRM isolation and protein precipitation to improve the solubility of transmembrane proteins. It enabled the resuspension of the precipitated proteins and had the advantage of being tolerated during tryptic digest and even facilitating protein cleavage.

To minimize the complexity of the experiment and to increase the chance to find differences, only two strains were analysed and compared: wild-type and *tea1Δ* mutant cells. The other mutants were no longer considered in the study. The cellular material was collected freshly from three exponentially growing cell cultures each from both yeast strains. The cell pellets were shock frozen and the deep-frozen pellets were ground in liquid nitrogen, the way it was described before. It was expected that the acquired routine for these steps allowed to obtaining more comparable samples due to a consistent treatment of the cultures.

The next part, the DRM isolation itself, had already worked reliably and reproducibly before and was not modified any further. In total, four DRM samples were prepared for each strain from the three individual cell cultures. This meant that one biological sample of each condition was used in duplicate. The eight DRM isolations had to be carried out on two different days because the ultracentrifuge only fits four samples. On both days, two wild-type and two mutant samples were prepared together. As before, the sample preparation process was followed with Western blots to control the success of the fractionation and to compare the different samples used for the experiment.

To minimize the variability, the next part was conducted simultaneously for all eight samples on the same day. The following step, transferring the proteins from the floating DRM fraction of the ultracentrifugation gradient to the mass spectrometry analysis, was expected to be one of the most difficult. The challenge was to transfer all proteins isolated in the DRM fractions into a detectable form (peptides) with minimal material loss during the experimental steps on the way. Like before, the proteins were precipitated with TCA and washed with ethanol to remove remaining Optiprep and Triton X-100 to avoid their interference with the MS analysis and the present protease inhibitors.

The ability to subsequently resuspend the proteins for tryptic digest was expected to be crucial for the identification in the MS analysis. Preliminary tests showed that concentrations of 1% RapiGest allowed the complete digestion of DRMs. The precipitated floating fractions were dissolved in RapiGest and digested with Trypsin. To control this step and to purify the resulting peptides before MS analysis, the tryptic digest was done in my hands instead of sending the dry TCA precipitated samples directly to the FGCZ. Finally, the samples were purified on Waters OASIS columns to remove any disturbing residuals from the cleaved peptides and dried as much as possible. The final peptide samples were analysed within the same MS experiment by the FGCZ.

2.4 Results: mass spectrometry screen 2 – Optimised method allows identifying functional links to Tea1

2.4.1 Summary of the second mass spectrometry screen

1093 proteins in 1069 clusters with 4 decoys have been identified in the mass spectrometry analysis of the eight samples prepared from wild-type and *tea1Δ* mutant cells based on a Mascot database search of the results (SwissProt, *S. pombe*). Two exclusive unique spectra were chosen as the minimum number of spectra required for the identification of a protein and also used as a rule for the candidate selection later. From all identified proteins, 875 (854 clusters) were detected in at least three out of the eight samples.

In general, the different samples were similar in composition. 60 proteins had a quantitative variance between the samples ≤ 10%, 164 proteins ≤ 15% and 262 proteins ≤ 20%. As intended with the improved isolation method, the variability between individual samples was low. The exclusive unique spectrum counts were very similar for the first hits. At the same time, the improved, stringent sample preparation and analysis allowed the detection of differences between wild-type and the *tea1Δ* mutant. The Venn diagram in Figure 12a illustrates the differential presence of proteins in the two strains (≥ 2 peptides). It illustrates that variations in the protein profile between the samples were detectable. To have a strict filtering for subsequent experiments, proteins were only considered when two peptides were detected in at least three samples. With these limitations, four proteins were identified that were only detected in *tea1Δ* mutant cells, while another 15 were only identified in the wild-type samples (Figure 12b, Table 2).

wild-type	SPBC2G2.13c SPAC11D3.18c Arm1 Ptr1 Clc1 Cip2 SPAC15E1.04 Pla1 Pre6 Mug64 SPBC17G9.06c Met8 Crm1 SPCC11E10.01
tea1Δ	Yak3 SPAC1805.16c SPCC1840.05c Pro1

Table 2: Proteins detected in one strain only

As in the first screen, GFP-Tna1 was detected in all samples, while Tea1 and the other classical polarity factors Tea3, Tea4, For3 and Mod5 were not detected in the mass spectrometry analysis at all. This is probably due to the fact that none of them is a transmembrane protein and their localisation to the membrane is very dynamic. Their membrane-association is probably too weak for the proteins to stay there during the DRM isolation. It might also be that their localisation is even further below the membrane (except the prenylated Mod5). Another possibility is that the concentration of these proteins was below the threshold for detection. Importantly, none of the proteins differentially detected in the two yeast strains were selected as candidates in the first screen. This shows the strength of the modified method to actually discover new factors in an unbiased way. However, all the proteins detected to be differentially present in DRMs were in the low abundance range and detected with only 2-4 peptide counts.

2.4.2 Selection of candidate genes/proteins for *in vivo* analysis

The mass spectrometry data were the main criteria for the selection of candidates to avoid any bias and to include novel factors in the next phase of the study. The potential candidates were chosen based on their presence in the MS data in one of the two strains. Again, a strict rule was applied stating that at least 2 peptides of a protein had to be found in a sample to be included in the analysis. A ranking was made, based on the number of times a protein was detected in wild-type vs. *tea1Δ* mutant cells. If a protein was present in all replicas from one and absent from all replicas from the other strain, it was placed on top of the list. Also, proteins found in three samples from one strain only were listed. Factors detected in all replica from one condition, but also in one from the other, were additionally considered. For the final selection for in vivo experiments, the (predicted) biological role was also examined.

Table 3 lists the top 13 candidate proteins/genes selected for further analysis. It shows in how many samples they were identified based on the Mascot search against the SwissProt *S. pombe* database. When searched against SwissProt all species, the results vary slightly. Some hits were missing compared to the *S. pombe* search or additional hits showed up, as shown in brackets. The results from the search against SwissProt *S. pombe* have mainly been considered to choose the candidates listed below.

protein	**size/kDa**	**detected in sample**
SPAC11D3.18c	55	4/4 wild-type; 0(-2)/4 *tea1Δ*
Hal3 (SPAC15E1.04) *	70	4/4 wild-type; 0/4 *tea1Δ*
Crm1 (SPAC1805.17), essential	124	4/4 wild-type; 0/4 *tea1Δ*
Cip2 (SPAC12G12.03)	62	4/4 wild-type; 0/4 *tea1Δ*
Dcd1 (SPBC2G2.13) *	36	3/4 wild-type; 0/4 *tea1Δ*
Rnc1 (SPCC757.09c)	43	1(-3)/4 wild-type, 4/4 *tea1Δ*
Yak3 (SPAC1F7.12 or SPAC21E11.01)	38	0(-2)/4 wild-type, (1-)3/4 *tea1Δ*
Asp1 (SPCC1692.06c)	106	(2-)3/4 wild-type, (0-)1/4 *tea1Δ*
SPBC18E5.01 or SPBC29A3.19	38	1/4 wild-type, 4/4 *tea1Δ*

Pre6 (SPBC106.16) * °	28	(2-)3/4 wild-type, 0/4 *tea1Δ*
Pro1 (SPAC821.11) °	49	0(-1)/4 wild-type, 3/4 *tea1Δ*
Vps74 (SPAC5D6.13)	38	4/4 wild-type, 1/4 *tea1Δ*
Lub1 (SPBC887.04c)	79	4/4 wild-type, 1/4 *tea1Δ*

Table 3: Candidate selection for *in vivo* screen 2 (TOP13)

Summary in which and how many samples the proteins were identified. Indicated by number in brackets, if the identification varied between the two databases (SwissProt all species in brackets).

2.4.3 Characterisation of deletion mutants of non-essential candidate genes

To study the biological role of the identified proteins, the deletion mutants were taken from the fission yeast deletion library and used for *in vivo* experiments. Unfortunately, not all deletion strains could be confirmed by PCR with the verification primers listed by the authors who created the fission yeast deletion library (Kim et al. 2010, http://pombe.kaist.ac.kr/nbtsupp/). They are marked with a star (*) in Table 3. It was decided that the missing deletion strains were not constructed at this point of the study and thus were excluded from the *in vivo* experiments. All confirmed strains were crossed to the standard laboratory wild-type strain to remove the auxotrophic markers and to clean up the genetic background. Only prototrophic strains were used for all further experiments shown in this thesis.

The fission yeast cells were starved for 3 days at 25° C, recovered by the addition of fresh medium and imaged during starvation exit. Filipin was used to stain SRMs and to follow the process of cell polarisation and the cell walls were stained with Rhodamine-Lectin to segment the imaged cells for quantification of the polarisation process. Details can be found in the Materials and Methods section and in chapter 4 (Kijowski et al., in preparation). The calculated polarisation ratio *rP* simply reflects the ratio of filipin signal at the cell tips relative to the sum of all filipin signal around the cell and gives values between 0 for an unpolarised and 1 for a perfectly polarised cell (for details compare section 1.6).

In the following section, the visual imaging results and the quantifications are shown in the figures for comparison.

Figure 13 shows the polarisation process of *asp1Δ, rnc1*Δ and *lub1Δ* mutant cells compared to wild-type cells. These three candidate mutants were found to differ from the wild-type behaviour during SE. As can be seen in the figure, wild-type cells showed the typical randomly distributed SRM domains stained with filipin after 30 min (P1) and were mainly polar after 60 min of SE (P2). After 120 min, the cells had already grown visibly (P3) and continued to grow until the first cells divided after approx. 300 min.

Some *asp1Δ* cells still showed filipin stainable dots in starvation in this experiment. Within 30 min in SE, SRM domains formed in all mutants (P1), while only a few *asp1Δ* and *rnc1Δ* cells had polar SRM caps after 120 minutes (P2 is delayed). The majority of cells still had lateral domains. In the *lub1Δ* mutant, none of the cells managed to polarise within 60 minutes. *Rnc1Δ* mutant cells showed a mainly polar localisation of SRMs only after 120 min, thus had a major delay in P2. The *asp1Δ* mutant was even more delayed in P2 and although from 120 min onwards, polar cells were visible, a number of unpolarised, patchy cells was still present. At the end of the experiment, cells became mainly polar, with some domains remaining at the side.

Lub1Δ mutant cells showed a strikingly different phenotype. The patches present after 30 min (P1) appeared to enlarge mainly at the lateral positions. After 120 min, many cells showed strong filipin staining at the cell sides, but little at the cell poles. Eventually, the first polar cells appeared after 180 min and all cells polarised within 240 min SE (strong delay in P2).

For all strains, the quantifications are presented in Figure 14. For this representation, two experimental repeats, imaging wild-type, *asp1Δ* and *rnc1Δ* together and *lub1Δ* data from a separate experiment, were used. The wild-type control of the *lub1Δ* experiment showed a typical behaviour and is not displayed here because the *lub1Δ* mutant will be studied and analysed in more detail later.

The graphical representation of the polarisation process during SE using the polarisation ratio *rP* further illustrates the polarisation modes of the mutant strains that all differ from the wild-type. While the *rP* values increase from 0 to 1 within 60 min in wild-type cells, the *rnc1Δ* mutant shows the same behaviour, but with an approx. 60 min time delay. The *asp1Δ* mutant shows an increasing *rP* value over time, but the population does not reach an *rP* of 1. In contrast, *lub1Δ* mutant cells have a rather high *rP* value at the initial phase of SE. The *rP* value is gradually decreasing even until 120 min of SE. This nicely reflects

the observed cellular behaviour seen in Figure 13, showing the large lateral filipin stainable regions. The transition to polar cells happening between 120 and 240 min is clearly represented in the quantification.

In agreement with the polarisation pattern, wild-type cells grew in length until 300 min, then the cell length dropped due to the appearance of dividing cells (Figure 14b). *Rnc1Δ* mutant cells showed the same behaviour, but at a shorter length compared to wild-type cells. In contrast, *asp1Δ* mutant cells were longer than the wild-type control in the starved condition and showed growth mostly as an increase in width (Figure 14c) rather than in length, while wild-type and *rnc1Δ* mutant cells kept the cell width constant.

The 1/3 inositol polyphosphate kinase Asp1 is part of the conserved Vip1 1/3 inositol polyphosphate kinase family. In fission yeast, it was found as a regulator of the Arp2/3 actin nucleator and as suppressor of the thiabendazole sensitivity of a *mal3* mutant and was later described to be essential for invasive growth (Feoktistova et al. 1999; Pöhlmann and Fleig 2010). Pöhlmann and Fleig showed that Asp1 regulates the switch to pseudohyphal growth from the single cell depending on the cyclic AMP protein kinase A pathway (cAMP PKA). During this growth mode, cells grow mainly monopolar. It was demonstrated that Asp1 has two domains with self-regulatory capacities: the C-terminal phosphatase domain negatively regulates the N-terminal kinase domain (Pöhlmann and Fleig 2010; Pöhlmann et al. 2014). *Asp1Δ* mutant cells lack a proper microtubule organization in interphase due to lower inositol pyrophosphate levels and independent of Mal3 (Pöhlmann et al. 2014).

The increased number of catastrophe events at lateral positions might be a possible reason why *asp1Δ* mutant cells are wider than wild-type cells in the SE experiment described above and explain why lateral SRM domains persisted throughout the recovery. However, the T-shaped cells described by Pöhlmann et al. upon shifting cells from stationary phase to fresh YE5S medium were not observed in the SE experiments. More recently, the Asp1-inositol pyrophosphate system was found to be important for proper chromosome segregation in fission yeast (Topolski, Jakopec, and Fleig 2016).

Rnc1 is a K homology domain containing RNA binding protein that suppresses the effects of a calcineurin deletion. It binds and stabilises the MAPK phosphatase Pmp1 mRNA which represses the activity of the MAPK Pmk1. The binding to its target mRNA is necessary for the essential export from the nucleus depending on the nuclear pore complex component Rae1. The transport from the nucleus to the cytoplasm is independent from the exportin Crm1, the essential candidate analysed in the following section (Satoh et al. 2017; Satoh, Hagihara, and Sugiura 2018).

The WD40 protein Lub1 was identified as a protein involved in the response to several types of stress in fission yeast. It was found to serve in the ubiquitin homeostasis pathway. It is important for proteasomal degradation and it interacts with Cdc48 (Ogiso et al. 2004). This essential factor binds ubiquitinylated proteins and is involved in the release of the sterol-regulatory element binding proteins (SREBPs) that regulate cellular cholesterol levels and general gene expression under hypoxic conditions (Hughes, Todd, and Espenshade 2005; Hughes, Nwosu, and Espenshade 2009; Stewart et al. 2011; Hwang et al. 2016).

2.4.4 The essential candidate Crm1 appears to stabilise the second pole

Among the 13 selected candidates for *in vivo* studies, one was an essential protein. It was thus not possible to analyse a deletion mutant to study its function. Therefore, the cold-sensitive mutant *crm1-809* was used to test the function of the exportin protein Crm1 during SE. The cells were starved at the permissive temperature of 30° C for two days and recovered from starvation at the restrictive temperature of 18° C.

The filipin stained cells are displayed in Figure 15a. The starved wild-type and *crm1-809* cells showed minor staining with filipin during starvation at the permissive temperature. Interestingly, after one hour of pre-incubation at the restrictive temperature, the staining appeared stronger and the stained regions slightly larger. The sequence of events during the polarisation process upon addition of fresh medium was the same as under the standard experimental conditions. However, due to the lower temperature, all phases occurred with a time delay as expected. Both wild-type and mutant strains formed patches within 30 min that persisted, enlarged and increased in strength until 120 min. The first polar wild-type cells appeared after 4 hours with some remaining SRM domains at the side. Wild-type cells were clearly polar only after 6 hours. *Crm1-809* mutant cells still had lateral SRM domains even in some cells that had polar SRM caps that were visible between 8 and 10 hours of SE. At the same time, T-shaped cells appeared. This shows that the remaining lateral SRM domains were selected as growth sides in the *crm1-809* cells. The first cell divisions happened in the wild-type strain after 13, in the *crm1-809* mutant after 16 hours.

The polarisation process was quantified based on the imaging data as described above (Figure 15b). The quantifications are based on a single experiment. Two other biological replicates qualitatively showed the same results regarding the polarisation process and the characteristic phenotype of the *crm1-809* mutant cells. However, because of technical problems with the temperature control during these experiments, they were not pooled with the experiment shown for the quantification. For the wild-type control, the polarisation ratio slowly increases until 13 hours in SE. The slight decrease in *rP* after 16 hours possibly reflects the emerging cell divisions. In contrast to experiments at higher temperatures, the polarisation ratio does not reach a value of 1 until 21 hours. It is clear from the imaging data that many polar cells still had remaining lateral SRMs at late stages of SE.

The slower polarisation process of *crm1-809* mutant cells in SE is also reflected in the *rP*. It stays below the polarisation ratio of wild-type cells at the same timepoint, with the exception of 10 hours when the median reaches a value of 1. At later points when the T-shaped cells are visible, the value stays in the range of about 0.8 and becomes 1 after 24 hours.

Crm1-809 mutant cells are longer than wild-type cells, but have slightly smaller cell width in starvation. The quantification of cell length illustrates that the growth of the mutants lags behind. While they are smaller when the wild-type reaches the maximum average length in this experiment after 16 hours, *crm1-809* reach that length after 18 hours when the average wild-type cell length is already lower due to cell divisions. For the *crm1-809* mutant, the cell width increases during the experiment in agreement with the emergence of the observed T-shaped cells. Additionally, the distribution of cell widths becomes larger from 10 hours on for the same reason.

Besides the cold-sensitive mutant *crm1-809,* I also tested *crm1-1*, a different allele that is sensitive to elevated temperatures (36° C) (Figure 17a). In agreement with the results above, the cells showed only a mild delay in SE. Many cells were not polar after 60 min in SE, while the wild-type control cells were mainly polar. The quantification also illustrates that the polarisation delay is minor (Figure 17b). However, although the polar cells are mainly monopolar, no T-shaped cells were observed in this mutant. The boxplots of *rB* in Figure 17c illustrate this observation quantitatively. However, it cannot be concluded from this experiment if the phenotype persists and one pole stays weaker, or if the cells will eventually become bipolar.

The exportin (export-karyopherin β) Crm1 recognizes leucine-rich nuclear export signals for nucleocytoplasmic transport of proteins via the nuclear pore complex (Satoh et al. 2017). In fission yeast, the localisation of 285 proteins was described to be regulated by Crm1, illustrating its potential to be involved in various cellular processes (Matsuyama et al. 2006).

Thus, it is likely that the observed phenotype was caused by the defective transport of another factor in the mutant *crm1* mutants. One described factor described to be

transported by Crm1 is Pap1. To test if the phenotype observed in the *crm1-809* mutant is due to the AP-1 like transcription factor Pap1 that is involved in oxidative stress response and multi-drug response and exported from the nucleus by Crm1 (Kawashima et al. 2012), the deletion mutant *pap1Δ* was analysed in a SE experiment (Figure 18a). While the majority of the wild-type cells polarised within one hour, *pap1Δ* mutant cells were delayed and polarised only within three hours. The quantifications underlined this finding, the *rP* value reached 1 within 60 min for the wild-type cells, for *crm1-809* it needed 180 min (Figure 18b).

By eye, one could speculate that *pap1Δ* cells also have a weaker second pole that the wild-type, similar to *crm1-1* mutant cells. This was tested with the quantification of the bipolarity ratio *rB* (Figure 18c). The graph shows a delay only. For the wild-type cells, *rB* values dropped after 120 min. The cells grow from one pole and have two SRM, a strong growing one and a weaker non-growing one. Later, the *rB* values increased again when the wild-type cells started to grow in a bipolar fashion. For the *pap1Δ* cells, a similar drop of *rB* appeared one hour later when these mutant cells were polarised. However, from these initial experiments it is not clear, if the *pap1Δ* actually does have a defect in stabilisation of the non-growing end. More replicates and longer recovery experiments should give more information in this regard.

I noted that none of the *pap1Δ* mutant cells started to grow in a T-shape under these conditions. To test if the T-shaped cells in the *crm1-809* mutant are only due to the low temperature, I repeated the SE experiment with the *pap1Δ* mutant at 18 °C. Yet, no T-shaped cells were observed for the *pap1Δ* mutant cells during SE at 18° C.

To further test the connection of *crm1* and *pap1* to the polarisation process and potentially *tea1*, the *crm1-1 pap1Δ* double mutant was starved at permissive and recovered at restrictive temperature (Figure 19). Strikingly, the double mutant was delayed severely in SE at the elevated temperature. Compared to wild-type cells that polarised within 60 min, it needed 180 min for polarisation. Again, the cells appeared rather monopolar to the eye. The quantification of bipolarity clearly shows here that *crm1-1 pap1Δ* double mutant cells are mainly monopolar. From 60 min on, the *rB* values were close to 0. Only a minority of cells was classified as bipolar until 45 min in SE. It is expected that during SE, a small

proportion of cells is classified as bipolar due to the random positioning of SRM patches, not because of actual polarisation.

To conclude, the essential candidate gene *crm1* appears to play a role in polarisation. Temperature sensitive mutants show similarities to a *tea1Δ* mutant phenotype. The more severe one, the cold sensitive mutant *crm1-809,* forms T-shapes during SE, the typical behaviour of *tea1Δ* mutant cells, while the *crm1-1* allele leads to mainly monopolar cells at elevated temperatures. It is a characteristic of *tea1Δ* mutant cells to grow only monopolar and fail to do NETO. However, to clarify if both phenotypes observed for the *crm1* mutants are actually linked or if they show two different functions of the protein needs further investigation.

The fact that the deletion mutant of the transcription factor Pap1, which is transported via Crm1, is delayed in SE further supports the hypothesis that there might actually be a link to the Tea1-dependent polarisation system. So far, the results presented can be regarded as an entry point into more comprehensive studies. Thus, a possibly novel part of the cell polarisation process and machinery was uncovered.

As a start into further explorations, Crm1 function could be specifically disrupted by chemical modification with the specific drug Leptomycin B (LMB) (Nobuaki Kudo et al. 1997; N. Kudo et al. 1999). It would be interesting to test if the full block of nuclear export via Crm1 leads to the observed T-shapes under normal growth conditions (25° C) as well. Li et al. 2014 showed that the essential phosphatidylinositol-4-phosphate 5-kinase (PI4P5K) Its3 accumulates in the nucleus upon LMB treatment. This phenotype was originally observed in their study by disruption of Ypt3 and Ryh1, two Rab family GTPases that are important for the localisation of Its3 to the plasma membrane. Adam Kijowski has already studied the role of *its3* during cell polarisation. Strikingly, the temperature sensitive mutant has a polarisation defect, leading to mainly monopolar cells and mildly T-shaped cells (unpublished data). Also, *ypt3* was previously identified to play a role in cell polarisation (Adam Kijowski, unpublished, our laboratory). It is possible that the observed phenotype in the *crm1* mutants was actually due to the effect on Its3 localisation. Yet, this hypothesis needs further evaluation. If and how the transcription factor Pap1 is

actually involved in the polarisation process also needs further investigation. However, the fact that *pap1Δ* single mutant cells are delayed might be a hint for a level beyond the Its3 system.

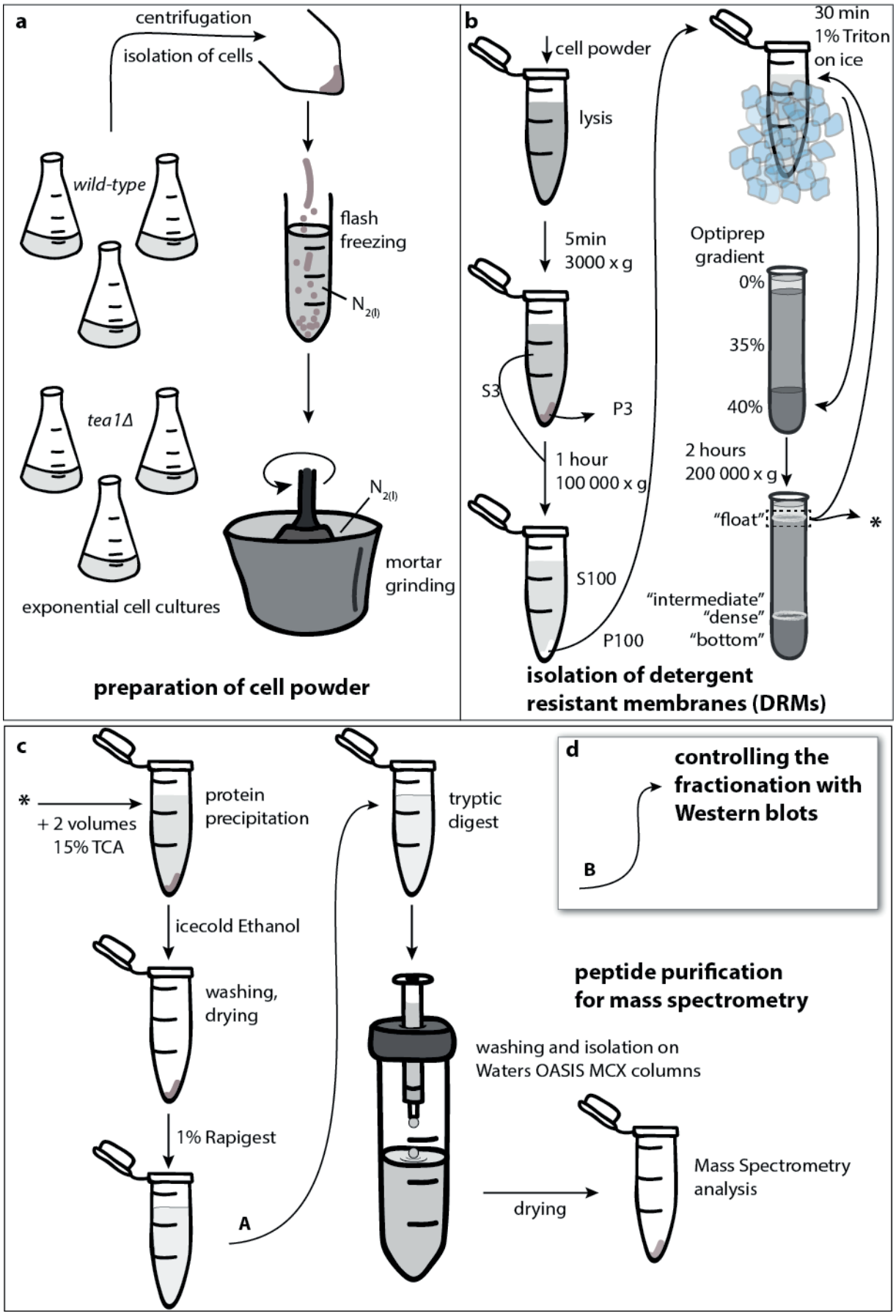

Figure 11: Detailed workflow of the final detergent-resistant membrane isolation protocol.

(a) Preparation of cell powder: flash freezing and grinding of cells in liquid nitrogen. (b) DRM isolation: Lysis of ground cells, differential centrifugation, detergent treatment and gradient centrifugation. (c) Peptide purification for mass spectrometry: Protein precipitation with 2 vol. 15% TCA, washing and drying, tryptic digest, peptide isolation and washing on OASIS MCX columns, drying before MS. (d) Western blotting to control the fractionation.

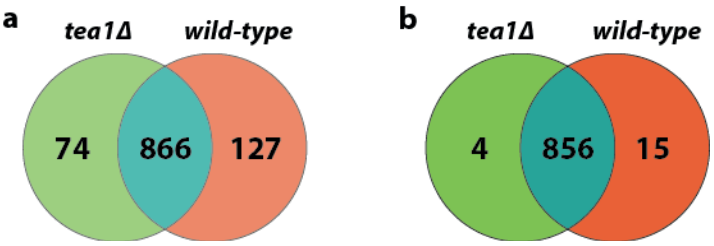

Figure 12: Venn diagrams summarising the mass spectrometry results

(a) Number of proteins identified by mass spectrometry (≥2 exclusive unique peptide counts) in *tea1Δ* (light green) compared to wild-type cells (light red). (b) Number of proteins identified by MS (≥2 exclusive unique peptide counts in ≥3 samples) in *tea1Δ* (green) compared to wild-type cells (red).

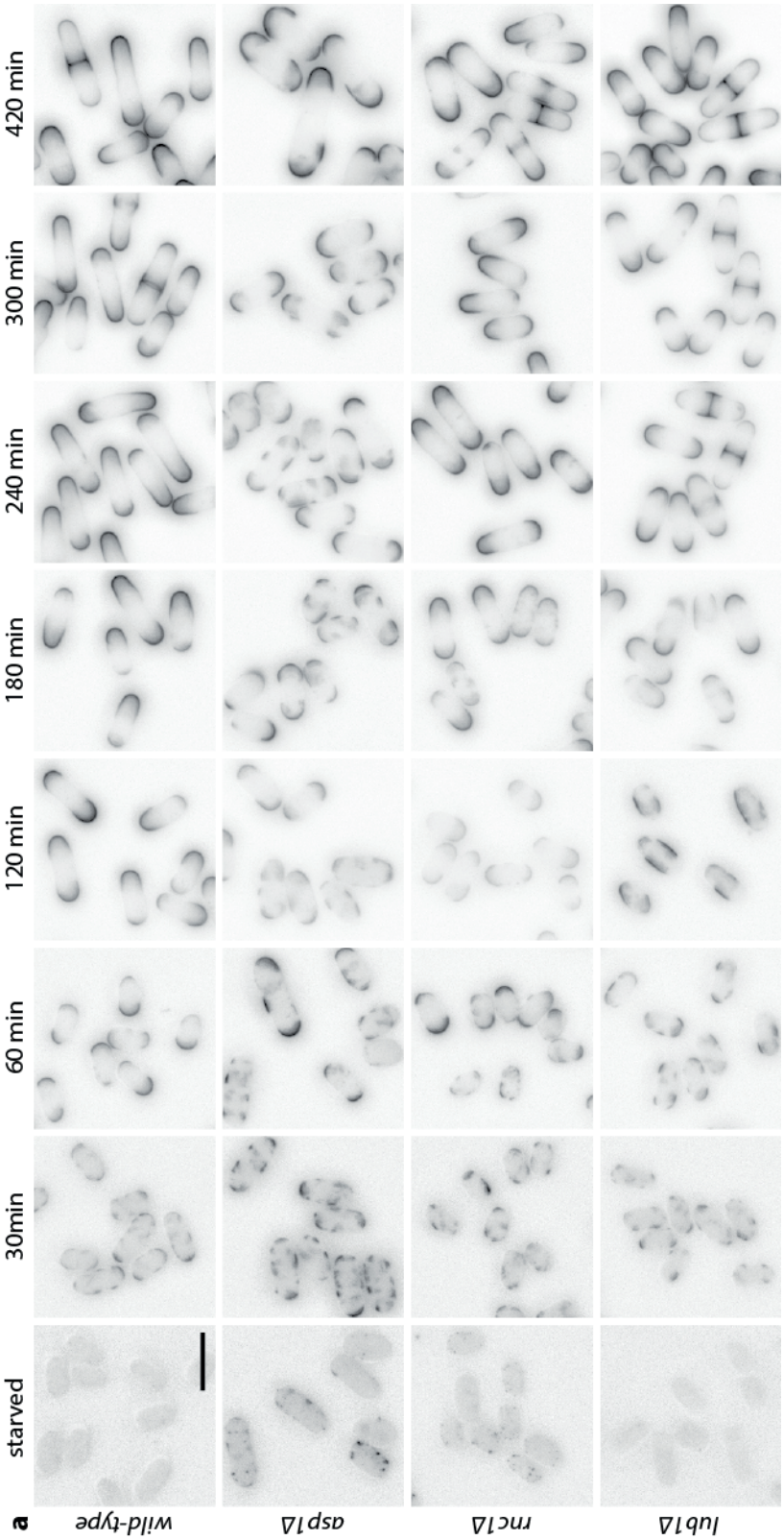

Figure 13: Starvation exit of *asp1Δ*, *rnc1Δ* and *lub1Δ*.

(a) Filipin-stained wild-type, *asp1Δ*, *rnc1Δ* and *lub1Δ* cells during SE. Scale bar: 10 µm.

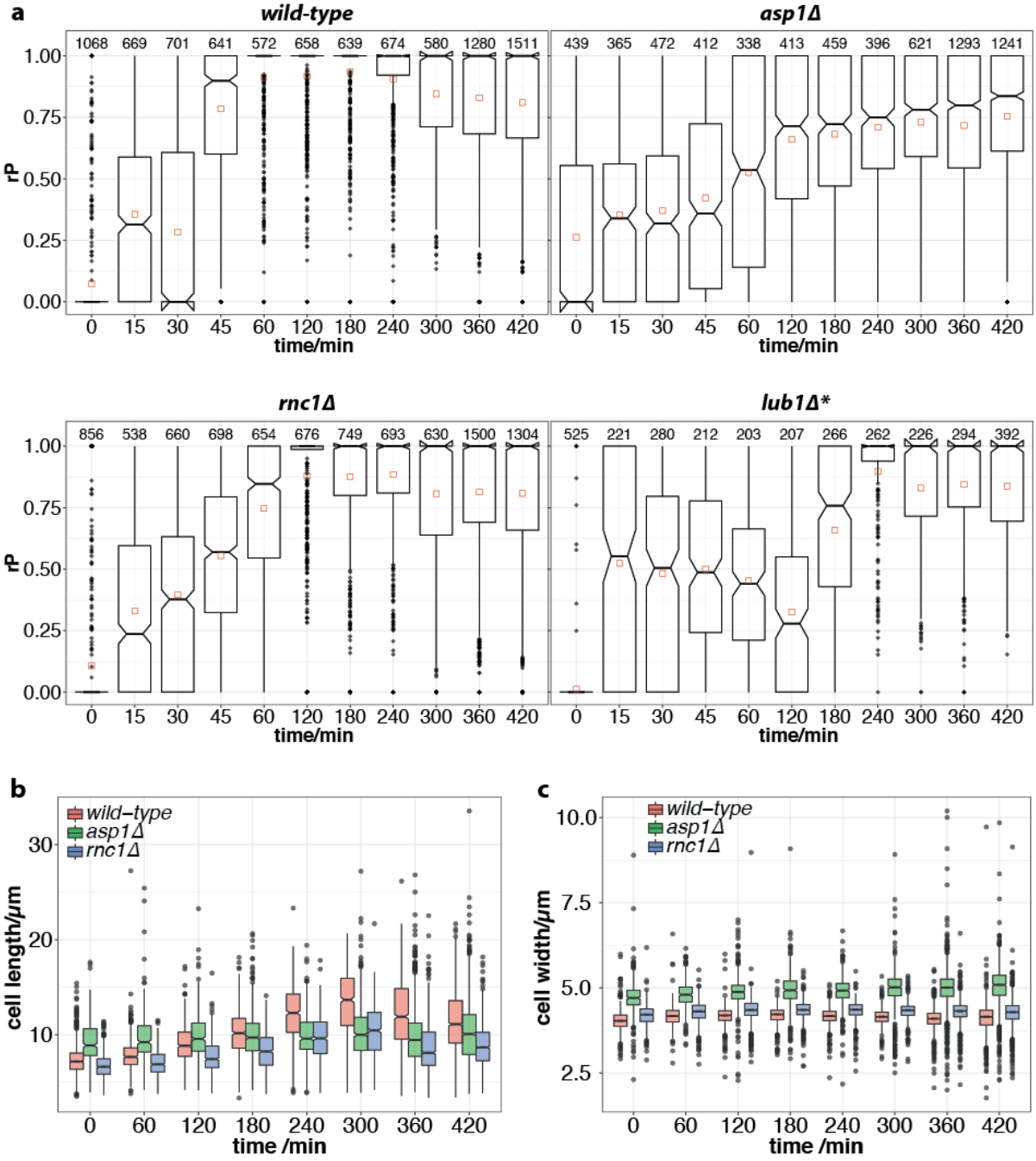

Figure 14: Quantification of starvation exit of *asp1Δ*, *rnc1* and *lub1Δ*.

(a) Notched boxplots showing *rP* during SE of wild-type, *asp1Δ*, *rnc1Δ* and *lub1Δ* cells. **Lub1Δ* cells were imaged in a separate experiment, the according wild-type control is not shown here (b)-(c) Notched boxplots summarising the cell length (b) and width (c) of wild-type, *asp1Δ* and *rnc1Δ* cells during SE.

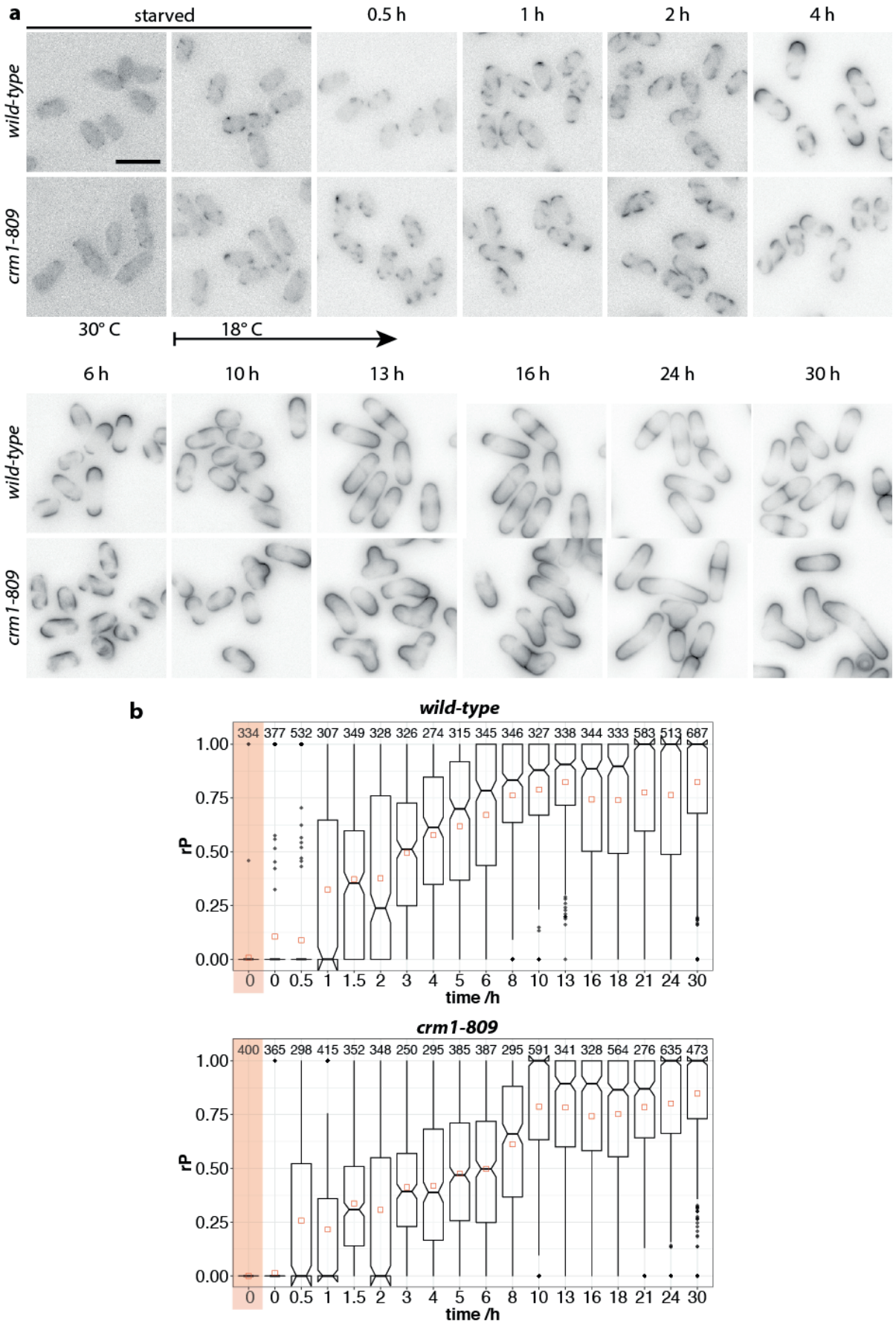

Figure 15: Starvation exit of *crm1-809* at restrictive temperature (18° C).

(a) Filipin-stained wild-type and *crm1-809* cells during SE at restrictive temperature (18 ° C). Cells were cultured at 30° C and starved for 2 days. Scale bar: 10 µm. (b) Notched boxplots showing *rP* during SE of wild-type and *crm1-809* cells, n above each boxplot.

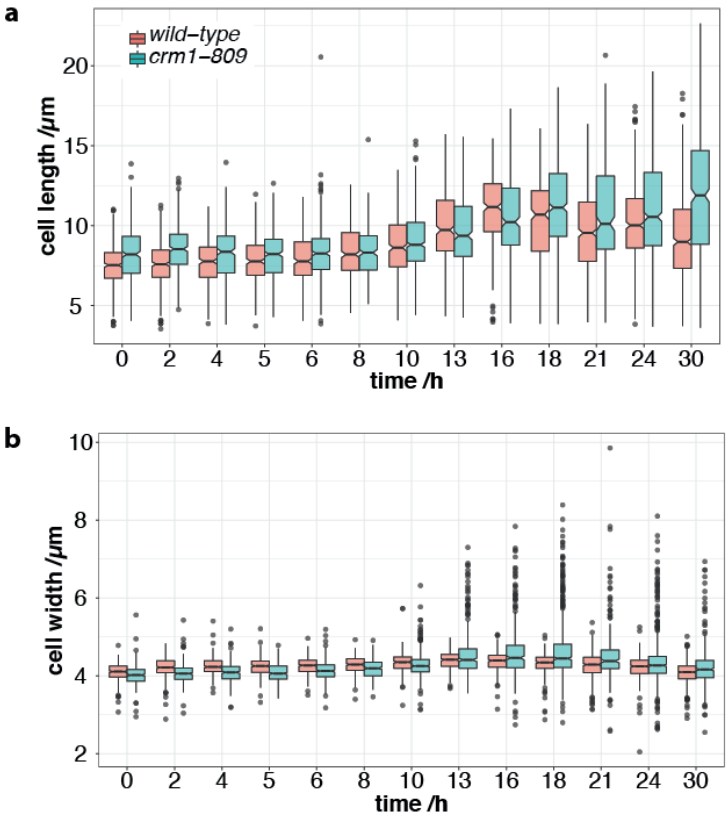

Figure 16: Cell length and width of *crm1-809* during starvation exit.

(a)-(b) Notched boxplots summarising the cell length (a) and width (b) of wild-type (red), and *crm1-809* cells during SE at restrictive temperature (18° C).

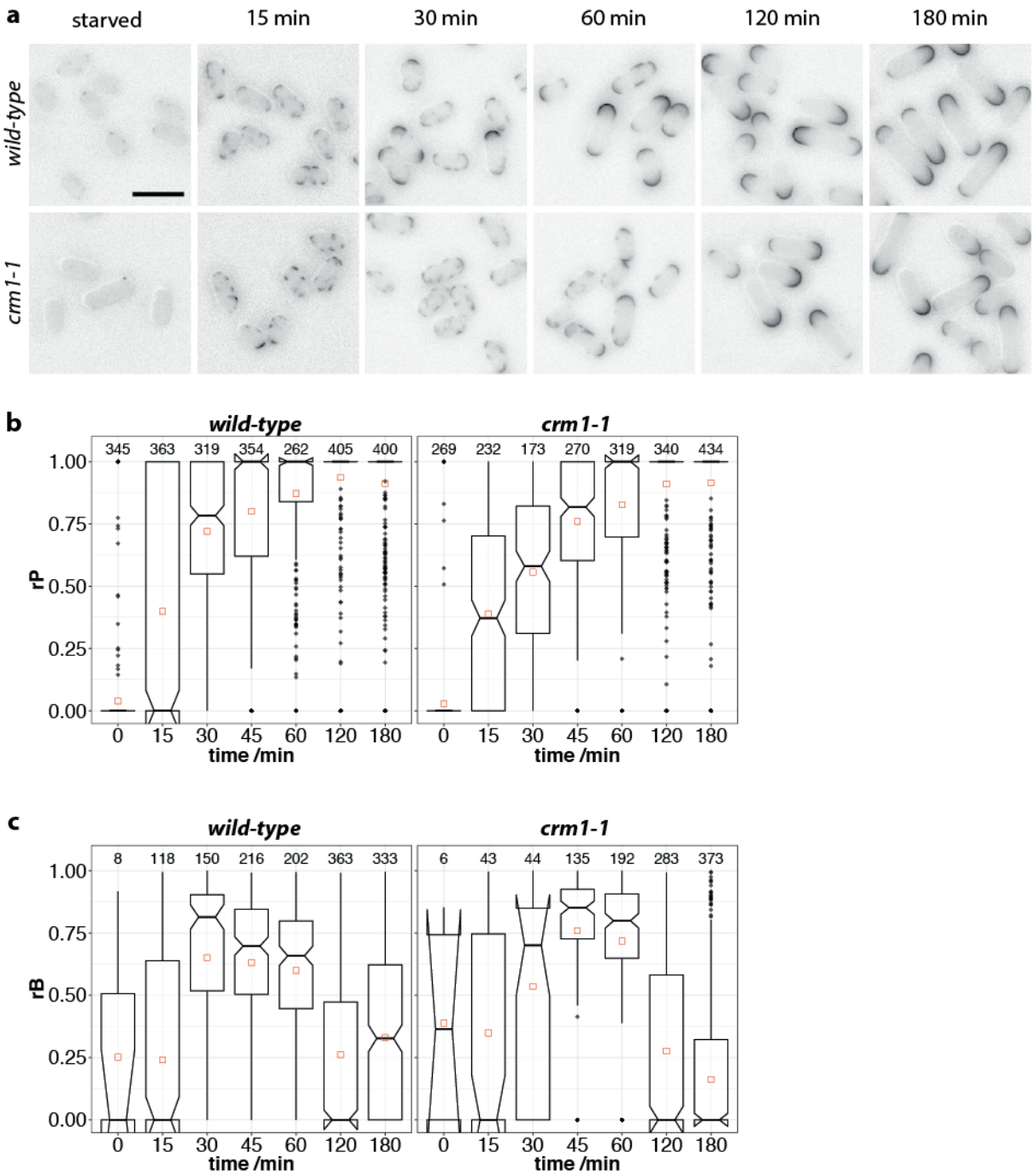

Figure 17: Starvation exit of *crm1-1* at restrictive temperature (36° C).

(a) Filipin-stained wild-type and *crm1-1* cells during SE at restrictive temperature (36 ° C). Cells were cultured at 25° C and starved for 3 days. Scale bar: 10 µm. (b)-(c) Notched boxplots showing *rP* (b) and *rB* (c) during SE of wild-type and *crm1-1* cells, n above each boxplot.

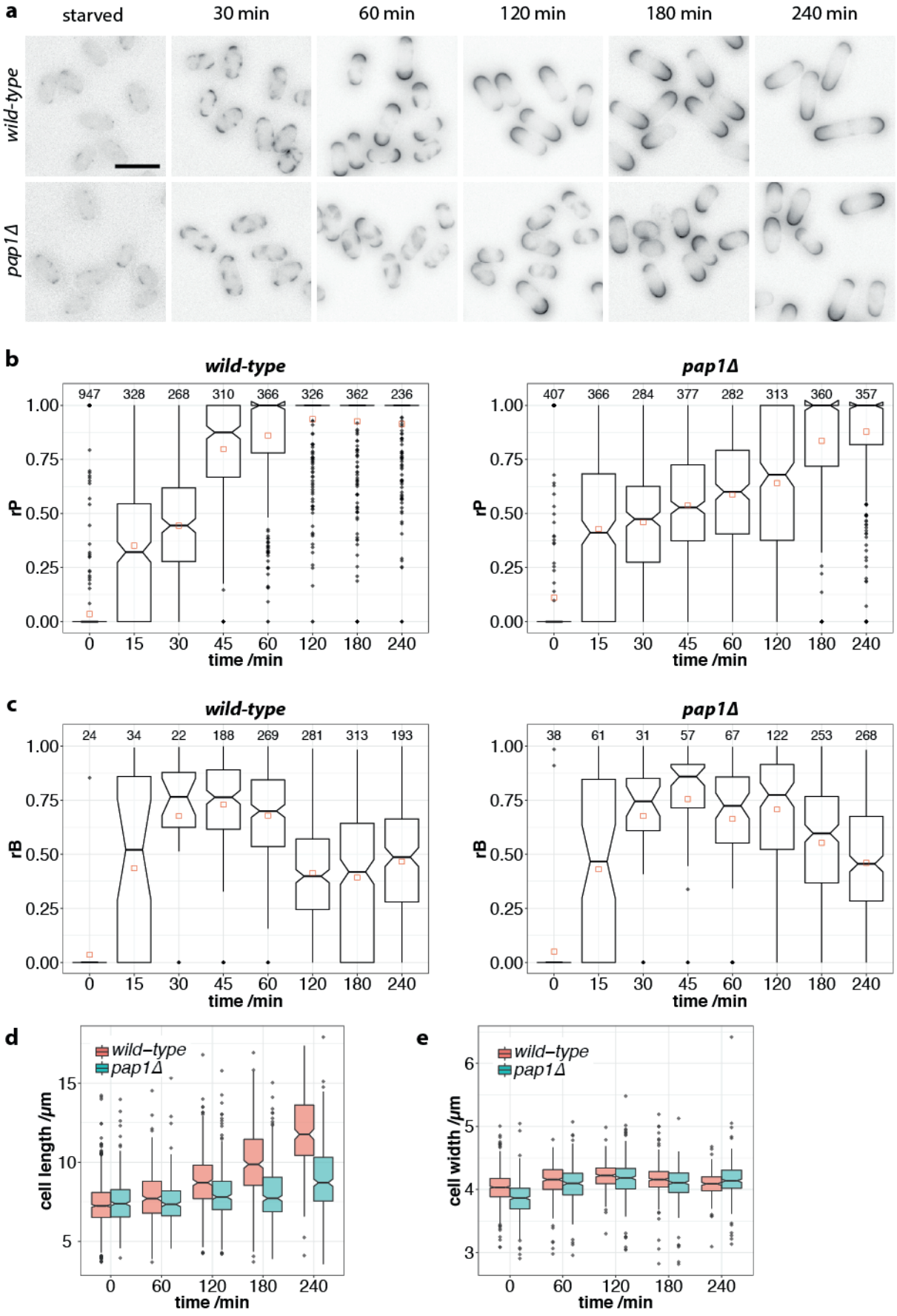

Figure 18: Starvation exit of *pap1Δ*.

(a) Filipin-stained wild-type and *pap1Δ* cells during SE at 25° C. Cells were starved for 3 days. Scale bar: 10 µm. (b)-(c) Notched boxplots showing *rP* (b) and *rB* (c) during SE of wild-type and *pap1Δ* cells, n above each boxplot. (d)-(e) Notched boxplots comparing cell length (d) and width (e) from wild-type (red) and *pap1Δ* (blue) cells during SE.

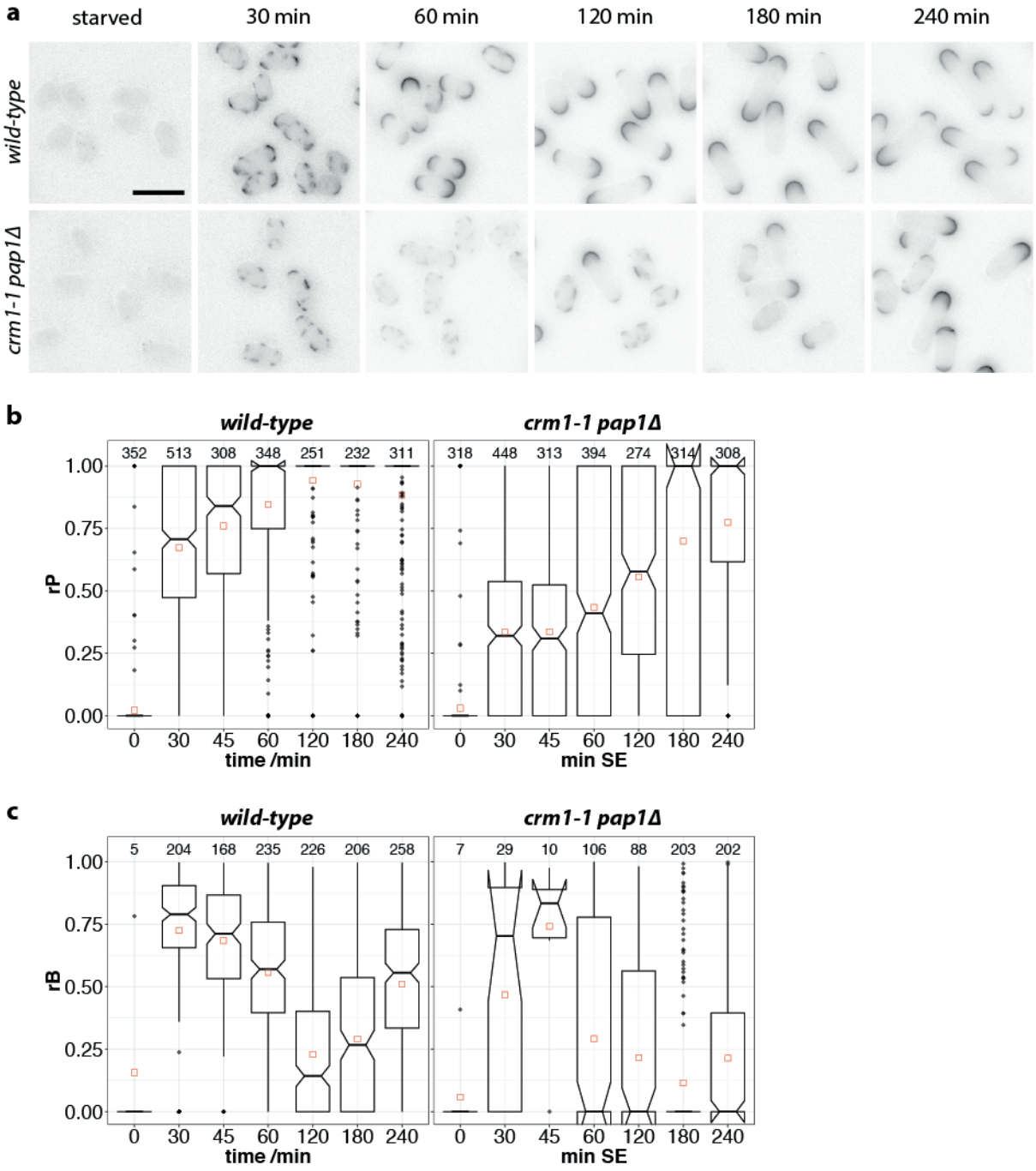

Figure 19: Starvation exit of *crm1-1 pap1Δ* at restrictive temperature (36° C).

(a) Filipin-stained wild-type and *crm1-1 pap1Δ* cells during SE at 36° C. Cells were starved for 3 days at 25° C. Scale bar: 10 µm. (b)-(c) Notched boxplots showing *rP* (b) and *rB* (c) during SE of wild-type and *pap1Δ* cells, n above each boxplot.

2.5 Characterisation of the WD40 protein Lub1 during SE

The deletion strain from the secondary *in vivo* screen that showed the most promising phenotype was *lub1Δ* (see 2.4.3, Figure 13Figure 14). During SE, the *lub1Δ* mutant had the most severe delay and showed a characteristic polarisation behaviour. The *lub1Δ* mutant cells failed to polarise during the first hour of SE. Instead, the cells polarised between the 3rd and 4th hour of SE. In the following section, this process will be analysed and described in more detail. The initial experiments to gain insight into the molecular mechanism of Lub1's involvement in polarisation will be presented and discussed.

So far, Lub1 has been described as playing a role in ubiquitin homeostasis in fission yeast, which was shown to be important during the response to stress (Ogiso et al. 2004). It contains a WD40 repeat domain at the N-terminus (Ogiso et al. 2004 and Pombase: Wood et al. 2012). WD40 repeat proteins recognise their binding partner via a conserved domain forming a circular β-propeller. They act as adaptors mediating protein-protein interaction in various cell functions (Li and Roberts 2001; Xu and Min 2011). For example, WD40 proteins are involved in the recognition of proteins for ubiquitination and subsequent degradation (C. Xu and Min 2011). Furthermore, they also play a role in signal transduction, the regulation of transcription, in vesicular trafficking and in apoptosis (D. Li and Roberts 2001).

2.5.1 The WD40 protein Lub1 plays a critical role during early polarisation (P2)

Lub1Δ mutant cells exiting starvation were imaged with increased time resolution to accurately describe the polarisation process (Figure 21). Samples were taken every 15 min during the first hour, after 2 hours and again every 15 min from 3 hours in SE on. As their appearance did not change much between 1 and 3 hours in SE in the initial experiments (compare Figure 13), only hourly samples were taken for this time period.

In the wild-type cells, the complete polarisation process happened during the first 60 min (Figure 21a). They formed the typical SRM domains in P1 that expanded at the cell tips and were removed from the sides in P2. In contrast, *lub1Δ* cells formed SRM domains in

P1 that subsequently expanded but were not removed from the cell sides. A strong delay in P2 led to the characteristic phenotype of the mutant with large, lateral SRM domains, spanning along the cell sides and often almost reaching the cell tip and leading to the impression that SRMs are being excluded from the cell tips. Already after 45 min in SE, some cells had SRM domains close to but not at the cell tips. Strikingly, from 180 min onwards, *lub1Δ* mutant cells started P2 by forming polar SRM caps and removing the lateral SRMs, and by 240 min into SE, most cells were polarised. Polar *lub1Δ* mutant cells subsequently entered P3 and started growing similar to wild-type cells.

The quantifications of the polarisation ratio values *rP* clearly illustrate the observed behaviour of the *lub1Δ* mutant (Figure 22a). In the wild-type culture, *rP* gradually increased from 0 to 1 within the first 60 min. For *lub1Δ* cells, the median *rP* values varied between 0.2-0.5 between 15-180 min in SE before the transition to 1 wa complete at 240 min. At first sight, the observed variations in the first 180 min might be confusing. However, they are at least partially due to the detection and calculation method. During the first 30 min in SE when the SRM domains are small, the *rP* values mainly depend on the relative distribution between polar to side localisations.

Strikingly, the first impression that *lub1Δ* mutant cells had more polar patches in early SE was supported by the higher *rP* value of 0.5 in the first 30 min compared to wild-type cells. After 45 min, the *rP* values dropped to 0.2, but went back up to 0.5 after 60 min. This shows that the expansion of the domains did not lead to polarisation at this timepoint, but the growing domains eventually touched the cell tip, leading to a more polar classification after 60 min. The continued expansion of the SRM domains at lateral positions were clearly visible in the low *rP* values after 120 and 180 min before the cells eventually polarised (P2) in a process similar to the wild-type cells. Although the absolute median values during the first 3 hours of SE varied between experiments, they all showed the same trend, namely that the *rP* values were unexpectedly high in early SE and low after 180 min.

Based on these observations, Lub1 appears to be essential during early SE (P2). Lub1 might be involved in the Tea1-mediated stabilisation of polar SRM domains. However, as

lub1Δ cells eventually polarise, either an alternative way to polarise takes over or the delay is due to another Lub1-mediated process slowed down in *lub1Δ* cells that is only complete after 180 min when these cells start to polarise.

Calculating the bipolarity ratio *rB* agreed with the observations described above and provided a complementary view on cell polarisation behaviour (Figure 22b). In the wild-type cells, the *rB* values increased to 0.7 until 60 min, when the majority of cells was polarised. The values then went down within the next two hours, reflecting the mainly monopolar cell growth in P3 before they increased again, showing the more equal size of the SRM caps during bipolar growth in P4. A closer look at the *lub1Δ* mutant revealed some details about its behaviour. In early SE, the random positioning of SRMs led to a proportion of cells classified as polar in case the random patch localised to a cell pole. As in wild-type, the *rB* was low in *lub1Δ* cells after 15 min, but with 0.7 surprisingly high after 30 min. This was also observed in other, yet not in all experiments (see for example Figure 41 andFigure 43). However, the drop of *rB* at 45 min fitted again with the lower *rP* value at that time point. From 60 min onwards, the *rB* values stayed at a high level in *lub1Δ*. After 225 min, for more than 50% of the *lub1Δ* cells – 491 out of 970 –the *rB* was calculated and the value has increased to 0.8. In comparison, more than 70% of the wild-type cells were polar, already after 60 min with an *rB* value of about 0.7 only. The observation that the *rB* values in the wild-type stayed significantly lower (<0.7 until 300 min) than in *lub1Δ* cells (≥0.8 from 240 min on) might indicate that Lub1 does not only have a function during SE, but is also important during normal growth. *Lub1Δ* mutant cells thus possibly grow more bipolar than wild-type cells after SE.

2.5.2 *De novo* polarised *lub1Δ* cells mainly grow bipolar and faster than the wild-type

To test the hypothesis that more *lub1Δ* mutant cells grow bipolar after SE, the polarisation process of individual cells was studied by live fluorescence imaging (Figure 23a). GFP-Tna1 was used as a live-marker during SE and the growth pattern was analysed based on kymographs (Figure 23b), (Makushok et al. 2016). In order to visualise the differences between wild-type and *lub1Δ* mutants, only a single representative cell is shown from both strains in Figure 23a. For this experiment, wild-type and *lub1Δ* mutant cells were

starved in liquid culture and SE and growth recovery was monitored in imaging dishes after addition of fresh growth medium. As reported above (see section 2.2.4), under these conditions, wild-type cells are also delayed compared to a recovery in liquid culture.

The sequence of events during the polarisation process was as observed when SRMs were labelled with filipin. The wild-type cell shown completed P2, was polar after 2-3 hours, and divided after 9 hours. The *lub1Δ* mutant cell showed the typical behaviour as observed before: SRM domains visualised with GFP-Tna1 formed and in time lapse-movies they appeared to move laterally on the membrane in a prolonged P2. Although the example cell appeared polar after 2-3 hours, it seemed as if any polar SRM is not functional or stable at this time point. After 4 and 5 hours, large lateral regions are covered with SRMs and the cell is fully polar only after 7 hours. After 10 hours the *lub1Δ* cell shown divided.

Kymographs were used to analyse when and where the cells initiated polar growth (Figure 23b). For this, a line of 35 px in width (yellow in Figure 23b) was drawn parallel to the long cell axis to virtually cover the entire cell in all frames of a time-lapse movie. In the resulting 2D time-resolved representation, the kymograph, each horizontal line of pixels represents the average signal of the 35 px wide line drawn through the cell for a single timepoint. The next timepoint is aligned below and so on. This simple method is able to illustrate the polarisation process and growth localisation over time. The kymographs presented in Figure 23b were generated on the cells presented in Figure 23a.

The wild-type cell started to grow from one pole first, once both polar GFP-Tna1 caps were formed after 1:50 hours (Figure 23 left; right arrowhead). After 4 hours, the other cell end started to grow as well (left arrowhead). In contrast, the right kymograph illustrates how the polarisation process was significantly prolonged in the *lub1Δ* mutant cell. Once the example cell was polar, it directly grew bipolar from 5:50 hours on.

From the kymographs of 36 wild-type and 67 *lub1Δ* cells, it was made clear that the majority of wild-type cells (75%) grew monopolar first and then switched to bipolar growth (P4) (Figure 23c). Only 6% of the cells appeared to grow directly bipolar and 17% only grew monopolar, thus did not enter P4. In contrast, half of the *lub1Δ* cells grew bipolar directly (51%), and a large proportion (42%) switched to bipolar growth, while no cell was detected that only grew monopolar. For a small proportion of cells (3% wild-type, 8% *lub1Δ* cells), the growth pattern was not clear from the kymographs.

Here, the results for the growth pattern differ from the description of growth phases by Makushok et al. (2016). They only observed 34% of the cells entering P4 (bipolar growth). In the study presented here, the time-lapse movies were obtained at 25°C, in contrast to 30° C in the Makushok study. Thus, the temperature difference might be responsible not only for a delay during SE, but also a different timing in the onset of growth. Thus, the results are not directly comparable in this regard.

However, due to the manual evaluation method, only a proportion of cells imaged was analysed in this study. Many cells started to move due to drift or detachment from the surface during growth. For some, the kymographs did not allow to identify clear growth initiation. Thus, it is possible that a more systematic analysis of preferably a larger number of cells will provide a better statistical representation of the different ways to grow for wild-type and *lub1Δ* cells.

Based on the same kymographs, the timepoints of growth initiation, bipolar growth initiation ("second end take-off" - SETO), septum formation and division after addition of fresh medium were measured (Figure 24a). The boxplots show that the analysed *lub1Δ* cells initiated polar growth significantly later than wild-type cells due to their polarisation delay. Most wild-type cells had already undergone SETO when *lub1Δ* cells initiated growth. Most, yet not all, *lub1Δ* mutant cells showed the bipolar phenotype described above. As for cells that grow bipolar straightaway, SETO was not defined. The timepoint of SETO is only displayed from the cells that switched to bipolar growth. For those, it happened already shortly after growth initiation. The timing of septum formation and division was, however, comparable for wild-type and *lub1Δ* mutant cells. As a consequence of the short growing time, *lub1Δ* mutant cells were significantly shorter than wild type cells at division (Figure 24b).

I hypothesised that the *lub1Δ* mutant cells might compensate for the short time they have to grow with an increased growth speed. To test this, growth speeds at both cell ends were measured based on the kymographs (Figure 24c). The growth speed of the slower and the faster end were compared. Strikingly, growth speeds at both the slower and faster growing end of *lub1Δ* cells were significantly higher than in wild-type cells. The speed of the slower growing ends in *lub1Δ* cells was almost in the range of the speed of the faster growing ends in wild-type cells. However, the growth speed difference between ends was the same in both strains (Figure 24d).

The results suggest that Lub1 plays a role in growth initiation at the second cell pole. The observation that *lub1Δ* mutant cells preferably grow bipolar during SE suggests that Lub1 might be involved in inhibiting growth at the second pole. The increased growth speed in *lub1Δ* might be an additional hint towards an inhibitory function of Lub1. Alternatively, it is possible that the observed bipolar growth is due to the delay and *lub1Δ* cells start to grow bipolar because with this timing in SE, they are already prepared to initiate bipolar growth (P4).

2.5.3 Microtubules and Tea1 localise normally in *lub1Δ* cells

To test if a mis-organisation of microtubules or mis-localisation of the polarity factor Tea1 is responsible for the *lub1Δ* polarisation defect, microtubule organisation and Tea1 localisation in *lub1Δ* mutant cells during SE were analysed (Figure 25).

To study the localisation of microtubules, GFP-tagged α-tubulin (GFP-atb2) was expressed in the wild-type and *lub1Δ* strains (Figure 25a, Pardo and Nurse 2005; Makushok et al. 2016). As previously described for wild-type (Laporte et al. 2015; Makushok et al. 2016), Microtubules were mostly depolymerized also in *lub1Δ* cells, leaving only short stumps. Upon glucose addition, microtubules quickly regrew to normal length and spanned the entire cell in a similar way in wild-type and *lub1Δ* cells. It was noted though that the GFP-tubulin signal was brighter in the *lub1Δ* mutant compared to the wild-type cells. Whether this was due to the function of Lub1 or a random phenomenon due to differences in the genetic background would need further investigation. However, I noticed before that the GFP-atb2 signal expressed with the SV40 promoter varied from strain to strain in other experiments (data not shown).

The localisation of Tea1 was analysed with a tagRFP-tagged version of the protein expressed at endogenous levels (tea1-HL-tagRFP, Makushok et al. 2016), (Figure 24b). During starvation, some tea1-HL-tagRFP signal remained at the cell ends in both strains. Upon glucose addition and microtubule regrowth, additional tea1-HL-tagRFP rapidly accumulated at the cell poles and was additionally visible as small intracellular dots. These dots probably show its localisation during its transport on microtubule plus ends (Mata and Nurse 1997). Regarding the localisation of tea1-HL-tagRFP, there was no difference

between *lub1Δ* and wild-type cells, although the fluorescence signal appeared weaker in the mutant.

These data further suggest that Lub1 might play a role in linking Tea1 and SRMs. For example, after 120 min large lateral SRMs are visible on the cell sides of mutant cells although the microtubules are oriented along the cell axis and Tea1 localises to the cell ends. Thus, although the microtubule organisation is not affected in *lub1Δ* cells and therefore Tea1 was properly localised as well, no polar SRMs could be stabilised until that point of SE.

2.5.4 *Lub1Δ* mutant cells grow in width during SE

Cell dimensions were quantified over time and are displayed in Figure 26. *Lub1Δ* mutant cells are slightly longer in starvation and start to grow in length later than the wild-type in agreement with the delayed polarisation (Figure 26a). Increased cell length is apparent in the quantification after 120 min for wild-type and 240 min for ub1Δ mutant cells, indicating growth initiation between 60-120 min and 180-240 min, respectively. According to the 120 min delay in *lub1Δ* cells, they grew less in length during the time frame of the experiment.

In contrast to wild-type cells that kept a constant cell width, however, *lub1Δ* mutant cells increased in width during SE (Figure 26b). After 120 min, an increased width was apparent in *lub1Δ* cells, thus demonstrating initiation of growth (P3) in unpolarised cells.

Lub1Δ cells had a larger area than wild-type cells in starvation (Figure 26d). Although the area of wild-type cells increased faster in SE due to the earlier length increase, the difference to *lub1Δ* mutant cells was less pronounced than for the length increase over time. At 120 min in SE, both cell length and area were comparable in *lub1Δ* and wild-type cells. While from 180 min onwards, the distributions (boxes) of cell length overlap merely minimally for both strains, they were more similar for the cell area. The growth in width of the *lub1Δ* mutant thus partially compensates for the lacking polar growth, leading to a more similar cell volume.

These results suggest that in absence of Lub1, growth is initiated with the same timing as in wild-type. It is, however, independent of successful polarisation. Thus, the data provide

further evidence that *lub1Δ* cells do not have a defect in growth initiation *per se,* but exclusively in polarisation.

2.5.5 The polarity marker Bud6 localises to ectopic SRM domains in *lub1Δ* cells

The cell width measurements above suggested that during SE, *lub1Δ* mutant cells can grow in width before polarising and initiating polar growth. To test for further support of this hypothesis, the localisation of the polarity marker Bud6 (Bud6-3GFP) was compared to recovering wild-type cells (Figure 27) (Glynn et al. 2001; Martin and Chang 2006). The protein by default localised to the randomly distributed SRM domains during the P1 phase of the polarisation process, while growth is only initiated later, once the cell is completely polar, as already described by Makushok et al. (2016).

Also, in my hands, the endogenously tagged Bud6-3GFP was delocalised in starvation in wild-type and in *lub1Δ* mutant cells. After glucose addition, Bud6-3GFP readily co-localised with filipin stained SRM regions and later, once the polarisation process was complete, to the cell poles. This included the large lateral SRM domains in *lub1Δ* cells during the prolonged P2 phase. Regarding the default localisation to SRMs, Bud6-3GFP thus behaved as a marker of SRM domains rather than a polarity marker as previously suggested (Makushok et al. 2016).

Although *lub1Δ* cells have a strong polarisation defect, the microtubule-independent polarity factor Bud6 localises to SRM domains already in P1. Thus, the ability of SRM domains to localise the polarity factor appears not to be affected in *lub1Δ* cells. While this is not the case in wild-type cells, the cell width measurements suggested that the large lateral domains formed during P1 in *lub1Δ* cells to which Bud6 localised are able to initiate growth. The next section will examine the validity of this hypothesis.

2.5.6 Cdc42 localises to and is activated at ectopic SRMs in *lub1Δ* mutant cells.

The localisation of the Rho GTPase Cdc42, its GEF Scd1 and the marker of Cdc42 activity CRIB-3GFP have been used to monitor Cdc42 activity, which correlates with growth (Miller and Johnson 1994; Tatebe et al. 2008). To further investigate growth initiation in *lub1Δ* cells, I analysed the localisation of the three proteins in these cells during SE (Figure 28-Figure 30).

During starvation, Cdc42-mCherry-SW localised to bright intracellular structures (Figure 28). After 120 min in SE, weak signal was detected at the plasma membrane, localising to the poles together with the SRMs in wild-type cells (Figure 28). In the delayed *lub1Δ* mutant cells, the signal also co-localised with lateral SRMs.

Similar, Scd1-3GFP co-localised with SRMs both in wild-type and in *lub1Δ* mutant cells from 60 min onwards (Figure 29). In *lub1Δ* cells, Scd1-3GFP was clearly visible at lateral SRM domains, indicating that Cdc42 is being activated there. Consistent with this conclusion, localisation of the Cdc42 activity marker CRIB-3GFP localisation was visible at lateral SRM domains of *lub1Δ* cells at 120 min confirming Cdc42 activity in these regions (Figure 30a).

This experiment demonstrates that the cdc42 system localises to and is active at the prominent lateral SRM domains in *lub1Δ* cells prior to cell polarisation. This supports the scenario of ectopic growth activity in these mutants causing the increase in cell width.

Importantly, during exponential growth, no difference was detectable between wild-type and *lub1Δ* cells regarding the localisation of Scd1-3GFP, Cdc42-mCherry-SW or CRIB-3GFP. All factors localised to the cell poles and to the division site in both strains, suggesting that the role of Lub1 in SRM domain- and growth site positioning is specific to Tea1 mediated *de novo* cell polarisation (Figure 30b).

Interestingly, the signal originating from mitochondria auto-fluorescence that was visible when imaging the weak fluorescence signal of Scd1-3GFP in wild-type cells during SE was absent in *lub1Δ* cells (Figure 29), (Rodrigues et al. 2011). The reason for this difference is not known.

2.5.7 *Cdc42-3 lub1Δ* double mutant cells polarise during starvation exit

Although Cdc42 is dispensable for *de novo* cell polarisation, it can eventually act as random polariser when the Tea1 pathway fails (Makushok et al. 2016, Kijowski et al., in preparation), (see also Figure 45). The timing of lateral growth initiation in *lub1Δ* cells coincided with the appearance and activation of Cdc42. It was tested if Cdc42 becomes essential for cell polarisation in this mutant.

Makushok et al. (2016) have shown that cells harbouring the *cdc42-L160S* allele are able to polarise during SE. However, the *cdc42-3* allele appeared to have stronger phenotype, as the mutation is lethal at restrictive temperature and was chosen for the following experiments (Tatebe et al. 2008).

Cdc42-3 lub1Δ double mutant cells were analysed in SE at the restrictive temperature (36° C) and compared to wild-type and the single mutants (Figure 31). At this temperature, *lub1Δ* mutant cells were almost completely polarised within 120 min already. The *cdc42-3* cells polarised despite some remaining lateral SRMs on the sides of the roundish cells. These are thought to be due to the roundish cell shape that hampers proper parallel microtubule orientation and consequently leads to inefficient bi-polar Tea1 deposition. The *cdc42-3 lub1Δ* double mutant cells were also able to polarise. Similar to the *cdc42-3* single mutant, however, they also had lateral SRM domains at timepoints when *lub1Δ* cells had fully polarised.

The polarisation process was quantified and is represented in the boxplots in Figure 31b. While in the quantification of the wild-type control, the transition of the *rP* from 0 to 1 happened gradually, it stayed low for *lub1Δ* mutant cells before a sudden increase to 1 after 120-180 min. *Cdc42-3* cells reached their most polar state after 120 min according to the *rP*. The *rP* values of *cdc42-3 lub1Δ* cells demonstrated that they were able to polarise similarly. If the double mutant polarised with a slight delay compared to *cdc42-3* cells is not clear from these results and would require further testing. Interestingly, the *cdc42-3 lub1Δ* double mutant was classified as more polar than the other strains in early SE. As the cells still had prominent lateral SRMs when polar caps are formed, the *rP* did not reach high values, similar to *cdc42-3* cells.

These results suggest that cell polarisation in *lub1Δ* cells does not depend on Cdc42. It rather appears to be controlled by Tea1; with a delay, however and the complication of round cell shapes leading to incomplete polarisation with remaining SRM domains at the cell sides.

In contrast to SE at 25° C (compare Figure 26), at which wild-type cells initiated growth earlier and grew longer than *lub1Δ* cells, both strains grew to the same length at the restrictive temperature (36° C) at 240 min (Figure 32a). As expected, the *cdc42-3* cells grew

very little in length during the monitored 300 min of SE at the restrictive temperature. In addition, *cdc42-3* and *cdc42-3 lub1Δ* cells did increase in width at a similar rate suggesting a low level of unpolarised growth. Accordingly, the double mutant *cdc42-3 lub1Δ* showed some resident unpolar growth. In contrast, both the *cdc42-3* single and the *cdc42-3 lub1Δ* double mutant grew in width. Although this had been observed in the *lub1Δ* mutant before, the *cdc42-3* single mutant grew more in width (approx. 0.8 µm) than the *cdc42-3 lub1Δ* double mutant (approx. 0.5 µm) between 60 and 300 min in SE. This might suggest that the growth defect in *cdc42-3* cells is enhanced by *lub1Δ*.

As an alternative measurement, the cell area of the strains was compared over time (Figure 32b). The area of wild-type, *lub1Δ* and *cdc42-3* cells significantly increased. From 240 min on, the cell area of *lub1Δ* cells was comparable to wild-type cells. Surprisingly, the area of *cdc42-3 lub1Δ* double mutant cells appeared not to increase. This apparent contradiction to the measured width increase would need further experimental investigation. It might also be due to artefacts from the analysis program. It is likely that with a cell shape becoming more and more spherical, the detection of long and short axis is less precise, thus leading to a width measurement that might be too high. Thus, comparing the segmented cell area might be more accurate.

2.5.8 Analysis of the *lub1Δ tea1Δ* double mutant during SE

To test if the delayed polarisation of *lub1Δ* is Tea1 dependent, *lub1Δ tea1Δ* double mutant cells were analysed during SE (Figure 33a). The characteristic lateral SMR domains typical for *lub1Δ* also appeared in the *lub1Δ tea1Δ* double mutant. Strikingly, T-shaped cells were visible already after 120 min and the micrograph showed branched cells after 180 min in SE. The *lub1Δ tea1Δ* cells did not grow much in length (Figure 33b), but they increased in width (c) until 180 min in SE. Reflecting this, the aspect ratio increased during SE (Figure 33d).

Thus, although *tea1Δ* mutants are only growing monopolar, the *tea1Δ lub1Δ* double mutant was able to grow from two poles (branching). Another surprise was that in contrast to *lub1Δ,* growth occurred in a pointed manner with the shape of a cell end. Although these data are not conclusive so far, they should be considered for future experiments and

should provide another piece of information in order to understand Lub1 function during cell polarisation.

2.5.9 Interaction of *lub1Δ* and oxysterol-binding protein mutants

An independent project in our lab has shown that the oxysterol-binding proteins Kes1 and Osh7 play a key role in the early stages of fission yeast cell polarisation (see chapter 4). Oxysterol binding proteins are lipid binding proteins that have the capacity to exchange lipids via non-vesicular transport between membranes that are in close proximity (Holthuis and Menon 2014; Mesmin and Antonny 2016). By generating *lub1Δ kes1Δ* and *lub1Δ osh7Δ* double as well as the *lub1Δ kes1Δ osh7Δ* triple mutants and analysing their SE, I tested if the non-vesicular transport system could be linked to Lub1 function (Figure 34).

The oxysterol-binding protein mutants *kes1Δ* and *osh7Δ* had filipin-stainable puncta in starvation. Especially in *osh7Δ* mutant cells, these could be seen to persist during SE. However, both single mutants *kes1Δ* and *osh7Δ* polarised within 120 min. Moreover, the double mutants *kes1Δ lub1Δ* and *osh7Δ lub1Δ* were also able to polarise, but with significant delays. Clearly polarised cells were only seen after 300 min. Notably, starved *kes1Δ lub1Δ* double mutants did not show the characteristic filipin puncta as observed in the single *kes1Δ* mutant. Strikingly, approximately 4% (n=385) of *kes1Δ lub1Δ* cells appeared to transiently activate growth at random positions, while only approximately 1% (n=420) of *osh7Δ lub1Δ* cells showed a bent shape (Figure 34, bent *osh7Δ lub1Δ* at 420 min in SE, marked with a "o"). In *kes1Δ lub1Δ* mutant cells, the phenotype was not observed at later time-points anymore. At 420 min in SE, remaining lateral bulbs without filipin staining were observed, suggesting that the ectopic growth sites that appeared additionally to polar ones in some cells were lost (Figure 34).

Although the *kes1Δ osh7Δ* double mutant is severely delayed compared to the single mutants and polarises within 300 min (see chapter 4), the additional deletion of *lub1* in the triple mutant *kes1Δ osh7Δ lub1Δ* did not lead to an additional delay in polarisation and the triple mutant cells polarised within 300-360 min (Figure 34a). Interestingly, ectopic growth was observed less than in the *kes1Δ lub1Δ* double mutant (1%, n= 242). However, all mutants grew in length (Figure 34b).

Quantification of the polarisation process in the mutant cells further clarified the observations from the imaging data (Figure 35). Wild-type cells polarised within 60 min, while *kes1Δ* and *osh7Δ* cells were polar only after 120 min. In both mutants the persisting filipin puncta described above led to higher *rP* values in early SE and to lower maximum *rP* values for the polarised *osh7Δ* mutant. As discussed before, *lub1Δ* cells polarised from 180 min onwards, after an extended delay, and were polar after 240 min. While *osh7Δ lub1Δ* mutant cells still polarised within 240 min, the polarisation delay appeared to be additive in the *kes1Δ lub1Δ* mutant cells, as the double mutant polarised within 300-360 min. This extended delay was similar in the triple mutant. Interestingly, the *rP* of the *kes1Δ lub1Δ* double mutant was lower during the first 30 min in SE than for either of the two single mutants. After an initial increase up to 120 min, it dropped to 0 again after 180 min and then led to a gradual polarisation of the cells. In contrast, the *kes1Δ osh7Δ lub1Δ* triple mutant showed an increase in *rP* throughout the whole SE process until the cells were polar.

The additive polarisation defect seen in *lub1Δ kes1Δ* cells suggests that Lub1 and Kes1 might work in parallel pathways.

2.5.10 Functional analysis of the C- and N-terminal domains of Lub1 during SE

In order to test which part of the Lub1 protein is responsible for its functions during cell polarisation, cells expressing truncated versions of the protein were generated and analysed during SE. The Lub1 truncation mutants were designed in a similar manner to those published by Ogiso et al. (2004), with the exception that they were generated as stable mutant strains. Ogiso et al. showed that the C-terminus is sufficient to partially rescue the sensitivity of *lub1Δ* mutant cells to elevated temperature. However, *lub1Δ* cells did not show heat sensitivity during SE experiments in this study.

The truncation Lub1(1-248) consisted of the N-terminal WD 40 domain, while the other truncated version Lub1(235-718) only contained the C-terminus. Both truncations were generated by homologous recombination at the endogenous locus such that no wild-type protein was present (see 6.1.1 for methods). This allowed to express Lub1(1-248) at endogenous level under control of the *lub1* promoter. In contrast, the N-terminally truncated version Lub1(235-718) had to be placed under the control of an exogenous

promoter. The chosen, strong *nmt1*-promoter allows the induced (over-)expression of proteins in absence of thiamine. Both its induction and repression are slow and need about 16 hours (Maundrell 1990). Intending to reach sufficient levels of the protein during SE, cells containing *lub1(235-718)* were grown on solid medium and to exponential growth in liquid culture without thiamine before starvation. As the *nmt1* promoter shuts off at day 2-3 of starvation, this aimed to ensure that the truncated protein is sufficiently present (M. Bächler and D. Brunner, unpublished).

Cells expressing Lub1(1-248) stained strongly with filipin already during P1 and P2 (Figure 36). While the deletion mutant *lub1Δ* is already polar after 240 min, in presence of the N-terminal domain Lub1(1-248), the lateral SRMs persisted until 300 min. However, clear polar caps started to form from 120 min onwards in *lub1(1-248)* cells. Interestingly, it seemed like the polar caps and the lateral SRMs were not connected, but instead interrupted by a small gap (arrowheads).

Thus, the *lub1Δ* WD40 domain appears to be involved in SRM formation, but not their removal from the cell sides.

Expression of the C-terminus produced filipin stainable puncta in starved cells (Figure 36). During SE, *lub1(235-718)* cells formed SRMs in P1 and some cells were able to proceed through P2 and polarised their SRM domains after 120 min. This shows that *lub1(235-718)* can potentially mediate normal polarisation and speed. Notably, the observed phenotypes varied from cell to cell probably due to the variable levels of protein. Consistently, after 180 min, only a proportion of the cells were polarised. Yet, some had already started to divide, although seemingly at a shorter cell length than the wild-type.

Figure 37 summarises the quantification of the SE experiments. Wild-type and *lub1Δ* mutant cells showed their typical polarisation behaviour. It was noted that *lub1Δ* mutant cells were slightly delayed and fully polar according to *rP* only after 300 min under these experimental conditions. A likely reason for this delay is the growth on minimal medium already on the solid medium (EMM2 instead of YE5S agar plates) when cells were woken up and for the subsequent liquid culturing. Although the quantification of SE dynamics of both truncated Lub1 versions show a general trend of an increasing *rP* over time, both strains never fully polarised. The *rP* values stayed below the deletion mutant due to

remaining lateral SRMs in *lub1(1-248)* cells (incomplete polarisation) and high variability in *lub1(235-718)* cells (not all cells polarise). Strikingly, after an initial decrease of *rP* in *lub1(1-248)* until 60 min in SE, *rP* values gradually increased. It would thus be interesting to test if *lub1(1-248)* cells eventually manage to polarise.

Together with the qualitative descriptions, these results suggest that the C-terminus might be sufficient for cells to polarise within 120 min. However, the rescue did not seem to be complete. Many cells were not able to polarise, and some polarised cells proceeded directly to division. To clarify if variable protein levels, due to usage of the *nmt1*-promoter, are responsible for the observed variability, it would be necessary to test the function of Lub1(235-718) at endogenous levels. However, the WD40 domain alone in *lub1(1-248)* cells allowed the formation of polar caps already after 120 min, although the full polarisation was even more delayed than in the full deletion mutant.

2.5.11 Overexpression of ubiquitin fully rescues the *lub1Δ* phenotype

In a next step, I investigated how the WD40 protein Lub1 might function during SE. WD40 proteins specifically interact with other proteins to guide them, for example, to ubiquitination and potentially degradation. This could therefore be a potential way of action for Lub1 as well. Alternatively, protein modification by polyubiquitination can also be proteasome-independent and lead to altered protein interaction or localisation. The latter one is also connected with mono-ubiquitination (Xu and Jaffrey 2012; Huang 2014). The previously reported hypersensitivity of *lub1Δ* cells to elevated temperatures and UV radiation was rescued by overexpression of polyubiquitin from the *ubi4* gene (Ogiso et al. 2004). Furthermore, it has been shown recently that deubiquitinating enzymes (DUBs) play a role during cell polarisation (Beckley et al. 2015). For example, they describe Cdc42 and Tea1 as potential targets of DUBs.

To test if Lub1 also works via ubiquitination in the cell polarisation process, I overexpressed *ubi4* in *lub1Δ* mutant cells. Ubi4 is a polyubiquitin made of five head to tail repeats of ubiquitin. Strains expressing polyubiquitin under control of the *nmt1* promoter were generated by homologous recombination at the endogenous *ubi4* locus (see 6.1.1 for methods). To maximize the induction of *ubi4* in absence of thiamine (-T) and its

repression in presence of thiamine (+T), all strains were grown on the according solid medium before transferring them to liquid culture for starvation. Wild-type and *lub1Δ* control cells were also kept without thiamine throughout the experiment.

Low expression levels of Ubi4 (*ubi4+*, +T) resulting from the leakiness of the thiamine-repressed promoter phenocopied the *lub1Δ* deletion phenotype (Figure 38). Under repressive conditions, *ubi4+* (+T) cells showed filipin signal in starvation. Similar to the *lub1Δ* mutant, they showed a lateral SRM localisation in SE. However, the filipin staining appeared stronger in *ubi4+* (+T) cells. Only after 180 min, the first polar caps appeared and polarisation was even delayed (≥360 min) compared to the *lub1Δ* mutant (240-300 min). In contrast, activating the full *nmt1*-mediated Ubi4 expression by the absence of thiamine (*ubi4+*, -T) was well tolerated and the polarisation process was not different from wild-type cells.

Repression of *ubi4+* in *lub1Δ* mutant cells (*lub1Δ ubi4+*, +T) completely disrupted cell polarisation within the investigated 360 min. In starvation, cells were covered with large SRM domains all over the cell with regions of variable staining intensity. The signal additionally varied from cell to cell. A substantial proportion of cells was dead under these conditions, as suggested by the bright filipin signal filling the cell bodies. Strikingly, overexpression of *ubi4* in the *lub1Δ* deletion mutant (*lub1Δ ubi4+*, -T) fully restored the wild-type behaviour. The polarisation process was not distinguishable from the wild-type in any way.

In agreement with these observations, the quantifications of *rP* illustrate the polarisation behaviour (Figure 39). While low ubiquitin levels led to a massive delay in wild-type cells (*ubi4+*, +T) and *lub1Δ* mutants completely failed to polarise with repressed *ubi4+* (*lub1Δ ubi4+*, +T), the quantifications further demonstrate that the polarisation process was indistinguishable from wild-type when Ubi4 is overexpressed either in wild-type or in *lub1Δ* mutant cells.

Cell length and width quantifications further support the finding that overexpression of *ubi4* in a *lub1Δ* background restores wild-type behaviour (Figure 40). *Lub1Δ* cells grow in length like wild-type when ubiquitin is overexpressed and growth in width is detected in otherwise wild-type cells when *ubi4* is repressed. It is not surprising at this point that the behaviour of *rB* followed these rules as well (Figure 41). Overexpression of ubiquitin

allowed the establishment of bipolarity. Interestingly, repression *ubi4* gave high *rB* values in the wild-type, but low ones in the *lub1Δ* background.

2.5.12 Cdc48 is needed for bipolarity

The chaperon-like ATPase Cdc48 interacts with the WD40 domain and thereby potentially stabilises Lub1 (Ogiso et al. 2004). Cdc48 (p97/VCP in higher eukaryotes) is an evolutionary conserved protein which has been called the "Swiss army knife of cell biology" by Baek et al. (2013) due to its essential regulatory role in many cellular processes. It consists of a conserved N-terminal domain, two AAA ATPase (ATPase associated with diverse cellular activities) domains and a C-terminal tail. Its active form is a hexameric ring. A range of cofactors, either recruiting or processing substrates, are known to interact mainly with both the N- and the C-terminal domain. In almost all Cdc48-controlled processes, ubiquitin plays a role (Baek et al. 2013). It is involved in ubiquitin-mediated proteolysis, in which pathway Lub1 was described to play a role like its budding yeast homologue Ufd3 (Ogiso et al. 2004; Baek et al. 2013). Furthermore, Cdc48 is important for the endoplasmic reticulum associated degradation (ERAD), a quality control system destroying misfolded proteins. Additionally, Cdc48 is involved in the activating cleavage to release the sterol-regulatory element-binding protein (SREBP) Sre1 in fission yeast that regulates the biosynthesis of sterols and plays a role in lipid homeostasis (Hughes, Todd, and Espenshade 2005; Hughes, Nwosu, and Espenshade 2009; Stewart et al. 2011; Hwang et al. 2016). Thus, Cdc48 acts in segregating ubiquitinated proteins from membranes or protein complexes (Bodnar and Rapoport 2017).

To test if the interaction of Cdc48 and Lub1 also plays a role during SE, strains carrying the temperature-sensitive mutant alleles *cdc48-ts* and *cdc48-353* of the essential gene *cdc48* were analysed during SE at the restrictive temperature (36° C) (Figure 42).

Similar to *lub1Δ* cells, SRM domains localised to the lateral sides in *cdc48-ts* and *cdc48-353* cells during early SE. Both mutants polarised with a delay and were polar after 120 min (Figure 42a). The quantification of *rP* (Figure 42b) illustrates this behaviour. Interestingly, in both temperature sensitive *cdc48* mutants, *rP* was in the medium range during the first 60 min in SE before the cells suddenly polarised as quantified with an *rP* value of

1. This is similar to the behaviour of *lub1Δ* cells, suggesting that Cdc48 and Lub1 work together during cell polarisation.

Interestingly, based on the filipin staining pattern, the polar cells from both mutants appeared to be monopolar. This is supported by the quantification of *rB* (Figure 42c*),* as values decreased during SE for *cdc48-ts* and *cdc48-353* cells and were low when the cells were polarised. After 120 min, when wild-type, *cdc48-ts* and *cdc48-353* cells were polar, the *rB* values of all three strains were also comparable. However, *rB* values were increased again from 180 min onwards in wild-type cells. In contrast, *rB* values were 0 for both *cdc48-ts* and *cdc48-353* cells from 180 min in SE onwards. Notably, monopolar growth is a hallmark of the *tea1Δ* phenotype.

Lub1Δ cdc48-ts and *lub1Δ cdc48-353* double mutants showed the same behaviour as the *cdc48* single mutants (Figure 43a, compare Figure 42). This meant that they polarised like *lub1Δ* cells, with the difference that they failed to become bipolar, just as the *cdc48-ts* and *cdc48-353* single mutants. Under these conditions, *lub1Δ, lub1Δ cdc48-ts* and *lub1Δ cdc48-353* mutants all had the characteristic decrease in *rP* until 60 min in SE before the sudden polarisation and transition to 1 between 120 and 180 min (Figure 43b). In contrast, the quantification of *rB* illustrates that *lub1Δ* cells were mainly bipolar from 120 min on, while *rB* decreased in the *lub1Δ cdc48*double mutants demonstrating their mono-polarity (Figure 43c).

Together, these results provide evidence that Lub1 and Cdc48 might work together in the same pathway in order to polarise the cells. At the restrictive temperature of 36° C used in this experiment, this happened within 120 min in SE. In contrast, in order for the cells to become bipolar, *cdc48* mutants appeared more similar to *tea1Δ* cells. Thus, Cdc48 might be involved in stabilising the non-growing end, potentially working together with Tea1.

Like for *lub1Δ* mutants, an increased width was measured for all *cdc48* mutant strains after 120 min (Figure 44b). Interestingly, all strains, including wild-type, showed a slightly increased width already after 60 min in SE. This might indicate that minor growth can also occur on unpolarised wild-type cells. However, the width increase was minor, while the *cdc48* mutants grew up to approx. 0.5 µm in width. In contrast, an increased length was detected after the cells had successfully polarised. This was after 120 min for wild-

type and to a lesser extend for *cdc48-ts*. All other strains only showed an increased cell length after 180 min.

2.5.13 Summary and discussion of *lub1*-related results

It was demonstrated in the section above that Lub1 plays a critical role during P2 (see chapter 2.5.1, Figure 21Figure 22). *Lub1Δ* deletion mutant cells were stuck in P1 and polarised from 180 min on. P2 was completed after ca. 240 min, three hours later than in wild-type cells.

Once *lub1Δ* cells were polarised, they initiated growth immediately from both cell ends (see chapter 2.5.2, Figure 23). The majority of the mutant cells grew bipolar directly upon growth initiation, in contrast to wild-type cells that mainly grew monopolar first. Surprisingly, the growth speed was significantly higher in *lub1Δ* mutant cells (Figure 24). They divided at the same time point during SE as wild-type cells at a shorter cell length due to the shorter growth time. Although the manual analysis of time-lapse movies used for this experiment is not perfectly accurate and causes additional variation, significant differences in the growth pattern, timing, and speed could be detected in comparison to the wild-type.

For more sound numbers, it would be beneficial to develop an automated analysis that also corrects for drift and rotations during imaging, ensuring that only real cell growth is detected and analysed. At the same time, more cells could be analysed to allow a better statistical analysis. Ideally, the setup would also allow tracking and analysing the growth mode and pattern of the offspring to test how the second generation after SE behaves. Furthermore, it would be interesting to analyse exponentially growing *lub1Δ* cells, to test if the observed growth pattern and speed are specific for *lub1Δ* cells during the SE period or are a general phenotype.

Both microtubules and Tea1 that are key system for cell polarisation in fission yeast localised normally in *lub1Δ* cells (see chapter 2.5.3, Figure 25). It was found that due to the polarisation delay, *lub1Δ* cells grew less in length during SE, but slightly increased in width compared to wild-type cells (see chapter 2.5.4, Figure 26). The growth marker Bud6-3GFP localised to the large lateral SRMs that formed during the extended P1 (see chapter 2.5.5Figure 27). As Cdc42, Scd1 and CRIB also localised to these ectopic SRMs,

they were activated as growth sites in *lub1Δ* mutant cells, explaining the increase in cell width (see chapter 2.5.6, Figure 28Figure 30).

As *lub1Δ cdc42-3* double mutant cells are still able to polarise to some extent, although with defective removal of lateral SRMs, the delayed polarisation does not appear to depend on Cdc42 (see chapter 2.5.7, Figure 31-Figure 32). If it is Tea1-dependent, as the results might indicate, is not yet clear and needs further investigation (see chapter 2.5.8, Figure 33).

In contrast, the polarisation delay appears to be additive in case the oxysterol-binding protein *kes1* is deleted in a *lub1Δ* background (see chapter 2.5.9, Figure 34 andFigure 35). Based on this, one could speculate that Kes1 and Lub1 usually work together during the polarisation process either in parallel pathways or in two consecutive, rate-limiting steps. Kes1 would be responsible for the initially polar deposition of SRMs in the *lub1Δ* mutant. In absence of Kes1 and Lub1, cells have to wait for the cdc42-dependent activation of Osh7 (see chapter 4), which might explain the additive effect.

Without Lub1, mainly lateral SRMs are stabilised even though Tea1 is correctly positioned at the cell ends. These ectopic SRMs are able to grow until yet another signal - possibly still directed by Tea1 - is able to quickly initiate polarisation in a backup program. The Tea1 system might also be weakened and only be able to work with a delay. In wild-type cells, Lub1 somehow leads to the stabilisation of SRMs at the cell poles or is involved in the removal of the laterally positioned SRMs. Thus, it is possible that a stabilisation of polar SRMs works via an interaction between Lub1 and Tea1. The WD40 protein Lub1 could work as a interaction mediator bringing Tea1 together with yet unknown factors, which eventually leads to the stabilisation of SRMs at the cell poles.

The *kes1Δ lub1Δ* double mutant did not only have an additional delay in polarisation, but a few cells also showed a bent or even the start of a T-shape in late SE (Figure 34). However, the shape was not stable and the double mutant cells eventually all grew in a normal, bipolar manner. Still, the observed T-shapes might be a hint that *lub1* and *kes1* are possibly functionally linked via *tea1*. It appears that Tea1 cannot properly function in absence of Lub1, leading to transiently T-shaped cells in the *lub1Δ kes1Δ* mutant. Notably, more experimental repeats and ideally an automated analysis would be necessary to make a clean statistical evaluation to improve the quantitative comparison of the appearance of

the observed bent or T-shaped phenotype in the *lub1Δ kes1Δ, lub1Δ osh7Δ* and *lub1Δ kes1Δ osh7Δ* mutants.

Furthermore, it was demonstrated that neither the N-terminal WD40 domain nor the C-terminal domain of Lub1 alone is sufficient for its full function (see chapter 2.5.10, Figure 36Figure 37). Although the results suggest that the C-terminal domain alone allows cell polarisation to occur, both domains are necessary for full function during SE. One could speculate that the WD40 domain facilitates the formation of lateral SRMs while the C-terminus is needed for their removal. Cells expressing the N-terminal WD40 domain only formed SRM domains in SE, but failed in removing lateral domains even when they successfully formed polar caps. In contrast, when the C-terminal domain was present, cells were able to remove lateral SRM domains. It is well possible that both domains interact during the cell polarisation process and/or are activated at different timepoints of SE to regulate the functions of the two domains. The result that the removal of lateral SRMs in *lub1(1-248)* was even more delayed than in the full deletion might be a hint that in absence of Lub1, another system takes over with a delay, while it is not activated or only with an additional delay in *lub1(1-248)* cells. It is also possible that the WD40 domain interacts with its partners, but in absence of the C-terminal domain, the necessary processes like protein modification or degradation cannot proceed due to a lack of interaction with the C-terminus or its potential binding partners. This might then block the system and be reminiscent of the deletion. It would be interesting to test in a next step if it is possible to restore the functionality of Lub1 when both truncated versions are present as two different parts in the cell or if the protein is only functional in a single piece.

Strikingly, the *lub1Δ* phenotype was completely suppressed by the overexpression of ubiquitin (*ubi4+*). In contrast, lower than normal levels of ubiquitin phenocopied the *lub1Δ* mutant (Figure 38). Taken together, these results demonstrate that the function of Lub1 during SE depends on sufficient ubiquitin levels. If the level is too low, it cannot fulfil its function during SE and the polarisation progresses with an even stronger delay than in the *lub1Δ* mutant. Ogiso et al. (2004) demonstrated that Lub1 is important for stress response via a function in ubiquitin homeostasis. They propose that Lub1 might negatively regulate ubiquitin degradation. Overexpression of ubiquitin thus compensates for the increased degradation of ubiquitin in absence of Lub1. It would be interesting to test if overexpression of Lub1 can speed up the polarisation process. However, as the

overexpression of ubiquitin did not lead to an increased polarisation speed (Figure 38 andFigure 39), it does not appear to be very likely.

The function of Lub1 might act at least partly via its interaction with Cdc48. This factor mediates interaction in various processes (Baek et al. 2013, see chapter 2.5.12 for a brief summary). The temperature-sensitive mutants *cdc48-ts* and *cdc48-353* also have characteristic lateral SMRs during starvation like *lub1Δ* cells (Figure 42). Based on these results, it is possible to speculate that the early function of Lub1 depends on interaction with Cdc48, as *cdc48* mutants phenocopy the *lub1Δ* mutant in early SE. Later in SE, defective *cdc48* allowed cell polarisation, but led to monopolar cells. This phenotype was similar to *tea1Δ* cells with the significant difference that the monopolar *cdc48* mutant cells were straight. These results demonstrated that Cdc48 or its interaction with Lub1 is critical for bipolarity. It has been described that Cdc48 stabilises Lub1, possibly by interacting with the WD40 domain (Ogiso et al. 2004). This means that in absence of Cdc48, Lub1 is destabilised, which in turn leads to destabilisation of ubiquitin. Thus, this would suggest that ultimately, ubiquitin is necessary for polarisation. Alternatively or additionally, Cdc48 could have a role independent of Lub1 during cell polarisation because *lub1Δ* mutant cells are able to polarise in a bipolar manner, or another redundant factor possibly takes over in absence of Lub1. This rather suggests a way of action via Tea1. The observation that *lub1(235-718)* cells are able to polarise earlier than *lub1Δ* cells (Figure 37), although the C-terminal part of the protein does not interact with Cdc48 due to the lack of the WD40 domain (Ogiso et al. 2004), supports this possibility. In other words, the results suggest that Lub1 protects the non-growing end before it initiates growth and Cdc48 is somehow involved in its formation and the initiation of bipolar growth. Under normal condition, *lub1* thus might negatively regulate *cdc48.* Upon NETO, it might be down-regulated, leading to *cdc48* activity and bipolar growth. In this context, the connection of Cdc48 to the sterol-pathway might also be of importance (Stewart et al. 2011). One could speculate that defect Cdc48 might lead to an altered sterol content and thus availability of SRM domains for polarisation in a way that stable SRM caps can only be stabilised at one cell end. From this point and these speculations on, further experiments are necessary to gain a deeper insight and understanding into how Lub1 might work during cell polarisation.

Figure 20 is a first attempt to graphically summarise these main results. It illustrates that from the experiments performed in this thesis, it is apparent that ubiquitin is somehow involved in the polarisation process, as Cdc48 stabilises Lub1 that in turn prevents the degradation of ubiquitin. In *lub1Δ* cells, overexpression of ubiquitin was able fully restore cell polarisation. The remaining question is, how. What are the interactors of Lub1 and Cdc48 in this context? Which domains are important at which step? Does Lub1 fulfil several functions during cell polarisation? It is likely that the Lub1 system acts in modifying other factors. What are the targets and how are they modified?

The results described in this chapter can be seen as an entry point into further experiments to tackle these questions. The analyses and the tools developed offer some possibilities for new experiments. For example, in order to test if the specific interaction of the Lub1 WD 40 domain is needed for bipolarity, the N-terminal truncation mutant could be analysed in a *cdc48* mutant background. Based on the observations in this study and described by Ogiso et al. 2004, the expression levels of *lub1* versions and ubiquitin should always be kept in mind and be part of the analysis. It would be beneficial to create more truncated versions of the Lub1 protein to learn more about the functions of the different domains and potentially identify the critical sequence for the polarisation process.

The presented results suggest a functional link between the Lub1 system and Tea1, but it is not clear how this connection might work at a molecular level. Although the localisation of Tea1 is not disturbed in *lub1Δ* cells, the cells fail to stabilise SRM domains at the cell poles during the first 3-4 hours of SE. In absence of functional Cdc48, only one cell pole is stabilised, reminiscent of *tea1Δ* mutant cells. However, the temperature sensitive *cdc48* mutants analysed in this study did not show T-shaped cells in SE, neither did the double mutants with *lub1Δ*. The possibility that the link works via temporal and special regulation of ubiquitination or de-ubiquitination of the involved factors is supported by the finding that factors of the polarisation system were identified as targets of DUBs (Beckley et al. 2015).

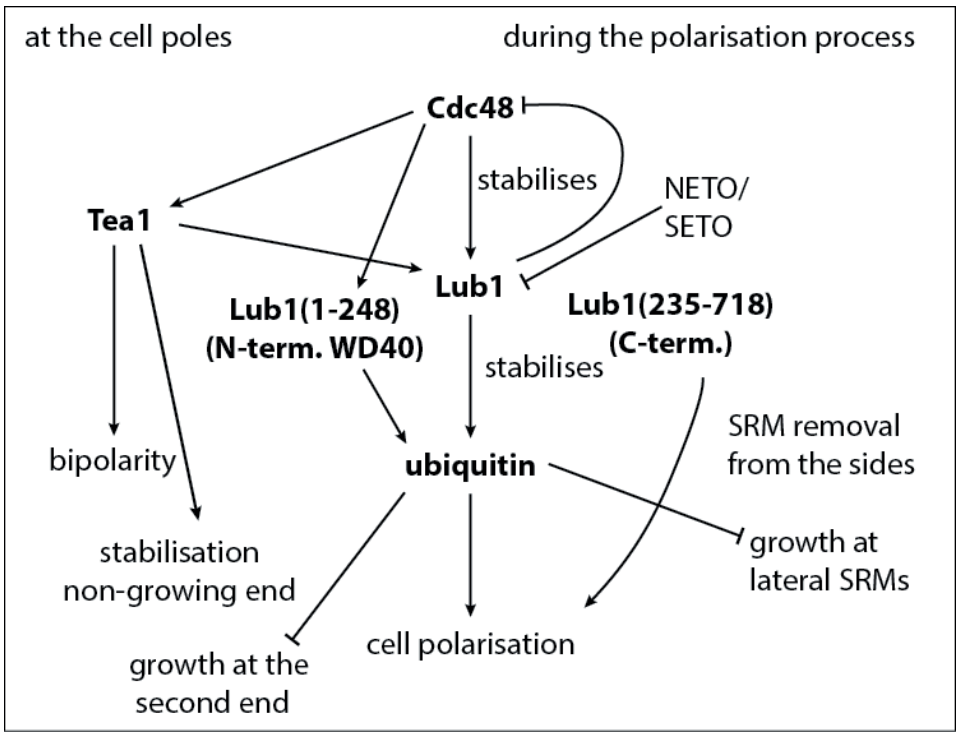

Figure 20: Summary of results.

Cdc48 stabilises Lub1 that prevents degradation of ubiquitin. Defects in any of the three lead to a delay in cell polarisation and growth at lateral SRM domains during SE. The Lub1/ubiquitin system appears to prevent growth at the non-growing end that might be stabilised by Cdc48 in a Tea1-dependent manner. Lub1 potentially inhibits Cdc48, preventing premature bipolar growth. Lub1 would thus have to be inhibited upon NETO/SETO, in order for the second end to start growing. Furthermore, the results suggested that the Lub1 N-terminus works via a stabilisation of ubiquitin, while the C-terminus might be necessary for the removal of lateral SRM domains.

In general, the ubiquitin-proteasome pathway plays various roles in different cellular processes, for example the stress response, not only in fission yeast, but also in budding yeast and *Candida albicans* (Finley, Özkaynak, and Varshavsky 1987; Leach et al. 2011). Polyubiquitin mutants of *Candida albicans* show morphological defects, are hypersensitive to stress and have an altered cell cycle (Leach et al. 2011). Interestingly, nitrogen and carbon starvation as cellular stresses have also been linked to ubiqutination in *Candida albicans* and budding yeast (Finley, Özkaynak, and Varshavsky 1987; Leach et al. 2011). The virulence of the fungal pathogen *Cryptococcus gatti* depends on the deubiquitinase Ubp5 (Meng et al. 2016). In budding yeast, protein degradation is involved in the reorganisation of polarised growth towards the location of membrane damage (Kono et al. 2012). In fission yeast, the CLIP-170 homologue Tip1, a key regulator of microtubule dynamics and polar Tea1 delivery, was proposed to be degraded by ubiquitin-mediated

proteolysis (Martín-García and Mulvihill 2009). However, microtubule organisation is not affected in *lub1Δ* cells, indicating that this link cannot be relevant for *de novo* cell polarisation during SE. To test if the role of Lub1 in this process is to mediate protein degradation rather than modification of the activity or the localisation of critical proteins needs further analysis. Genetic or drug mediated interference with the proteasome, for example by application of the specific proteasome inhibitor MG132, is an obvious way to go (Lee 1998; Ogiso et al. 2004).

Interestingly, a recent publication describes the segregation of the permease Mup1 in budding yeast into different membrane domains. It is stabilised by clustering in the plasma membrane. Substrate addition leads to a conformational switch and re-localisation into a disperse network, subsequently leading to its ubiquitination, internalisation and degradation (Busto et al. 2018). However, Mup1 re-localisation does not depend on ubiquitination. Thus, Lub1 might play a role in this uncovered interplay between protein segregation and turnover on the degradation side. Strikingly, the lateral SRM domains that are not removed during P2 could be due to altered endocytosis in these regions. This would suggest that during SE, Lub1 is involved in marking unknown factors in the plasma membrane for internalisation and degradation, necessary for polarisation. This process might be delayed in *lub1Δ* cells and another factor might have to take over to fulfil Lub1's function.

In summary, this study now provides a first insight and motivates to further investigate how Lub1 and ubiquitination are involved in cell polarisation of fission yeast.

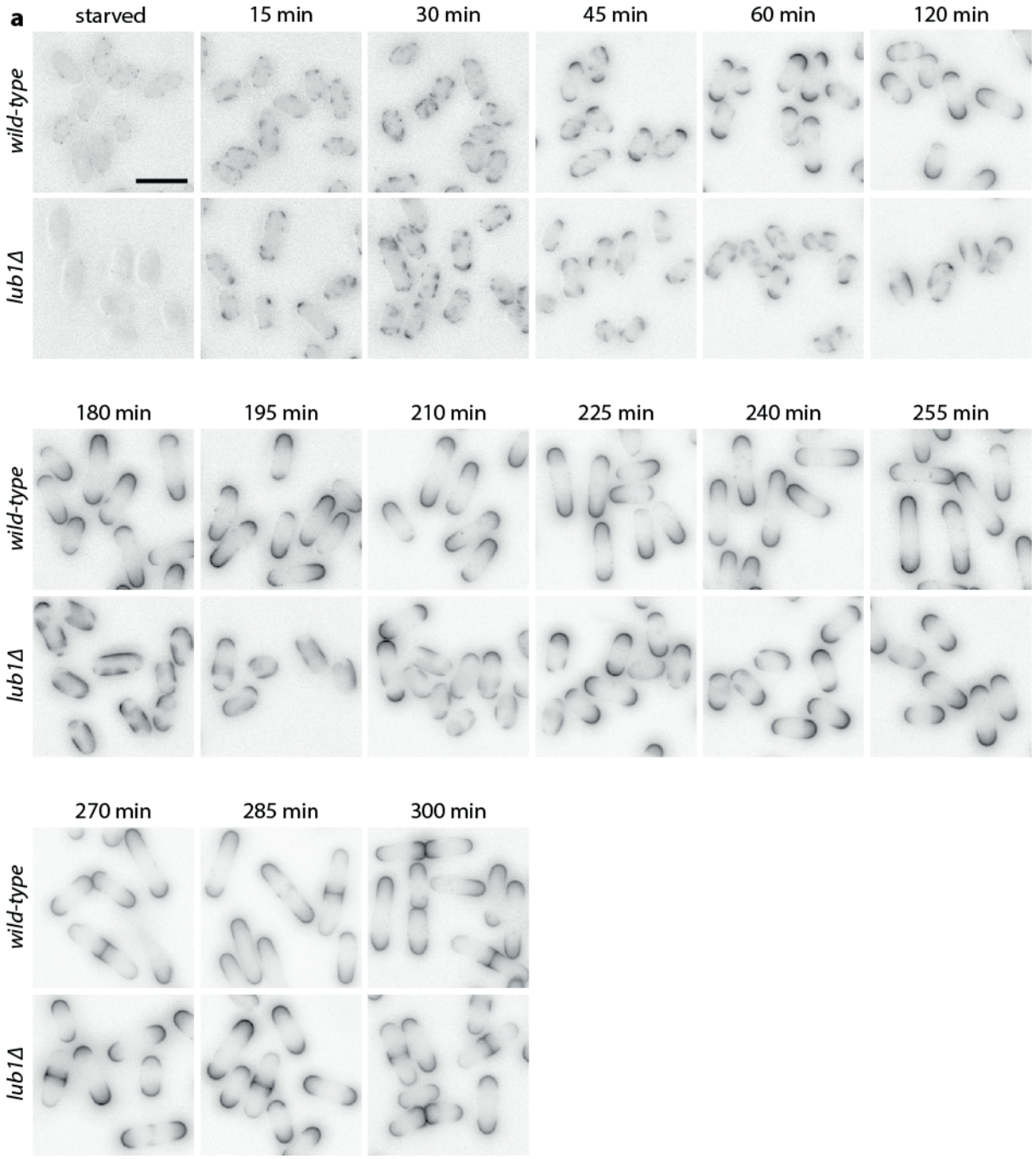

Figure 21: Detailed starvation exit of *lub1Δ*.

(a) Filipin-stained wild-type and *lub1Δ* cells during SE. Scale bar: 10 µm.

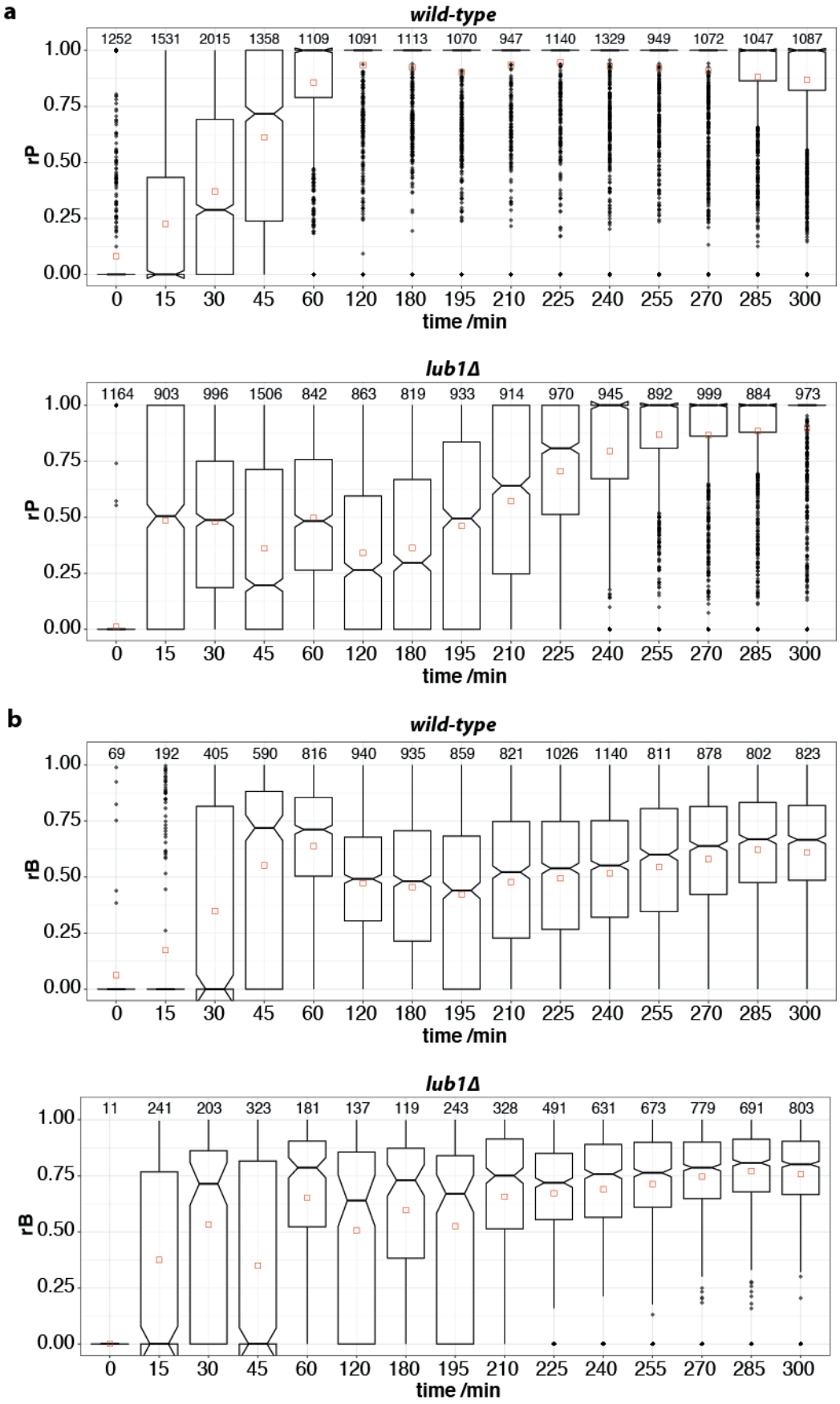

Figure 22: Quantification of starvation exit of *lub1Δ*.

(a) and (b) Notched boxplots showing *rP* (a) and *rB* (b) during SE of wild-type and *lub1Δ* cells, n above each boxplot.

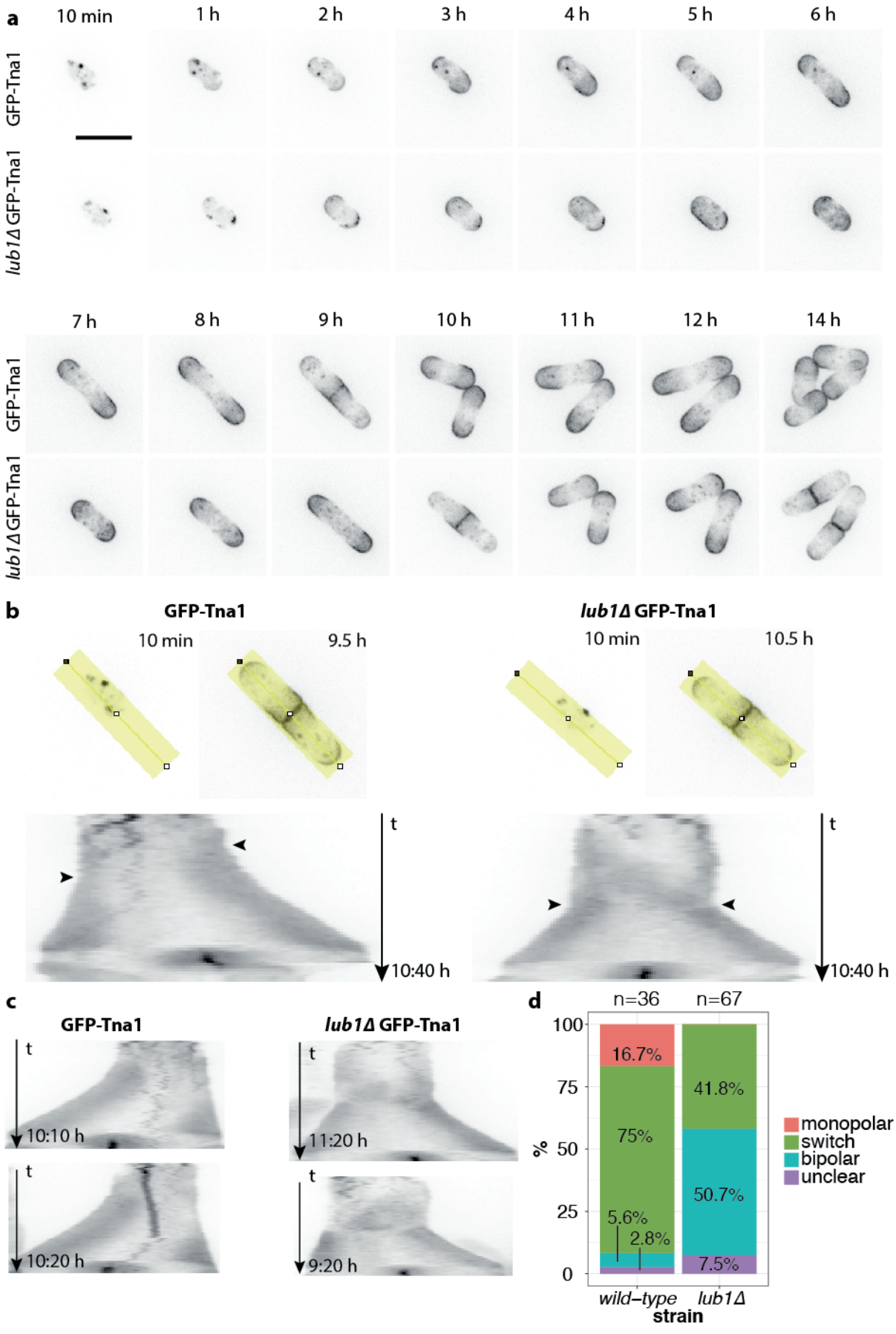

Figure 23: *Lub1Δ* grows mainly bipolar during starvation exit.

(a) Example cells showing GFP-Tna1 localisation in wild-type and *lub1Δ* during SE. (b) Kymographs of the cells shown in (a). Top: selecting the region of the kymograph with a 35 px line (yellow) spanning the cell from 10 min onwards until it divides (9.5 h for wild-type, 10.5 h for *lub1Δ*). Bottom: resulting kymographs. Arrowheads: growth initiation. (c) Additional example kymographs of wild-type (left) and *lub1Δ* cells (right) expressing GFP-Tna1 during SE. (d) Stacked barplots summarising the observed growth modes in wild-type and *lub1Δ*. Scale bar: 10 µm.

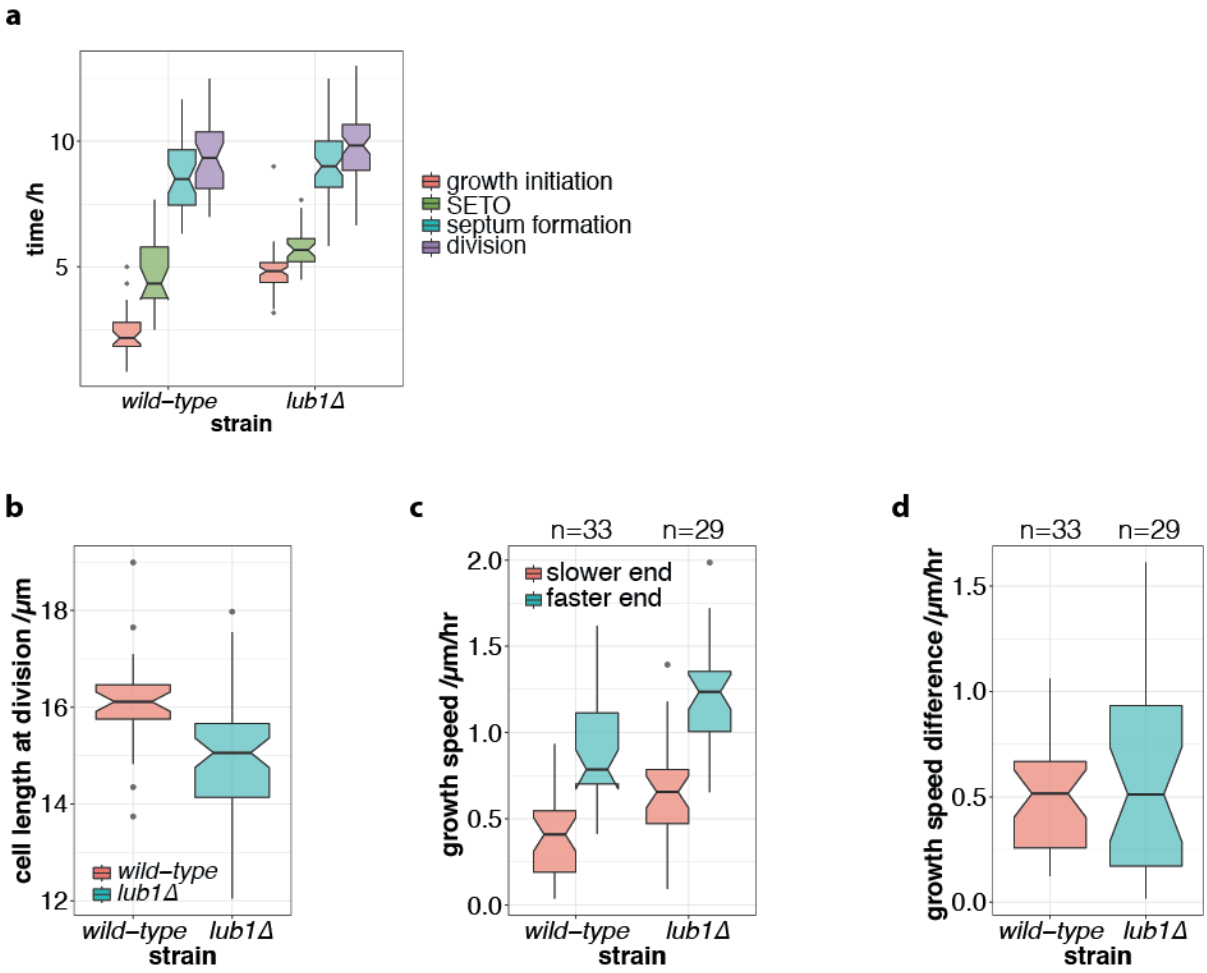

Figure 24: *Lub1Δ* grows faster than wild-type.

(a) Timing of growth during SE in wild-type compared to *lub1Δ* cells: growth initiation (red), second end take-off (SETO) (green), septum formation (blue) and division (violet). (b)-(d) Cell length at division (b), growth speed (c) and growth speed difference at the two growing ends (d) in wild-type compared to *lub1Δ*.

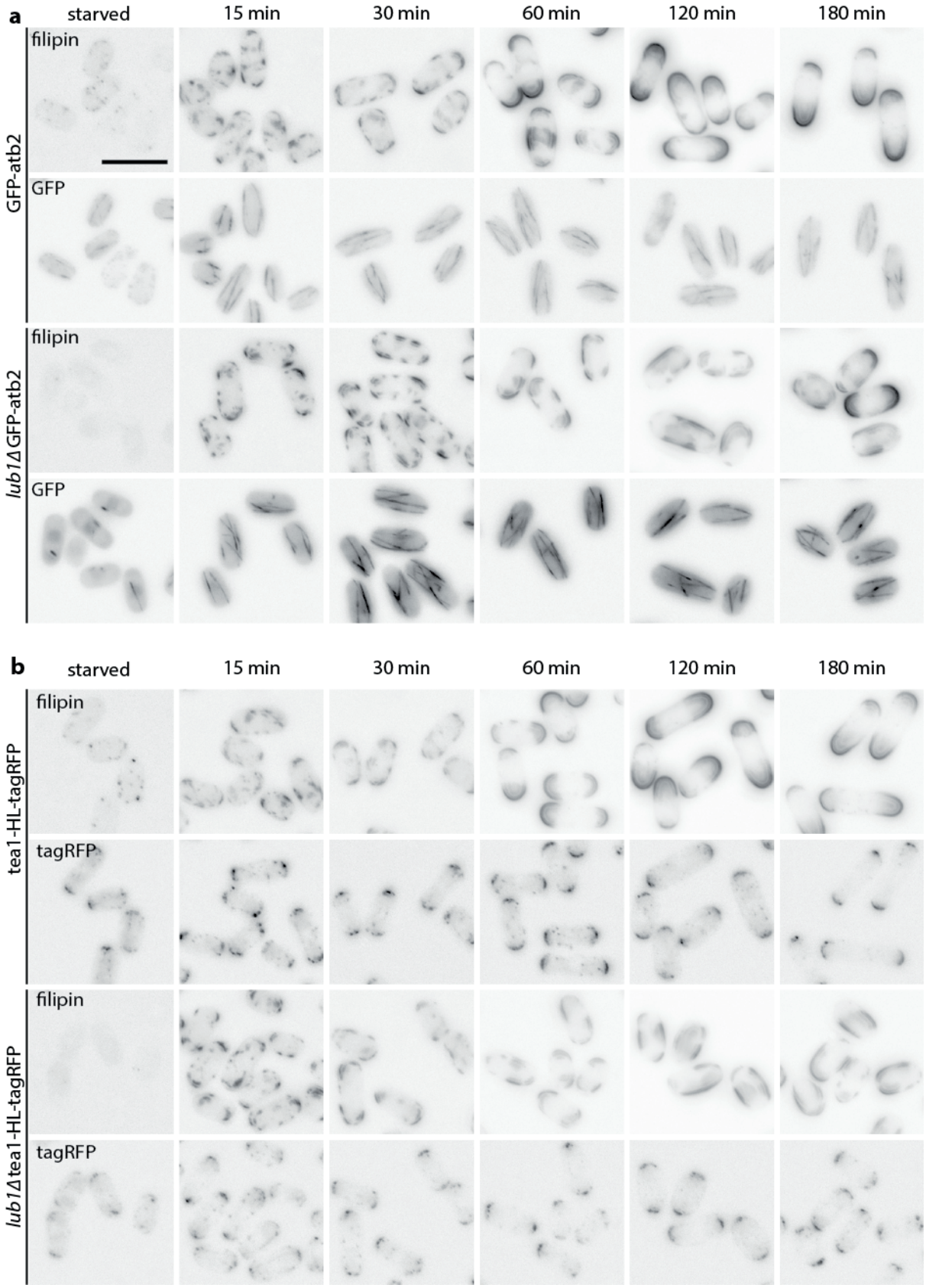

Figure 25: Microtubules and Tea1 localise normally in *lub1Δ*.

(a) GFP-atb2 localisation and filipin staining in wild-type (top) compared to *lub1Δ* (bottom) cells during SE. (b) Tea1-HL-tagRFP localisation and filipin staining in wild-type (top) compared to *lub1Δ* (bottom) cells during SE. Scale bar: 10 µm.

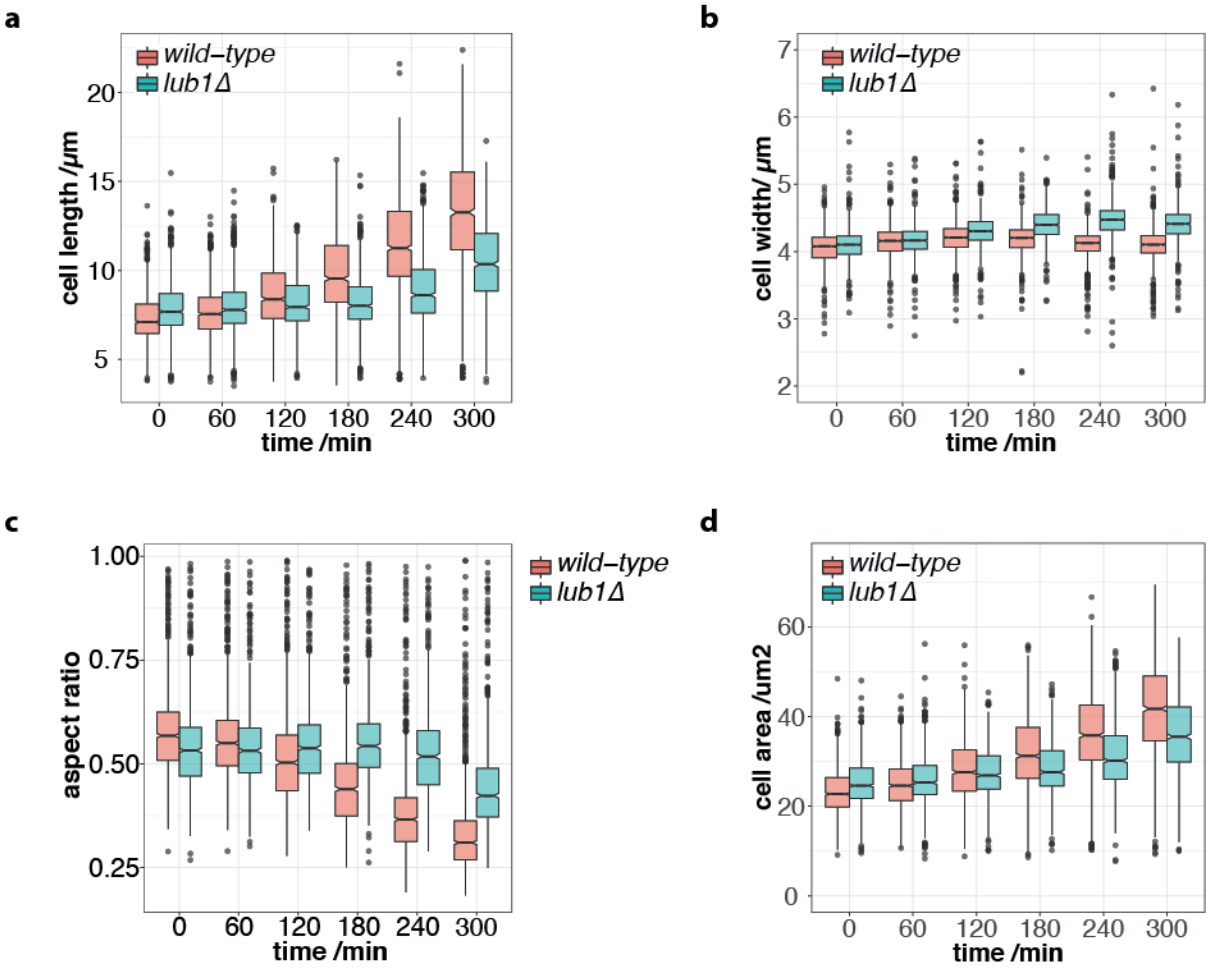

Figure 26: *Lub1Δ* grows in width during SE.

(a)-(d) Comparing cell length (a), cell width (b), aspect ratio (c) and cell area (d) of wild-type (red) and *lub1Δ* (blue) during SE.

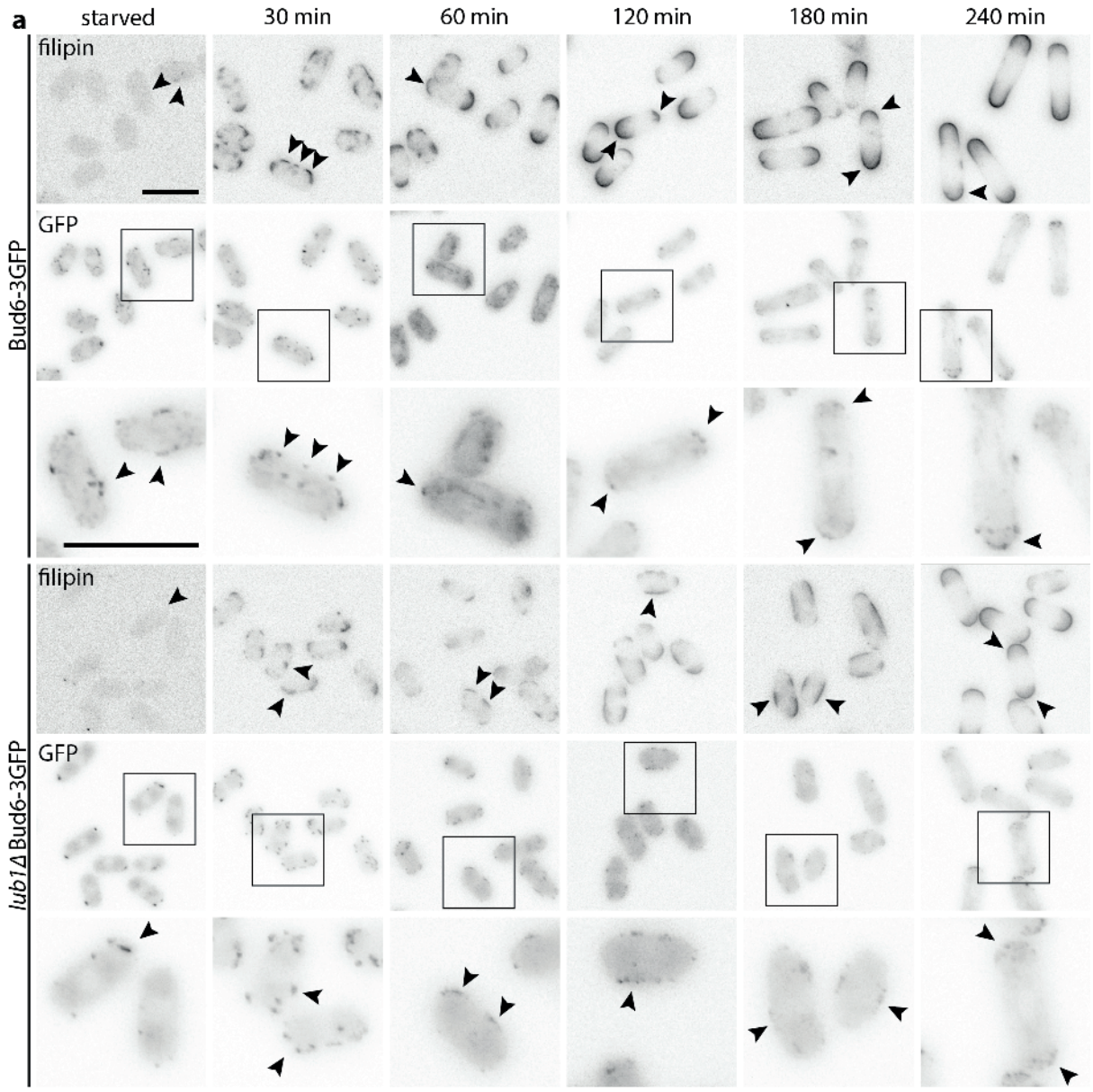

Figure 27: Bud6-3GFP localises to ectopic SRMs in *lub1Δ* mutant cells.

(a) Filipin staining and Bud6-3GFP localisation in wild-type (top) compared to *lub1Δ* cells (bottom) during SE. Regions of close-ups shown below the Bud6-3GFP images are marked. Arrowheads: Bud6-3GFP-filipin co-localisation. Scale bars: 10 µm.

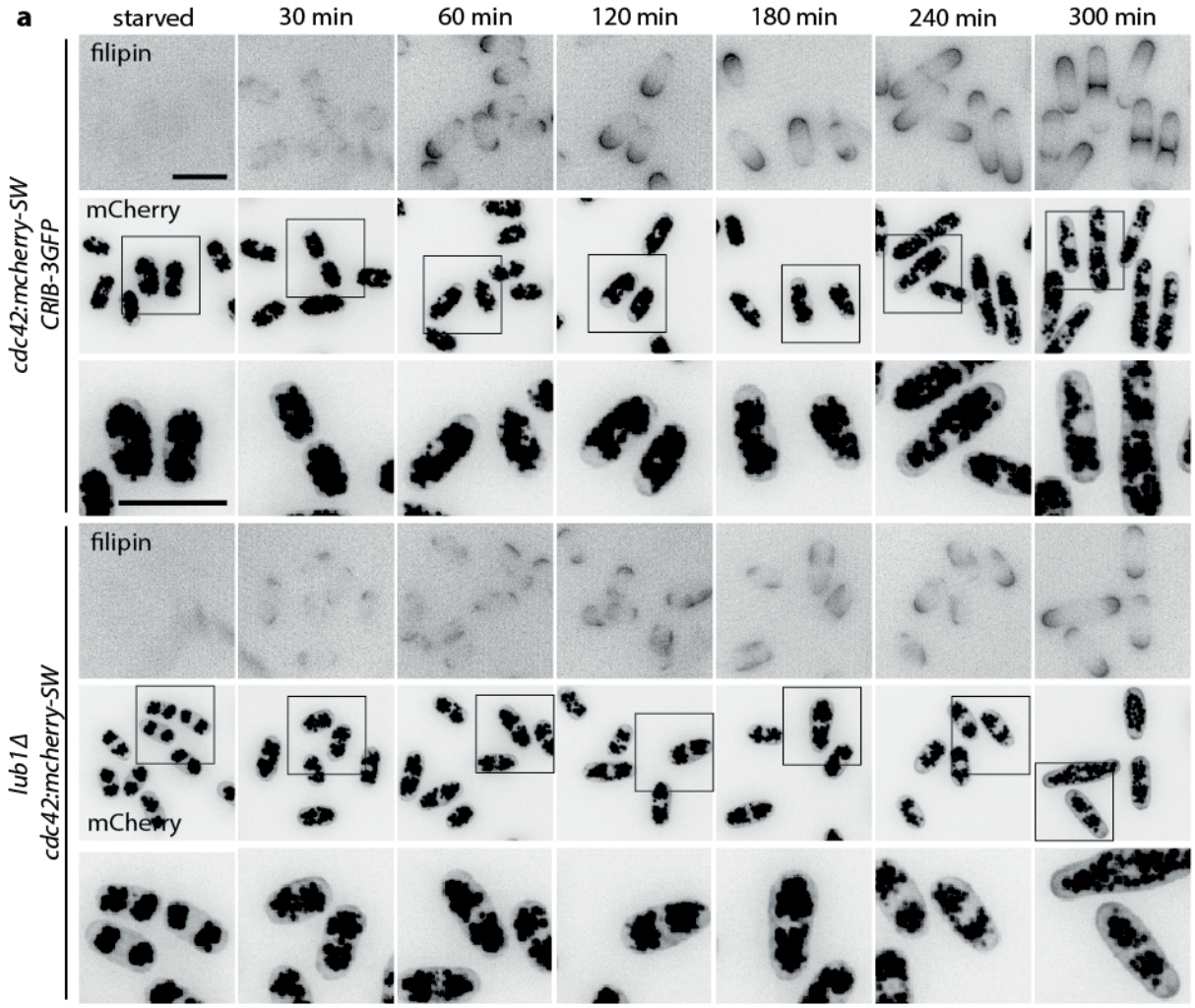

Figure 28: Cdc42-mCherry-SW localises to ectopic SRMs in *lub1Δ* mutant cells.

(a) Filipin staining and Cdc42-mCherry-SW localisation in wild-type (top) compared to *lub1Δ* cells (bottom) during SE. Regions of close-ups shown below the Cdc42-mCherry-SW images are marked. Scale bar: 10 µm.

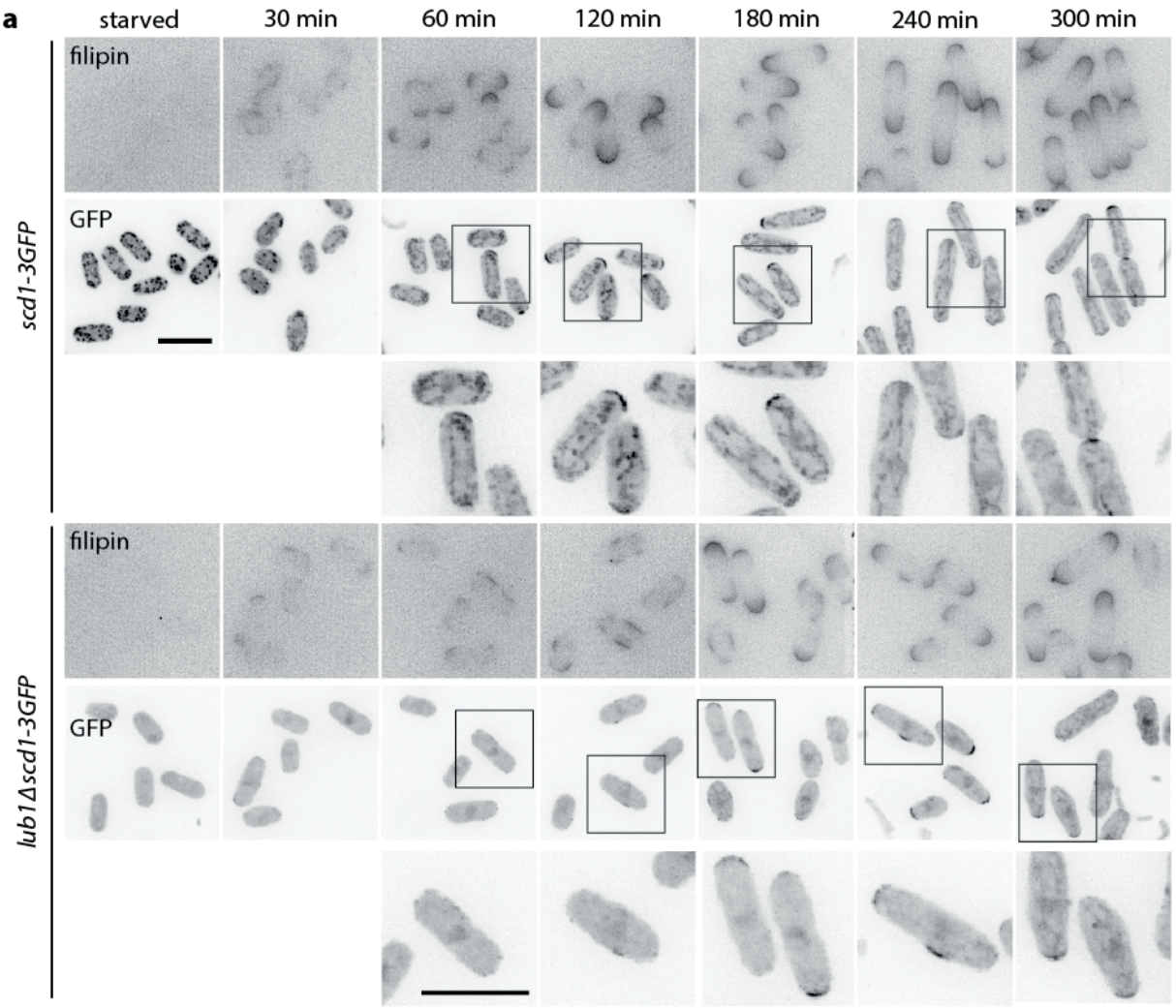

Figure 29: Scd1-3GFP localises to ectopic SRMs in *lub1Δ* mutant cells.

(a) Filipin staining and Scd1-3GFP localisation in wild-type (top) compared to *lub1Δ* cells (bottom) during SE. Regions of close-ups shown below the Scd1-3GFP images are marked. Scale bar: 10 µm.

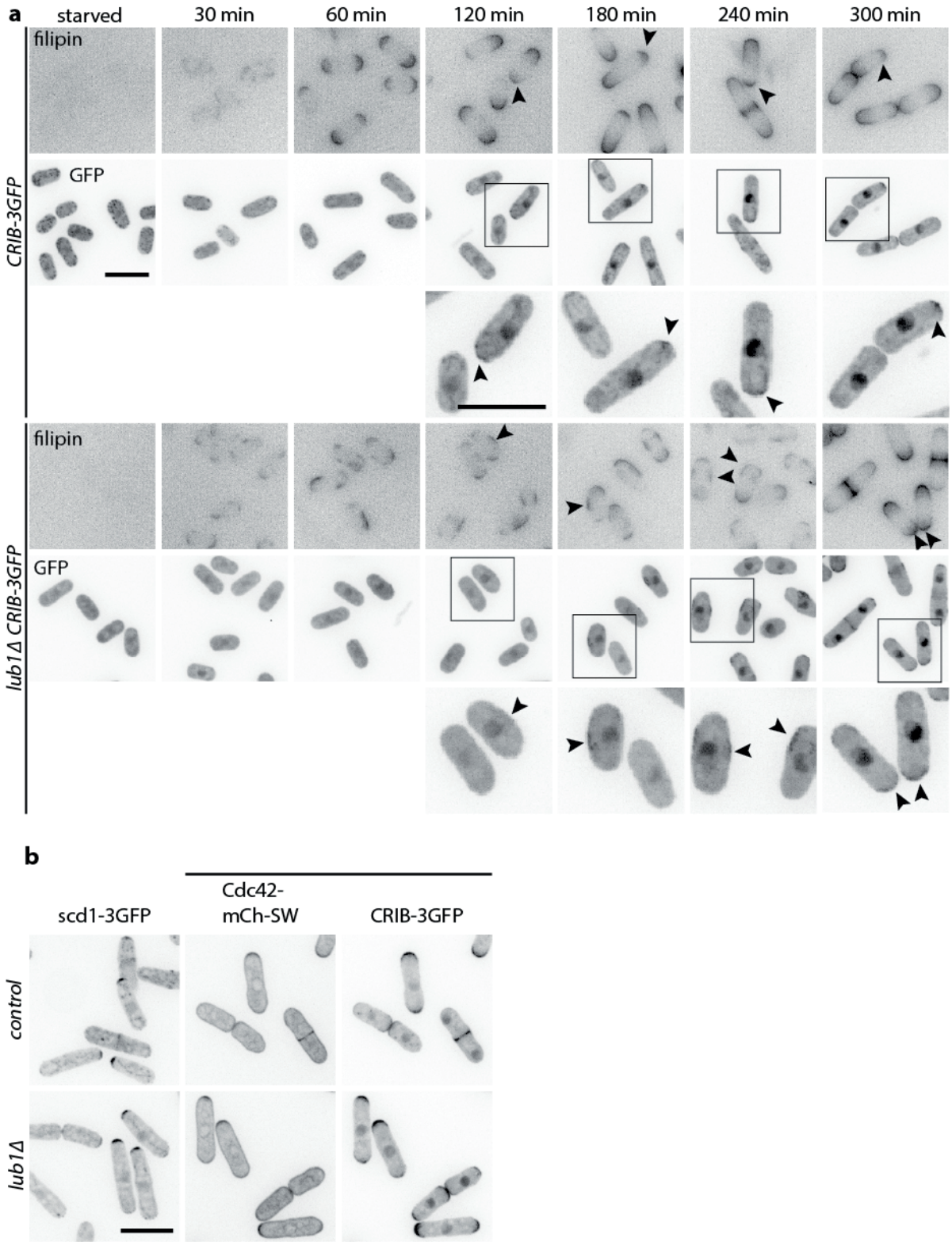

Figure 30: Cdc42 is activated at ectopic SRMs in recovering *lub1Δ* mutant cells.

(a) Filipin staining and CRIB-3GFP localisation in wild-type (top) compared to *lub1Δ* cells (bottom) during SE. Close-up regions shown below the CRIB-3GFP images are marked. Arrowheads: CRIB-3GFP-filipin co-localisation. (b) Scd1-3GFP, Cdc42-mCherry-SW and CRIB-3GFP localisation in exponentially growing cells. Scale bar: 10 µm.

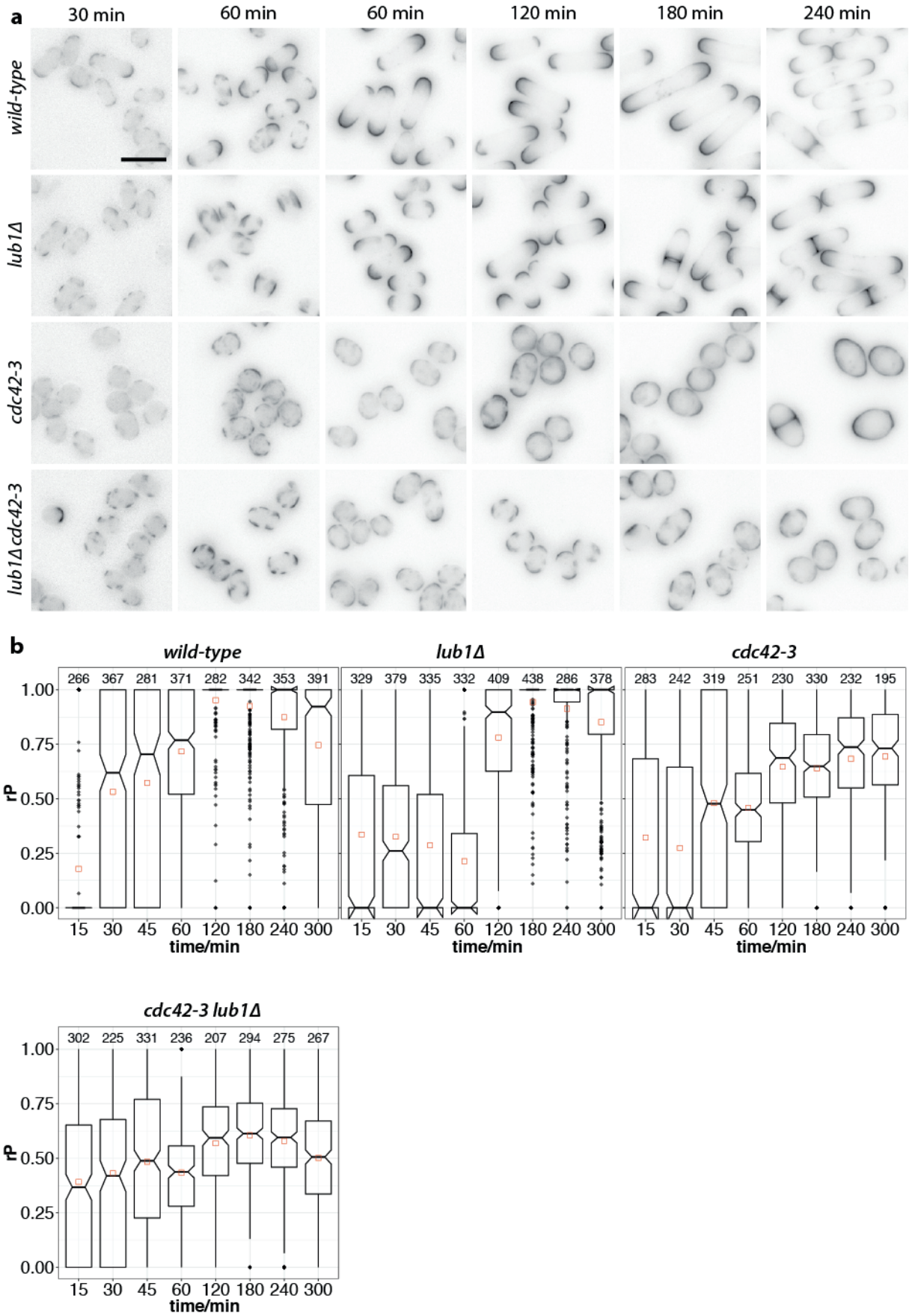

Figure 31: *Lub1Δ* polarisation does not depend on Cdc42.

(a) Filipin-stained wild-type, *lub1Δ*, *cdc42-3* and *lub1Δ cdc42-3* cells during SE at restrictive temperature (36° C). (b) Notched boxplots showing *rP* during SE of wild-type, *lub1Δ*, *cdc42-3* and *lub1Δ cdc42-3* cells.

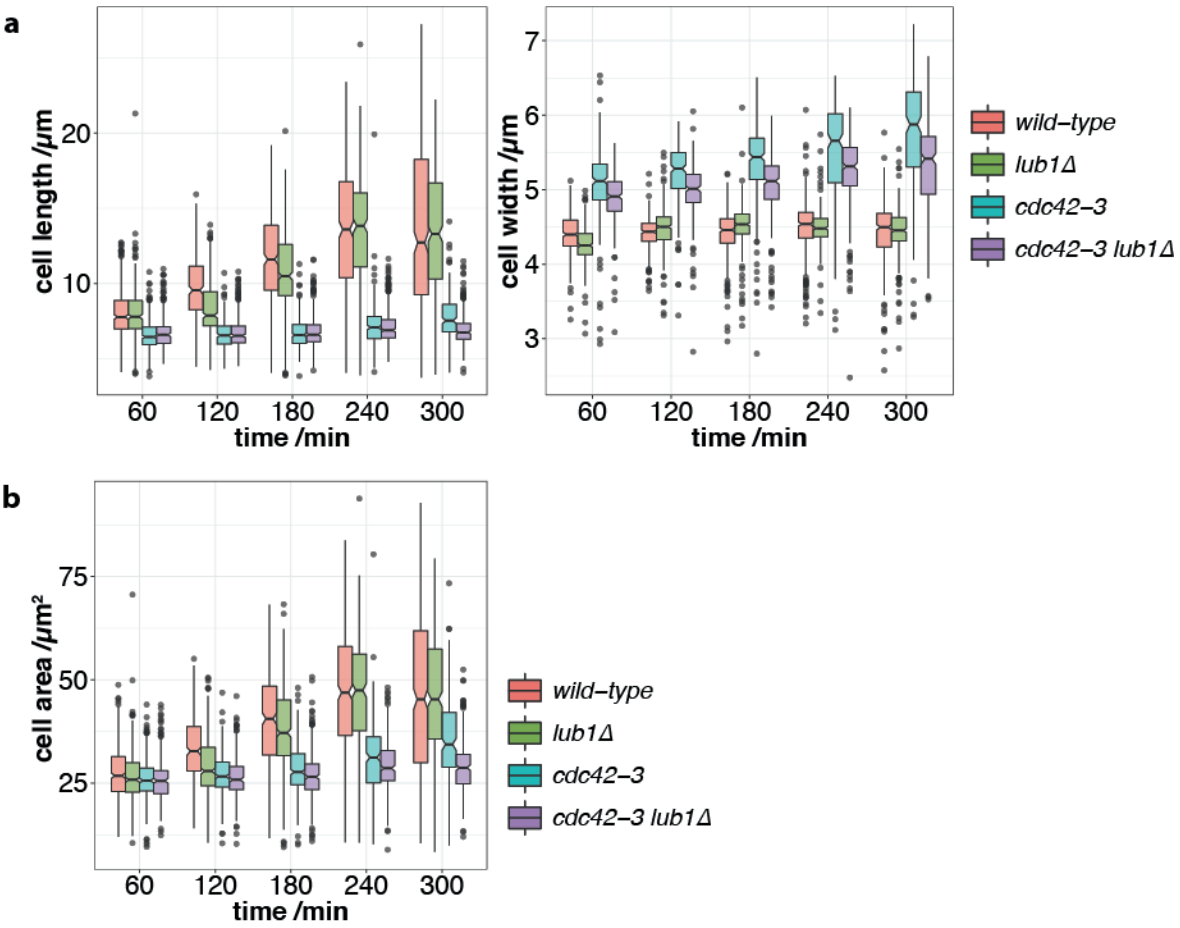

Figure 32: *Lub1Δ cdc42-3* cells grow less at restrictive temperature (36° C) than *cdc42-3* alone.

(a)-(b) Notched boxplots comparing cell length and width (a) and cell area (b) for wild-type (red), *lub1Δ* (green), *cdc42-3* (blue) and *cdc42-3 lub1Δ* (violet) cells during SE at restrictive temperature (36° C).

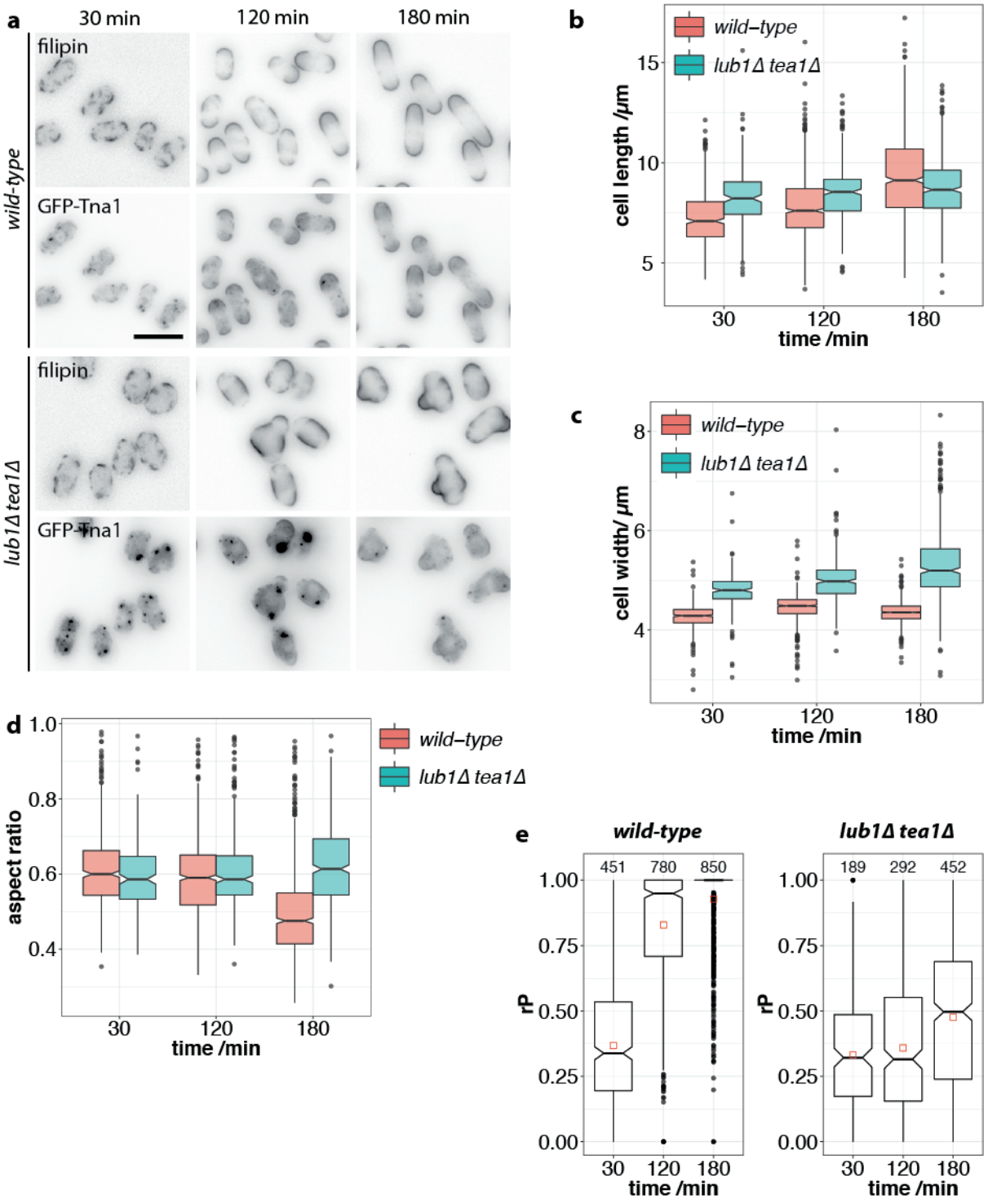

Figure 33: *Lub1Δ tea1Δ* cells branch during SE.

(a) GFP-Tna1 localisation and filipin staining during SE in wild-type (top) and *lub1Δ* cells (bottom) expressing GFP-Tna1. (b)-(d) Comparison of cell length (b), cell width (c) and the aspect ratio (d) of wild-type (red) and *lub1Δ* cells (blue) during SE. (e) Notched box-plots of *rP* during SE of wild-type and *lub1Δ* cells expressing GFP-Tna1. Scale bar: 10 µm.

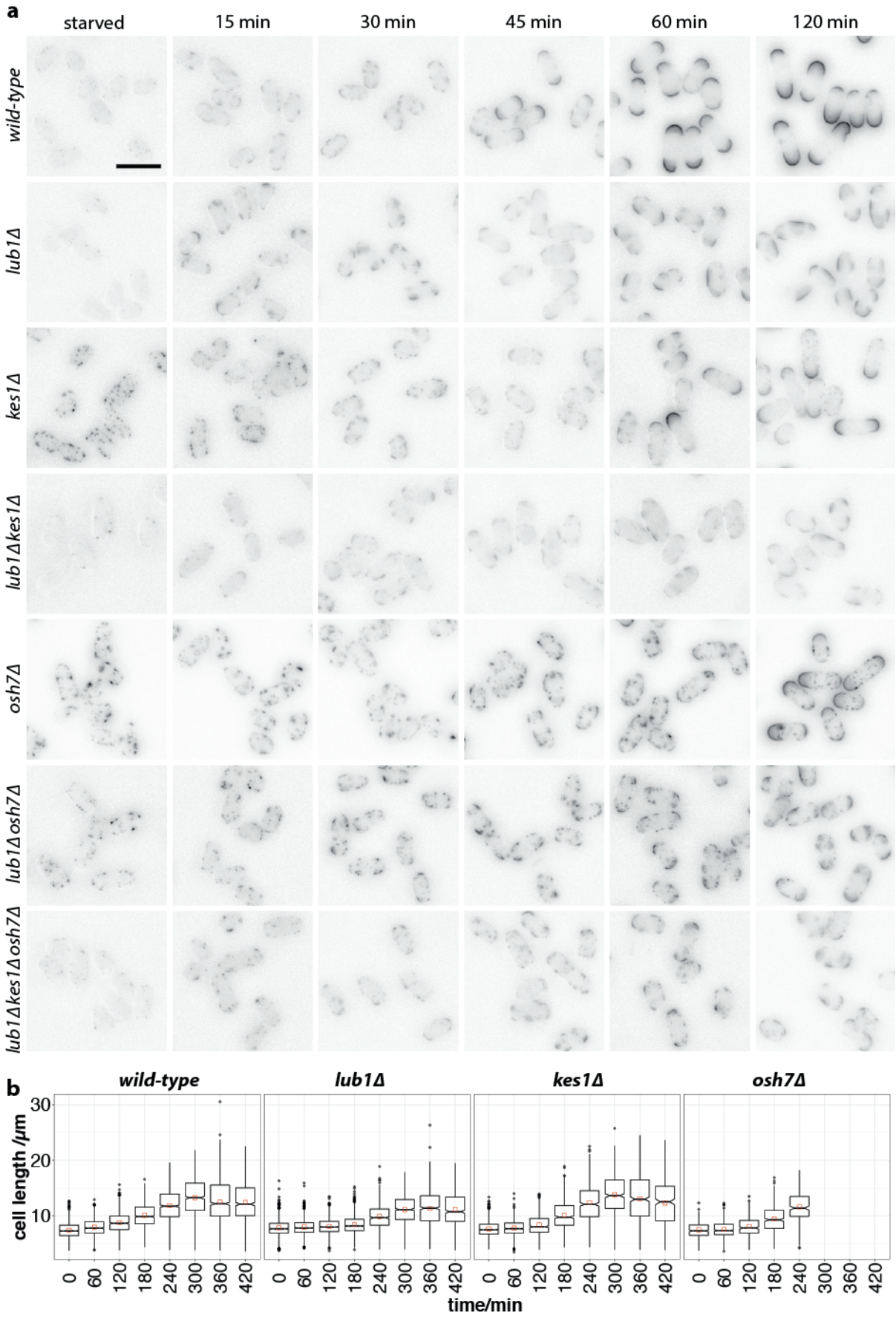
a
starved
15 min
30 min
45 min
60 min
120 min
wild-type
lub1Δ
kes1Δ
lub1Δkes1Δ
osh7Δ
lub1Δosh7Δ
lub1Δkes1Δosh7Δ
b
wild-type
lub1Δ
kes1Δ
osh7Δ
cell length /μm
30
20
10
0
60
120
180
240
300
360
420
time/min

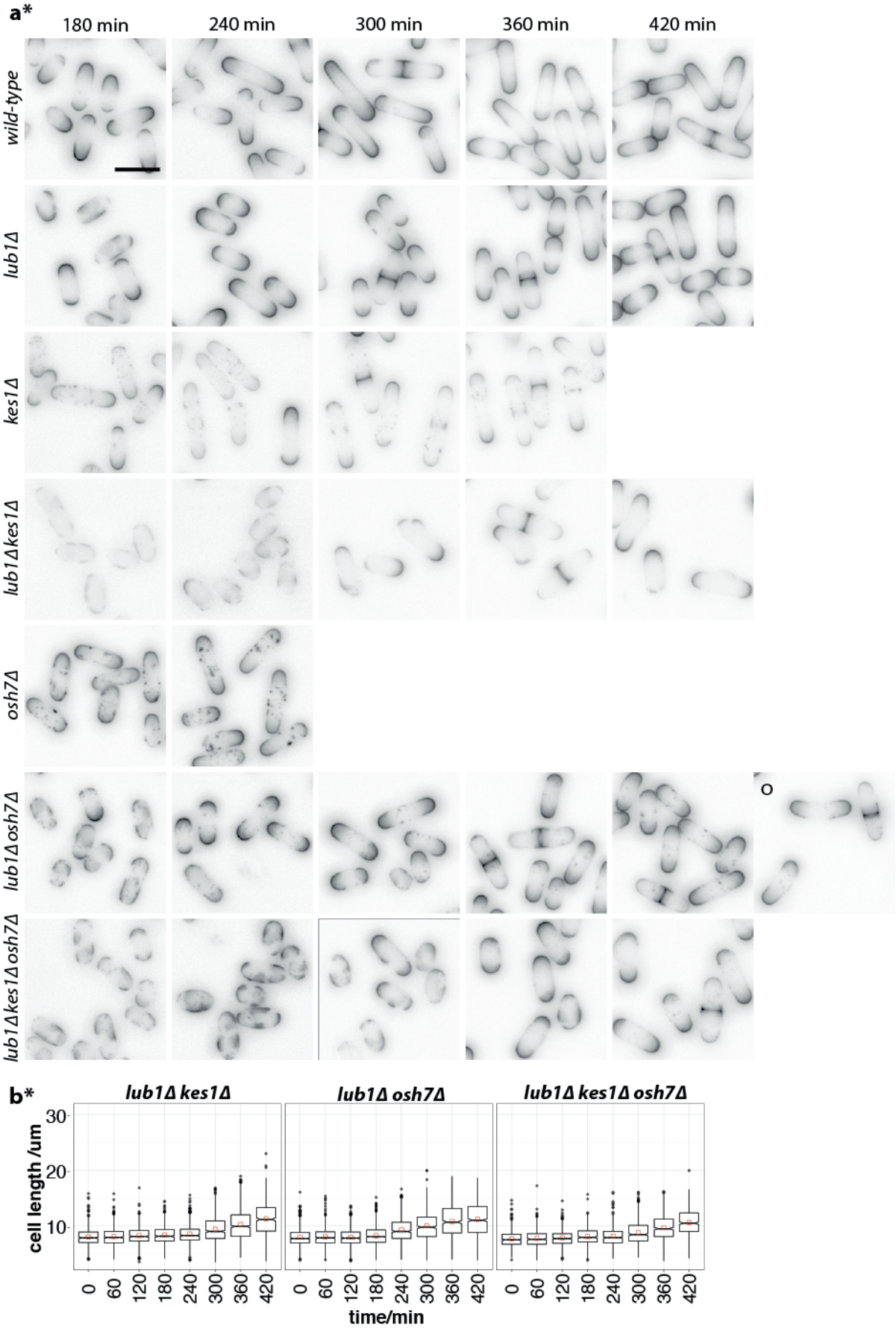

Figure 34: *Lub1Δ kes1Δ* cells transiently grow T-shaped.

(a) Filipin stained wild-type, *lub1Δ, kes1Δ, lub1Δ kes1Δ, osh7Δ, lub1Δ osh7Δ,* and *lub1Δ kes1Δ osh7Δ* cells during SE. Contrast for *osh7Δ* set separately, due to their much higher brightness. (b) Cell length of wild-type, *lub1Δ, kes1Δ, lub1Δ kes1Δ, osh7Δ, lub1Δ osh7Δ,* and *lub1Δ kes1Δ osh7Δ* cells during SE. Scale bar: 10 μm.

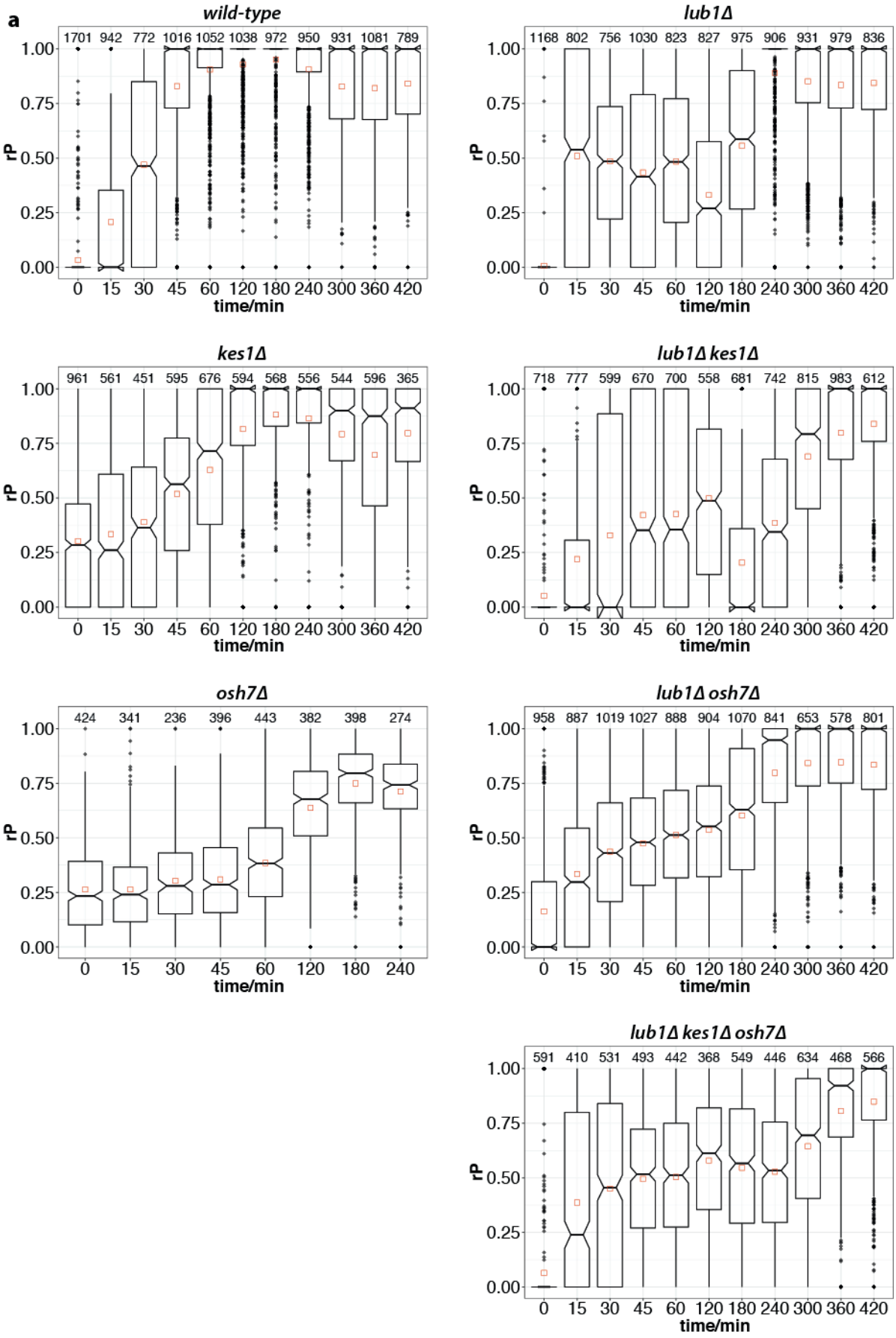

Figure 35: Quantification of polarisation (*rP*) during SE of wild-type, *lub1Δ*, *kes1Δ*, *lub1Δ kes1Δ*, *osh7Δ*, *lub1Δ osh7Δ*, and *lub1Δ kes1Δ osh7Δ* cells.

(a) Notched boxplots showing rP during SE of wild-type, *lub1Δ*, *kes1Δ*, *lub1Δ kes1Δ*, *osh7Δ*, *lub1Δ osh7Δ*, and *lub1Δ kes1Δ osh7Δ* cells.

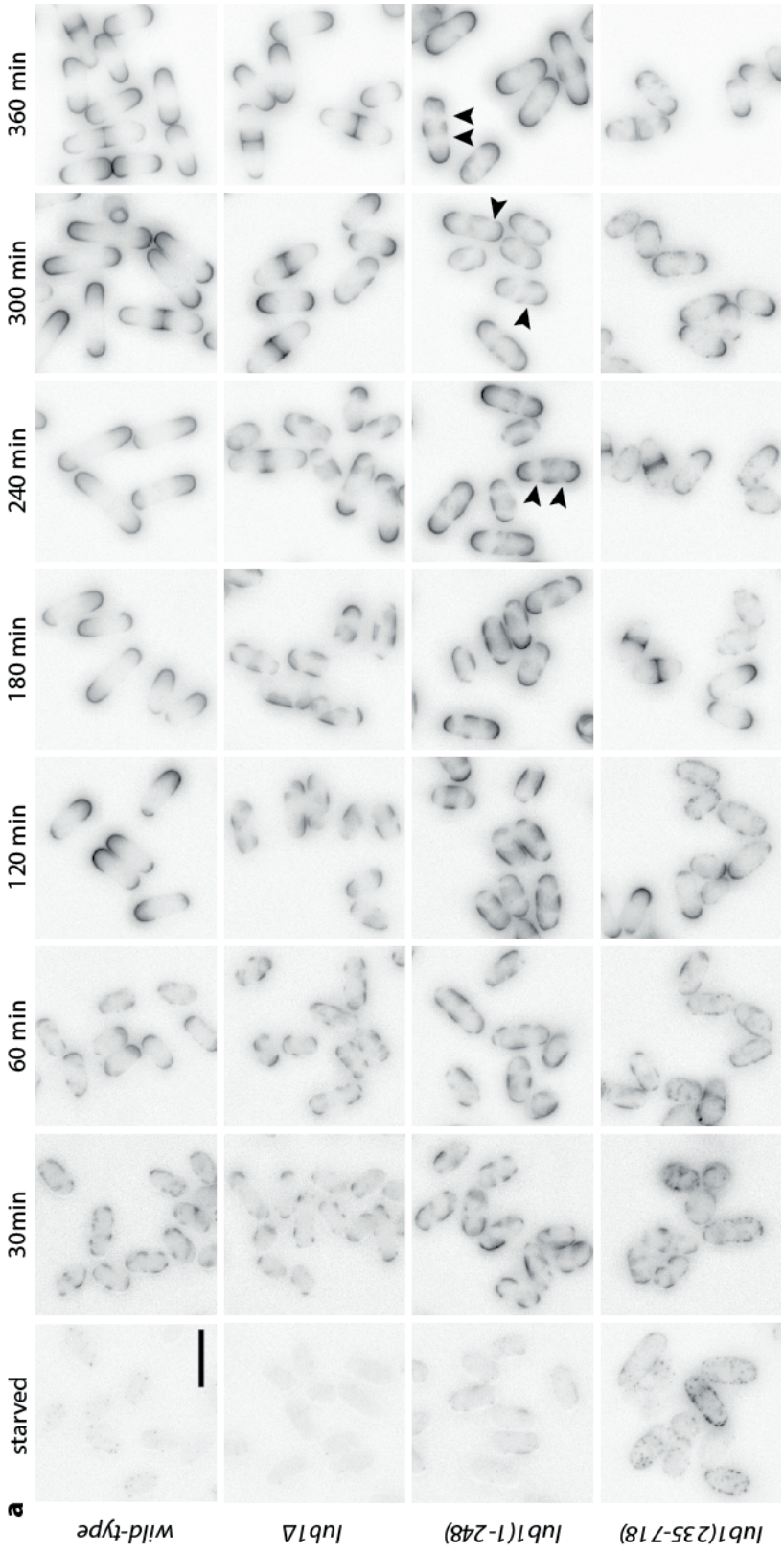

Figure 36: The Lub1 C-terminus partially rescues the *lub1Δ* cell polarisation defect.

(a) Filipin-stained wild-type, *lub1Δ*, *lub1(1-248)* and *lub1(235-718)* cells during SE. Arrowheads: gaps between filipin-stained SRM domains. Cells were woken up on EMM2 before culturing. Scale bar: 10 µm.

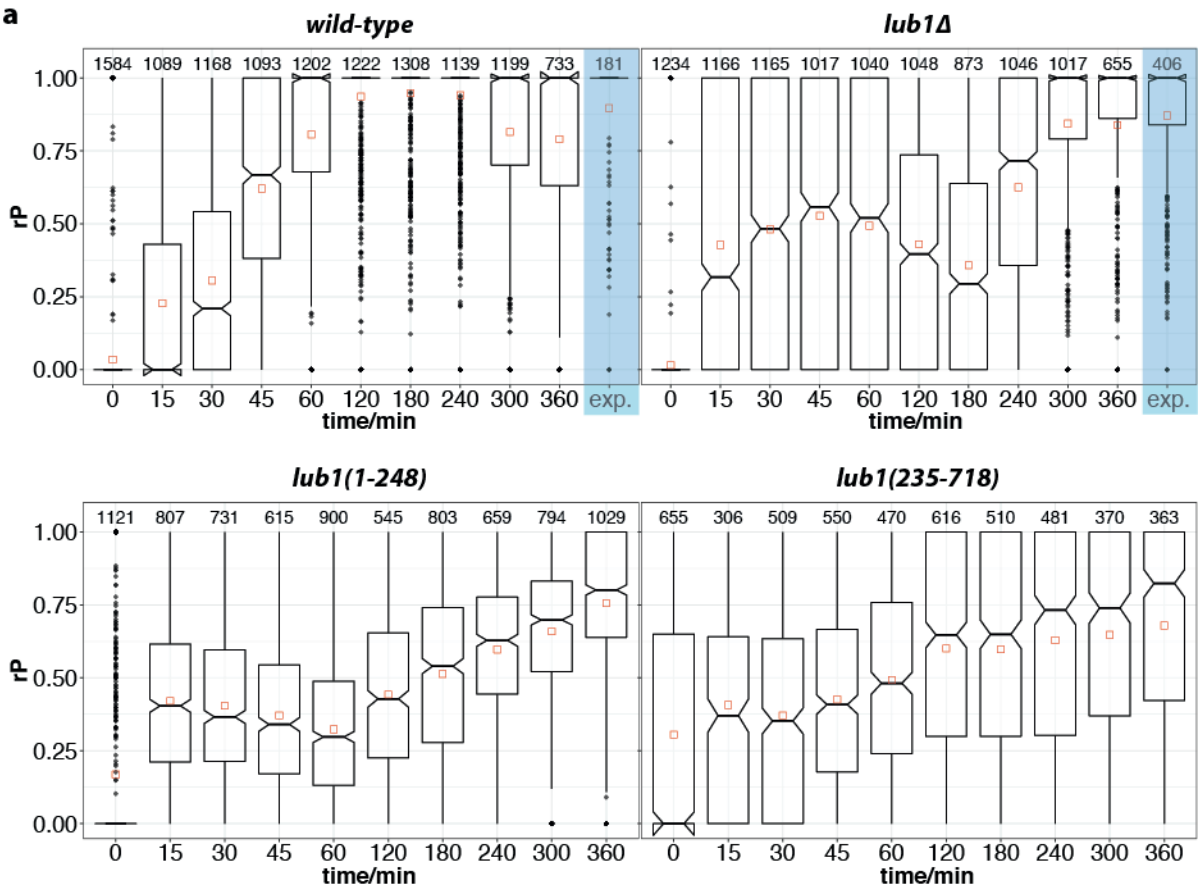

Figure 37: Quantification of polarisation (*rP*) during SE of *lub1Δ* truncations.

(a) Notched boxplots showing rP during SE of wild-type, *lub1Δ*, *lub1(1-248)* and *lub1(235-718)* cells and during exponential growth (blue).

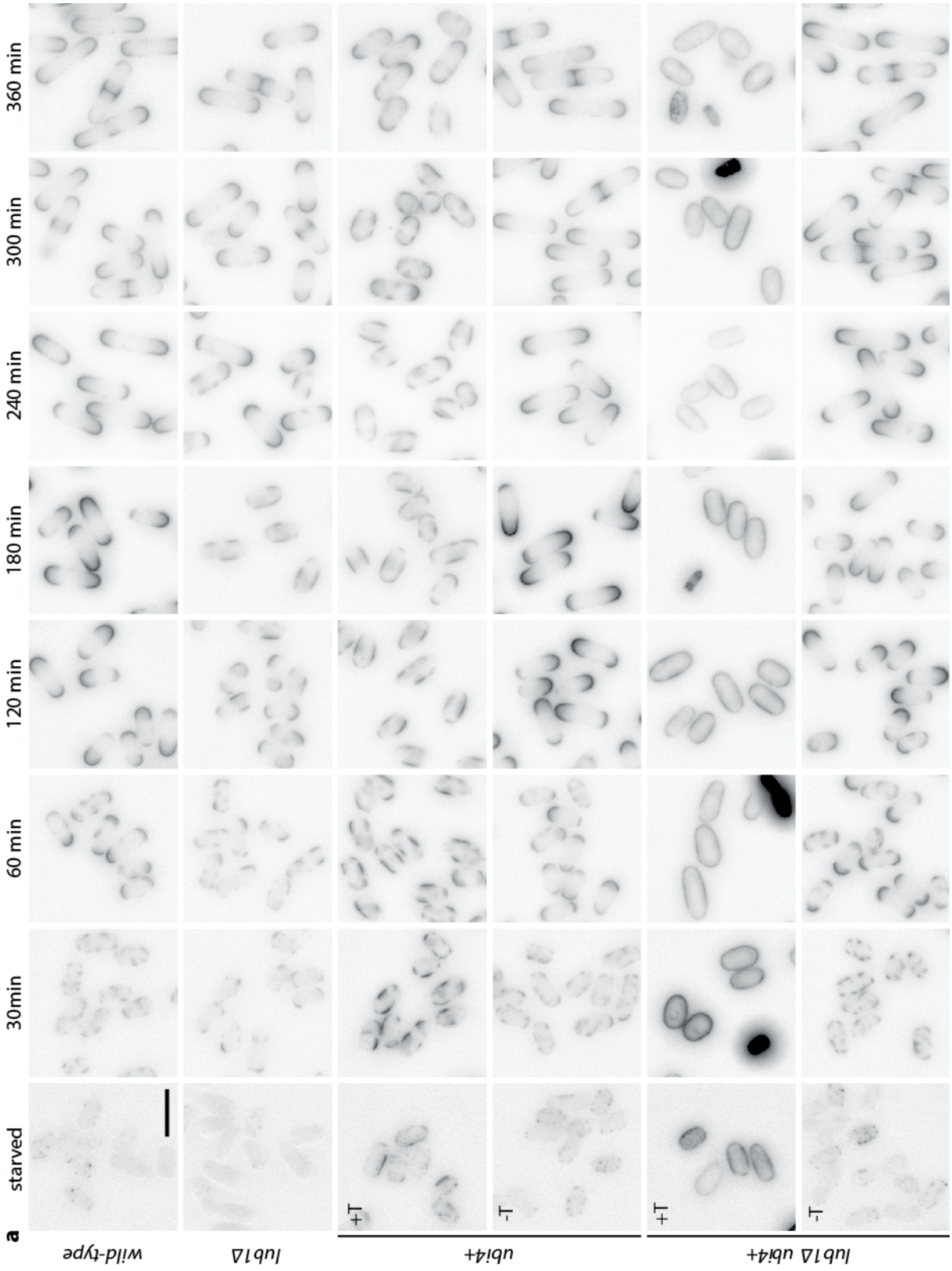

Figure 38: Overexpression of *ubi4* in *lub1Δ* fully rescues their cell polarisation defect.

(a) Filipin-stained wild-type, *lub1Δ*, *ubi4+* and *lub1Δ ubi4+* cells during SE. Thiamine-repressed *ubi4+* (+T) expression and its overexpression in Thiamine absence (-T) as indicated. Scale bar: 10 µm.

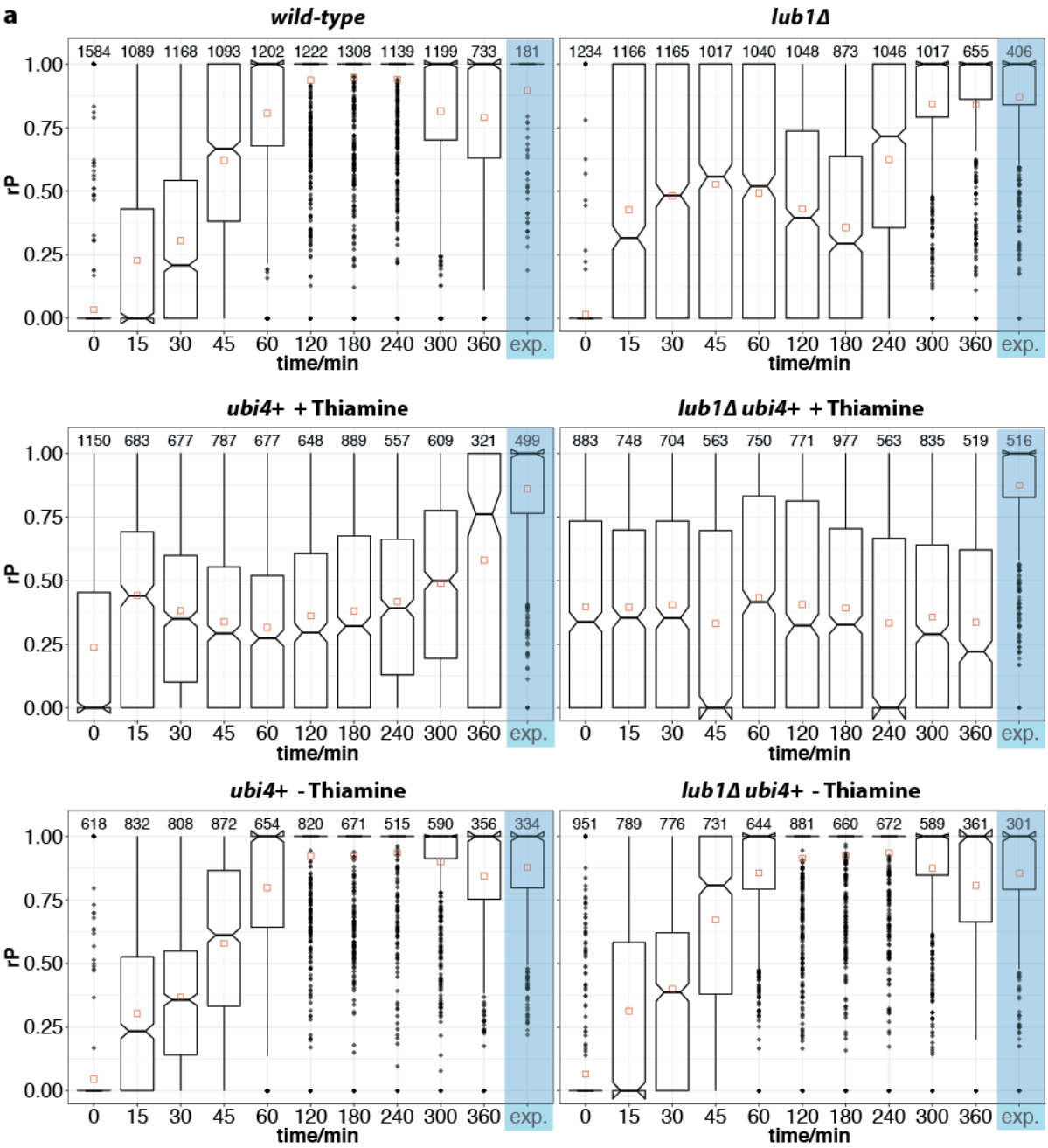

Figure 39: Quantification of polarisation (*rP*) in *lub1Δ* cells overexpressing *ubi4*.

(a) Notched boxplots showing rP during SE of wild-type, *lub1Δ*, *ubi4+* and *lub1Δ ubi4+* cells and during exponential growth (blue). Thiamine-repressed *ubi4+* (+T) expression and its overexpression in Thiamine absence (-T) as indicated. The wild-type and *lub1Δ* controls are the same as in Figure 37. Because both experiments were done on the same days, the mutual controls were pooled for the quantification.

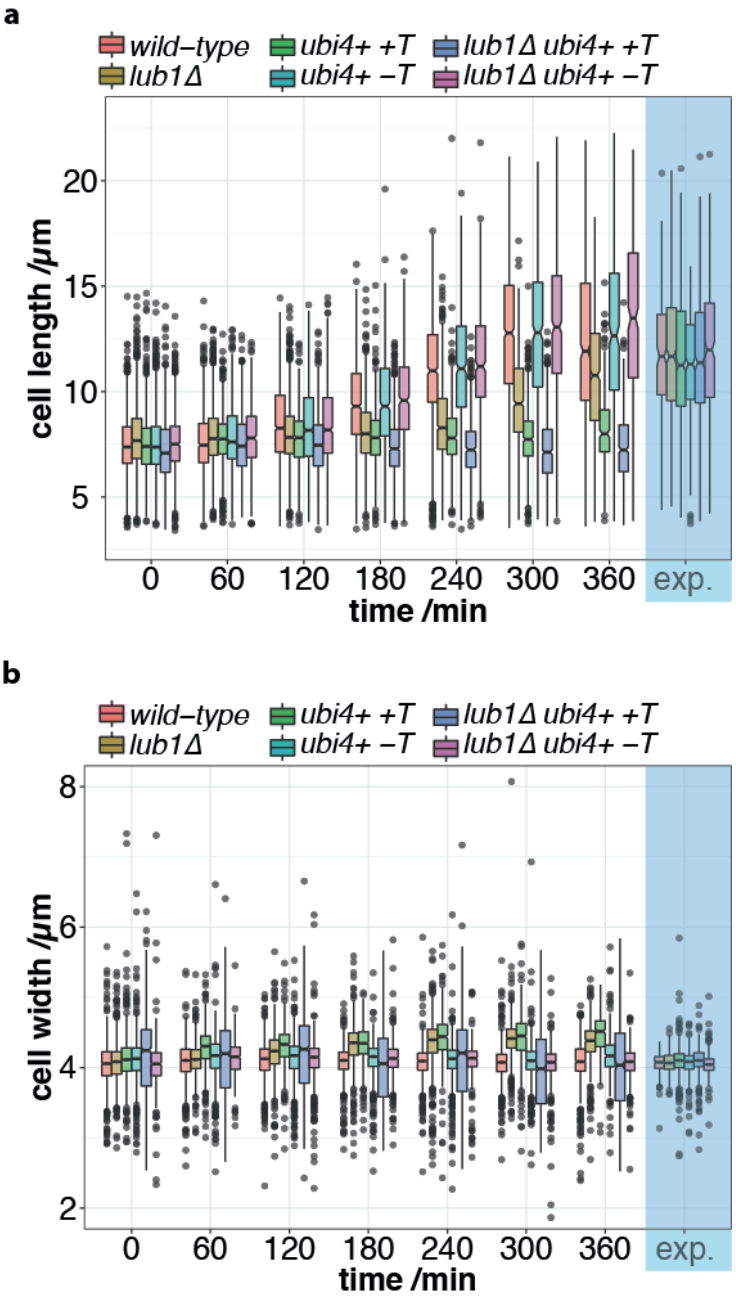

Figure 40: Overexpression of *ubi4* restores growth in length in *lub1Δ* cells.

(a) Cell length of wild-type (red), *lub1Δ* (yellow), *ubi4+* (+T green, -T blue) and *lub1Δ ubi4+*(+T dark blue, -T violet) cells during SE. *Ubi4+* expression repressed (+T) or over-expressed (-T) as indicated.

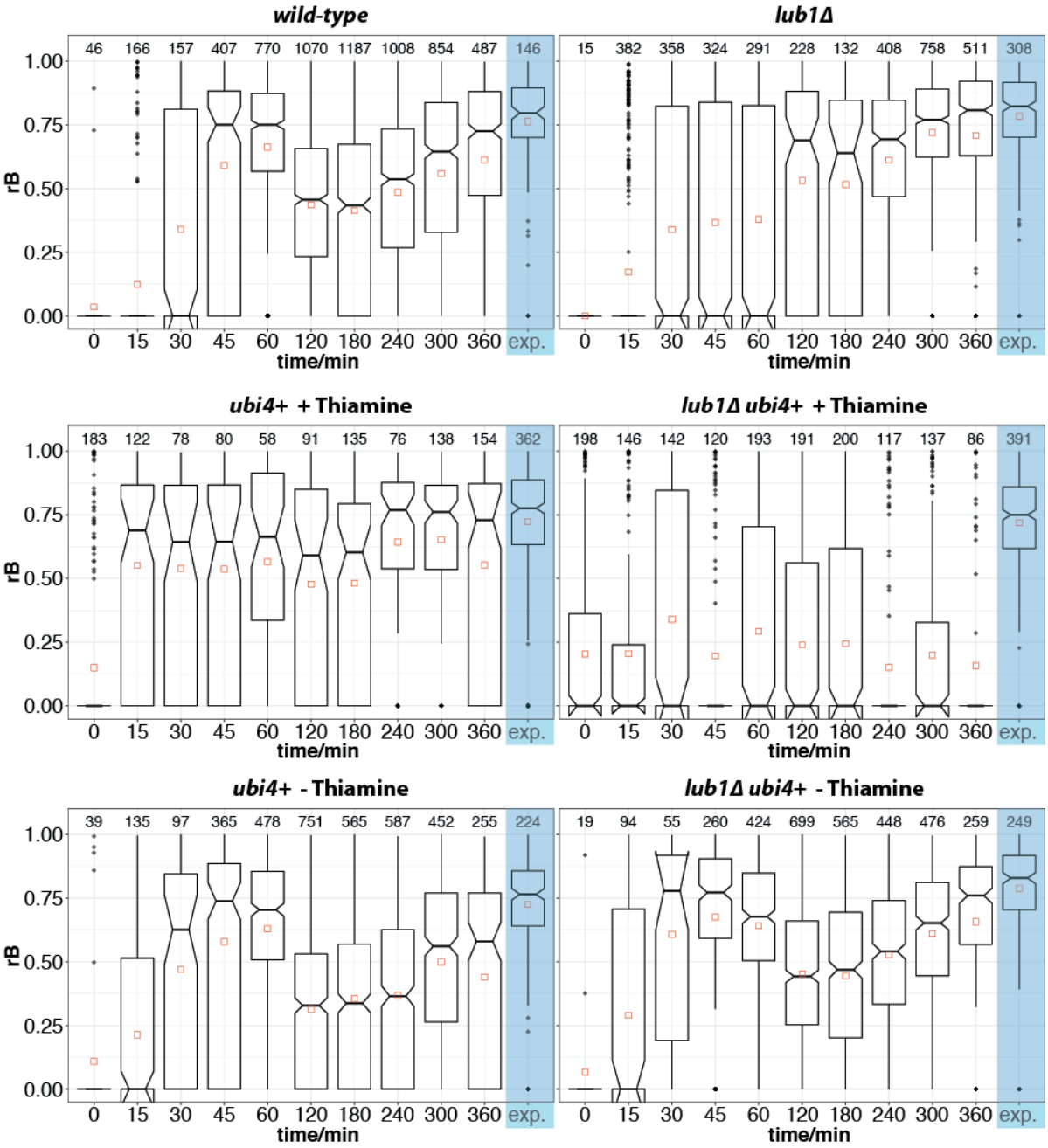

Figure 41: Quantification of bipolarity (*rB*) during SE of *lub1Δ* mutant cells overexpressing *ubi4*.

(a) Notched boxplots showing *rB* during SE of wild-type, *lub1Δ*, *ubi4+* and *lub1Δ ubi4+* cells and during exponential growth (blue). Thiamine-repressed *ubi4+* (+T) expression and its overexpression in Thiamine absence (-T) as indicated. The data from wild-type and *lub1Δ* controls are the same as in Figure 37. Because both experiments were done on the same days, the mutual controls were pooled for the quantification.

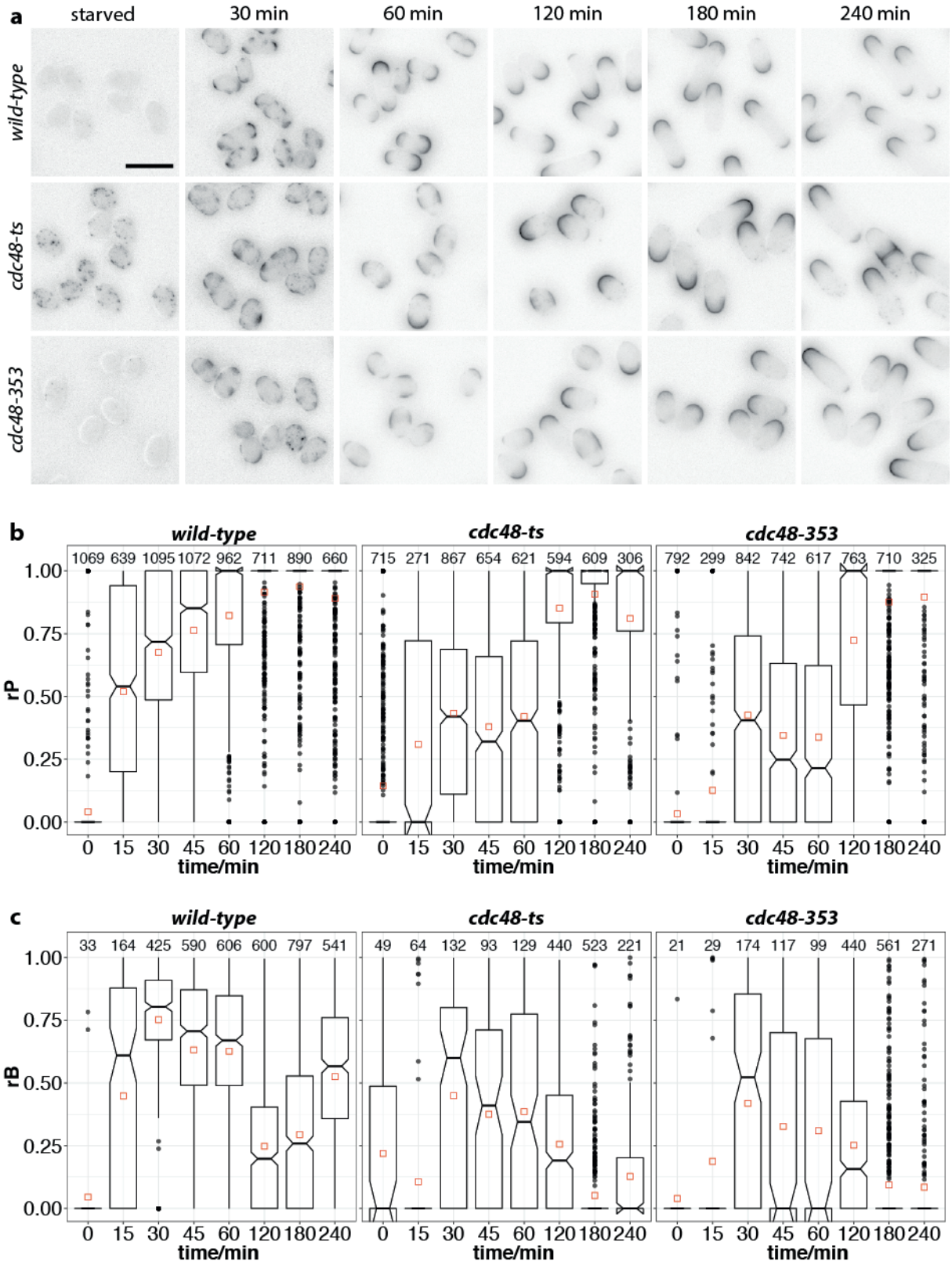

Figure 42: Temperature-sensitive *cdc48* mutants become monopolar during SE at restrictive temperature (36° C).

(a) Filipin-stained wild-type, *cdc48-ts* and *cdc48-353* cells during SE at restrictive temperature (36° C). (b)-(c) Notched boxplots showing *rP* (b) and *rB* (c) during SE of wild-type, *cdc48-ts* and *cdc48-353* cells at restrictive temperature (36° C). Scale bar: 10 µm.

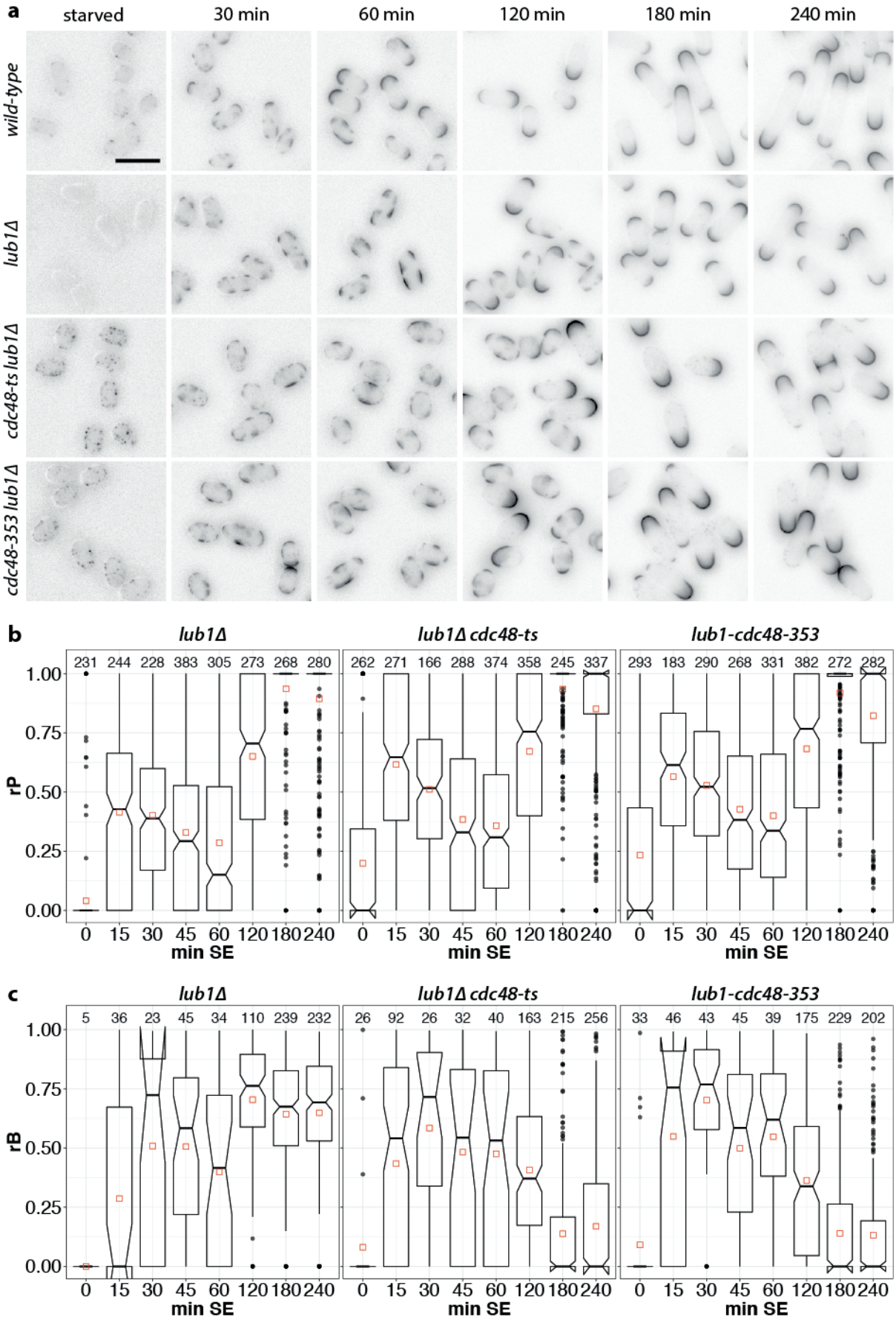

Figure 43: Temperature-sensitive *lub1Δ cdc48* double mutants become monopolar during SE at restrictive temperature (36° C).

(a) Filipin-stained wild-type, *lub1Δ*, *lub1Δ cdc48-ts* and *lub1Δ cdc48-353* cells during SE at restrictive temperature (36° C). (b)-(c) Notched boxplots showing *rP* (b) and *rB* (c) during SE of *lub1Δ*, *cdc48-ts* and *cdc48-353* cells at restrictive temperature (36° C). Scale bar: 10 µm.

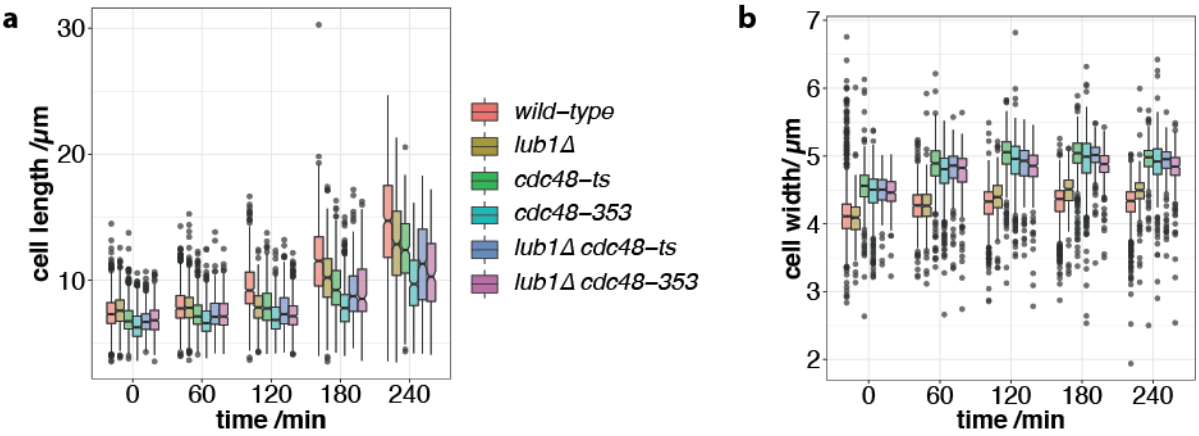

Figure 44: Temperature-sensitive *cdc48* mutants grow in width during SE at restrictive temperature (36° C).

(a)-(b) Cell length (a) and cell width of wild-type, *lub1Δ*, *cdc48-ts*, *cdc48-353*, *lub1Δ cdc48-ts* and *lub1Δ cdc48-353* cells during SE at restrictive temperature (36° C).

3 Summary and Discussion

In my PhD project, I aimed to identify a factor that links Tea1 to the sterol-rich membranes, allowing Tea1 to stabilise those during cell polarisation when cells exit glucose starvation. The approach was to isolate detergent resistant membranes from wild-type and *tea1Δ* mutant cells to compare the protein composition by mass spectrometry.

Within this thesis, the development process of a method to isolate detergent-resistant membranes from fission yeast cells for mass spectrometry was described. The comparison of DRMs from wild-type and *tea1Δ* mutant cells identified novel factors involved in *de novo* cell polarisation, which were characterised subsequently.

3.1 Method development and mass spectrometry screen 1

Chapter 2.1 describes the general method development. The final protocol started with the shock freezing of exponentially growing fission yeast cells in liquid nitrogen followed by mortar grinding also in liquid nitrogen (Figure 2, see also Figure 11). Fluorescent signal originating from the SRM live-marker GFP-Tna1 was preserved and still detected in the ground cells. From this cell powder, DRMs were isolated on an Optiprep step gradient as a floating fraction resistant to Triton X-100 treatment on ice (Figure 4). It was shown by Western blot analysis that GFP-Tna1 localising to fission yeast SRMs *in vivo* and the commonly used DRM marker Pma1 also localised with the floating DRM fraction, while the ER was depleted.

For the first mass spectrometry screen (see chapter 2.2), several DRM samples from wild-type and *tea1Δ* mutant cells were compared. Their protein composition was analysed with MS. Additionally, single samples from *myo1Δ* (SRMs covering the whole plasma membrane), *cdc10-129* (grow monopolar at restrictive temperature) and *cdc25-22* (grow bipolar at restrictive temperature) mutant cells and a sample from a 3-day starvation culture were prepared and analysed (see Table 1 for details).

By analysing the additional mutants, I hoped to identify proteins that vary clearly in their abundance between strains with different growth modes (chapter 2.2.1). This was not the case. Although the isolation protocol worked reliably for all strains, no clear differences in the protein composition were identified with this first approach. However, from the

proteins identified to localise to the isolated DRM fractions by MS, candidate genes were selected for an *in vivo* screen (see chapter 2.2.2). 153 deletion mutant strains were taken from the fission yeast deletion library and analysed at 90 min in SE to screen for strains with a polarisation defect to identify factors involved in cell polarisation. (Table 6, Figure 5). The appearance of the filipin staining of SRMs was classified manually. 18 Deletion mutants either showed a delay in polarisation as they were still in P1 after 90 min, or monopolar SRM localisation, similar to the *tea1Δ* deletion mutant (Figure 6). However, no branching cells were observed. Other phenotypes were characterised by SRMs all over the plasma membrane, detected in three mutant strains, or filipin stainable puncta or dots (classified as dotty), identified in eight strains (Figure 7).

As a start, three deletion mutants – *cfr1Δ, mfs3Δ* and *fzo1Δ* - were selected for further analysis. However, none of them showed a strong delay in polarisation as single mutants (chapter 2.2.4, Figure 8). Additionally, mutant strains initially characterised by their dotty filipin staining during the screen were analysed during full SE experiments at a later stage of the project (chapter 2.2.7, Figure 9 and 9). A method to quantitatively describe the polarisation process by assigning a polarisation ratio (*rP*) value to every cell was developed in the group in the meantime (see chapters 1.6 and 6.2 and Figure 1). This was used to quantitatively analyse the SE of these candidates. The observed dotty filipin staining pattern could not be reproduced in these strains and they all polarised similar to wild-type. I concluded and discussed in chapter 2.2.7 that the experimental setup possibly introduced some artefacts, leading to the observed filipin puncta in the previous experiments.

3.2 Method improvement and mass spectrometry screen 2

As described above, the first attempt to identify factors associated with sterol-rich membranes linking to Tea1 was not successful. However, as the DRM isolation method worked reproducibly, I decided to further improve the method for a second MS screen (see chapter 2.3).

Briefly, RapiGest was introduced to solubilize the precipitated proteins from the DRM fraction as a detergent tolerated during and facilitating tryptic digest. The cleaved peptides were further cleaned from remaining detergent and gradient medium by

purification on MCX columns before MS analysis. All sample preparation steps were carried out by me and only the mass spectrometry analysis was performed externally by the FGCZ.

Importantly, for this second approach, only samples from wild-type and *tea1Δ* mutant samples were prepared, and all samples were analysed within the same MS experiment (see chapter 2.4). This led to the identification of proteins that were differentially present in these two yeast strains (see chapter 2.4.1, Figure 12). Now based on their differential presence in either wild-type or *tea1Δ* cells, 13 candidate genes were selected for *in vivo* analysis during SE to test for a role during cell polarisation (see chapter 2.4.2, Table 3).

Three deletion mutants – *asp1Δ, rnc1Δ* and *lub1Δ* – showed a polarisation delay during SE (see chapter 2.4.3, Figure 13). One of them, the 1/3 inositol polyphosphate kinase Asp1, has been described before as playing a role in polarised growth and is important for invasive growth (Pöhlmann and Fleig 2010; Pöhlmann et al. 2014). However, the described T-shape formation during exit from stationary phase was not reproduced under my experimental conditions (Pöhlmann et al. 2014). As deletion of *asp1* (*asp1Δ*) and the RNA-binding protein Rnc1 (*rnc1Δ*) only led to a minor delay in SE, they were not studied in detail in this work (Figure 14). In contrast, deletion mutant cells of the WD40 protein Lub1 (*lub1Δ*) showed a severe polarisation defect. Therefore, this mutant was subject to further investigations and the results will be summarised below.

One essential gene was identified among the candidates selected for i*n vivo* studies: *crm1*. It encodes for the exportin Crm1, which exports proteins from the nucleus to the cytoplasm (Satoh et al. 2017). Two different temperature sensitive mutants were analysed during SE at their restrictive temperatures (see chapter 2.4.4). The cold-sensitive mutant *crm1-809* (Figure 15 and 15) was delayed compared to wild-type cells during SE at 18° C and started to grow in a T-shape, similar to *tea1Δ* cells. In contrast, the mutant *crm1-1* sensitive to elevated temperature did not show this behaviour at its restrictive temperature 36° C (Figure 17). However, although not delayed in polarisation, this mutant preferably polarised in a monopolar fashion, similar to the strictly monopolar growing *tea1Δ* mutant. Strikingly, deletion mutant cells of the transcription factor Pap1 (*pap1Δ*), involved in stress response and exported from the nucleus by Crm1 (Kawashima et al. 2012), were delayed in polarisation and resembled the monopolar polarisation seen in *tea1Δ* mutants (Figure 18). However, the monopolar phenotype was rather mild

compared to *crm1-1* cells. The double mutant *crm1-1 pap1Δ* was similarly delayed at 36° C compared to the *pap1Δ* single mutant (at 25° C), but was more clearly polarising in a monopolar manner (Figure 19).

Thus, these preliminary experiments demonstrated a potential role of Crm1 in stabilising the second pole during cell polarisation. *Tea1Δ* mutant cells also fail to stabilise SRMs at the second cell end, leading to monopolar growth in exponentially growing cells and to mainly branched or bent cells during SE. This might indicate a functional link between Crm1 and Tea1. However, as Crm1 is localised to the nucleus and involved in the export of almost 300 proteins (Matsuyama et al. 2006), the link is probably indirect and might be mediated via additional factors.

3.2.1 Lub1 as a potential novel regulator of cell polarity

Lub1Δ mutant cells showed the most severe polarisation defect during SE and their cell polarisation during SE was analysed with higher time resolution (see chapter 2.5, Figure 21 and 20). A more detailed discussion of the *lub1*-related results can be found in chapter 2.5.13 and only the key results are presented here.

Characteristic for the *lub1Δ* mutant was the initially higher cell polarisation based on *rP* values compared to wild-type. The values decreased until 180 min in SE before the cells suddenly polarised until 240 min in SE (chapter 2.5.1). The quantifications of the bipolarity ratio (*rB*) indicated that *lub1Δ* cells become more bipolar during SE than the wild-type, meaning the polar SRM caps were of more comparable size/intensity in (bi)polar cells (Figure 22). This finding was further supported by the analysis of time-lapse movies from live-cell imaging, demonstrating that the *lub1Δ* cells indeed grew mainly bipolar, directly after polarising successfully (Figure 23). Interestingly, their growth speed was found to be higher than in wild-type cells (Figure 24). Thus, Lub1 appears to be involved in stabilising polar SRM domains in early SE and might have a role in inhibiting growth at the second end and potentially in general.

Another characteristic of the *lub1Δ* mutant in SE was the prominent lateral localisation of large SRM domains in P1 before the cells polarised. Strikingly, these domains were able to serve as active growth sites with the same timing as polar SRM caps in wild-type cells

(see chapters 2.5.4-6). This was indicated by an increased cell width instead of cell length after 120 min in SE (Figure 26).

Lateral SRM domains in *lub1Δ* cells were able to recruit the polarity marker Bud6, adding further evidence that Bud6 localisation depends on SRMs (see chapter 2.5.5, Figure 27). It was further shown that Cdc42 localises to and is activated at these lateral SRM domains, demonstrating that *lub1Δ* cells are able to initiate growth (P3) before P2. The delayed polarisation appears to be independent of *cdc42-3,* as the *cdc42-3 lub1Δ* double mutant is still able to polarise (see chapter 2.5.7, Figure 31). These results add further evidence for a potential role of Lub1 in preventing growth before cells are polarised.

Microtubules and Tea1 were shown to localise normally in *lub1Δ* mutant cells (see chapter 2.5.3, Figure 25). However, it is not clear whether the delayed polarisation of *lub1Δ* depends on Tea1 (see chapter 2.5.8, Figure 33).

Double mutants with deletions of the oxysterol-binding protein Kes1 gene (*lub1Δ kes1Δ*) showed transient ectopic growth, leading to a low percentage (approx. 4%) of bent or branched cells (Figure 34 Figure 35). However, this ectopic growth was not stable and left cells with lateral bulbs that did not stain with filipin anymore. Still, this might be a hint towards a connection of *lub1Δ* and *tea1Δ,* as *kes1Δ* is also controlled via the microtubule/Tea1 system (see also the manuscript in chapter 4).

Truncation experiments testing the role of the N-terminal WD40 domain of Lub1 (*Lub1(1-248)*) vs. the C-terminal domain (*lub1(235-718)*) did not indicate clearly which part of the protein might be more important during SE (see chapter 2.5.10, Figure 36 Figure 37). However, polarised cells were visible at 120 min in SE in case of *lub1(235-718),* indicating that the C-terminus might be responsible for successful cell polarisation in SE. As discussed in chapter 2.5.13, the unclear result might originate from the high expression level caused by the nmt1 promoter.

Lub1 was previously described to be important for ubiquitin homeostasis and *lub1Δ* mutant stress hypersensitivity phenotypes have been rescued by overexpression of ubiquitin (Ogiso et al. 2004). Strikingly, the overexpression of polyubiquitin by *ubi4* in *lub1Δ* cells also fully rescued the polarisation defect and cells were able to recover from starvation just like wild-type cells (see chapter 2.5.11, Figure 38-Figure 41). Thus, ubiquitin-homeostasis also seems to be important for Lub1 function during SE. It was suggested by Ogiso

et al. (2004) that Lub1 plays a role in polyubiquitination to mark proteins for proteasomal degradation. Whether Lub1 also works like this during SE needs further investigation. Alternatively, ubiquitin could also serve as marker for localisation or modification of other proteins.

I further tested if the observed *lub1Δ* phenotype depends on Lub1's interaction with the essential protein Cdc48 (see chapter 2.5.12, Figure 42Figure 43). This stress-induced, chaperone-like protein is involved in protein degradation, the ERAD pathway and is needed for cleavage activation of the sterol-regulatory element-binding protein (SREBP) Sre1 that regulates biosynthesis of sterols and plays a role in lipid homeostasis (Baek et al. 2013; Hwang et al. 2016). Interestingly, both analysed temperature sensitive mutants – *cdc48-ts* and *cdc48-353* – showed a similar lateral SRM domain distribution in early SE at the restrictive temperature. Furthermore, they initiated growth on the lateral SRM domains like *lub1Δ* cells (Figure 44). They polarised within 120 min and thus polarised 60 min earlier than *lub1Δ* under the same conditions (compare Figure 42Figure 43). However, both *cdc48-ts* and *cdc48-353* polarised in a monopolar manner. This is again reminiscent of *tea1Δ* mutant cells, although the *cdc48* mutants are able to polarise the SRM domains to the cell poles.

3.3 Overall discussion

To conclude, the method I developed to compare DRMs from different fission yeast strains as a mean to study the differences in the composition of SRM domains was able to identify factors involved in cell polarisation of fission yeast. To be able to select candidate proteins for *in vivo* studies based on their detection in isolated DRMs, I modified and improved the protocol used for the first MS screen (see chapter 2.1) for the second attempt (see chapter 2.3).

Probably the most important change that led to comparable results from the analysed wild-type and *tea1Δ* samples was the analysis within the same MS experiment. It was not optimal to compare results originating from different MS experiments before to make use of the generated results. Although I did not test this systematically, I expect that also the use of RapiGest to dissolve the precipitated proteins from the DRMs improved the accessibility of otherwise insoluble proteins for tryptic digest and identification by MS,

therefore adding factors otherwise not identifiable. At the same time, I expect that other proteins might have been less accessible for analysis due to the potentially changed protein composition in the samples. Comparing both MS screens, I noticed that the proteins selected as candidates based on the second analysis would not have been selected based on the results from the first screen. Some candidate proteins were identified in both strains in the first screen and only in one in the second or not identified in one of the experiments. This indicates that the proteins detectable varied between the two sets of experiments. It is possible that the differences reflect the difficulty to detect the proteins in the lower abundance range with the applied method and thus they are sometimes identified, sometimes not. However, for this reason very strict rules were applied when selecting candidates for further analysis (≥2 peptides in ≥3 samples). Additionally, I expected that the DRM isolation improved due to the handling practice gained within the first screen. The freshly prepared samples for the second screen should have been as comparable as possible. Thus, the most important improvement regarding the results was the detection of differences between the two strains to select candidate genes/proteins in an unbiased way. In this regard, the rule that at least two peptides of a protein had to be identified for me to consider it might have introduced another bias. For example, while they appeared to be only present in either strain, at least one spectrum from Asp1, Rnc1 and Lub1 was identified also in the other strain. From the candidates studied in more detail, only Crm1 was detected in wild-type samples only.

Despite these problems, I demonstrated that factors involved in cell polarisation were identified with the preliminary analysis of the deletion mutants presented in this thesis. With Lub1, a potential link between the polarity factors and SRM domains has been found. This can be regarded as a proof of concept that the applied method is able to pull out new factors of DRMs from fission yeast.

3.4 Outlook

Lub1 appears as a promising factor to be analysed in more detail. It would be interesting to test if Lub1 is enriched in the floating fraction when isolating DRMs on an Optiprep gradient. GFP-tagged Lub1 did not show any prominent localisation to the cell poles, and only weak, cytoplasmic localisation was detected in exponentially growing cells (data not

shown). Thus, it would be interesting to test its localisation during SE, which might require a stronger fluorescent signal.

Furthermore, inhibition of the proteasome with specific drugs should provide more information if Lub1 function during SE depends on ubiquitin-mediated, proteasomal degradation. It would also be interesting to test if overexpression of ubiquitin in the *cdc48* mutant background is able to rescue the monopolar polarisation phenotype.

The MS results I generated during my PhD project can serve as an entry point for further studies. They provide a resource to select additional candidate genes/proteins to be tested *in vivo*. As discussed above, due to the rules applied for the selection of candidates in this work, many potentially interesting factors were left out that were detected in only one of the strains but with less peptide spectra. Among these, more interesting factors involved in cell polarisation might be hidden.

Additionally, the fractionation protocol could now be used to analyse DRMs isolated from fission yeast cells at different timepoints during SE, for example. I expect that it should be possible to identify factors that vary during SE. Also, the analysis of DRMs from mutants studied within this thesis might provide insights into their function. For example, it would be interesting to isolate DRMs from *lub1Δ* cells while they still have lateral SRMs and compare them with the polar ones. Analysing the proteins associated with the DRM fraction of monopolar *cdc48-ts* or *cdc48-353* mutants might thus provide some insight into their interaction with Lub1 during cell polarisation.

As the results between the different experiments appear to vary greatly, it would be interesting to analyse a subset of proteins that were identified as (potential) candidates in a quantitative mass spectrometry experiment. By selecting only those low-abundance proteins that might differ between strains for selected reaction monitoring (Lange et al. 2008; Picotti et al. 2009) to quantify their abundance, it could be tested if they do vary or if the differences I observed were rather due to minor variations between the individual samples.

However, in any case it is well possible to miss the actual link to SRM domains with the applied method. Besides preparational and detection problems, it is not unlikely that the factor I was looking for transiently interacts with Tea1 to stabilise polar SRM domains, but does not associate strongly enough with SRM domains to be isolated with DRMs. Although this potential problem should be considered for future experiments, the presented work so far supports the assumption that factors involved in cell polarisation during SE can successfully be isolated and identified within DRM from fission yeast.

4 Manuscript in preparation

The microtubule/tea1p system controls cell polarisation via non-vesicular lipid transport

Adam Rafal Kijowski[1], **Michèle Gemünden**[1], David Dreher[1], Robin W. Klemm[1] and Damian Brunner[1]*

[1] Department of Molecular Life Sciences, University of Zurich, Winterthurerstrasse 190, 8057 Zurich, Switzerland

Summary paragraph

Cell polarisation is a fundamental process in proliferating and differentiating cells. The *de novo* polarisation of fission yeast cells exiting from starvation provides a powerful experimental model for investigating this process. Polarisation and growth initiation depends on *de novo* biosynthesis of sterols and their enrichment in distinct plasma membrane domains that define prospective growth sites[1]. The proper polar positioning of these domains is cdc42p-independent but requires microtubules, which deposit the key polarity factor tea1p at cell poles[1,2]. The mechanisms underlying the initial cell surface delivery of sterols into multiple distinct domains, and their subsequent polarisation by microtubules and tea1p are largely unknown. Here we show that the formation and polarisation of sterol-rich membrane domains does not depend on vesicular membrane traffic. Rather it occurs through non-vesicular lipid transport involving the oxysterol-binding protein kes1p. It has been proposed that oxysterol-binding proteins exchange sterols between closely apposed membranes[3]. In cells lacking kes1p, cell polarisation becomes cdc42p-dependent. Intriguingly, the cdc42p function employs a second non-vesicular

sterol transport system, involving the oxysterol-binding protein osh7p. Eliminating phosphoinositide-4-(PI4)kinase activity hampers cell polarisation and growth initiation similar to the simultaneous deletion of *kes1* and *osh7*, providing *in vivo* support for a previously proposed mechanism in which oxysterol-binding proteins deliver sterols in exchange with PI4P[4]. Our study assigns a specific role to non-vesicular lipid transport in cell polarisation and disentangles redundant, microtubule/tea1p-mediated polarity pathways.

Main

To determine how the MT/tea1p system controls sterol-rich membrane (SRM) domain polarisation, we carried out functional perturbation experiments using small molecule inhibitors and genetics. We developed automated image analysis to quantify the degree of cell polarisation in comparison to wild type cells (Supplementary Information). Since sterols are produced in the endoplasmic reticulum (ER), we hypothesised that their plasma membrane delivery requires vesicular membrane traffic via the Golgi apparatus. To test this, we first added Brefeldin A (BFA), a drug that interferes with Golgi integrity, to cells in starvation exit (SE) (Methods)[5]. We confirmed drug action by showing that BFA efficiently interfered with the delivery of the multi-pass transmembrane protein GFP-tna1p, which brightly labels SRM domains during SE in untreated cells (Extended Data Fig. 1a)[1]. Intriguingly, BFA did not prevent SRM domain formation and polarisation (Fig. 1a). Since sterol delivery to the plasma membrane can bypass the Golgi apparatus in mammalian cells, we tested whether *de novo* cell polarisation is defective in strains carrying temperature-sensitive (ts) alleles of essential vesicular trafficking components (Methods)[6,7]. SE of wild type cells occurred through the same sequence of events at permissive (25°C) and restrictive (36°C) temperatures and merely showed different kinetics compared to previously published experiments carried out at 30°C (Extended Data Fig. 1b)[1]. Unfortunately, surface transport of GFP-tna1p was impaired at 36°C, precluding its use as a marker in our ts-mutant analysis (Extended Data Fig. 1c). We therefore analysed SE of trafficking mutants by monitoring Filipin-stained SRM localisation. Despite the strong block in secretion in these mutants, SRM domain formation and polarisation occurred (Extended Data Fig. 1d)[8-11]. To increase interference with vesicular trafficking, we combined *sec3-916* and *sec8-1* ts-mutants, which cause proliferation arrest at 36°C, with

deletions of *exo70* and *for3* respectively[8,11-13]. The latter are known to interfere with the late secretory pathway. We found that the double mutants formed and polarised SRM domains at 36°C, even when additionally treated with BFA (Fig. 1b; Extended Data 1e). Thereby, we only detected a slight delay in completion of SRM domain polarisation. To exclude the activity of an unknown vesicular transport pathway, we attempted to block fusion of intracellular membrane systems with the plasma membrane. For this we used cells simultaneously expressing ts alleles of the essential plasma membrane-resident t-Snares psy1p and sec9p[14,15]. These cells formed and polarised SRM domains at the restrictive temperature of 36°C (Fig. 1c). Altogether these results indicate that the formation and polarisation of SRM domains does not critically depend on the vesicular transport machinery.

An alternative pathway mediating lipid exchange between different organelles occurs via a non-vesicular transport system comprised of the evolutionarily conserved family of oxysterol-binding proteins (OSBPs)[3,16-18]. Fission yeast has six predicted OSBPs, none of which is essential (Extended Data Fig. 2; Supplementary Information)[7]. To test for a role of these proteins in SE, we analysed deletion strains of each of these genes (Methods). During SE, only deletion of *kes1* (*kes1Δ*) and *osh7* (*osh7Δ*) indeed showed a detectable delay in initiating SRM domain formation and polarisation (Fig. 2a, Extended Data Fig. 3a). Notably, the measured polarisation ratios in these cells started at a higher value than the wild type and did not reach the maximal polarisation rate in the first cell cycle of SE. This was due to Filipin-stained punctae that were present all over the cell periphery in starved *kes1Δ* and *osh7Δ* cells, indicating defective sterol removal from the plasma membrane during starvation entry (Fig. 2a)[19,20]. The sterol punctae persisted throughout SE and did not enter newly grown plasma membrane regions, indicating that they were immobile and did not contribute to new SRM domain formation (Extended Data Fig. 3b).

Since *kes1Δ* and *osh7Δ* cells merely showed delayed SRM domain polarisation, we tested these proteins for functional redundancy with each other, or with the other OSBPs by generating double mutant combinations. Only in *kes1Δ osh7Δ* double mutants was the phenotype of the single mutants enhanced. The enhancement was substantial with the first cells showing polarised SRM domains only after 3-4 hours and even after 6 hours their number remained low (Fig. 2b). This reveals a crucial role for non-vesicular lipid transport in SRM domain formation and polarisation, mediated by kes1p and osh7p.

Non-vesicular sterol trafficking by some OSBPs was proposed to involve counter-flow

transport of sterols and phosphatidylinositol 4-phosphate (PI4P)[21]. To test if such lipid exchange occurs during cell polarisation, we analysed SE of cells expressing a temperature-sensitive variant of pik1p (*pik1-td*), the kinase producing PI4P[22]. Compared to *kes1Δ osh7Δ* cells, *pik1-td* cells exiting starvation at the restrictive temperature were even more inhibited in their ability to form and polarise SRM domains, and after 6 hours only very few of these domains were polar (Fig. 2c). This suggests that phosphoinositides act together with the OSBPs to form and polarise SRM domains at the plasma membrane, which may well involve the previously proposed OSBP-mediated counter flow of sterols and PI4P.

The fact that *kes1Δ osh7Δ* cells eventually still manage to form and polarise SRM domains, suggests that these cells may compensate for the loss of non-vesicular transport by switching to vesicular transport. However, BFA-treatment of *kes1Δ osh7Δ* cells did not noticeably change the mutant phenotype indicating that this is not the case (Fig. 2d).

Cdc42p, was previously shown to spontaneously polarise yeast cells[23,24]. In wild type cells polarising *de novo* during SE, cdc42p was shown to be dispensable and its activity was detected only after cells had completed SRM domain polarisation. We hypothesised that this activity may be responsible for the delayed rescue of polarisation in a subset of *kes1Δ osh7Δ* cells. To investigate this possibility, we combined the *kes1Δ* and *osh7Δ* deletions with the *cdc42* ts-allele *cdc42-3*[25]. *Cdc42-3* causes a particularly strong loss-of-function that generates cells that grow with a rounded morphology even at permissive temperatures (Fig. 3a). Notably, when exiting starvation, such rounded cells could not produce the bipolar microtubule arrangement known to be required for polarised tea1p deposition (Fig. 3b). Consequently, SRM domain polarisation - which was shown to depend on polar tea1p - was delayed at permissive and restrictive temperatures (Fig. 3c, Extended Data Fig. 3c)[1]. Yet these cells formed the typical SRM caps at both cell poles confirming an otherwise functional cell polarisation process. This was very different from *kes1Δ cdc42-3* double mutant cells, which were unable to polarise their SRMs and usually ended up with a single, prominent, but randomly positioned SRM domain (Fig. 3d). This indicates that SRM domain polarisation in *kes1Δ* mutants is fully dependent on cdc42p. It further shows that osh7p no longer can compensate for the loss of kes1p, suggesting that its rescuing activity in *kes1Δ* cells requires cdc42p. Conversely, kes1p activity is independent of cdc42p, since *osh7Δ cdc42-3* double mutants can form and polarise SRM domains similarly to the *cdc42-3* single mutant (Fig. 3c, 3e). We conclude that cdc42p/osh7p

provide a redundant non-vesicular sterol trafficking pathway that rescues SRM domain formation and polarisation in the absence of kes1p, and that becomes activated only after the kes1p pathway has completed cell polarisation in wild type cells. Notably, the few SRM domains slowly forming in *kes1Δ cdc42-3* cells hint at a cdc42p-independent osh7p activity that may contribute to the formation of the first, randomly positioned SRM domains.

Since in *kes1Δ* and *kes1Δ osh7Δ* cells the rescuing cdc42p activity reliably positions growth sites at the cell poles, it should be under tea1p control as previously suggested in polarizing spheroplasts[26]. In support of this model, additional deletion of *tea1* (*tea1Δ*) in *kes1Δ* cells resulted in the random selection of one of the SRM domains as a polarized growth site - similar to what was previously reported for *tea1Δ* single mutants (Extended Data Fig. 3d)[1].

SRM domain polarisation may occur through direct control of non-vesicular sterol transport by tea1p, for example, by localising pik1p, or kes1p and osh7p. However, during SE, functional GFP-tagged versions of these proteins did not specifically localised to the cell poles (Extended Data Fig. 4; Methods)[22]. While all three proteins stained the entire cell volume, GFP-pik1p and osh7p-GFP additionally accumulated in few sub-cellular spots and the nucleus. During SE, kes1p-GFP and osh7p-GFP - but not GFP-pik1p - started accumulating all over the cell periphery. Consistent with its early role, kes1p-GFP did so after 15minutes, while peripheral osh7p-GFP only became visible at around 45 minutes - fitting well with its dependence on cdc42p activation. Kes1p-GFP accumulated in additional sub-cellular structures at around the time when growth started. This indicates additional functions in growth homeostasis, as suggested in budding yeast[19,21]. We conclude that tea1p does not function by localising the factors mediating non-vesicular sterol transport, but more likely by promoting the recruitment of other, key regulatory activities.

In summary, our results suggest that during SE of wild type cells, kes1p provides non-vesicular sterol transport to form and subsequently polarise SRM domains under tea1p control (Fig. 4). Cells lacking kes1p wait until sufficient cdc42p activity has built up to activate osh7p-dependent, non-vesicular lipid transport. Whether kes1p activity depends on a GTPase similar to cdc42p remains to be shown.

Despite good evidence that non-vesicular transport is an important mechanism of lipid transfer between various membranes, specific cell biological function for this pathway

had not been identified. Our data provide first evidence that non-vesicular delivery of *de novo* synthesised sterols from the ER to the plasma membrane is central to the generation of *de novo* cell polarity, a fundamental event in eukaryotic cells. Future work will address how tea1p is able to confine the non-vesicular sterol transport pathway to the cell poles. It is conceivable that this change involves a yet unknown activity that would provide a critical molecular link between microtubule-dependent polarity control and the non-vesicular lipid transport systems. It will be interesting to investigate whether OSBP-mediated cell polarisation - as described here - occurs in cells of higher eukaryotes where microtubules are involved in polarity control.

Acknowledgements

We thank Darren Gilmour, Stephen M. Huisman and Angela Lloyd for critical reading of the manuscript. We are grateful to Yauhen Yakimovic and Maria B. Heimlicher for advice on image segmentation. This work was funded by a grant from the Swiss National Science Foundation to DB.

Figures and Figure legends

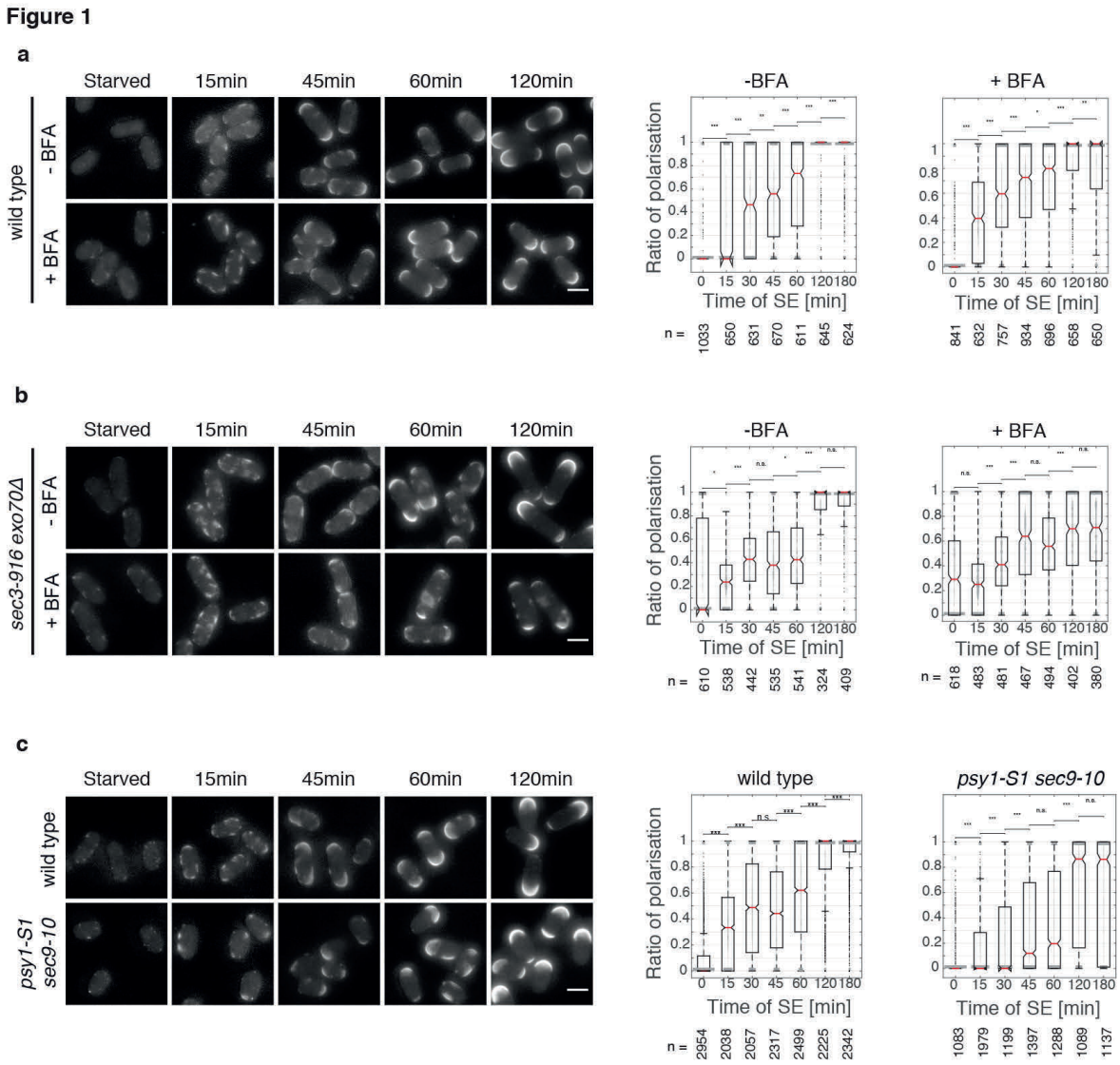

Figure 1: Sterol delivery is independent of vesicular transport. a, SRM domain formation and polarisation during SE at 36°C of wild type cells treated with BFA dissolved in DMSO (+BFA) and DMSO alone (-BFA control). Notched box plots show the polarisation rates at different time points during SE with p-values whereby * represents p≤0.05, ** represents p≤0.01, *** represents p≤0.001 and "n.s." stands for non-significant difference in this and all following figures (Methods). **b,** SRM domain formation and polarisation during SE at restrictive temperatures (36°C) of *sec3-916 exo70Δ* double mutant cells treated with DMSO (-BFA control) and BFA in DMSO (+BFA). Notched box plots show the polarisation rates at different time points during SE with p-values. **c,** SRM domain formation and polarisation during SE at restrictive temperatures (36°C), comparing

Filipin-stained wild type and *psy1-S1 sec9-10* double mutant cells. Notched box plots show the polarisation rates at different time points during SE with p-values. Scale bars: 5µm.

Figure 2

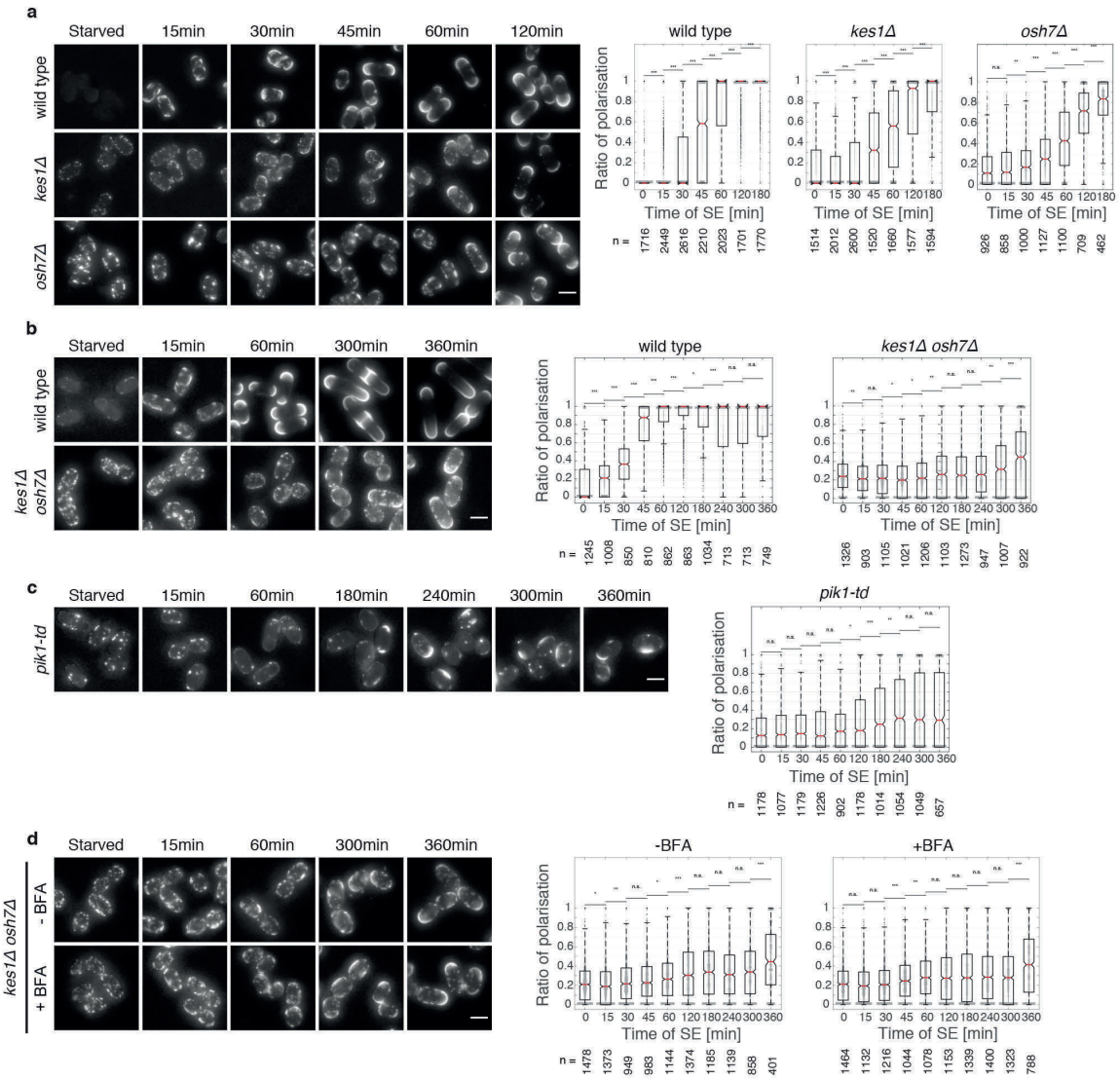

Figure 2: Non-vesicular transport mediates sterol delivery. a, SRM domain formation and polarisation during SE, comparing Filipin-stained wild type, *kes1Δ* and *osh7Δ* cells. Notched box plots show the polarisation rates at different time points during SE with p-values. **b,** SRM domain formation and polarisation during SE, in Filipin-stained wild type and *kes1Δ osh7Δ* double mutant cells. Comparative quantification of polarisation rates for wild type and *kes1Δ osh7Δ* cells. Notched box plots show the polarisation rates at different time points during SE with p-values. **c,** SRM domain formation and polarisation during SE at the restrictive temperature (36°C) of *pik1-td* cells. Comparative quantification of polarisation rates for *pik1-td* cells. Notched box plots show the polarisation rates at different time points during SE with p-values. **d,** SE of *kes1Δ osh7Δ* cells treated with DMSO (-BFA control) and BFA in DMSO (+BFA). Comparative quantification of polarisation rates for control- and BFA-treated *kes1Δ osh7Δ* cells. Notched box plots show the polarisation rates at different time points during SE with p-values. Scale bars: 5µm.

Figure 3

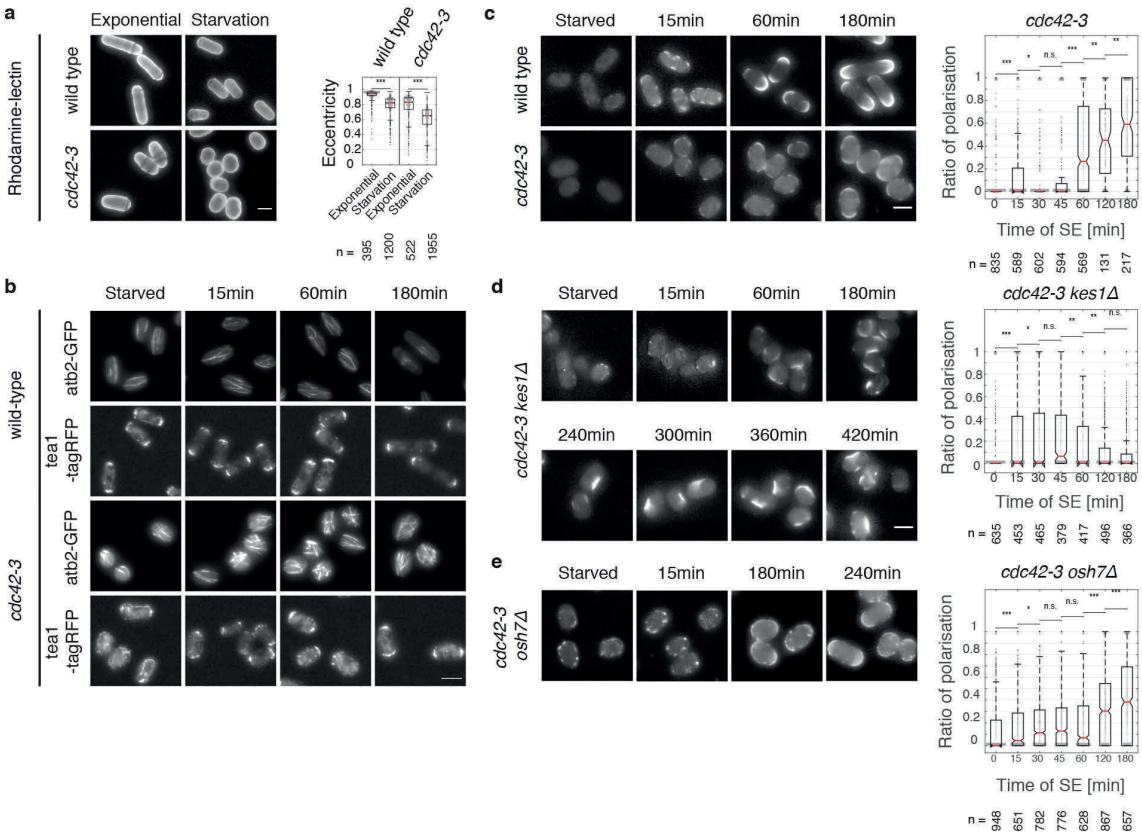

Figure 3: Polarisation pathway redundancies. a, Qualitative and quantitative comparison of Rhodamine-lectin-stained wild type and *cdc42-3* mutants grown at the permissive temperature (25°C) and imaged in exponential growth or in starvation after 3 days of culturing. Notched box plots show the distribution of cellular shape eccentricity (Methods). **b,** Comparison of microtubule organisation and tea1p localisation in wild type and *cdc42-3* mutant cells expressing GFP-tagged α2-tubulin (atb2-GFP) or tagRFP-tagged tea1p (tea1-tagRFP) at different time points during SE at the restrictive temperature (36°C). **c,** SRM domain formation and polarisation during SE at the restrictive temperature (36°C), comparing Filipin-stained wild type and *cdc42-3* cells. Notched box plots show the polarisation rates at different time points during SE with p-values. **d,** SRM domain formation and polarisation of Filipin-stained *cdc42-3 kes1Δ* cells at different time-points during SE at the restrictive temperature (36°C). Notched box plots show the polarisation rates at different time points during SE with p-values. **e,** SRM formation and polarisation of Filipin-stained *cdc42-3 osh7Δ* cells at different time-points during SE at the restrictive temperature (36°C). Notched box plots show the polarisation rates at different time points during SE with p-values.

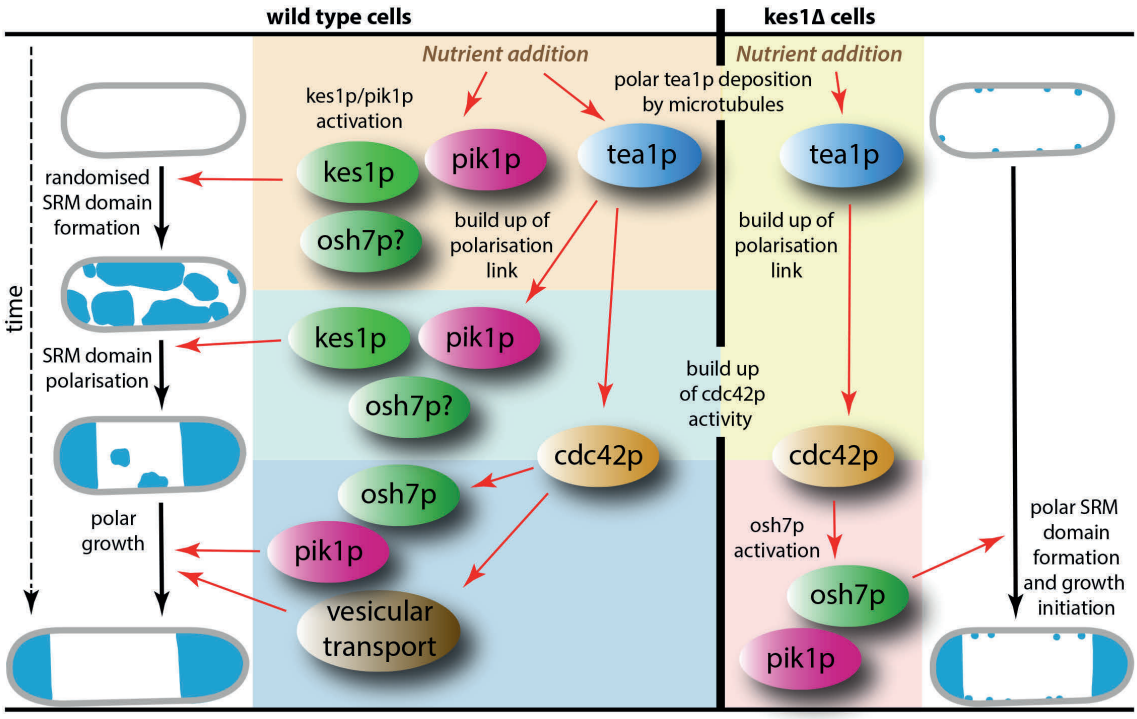

Figure 4: Cartoon of *de novo* cell polarisation. The cartoon shows the sequence of events we propose for microtubule/tea1p-guided SRM domain formation and polarisation during SE in wild type (left) and *kes1Δ* (right) cells. It depicts the time line of the protein activities we identified. Red arrows indicate the proposed regulatory hierarchy, without proposing direct interaction.

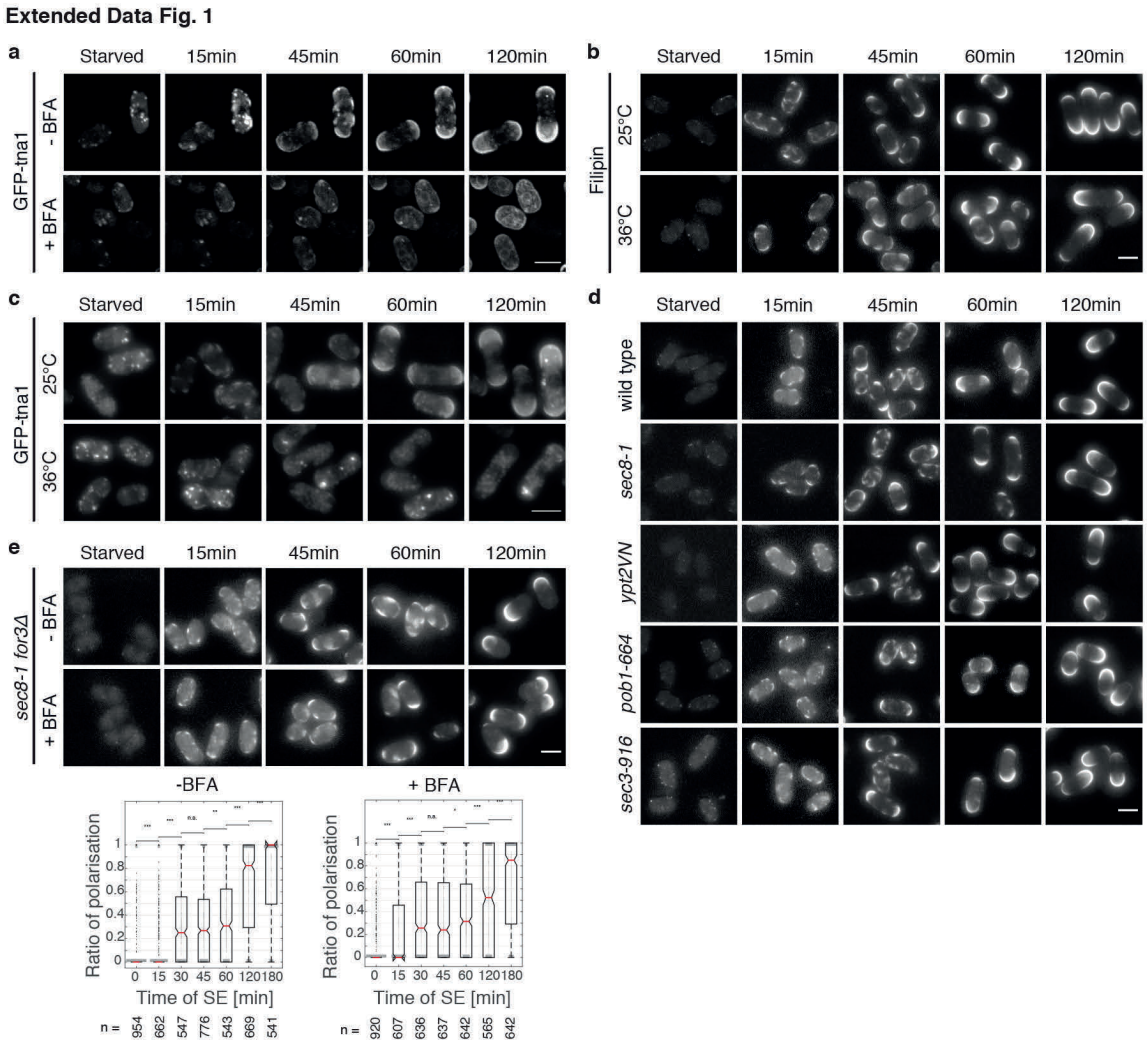

Extended Data Figure 1: Sterol delivery is independent of the Golgi apparatus and vesicular transport. a, Localisation of GFP-tagged tna1p during SE of wild type cells treated with DMSO (-BFA control) and BFA in DMSO (+BFA). **b,** SRM domain formation and polarisation during SE, comparing Filipin-stained wild type cells at 25°C and 36°C. **c,** Qualitative comparison of localisation of GFP-tagged tna1p during SE of wild type cells at 25°C and 36°C. **d,** SRM domain formation and polarisation during SE at the restrictive temperature (36°C), comparing Filipin-stained wild type cells with different mutants of vesicular secretion. **e,** SRM domain formation and polarisation during SE at the restrictive temperature (36°C) of Filipin-stained *sec8-1 for3Δ* cells treated with DMSO (-BFA control) and BFA in DMSO (+BFA). Notched box plots show the polarisation rates at different time points during SE with p-values.

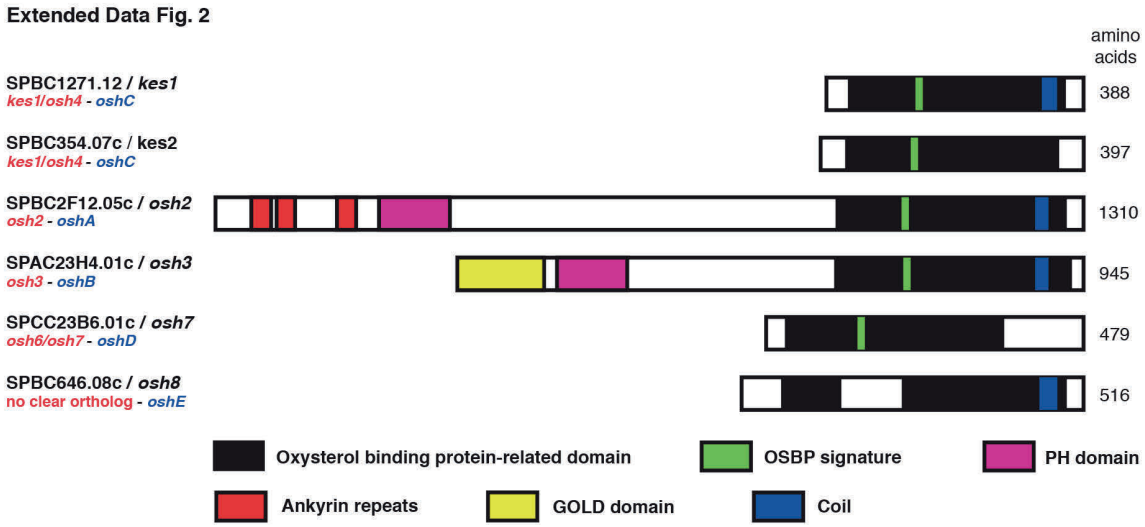

Extended Data Figure 2: Domain structure of *S. pombe* OSBPs. Protein domains as annotated in Pombase are highlighted in colour[7]. Where missing, gene names were assigned based on closest protein sequence homology to OSBPs in budding yeast (names in red) and *Aspergillus nidulans* (names in blue).

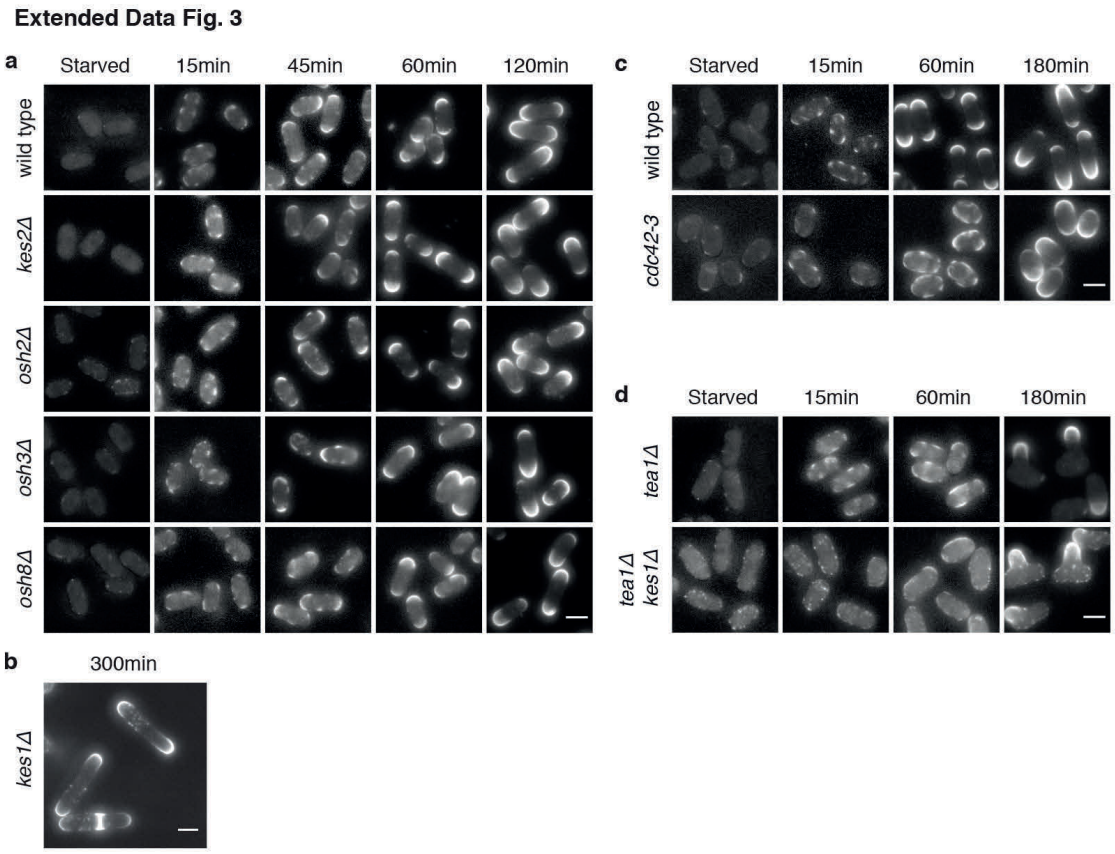

Extended Data Figure 3: SE of cells carrying gene deletions of oxysterol-binding proteins. a, SRM domain formation and polarisation during SE of wild type cells and of mutants stained with Filipin and carrying gene deletions of oxysterol-binding proteins (*kes2Δ*, *osh2Δ, osh3Δ, osh7Δ and osh8Δ*). **b,** Asymmetric distribution of the residual Filipin- stained sterol punctae in *kes1Δ* cells at the time of the first cell division during SE. **c,** SRM domain formation and polarisation in Filipin-stained wild type and *cdc42-3* cells during SE at the permissive temperature (25°C). **d,** SRM domain formation and polarisation during SE, comparing Filipin-stained *tea1Δ* and *tea1Δ kes1Δ* cells.

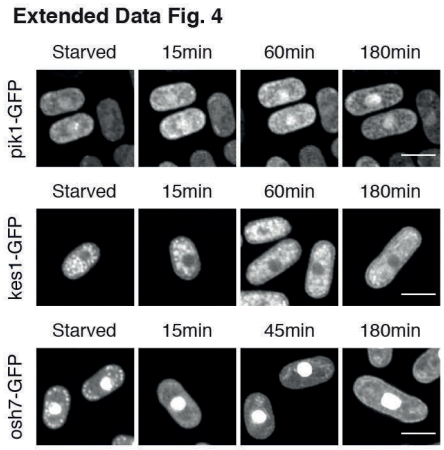

Extended Data Figure 4 Non-polar localisation of sterol delivery components. Localisation of GFP-tagged pik1p, GFP-tagged kes1p and GFP-tagged osh7p during SE.

References

1. Makushok, T., Alves, P., Huisman, S. M., Kijowski, A. R. & Brunner, D. Sterol-Rich Membrane Domains Define Fission Yeast Cell Polarity. *Cell* **165,** 1–37 (2016).
2. Mata, J. & Nurse, P. tea1 and the Microtubular Cytoskeleton Are Important for Generating Global Spatial Order within the Fission Yeast Cell. *Cell* **89,** 939–949 (1997).
3. Holthuis, J. C. M. & Menon, A. K. Lipid landscapes and pipelines in membrane homeostasis. *Nature* **510,** 48–57 (2014).
4. Mesmin, B. *et al.* A four-step cycle driven by PI(4)P hydrolysis directs sterol/PI(4)P exchange by the ER-Golgi tether OSBP. *Cell* **155,** 830–843 (2013).
5. Pelham, H. R. B. Multiple targets for brefeldin A. *Cell* **67,** 449–451 (1991).
6. Delic, M. *et al.* The secretory pathway: exploring yeast diversity. *FEMS Microbiology Reviews* **37,** 872–914 (2013).
7. Wood, V. *et al.* PomBase: a comprehensive online resource for fission yeast. *Nucleic Acids Research* **40,** D695–D699 (2011).
8. Wang, H. *et al.* The multiprotein exocyst complex is essential for cell separation in Schizosaccharomyces pombe. *Mol. Biol. Cell* **13,** 515–529 (2002).
9. Craighead, M. W., Bowden, S., Watson, R. & Armstrong, J. Function of the ypt2 gene in the exocytic pathway of Schizosaccharomyces pombe. *Mol. Biol. Cell* **4,** 1069–1076 (1993).
10. Nakano, K. *et al.* Pob1 Ensures Cylindrical Cell Shape by Coupling Two Distinct Rho Signaling Events During Secretory Vesicle Targeting. *Traffic* **12,** 726–739 (2011).
11. Jourdain, I., Dooley, H. C. & Toda, T. Fission yeast sec3 bridges the exocyst complex to the actin cytoskeleton. *Traffic* **13,** 1481–1495 (2012).
12. Bendezú, F. O., Vincenzetti, V. & Martin, S. G. Fission Yeast Sec3 and Exo70 Are Transported on Actin Cables and Localize the Exocyst Complex to Cell Poles. *PLoS ONE* **7,** e40248 (2012).
13. Bendezu, F. O. & Martin, S. G. Actin cables and the exocyst form two independent morphogenesis pathways in the fission yeast. *Mol. Biol. Cell* **22,** 44–53 (2011).
14. Maeda, Y., Kashiwazaki, J., Shimoda, C. & Nakamura, T. The Schizosaccharomyces pombe syntaxin 1 homolog, Psy1, is essential in the development of the

forespore membrane. *Bioscience, Biotechnology and Biochemistry* **73,** 339–345 (2009).

15. Nakamura, T., Kashiwazaki, J. & Shimoda, C. A Fission Yeast SNAP-25 Homologue, SpSec9, Is Essential for Cytokinesis and Sporulation. *Cell Struct. Funct.* **30,** 1–10 (2005).
16. Du, X., Brown, A. J. & Yang, H. Novel mechanisms of intracellular cholesterol transport: oxysterol-binding proteins and membrane contact sites. *Curr. Opin. Cell Biol.* **35,** 37–42 (2015).
17. Holthuis, J. C. M. & Levine, T. P. Lipid traffic: floppy drives and a superhighway. *Nat. Rev. Mol. Cell Biol.* **6,** 209–220 (2005).
18. Mesmin, B., Antonny, B. & Drin, G. Insights into the mechanisms of sterol transport between organelles. *Cellular and Molecular Life Sciences* **70,** 3405–3421 (2013).
19. Raychaudhuri, S., Im, Y. J., Hurley, J. H. & Prinz, W. A. Nonvesicular sterol movement from plasma membrane to ER requires oxysterol-binding protein–related proteins and phosphoinositides. *J. Cell Biol.* **173,** 107–119 (2006).
20. Beh, C. T., McMaster, C. R., Kozminski, K. G. & Menon, A. K. A Detour for Yeast Oxysterol Binding Proteins. *J. Biol. Chem.* **287,** 11481–11488 (2012).
21. de Saint-Jean, M. *et al.* Osh4p exchanges sterols for phosphatidylinositol 4-phosphate between lipid bilayers. *J. Cell Biol.* **195,** 965–978 (2011).
22. Park, J.-S., Steinbach, S. K., Desautels, M. & Hemmingsen, S. M. Essential Role for Schizosaccharomyces pombe pik1 in Septation. *PLoS ONE* **4,** e6179 (2009).
23. Wedlich-Soldner, R. & Li, R. Yeast and fungal morphogenesis from an evolutionary perspective. *Seminars in Cell & Developmental Biology* **19,** 224–233 (2008).
24. Bendezú, F. O. *et al.* Spontaneous Cdc42 Polarization Independent of GDI-Mediated Extraction and Actin-Based Trafficking. *PLOS Biology* **13,** e1002097 (2015).
25. Tatebe, H., Nakano, K., Maximo, R. & Shiozaki, K. Pom1 DYRK Regulates Localization of the Rga4 GAP to Ensure Bipolar Activation of Cdc42 in Fission Yeast. *Current Biology* **18,** 322–330 (2008).
26. Kelly, F. D. & Nurse, P. De Novo Growth Zone Formation from Fission Yeast Spheroplasts. *PLoS ONE* **6,** e27977 (2011).

Methods

Yeast Culturing, Constructs and BFA treatment

For SE cells were cultured for 3 days at 25°C as described in Moreno et al. (1991)[1] in EMM with 0.5% glucose[2]. Supplementing cells with EMM2 1:4 (starved culture:EMM2) triggered SE, which was done at 25°C unless stated differently. Starved temperature-sensitive mutants were pre-incubated at 36°C for 1h prior to SE at the restrictive temperature (36°C), which was triggered by adding pre-warmed EMM2. Cells were then kept at 36°C throughout SE. GFP-pik1 and *pik1-td* strains were cultured in continuous presence of thiamine[3]. The strains used are listed in Supplementary Information, Table 1.

To generate kes1p-GFP and osh7p-GFP strains by homologous recombination as previously described using the primer pairs listed in Supplementary Information, Table 2, and plasmid pFA6A-HLGFP-kanMX6 (SM. Huismann and D. Brunner, unpublished)[4,5]. Strains carrying OSBP gene deletions (except *osh8Δ*) were taken from the 5. edition Bioneer gene deletion library[6]. Deletions were confirmed by colony PCR and auxotrophic markers were crossed out. The *osh8Δ* strain was generated with the primer pair listed in Supplementary Information, Table 2, and the plasmid KS-ura4 as previously described[4]. Our OSBP naming procedure is described in the Supplementary Information.

BFA (LC Laboratories) was dissolved 50mg/ml in DMSO and used at 200µg/ml final concentration in the respective medium. Starved cells were pretreated 1h with BFA. SE was initiated by adding BFA-containing EMM2 medium.

Microscopy/Image Analysis

Filipin staining is described in Takeda et al. (2004)[7] and Makushok et.al. (2016)[8]. The cell wall was labelled with Rhodamine Grifonia Simplicifolia-Lectin I (GFL I, BSL I), (Vector laboratories; 4µg/ml) as described in May and Mitchison (1986)[9]. For imaging, samples of cells taken at defined time points of SE were stained and placed on a lectin-coated glass-bottom dish (Ibidi) and centrifuged at low speed. Imaging was performed on standard epifluorescence and spinning disc confocal microscopes as described in Makushok et al. (2016)[8], using 40x (NA 1.3), and 100x (NA 1.4) oil objectives and CCD or sCMOS

cameras for detection.

Routine image processing was done using ImageJ. Images in Extended Data Fig. 4 were acquired as single plane images and deconvolved using Huygens deconvolution (Scientific Volume Imaging) (detailed description in the Supplementary Information). p-values were calculated based on a Wilcoxon rank sum test (https://ch.mathworks.com/help/stats/ranksum.html)[10].

1. Moreno, S., Klar, A. & Nurse, P. in *Guide to Yeast Genetics and Molecular Biology* **194,** 795–823 (Elsevier, 1991).
2. Zaitsevskaya-Carter, T. Spm1, a stress-activated MAP kinase that regulates morphogenesis in S.pombe. *EMBO J.* **16,** 1318–1331 (1997).
3. Park, J.-S., Steinbach, S. K., Desautels, M. & Hemmingsen, S. M. Essential Role for Schizosaccharomyces pombe pik1 in Septation. *PLoS ONE* **4,** e6179 (2009).
4. Bähler, J. *et al.* Heterologous modules for efficient and versatile PCR-based gene targeting inSchizosaccharomyces pombe. *Yeast* **14,** 943–951 (1998).
5. Jankovics, F. & Brunner, D. Transiently Reorganized Microtubules Are Essential for Zippering during Dorsal Closure in Drosophila melanogaster. *Dev. Cell* **11,** 375–385 (2006).
6. Kim, D.-U. *et al.* Analysis of a genome-wide set of gene deletions in the fission yeast Schizosaccharomyces pombe. *Nature Biotechnology* **28,** 617–623 (2010).
7. Takeda, T., Kawate, T. & Chang, F. Organization of a sterol-rich membrane domain by cdc15p during cytokinesis in fission yeast. *Nat. Cell Biol.* **6,** 1142–1144 (2004).
8. Makushok, T., Alves, P., Huisman, S. M., Kijowski, A. R. & Brunner, D. Sterol-Rich Membrane Domains Define Fission Yeast Cell Polarity. *Cell* **165,** 1–37 (2016).
9. May, J. W. & Mitchison, J. M. Length growth in fission yeast cells measured by two novel techniques. *Nature* **322,** 752–754 (1986).
10. Wilcoxon, F. Individual Comparisons by Ranking Methods. *Biometrics Bulletin* **1,** 80–83 (1945).

Supplementary Information

Naming of OSBPs

Pombase, the fission yeast genome database, lists six OSBP protein family members (Extended Data Figure 2)[1]. Two of them, kes1 and osh3, were previously given gene names. The other we named based on the annotated protein domains (Extended Data Figure 2) and homology to presumptive *S. cerevisiae* genes. Also, *A. nidulans* orthologs were considered as published by Bühler et al. 2015[2]. *osh8* was most similar to *A. nidulans oshE* with no clear *S. cerevisiae* homolog, which is why we simply applied successive numbering to fullfil *S. pombe* naming requirements.

Image processing and segmentation

To analyse and quantify SRM domain formation and polarisation dynamics, cells were stained with Filipin and Rhodamine Grifonia Simplicifolia-Lectin I (Rhodamine-lectin). Image stacks of 5 z-slices with 1µm steps were acquired for both fluorescence signals. For each z-slice of Filipin and Rhodamine-lectin-stained cells we subtracted the background before performing a maximum projection (rolling ball radius 100px). The Rhodamine-lectin signal was normalized using the *Enhance Contrast* plugin of ImageJ. For cell segmentation object probabilities were estimated using Ilastik software on the processed Rhodamine-lectin images[3]. The following steps of cell segmentation were done using the adapted custom made processing pipeline of CellProfiler 2.0, as previously described[4,5,6]. Segmentation quality was controlled by overlaying boundaries of segmented cells with the Rhodamine-lectin and filipin staining images. Artefacts were minor, showing that the segmentation procedure was very robust.

Quantification of cell polarisation states

To quantify the polarisation state of individual *S. pombe* cells microscopy images were segmented as described above. For further analysis custom software was written in Matlab (MathWorks Inc.). A detailed description will be presented elsewhere. In short: An estimate of the membrane was computed from the segmentation and local normals were

fitted to the membrane curvature. Along these normals either mean or maximum intensities were measured. The corresponding intensity values for each pixel of the membrane curvature were interpolated to a reference curvature length and a designated signal processing and peak detection routine identifies regimes of high intensities guided by user-supplied parameters. These high intensity regions were classified as being at the poles or inbetween the poles of the fission yeast cells based on position information on the reference curvature. Each region was scored based on its size and mean intensity. A total polarisation score was then defined as the ratio of scores attributed to cell poles and to the cell regions in between the poles.

Measurement of cell eccentricity (Fig. 3a)

The eccentricity is defined as the ratio of distance between foci and the major axis length of the inertia ellipse fit to the object. The value is between 0 and 1, where 0 corresponds to a circle-like and 1 to a line-like object. This was computed by Matlab's built-in regionprops function (https://ch.mathworks.com/help/images/ref/regionprops.html).

List of strains used in this study

see Supplementary Information, Table 1

List of primers used in this study

see Supplementary Information, Table 2

1. Wood, V. *et al.* PomBase: a comprehensive online resource for fission yeast. *Nucleic Acids Research* **40,** 695–699 (2011).
2. Bühler, N., Hagiwara, D. & Takeshita, N. Functional Analysis of Sterol Transporter Orthologues in the Filamentous Fungus Aspergillus nidulans. *Eukaryotic Cell* **14,** 908–921 (2015).
3. Sommer, C., Straehle, C., Kothe, U. & Hamprecht, F. A. Ilastik: Interactive learning and segmentation toolkit. in 230–233 (IEEE, 2011).
4. Carpenter, A. E. *et al.* CellProfiler: image analysis software for identifying and

quantifying cell phenotypes. *Genome Biol.* **7,** 100 (2006).

5. Dimopoulos, S., Mayer, C. E., Rudolf, F. & Stelling, J. Accurate cell segmentation in microscopy images using membrane patterns. *Bioinformatics* **30,** 302–2651 (2014).
6. Frechin, M. *et al.* Cell-intrinsic adaptation of lipid composition to local crowding drives social behaviour. *Nature* **523,** 88–91 (2015).

Supplementary Information, Table 1

Strain	Genotype	Source	Adapted from
DB558	*h-*	Leupold U. (1950)	
DB1886	*h- P3nmt1-GFP-tna1p::kanMX6*	Makushok et al. (2016)	
DB4009	*h- ypt2VN::ura4 ura4*	This study	Craighead et al. (1993)
DB4018	*h- pob1-664*	This study	Toya et al. (1999)
DB4020	*h+ cdc42-3::kanR*	This study	Tatebe et al. (2008)
DB4026	*h- sec8-1*	This study	Wang et al. (2002)
DB4148	*h- osh3Δ::kanMX6*	This study	Kim et al. (2010)
DB4168	*h- sec3-916::HphR*	This study	Jourdain et al. (2012)
DB4178	*h- osh2Δ::kanMX6*	This study	Kim et al. (2010)
DB4184	*h+ kes1Δ::kanMX6*	This study	Kim et al. (2010)
DB4416	*h+ osh7-HL-GFP::kanMX6*	This study	
DB4826	*h+ osh7Δ::kanMX6*	This study	Kim et al. (2010)
DB4847	*h? kes1-HL-GFP::kanMX6*	This study	
DB4848	*h+ kes2Δ::kanMX6*	This study	Kim et al. (2010)
DB4850	*h? pik1Δ::ura4 pREP41X-Ub-R-DHFRts-pik1* (referred as pik1-td cells) *leu1-32 ura4-D18*	This study	Park et al. (2009)
DB4853	*h? sec8-1 for3Δ::kanMX6*	This study	Wang et al. (2002), Feierbach & Chang (2001)
DB4869	*h? pik1Δ::ura4 ade6-M210 leu1-32 ura4-D18, pREP41-2XeGFP-pik1*	This study	Park et al. (2009)
DB4885	*h? sec3-916::HphR exo70Δ::kanMX6*	This study	Jourdain et al. (2012), Kim et al. (2010)
DB4934	*h- osh8Δ::ura4 ura4-D18*	This study	
DB4939	*h? kes1Δ::kanMX6 osh7Δ::kanMX6*	This study	Kim et al. (2010)
DB4940	*h? kes1Δ::kanMX6 cdc42-3::kanR*	This study	Kim et al. (2010), Tatebe et al. (2008)
DB4941	*h? osh7Δ::kanMX6 cdc42-3::kanR*	This study	Kim et al. (2010), Tatebe et al. (2008)
DB4960	*h? kes1Δ::kanMX6 tea1Δ::ura4 ura4-D18*	This study	Kim et al. (2010), Makushok et al. (2016)
DB5164	*h+ leu1::sec9-10 sec9::ura4 psy1-S1::ura4+ ura4-D18*	This study	YGRC/NBRP Japan
DB5415	*h? tea1HL-tagRFP::kanR*	This study	Makushok et al. (2016)
DB5416	*h? leu2::sv40-GFP-atb2*	This study	Pardo M. & Nurse P. (2005)
DB5417	*h? tea1HL-tagRFP::KanR cdc42-3::kanR*	This study	Makushok et al. (2016), Tatebe et al. (2008)
DB5418	*h? leu2::sv40-GFP:atb2 cdc42-3::kanR*	This study	Pardo M. & Nurse P. (2005), Tatebe et al. (2008)

Supplementary Information, Table 2

Strain	Primer	Sequence
kes1-HL-GFP::kanMX6	DPE 1070	AAGATAAAGATGAGGGCTTTGAAGAAGCTACTAAGTGTCTTAGACAGCCTGTTAAAGAAGGTTTCTGGTATTATCTTAGAATCCTTGGAGCTCCTTCAGG
	DPE 1071	TTCACTTCAACTTAACCAAAGTCGTTAATGAAAGCCAGAGAGGAAATATATCTTACCATGAACAAGCTCGTAAAAGTGAAGAATTCGAGCTCGTTTAAAC
osh7-HL-GFP::kanMX6	DPE 1312	CGGTTGATGAATATCATGACGCTCAACTCCCTGACCCTAATACTCTATCAAAGTTACATGAAGAACAGGATCCAGCTTTAATCCTTGGAGCTCCTTCAGG
	DPE 1313	AATAGGTTAATAGTGTATAAAGAACTAAATCCCAATTAAGGAAAAAATATGGTAAATAACAACGTTGCAATTTATCTCTCTGAATTCGAGCTCGTTTAAAC
osh8Δ::ura4 ura4-D18	DPE 1279	GTGCCACCAACATTTATCAACGCAAAGATATCTCTTGAAAAGAATAGATTTTTGGTCAGTAGTAGGACCAGGACCCTAAAGCGCCAGGGTTTTCCCAGTCACGAC
	DPE 1280	AAGGTAGGGAAAAAGTTCTAAATGCACGCCAATTAAAGAGTTTGTGAAAAGGGTTAAAAATTAACGTTTTATGAAAGACAAGCGGATAACAATTTCACACAGGA

5 Additional, not included experiments for manuscript in preparation

"The microtubule/tea1p system controls cell polarisation via non-vesicular transport"

The following section summarises a set of complementary experiments done for the project in collaboration with Adam Kijowksi (see chapter 4). The collaboration led to a publication that is currently under revision. Here, only a brief introduction into the topic will be given, more details can be found in the manuscript in chapter 4.

5.1 Introduction

During his PhD project, Adam Kijowski focussed on the question how the SRMs reach the plasma membrane. Together, we show in the manuscript that the formation of SRMs on the plasma membrane during SE is independent of vesicular trafficking, the classical pathway from ER through Golgi to the plasma membrane. Instead, it depends on the oxysterol-binding protein kes1. We have good evidence that the process works via direct lipid transport of sterols synthesised in the ER to the plasma membrane via non-vesicular transport.

5.2 Experiments done for the manuscript

In general, the strains listed below, were analysed by imaging SE experiments as described in chapter 4 (see also section 6.1.2).

sec8-1 GFP-Tna1 and *sec3-916* GFP-Tna1*:* Repeated the experiment with GFP-Tna1 to confirm the results (not included in the manuscript).

psy1-S1 sec9-10: Generated the strain, performed the experiments.

Additional, not included experiments for manuscript in preparation

kes1Δ, osh7Δ and *kes1Δ osh7Δ*: Additional experimental repeats for statistical analysis.

cdc42-3: Performed the experiments.

cdc42-3 kes1Δ and *cdc42-3 osh7Δ*: Repeated the experiments to confirm the results.

cdc42-3 kes1Δ osh7Δ: Generated the strain, performed the experiments. The observed phenotype was the same as *cdc42-3 kes1Δ* during SE (data not shown, not included in the manuscript).

5.3 Additional experiments that are not included in the manuscript

5.3.1 Cell polarisation is independent of Cdc42 but Tea1-dependent

Tea1Δ mutant cells polarise with a delay and form bent or T-shaped cells in SE. During P2, they fail to stabilise polar SRMs and any random SRM patch is chosen as future growth site leading to the characteristic shape phenotypes. We hypothesised that this step is Cdc42-dependent although cell polarisation is independent of Cdc42 (Makushok et al. 2016). To test this hypothesis, *cdc42-3 tea1Δ* double mutant cells were recovered at the restrictive temperature of 36° C (Figure 45 and 42).

As expected, the double mutant *cdc42-3 tea1Δ* fails to polarise, although *cdc42-3* cells are able to polarise (Figure 45 and Figure 47). In absence of Cdc42, Tea1 still serves for the polar SRM caps and cell polarisation. In contrast, if Tea1 is missing, no polar caps form in P2 and without Cdc42 the cells remain in this state, unable to polarise and no SRM can be selected for polarised growth. However, the quantifications of the cell dimensions during SE in Figure 46 demonstrate, that both the *cdc42-3* single and the *ccd42-3 tea1Δ* double mutant cells grow slightly in length and even more in with. The more pronounced increase in cell width for *cdc42-3 tea1Δ* cells results in an almost spherical cell shape. The aspect ratio is close to 1 after 540 min in SE. Although the single mutant also grows in width, the aspect ratio decreases during the experiment until 360 min, due to the polarisation and minimal length increase that is happening in these cells.

As a control, the same experiment was repeated at permissive temperature (25° C) (Figure 48). Already at low temperatures, *cdc42-3* cells show a mild shape phenotype. They are wider than wild-type cells, and thus start with a rounded shape in starvation. *Cdc42-3* cells fully polarise within 120 min. In these cells, Tea1 deposition at the cell end is not as

precise as in elongated shapes due to the misalignment of microtubules resulting from the rounded shape (compare chapter 4). This leads to a delay in polarisation. The *cdc42-3 tea1Δ* double mutant is also slightly round in starvation. However, at permissive temperature they are able to focus the SRMs onto one growth site like the *tea1Δ* single mutant can. The resulting T-shapes demonstrate that *cdc42-3* was still functional under these conditions.

5.3.2 Cell polarisation depends on ER morphology – VAP mutants recover with a similar delay as the oxysterol-binding protein mutants

We speculate that the non-vesicular lipid transfer mediated by oxysterol-binding proteins occurs at ER-PM contact sites during SE. To test this hypothesis, we studied the ER morphology mutant *scs2Δ scs22Δ* (Figure 49). In these cells, the ER-PM contact sites are disrupted and the cortical ER is not tethered to the plasma membrane anymore (Zhang, Vjestica, and Oliferenko 2012).

Indeed, *scs2Δ scs22Δ* cells are delayed in SE, they polarise within 120 min and show bending cell ends. The polarisation defect is similar to the one observed in the *kes1Δ* and *osh7Δ* single mutants, although they do not show shape phenotypes. The ability of *scs2Δ scs22Δ* to polarise only with a mild delay is probably due to the ER dynamics. Although in the *scs2Δ scs22Δ* double mutant, the tethering to attach the cortical ER to the PM is missing, the ER is still dynamic and can still touch the PM from time to time. The temporary interaction happening over time might thus be enough to allow the transfer of ergosterol to the plasma membrane by non-vesicular transport.

5.3.3 GFP-Tna1 does not localise to filipin puncta in *kes1Δ* and *osh7Δ* mutant cells

The localisation of the SRM life-marker GFP-Tna1 was analysed in *kes1Δ, osh7Δ* and *kes1Δ osh7Δ* mutant cells (Figure 50). In all mutant strains, GFP-Tna1 localised to larger SRM patches but not to the bright filipin stained puncta that were present in starved cells, persisted through SE and that are characteristic for these oxysterol-binding protein mutants. This suggests that the observed puncta are no functional SRMs that can participate in the SE process.

5.3.4 *Cdc42-3 sec9-10* cells fail to polarise within 4 hours in SE

In an experiment related to this project, I tested the connection of the essential plasma membrane t-SNARE *sec9* and *cdc42.* Both single mutants *sec9-10* and *cdc42-3* are able to polarise at restrictive temperature. Also, the double mutant of both essential t-SNARES *sec9-10 psy1-S1* polarises. However, the double mutant *sec9-10 cdc42-3* failed to polarise within 4 hours in SE (Figure 51). Although we do not understand the described results, so far, they show that there is probably still much more in the polarisation system of fission yeast to be discovered. How Cdc42 and sec9 are connected as this experiment suggests, needs further investigations.

To test if the roundish cell shape of this double mutant is involved in the polarisation defect, I tested the effect of the cell shape on the polarisation. The *rP* values were plotted against the aspect ratio (Figure 52). In wild-type, cells start with an aspect ratio around 0.5, then they polarise, start to grow and the aspect ratio goes down. *Psy1-S1 sec9-10* double mutant cells show the same behaviour overall. In contrast, the aspect ratios of *cdc42-3 sec9-10* cells were higher throughout the experiment because of the round cell shape. The polarisation ratio was independent of aspect ratio and SE progression (time). Although indirect, this comparison demonstrates that even though it is expected that roundish cells have more difficulties to polarise due to the mis-alignment of microtubules leading to mis-localisation of Tea1, there is no one-to-one connection of cell shape and *rP*. If it would only be the shape that leads to the ability to polarise or not, the more elongated cells should be able to polarise and have a higher *rP* and the round ones should not, leading to two populations in the plot.

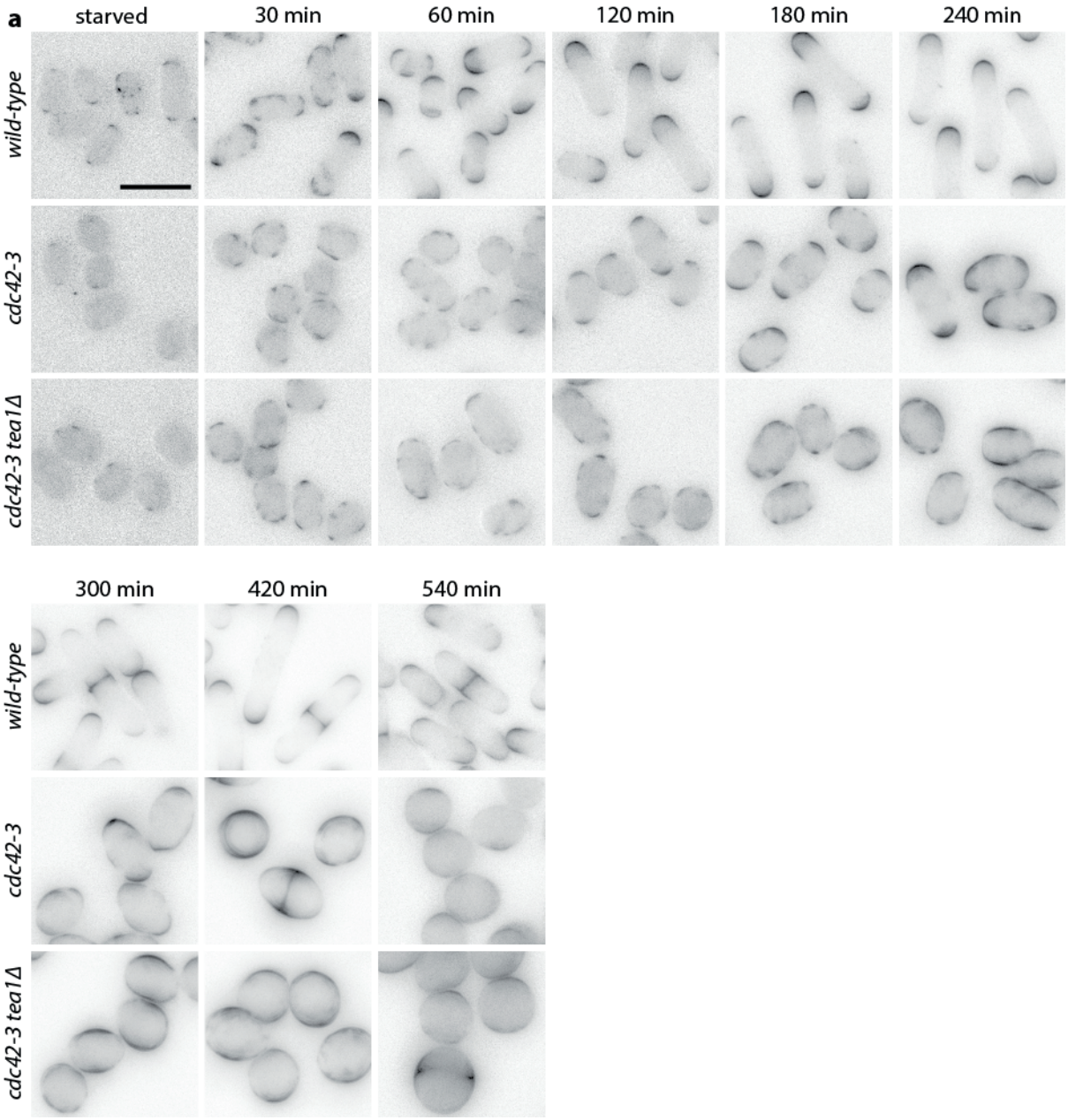

Figure 45: *Cdc42-3 tea1Δ* cells fail to polarise at restrictive temperature (36° C).

(a) Filipin-stained wild-type, *cdc42-3* and *cdc42-3 tea1Δ* cells during SE at restrictive temperature (36° C). Scale bar: 10 µm.

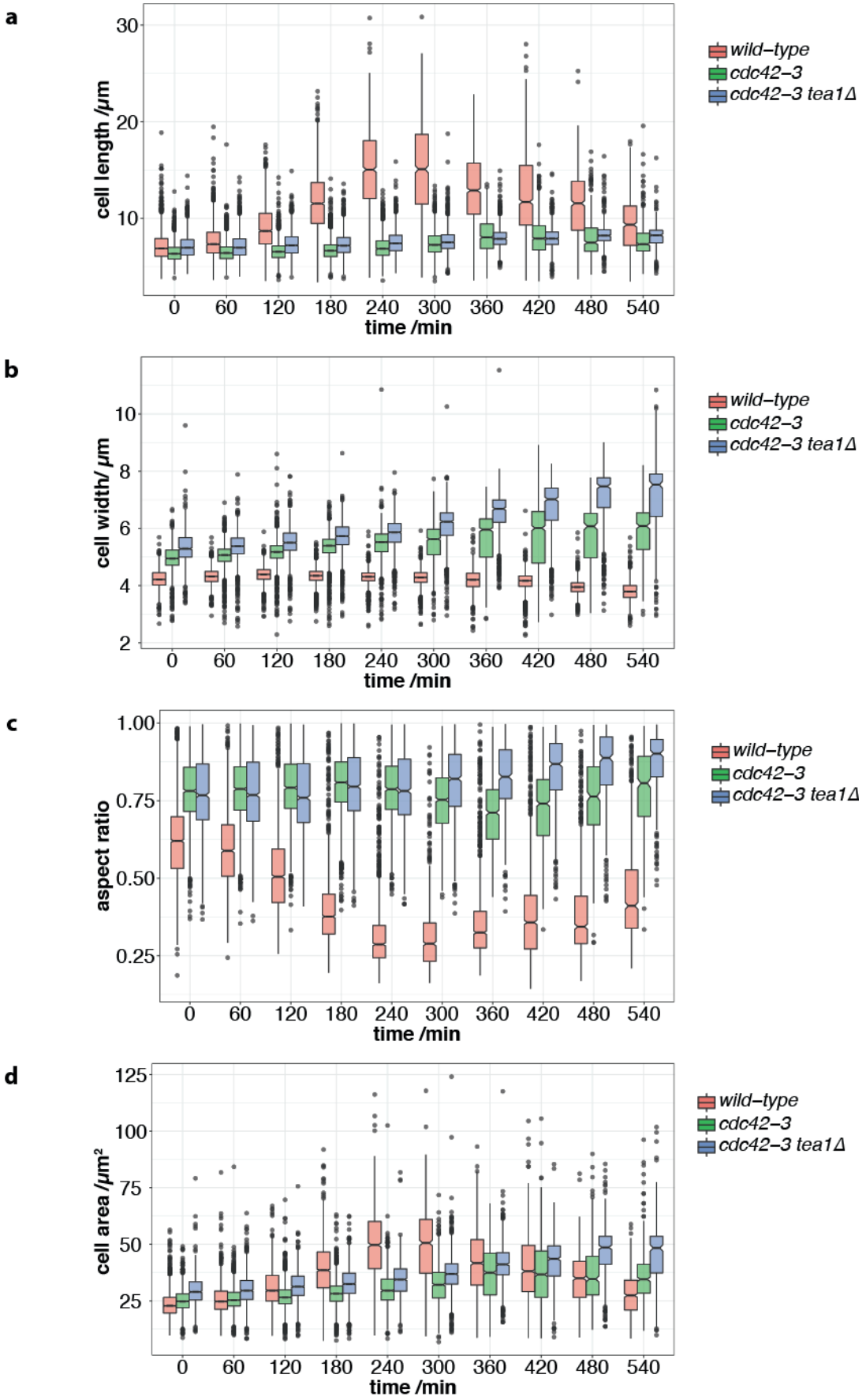

Figure 46: Cell dimensions of *cdc42-3 tea1Δ* cells during SE at restrictive temperature (36° C).

(a)-(d) Cell length (a), cell width (b), aspect ratio (c) and cell area (d) during SE of wild-type, *cdc42-3* and *cdc42-3 tea1Δ* cells at restrictive temperature (36° C).

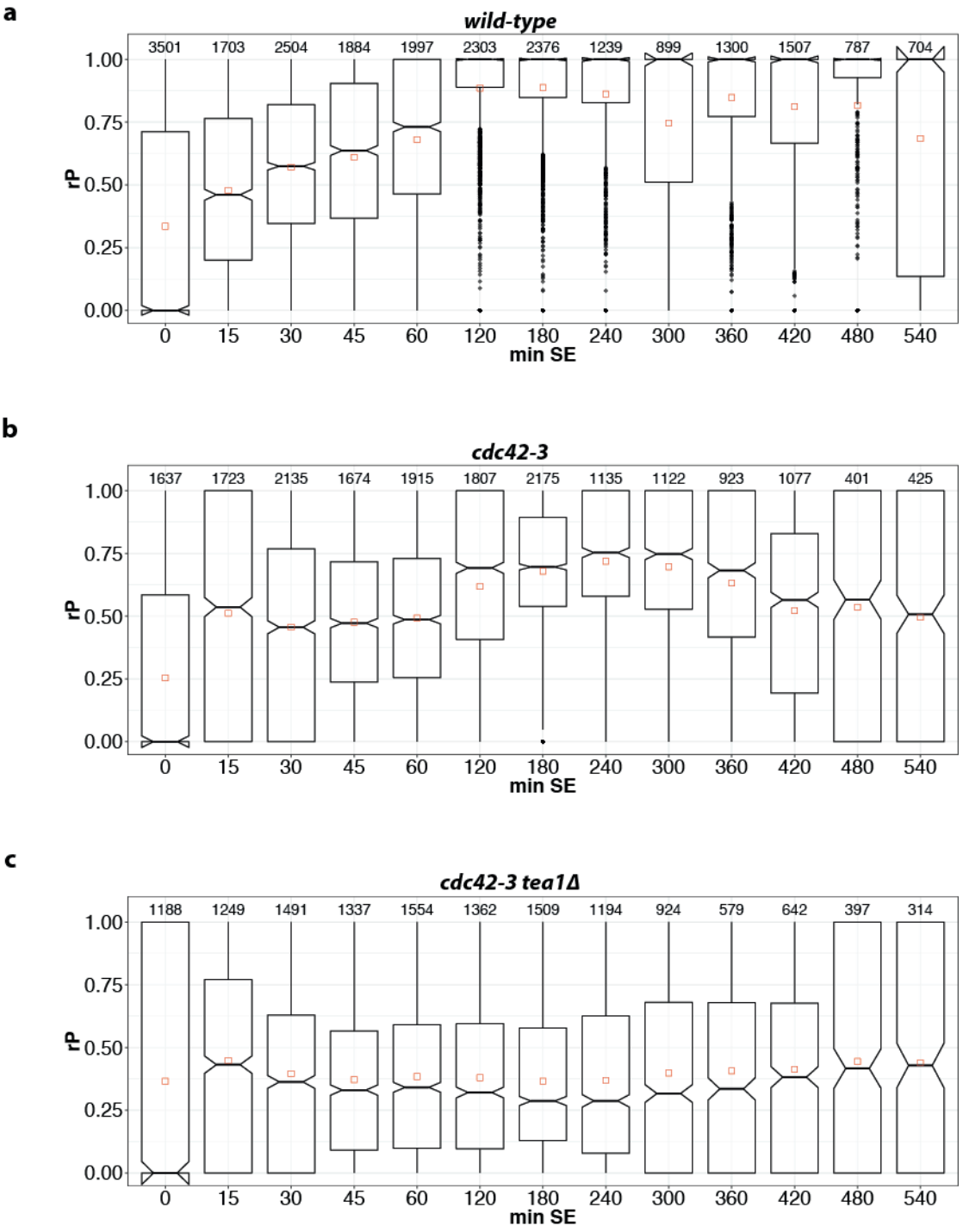

Figure 47: Quantification of polarisation (*rP*) of *cdc42-3 tea1Δ* double mutant cells at restrictive temperature (36° C).

(a) Notched boxplots showing *rP* during SE of wild-type, *cdc42-3* and *cdc42-3 tea1Δ* cells at restrictive temperature (36° C).

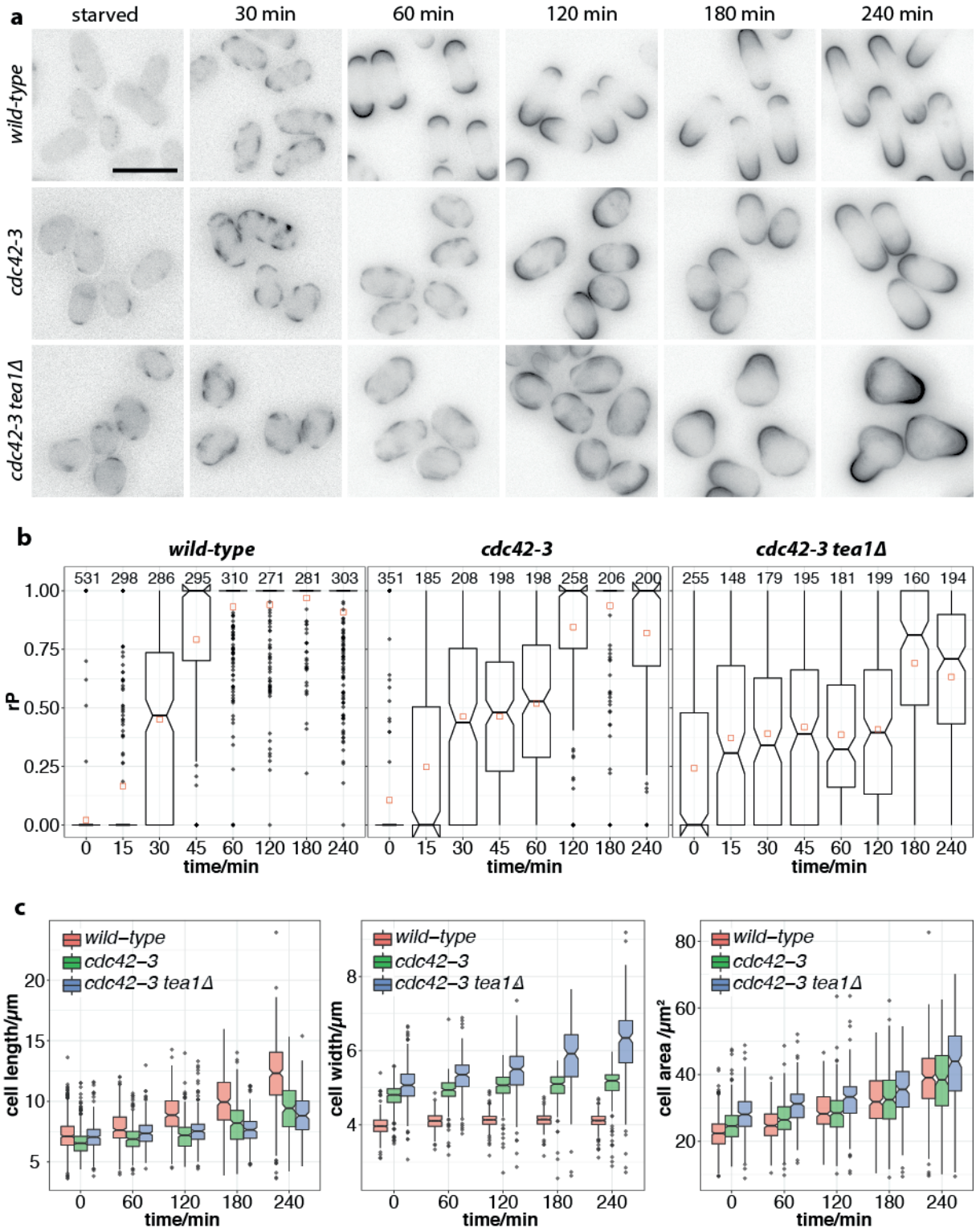

Figure 48: *Cdc42-3 tea1Δ* cells are able to polarise at permissive temperature (25° C).

(a) Filipin-stained wild-type, *cdc42-3* and *cdc42-3 tea1Δ* cells during SE at permissive temperature (25° C). (b) Notched boxplots showing *rP* during SE of wild-type, *cdc42-3* and *cdc42-3 tea1Δ* cells at permissive temperature (25° C). (c) Cell length (left), width (middle) and area (right) of wild-type (red), *cdc42-3* (green) and *cdc42-3 tea1Δ* cells (blue) during SE at permissive temperature (25° C). Scale bar: 10 µm.

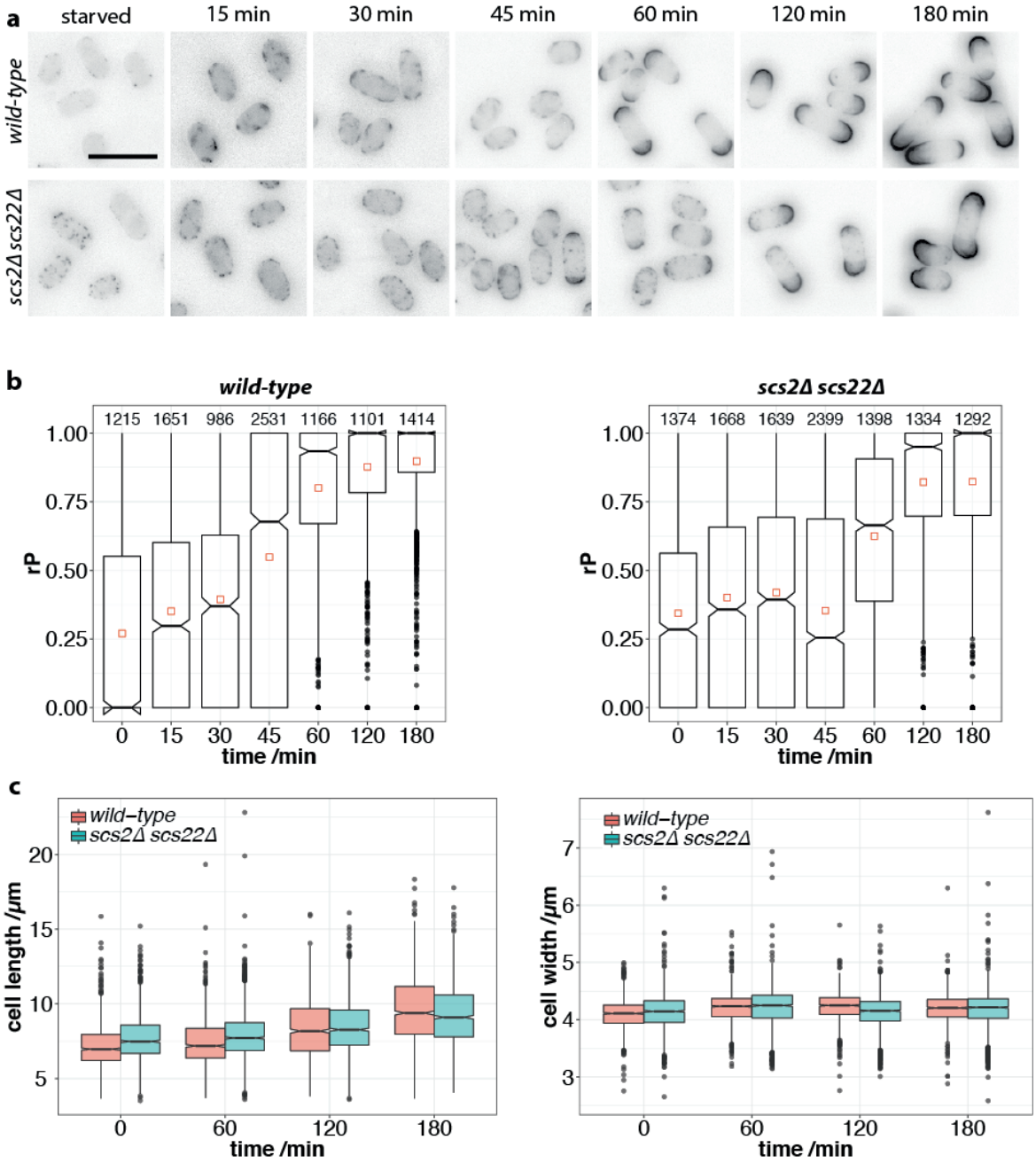

Figure 49: Polarisation during SE depends on ER morphology.

(a) Filipin-stained wild-type and *scs2Δ scs22Δ* cells during SE. (b) Notched boxplots showing *rP* during SE of wild-type and *scs2Δ scs22Δ* cells. (c) Cell length (left) and width (right) of wild-type (red), *scs2Δ scs22Δ* cells (blue) during SE. Scale bar: 10 µm.

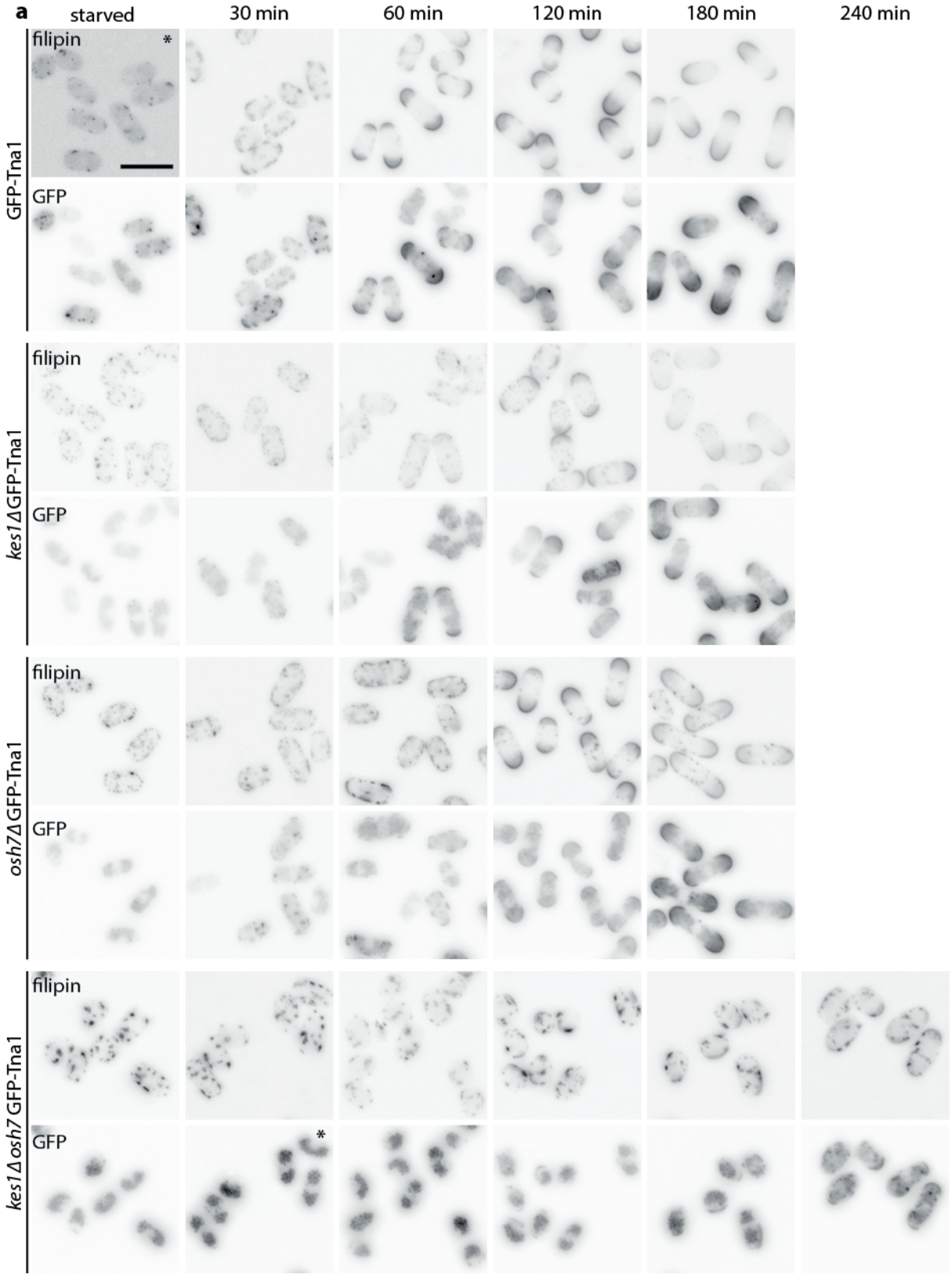

Figure 50: GFP-Tna1 localisation in *kes1Δ, osh7Δ* and *kes1Δ osh7Δ* mutant cells during SE.

(a) Filipin-stained wild-type, *kes1Δ, osh7Δ* and *kes1Δ osh7Δ* cells expressing GFP-Tna1, during SE. Scale bar: 10 µm.

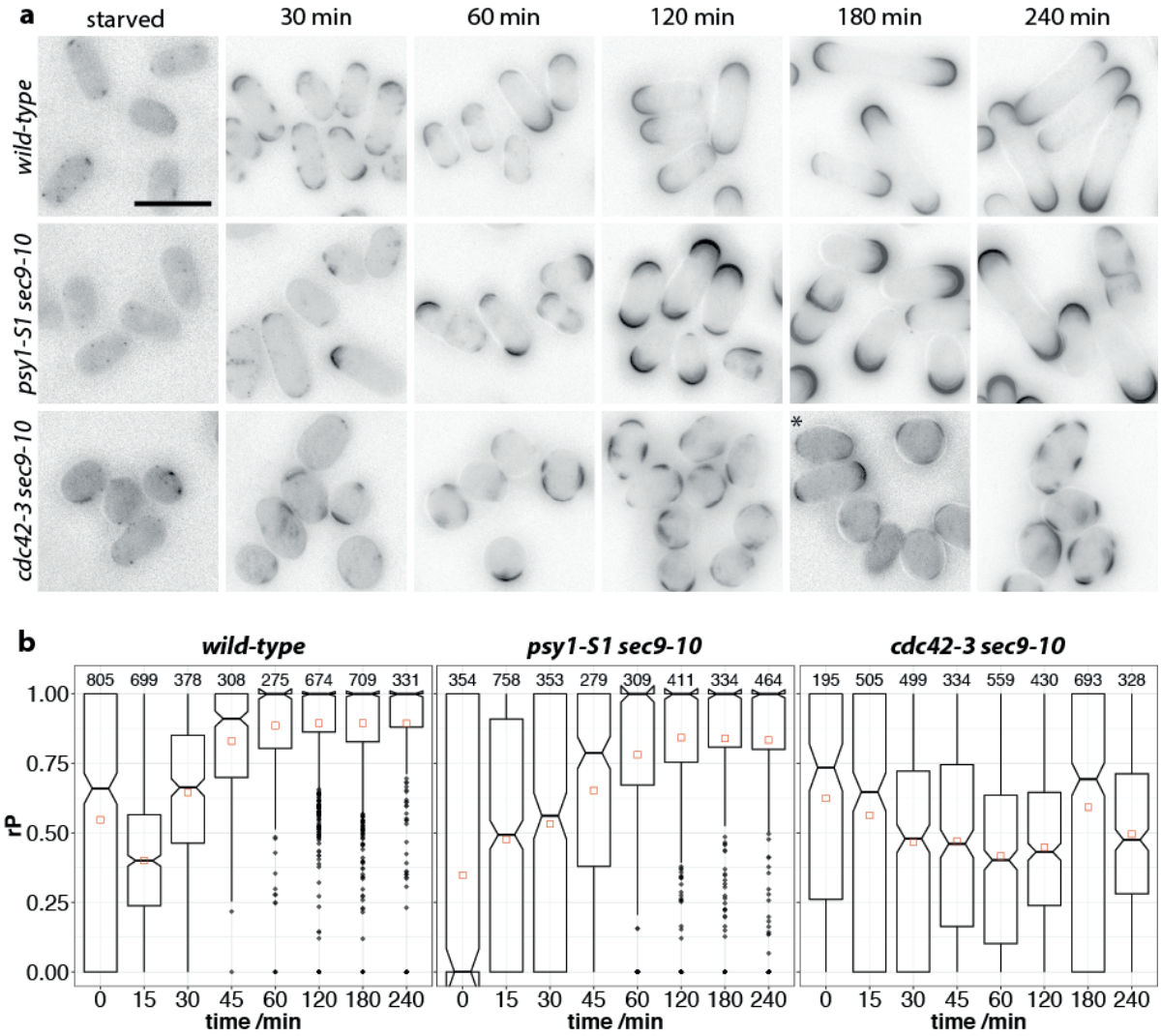

Figure 51: *Cdc42-3 sec9-10* cells fail to polarise at restrictive temperature (36° C).

(a) Filipin-stained wild-type, *psy1-S1 sec9-10* and *cdc42-3 sec9-10* cells during SE at restrictive temperature (36° C). (b) Notched boxplots showing *rP* during SE of wild-type, *psy1-S1 sec9-10* and *cdc42-3 sec9-10* cells at restrictive temperature (36° C). Scale bar: 10 µm.

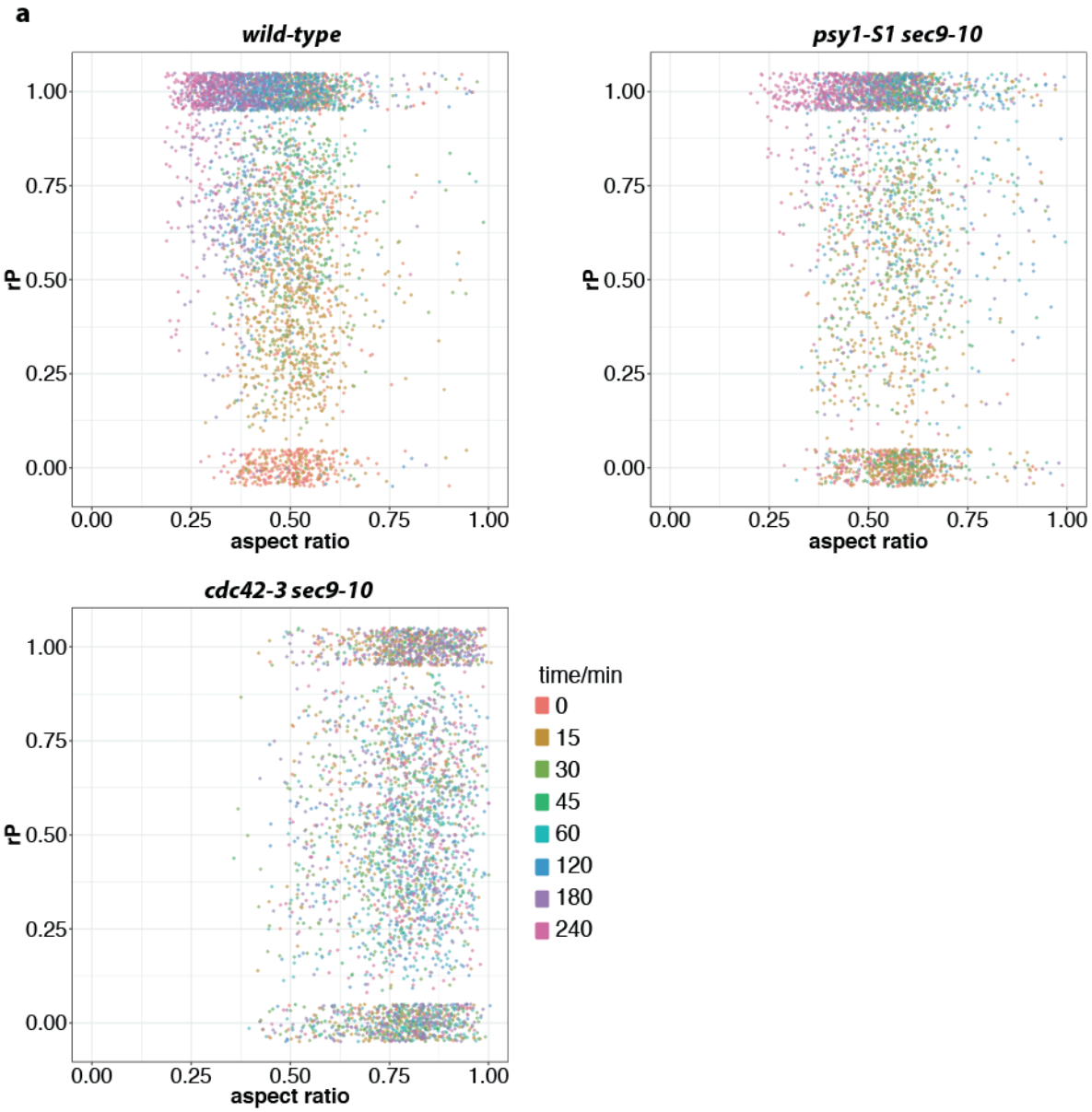

Figure 52: Testing the dependence of polarisation (*rP*) on the aspect ratio.

(a) *rP vs.*aspect ratio of wild-type, *psy1-S1 sec9-10* and *cdc42-3 sec9-10* cells during SE at restrictive temperature (36° C).

6 Materials and Methods

6.1 Yeast handling

6.1.1 Yeast strains

All strains used for the thesis are listed in Table 4. If not stated otherwise, cells were cultured at 25° C in Edinburgh minimal medium (EMM) supplemented with amino acids and 0.2 µM thiamine, if necessary. Strains were generated with standard methods either via crossing of existing strains or by the PCR-based method to replace or modify a gene (Moreno, Klar, and Nurse 1991; J Bähler et al. 1998). The primers used for PCR-based genetic modifications are listed in **Error! Reference source not found.**. Colony PCR was used to screen the colonies growing in presence of the according antibiotic drug to find the correct clones.

6.1.2 Starvation exit experiments

Starvation experiments were done as described before (Zaitsevskaya-Carter and Cooper 1997; Makushok et al. 2016). If not stated differently, exponentially growing cells were transferred to EMM2 medium with 0.5% glucose at an initial OD of 0.2 and grown for 3 days at 25° C. For SE, the starved culture was mixed with EMM2 with 2% glucose in a 1:4 ratio to induce SE. When temperature-sensitive strains were used, the cultures and media were transferred to the according restrictive temperature one hour prior to the SE experiment.

6.2 Microscopy and Image Analysis

6.2.1 Imaging

Samples of the SE cultures were taken from the liquid culture and imaged in 8-well glass- or plastic-bottom imaging dishes (ibidi) coated with lectin (Vector Laboratories). Cell outlines were labelled with 4 µg/ml Rhodamine Griffonia Simplicifolia Lectin I (Vector Laboratories) and Filipin (Sigma, F9765-50MG) was used to stain SRMs (May and Mitchison 1986; Takeda, Kawate, and Chang 2004; Makushok et al. 2016). Filipin was used at a concentration of 5 µg/ml from a 4000x stock in DMSO, from chapter 2.2.7

onward, a new filipin batch was used at a concentration of 2.5 µg/ml with the same signal and reduced toxicity. SE experiments were imaged on standard epifluorescence and spinning disc confocal microscopes with 40x (NA 1.3), 63x (NA 1.4) or 100x (NA 1.4) oil objectives, equipped with a CCD or sCMOS camera. When imaging with 40x magnification for quantification of SE, 5 z-stacks were imaged with a 1 µm distance. For higher magnifications 11 z-stacks with 0.5 µm distance were acquired. Image processing routines were done with ImageJ. If not stated otherwise, in images displaying filipin signal, the contrast settings were equalised for all strains displayed in the figure for each timepoint individually.

6.2.2 Image processing and cell segmentation

To quantify the polarisation process during starvation exit, cell segmentation is necessary. A segmentation pipeline mainly developed by Maria Barbara Heimlicher and Adam Kijowski was used and modified slightly (unpublished, (Kijowski et al., n.d.), in preparation). More details can also be found in (chapter 4). All imaging data for quantification of SE and its visualisations were acquired on the epifluorescence microscope with 40x magnification. The background was subtracted (rolling ball, 100 px) prior to the maximum projection. To normalize the cell outline signal, Rhodamine-lectin images were normalised with the *Enhance Contrast* plugin in ImageJ (0.4% saturated pixels, normalized). The cell outlines were used to generate an ilastik training (version 1.1.7), defining *cell seeds*, *cell outline* and *background*. The training was run over all cell outline images. The resulting probability images were fed into a CellProfiler (version 2.0) pipeline provided by Adam Kijowski that takes the cell seeds as starting point to segment the cells in the original image. Briefly, the cell seeds were filled, filtered by shape and size parameters to match the typical cell dimensions, were overlaid with the original image and expanded until they reach the imaged cell outline signal. The final step, reducing the size of the segmented cell by 1 px from the outside gives the resulting segmentation. The cell outline used for the quantification of cell polarisation, is the outline of the segmented cells. The overlay with the original images also served as control of the segmentation method and showed that segmentation artefacts were rare.

6.2.3 Quantification of the cell polarisation process

A MATLAB program, written by David Dreher (unpublished, in preparation) read the filipin signal along the outline of the segmented cells. For each individual cell, the program calculated the polarisation ratio *rP,* the bipolarity ratio *rB,* and provided additional information of each segmented cell like cell length and width, area and eccentricity.

For the quantification of polarisation and the calculation of *rP* and *rB,* it detected the position of the filipin signal relative to the cell dimensions and used this information to classify how polar a cell is. The polarisation ratio *rP* simply was the ratio of filipin signal at the cell tips relative to the sum of all filipin signal around the cell. It gave a ratio between 0 and 1, with 0 for an unpolarised cell having no SRMs detected or only signal at the cell sides and 1 for a cell with a perfectly polar SRM cap or a bipolar cell.

The polar signal *PolarSum* was calculated based on the signal intensity *PolarInt* and the signal width *PolarWidth* as:

$$PolarSum = (PolarInt_1 * PolarWidth_1) + (PolarInt_2 * PolarWidth_2).$$

Similar, the lateral signal at the cell sides was calculated as the *SideSum* base on the signal intensity at the cell side *SideInt* and the width of the signal *SideWidth*:

$$SideSum = \sum(SideInt_i * SideWidth_i).$$

Based on these, the Polarisation ratio was calculated as

$$rP = \frac{PolarSum}{PolarSum + SideSum}$$

and could be used as a quantitative measure of polarisation progress during SE.

At this stage, the calculation did not distinguish, if a cell was mono-or bipolar. To test the bipolarity, the ratio of bipolarity was calculated for cells with polar signal as ratio of the two polar signals as

$$rB = \frac{(PolarInt_1 * PolarWidth_1)}{(PolarInt_2 * PolarWidth_2)}$$

with the larger polar SRM cap as pole 2. In the analysis, a cell with only one pole received an *rB* value of 0, if more than two poles were detected, it was not defined (NaN).

For this study, except chapter 4, the latest version of the MATLAB script with a graphical user interface that allowed the modification of filtering and measuring parameters was used. The parameters were chosen as follows:

- Filter parameters: Gaussian filter with l=100 and σ=20
- Peak detection parameter:
  Findpeaks parameter: MinPeakHeight=100, MinPeakProminence=50, Threshold=0, WidthReference=halfprom, MinPeakDistance=20, MinPeakWidth=20, MaxPeakWidth=Inf, NPeaks=Inf
  Width measurement: Reference=heightcorr, Reference level=0.75,
  Sign. minima depth=30, Sign. nb. max height=5

6.2.4 Data Analysis and Visualisation

The Data generated with MATLAB were analysed and plotted with R using the *ggplot2*, *reshape2*, *EnvStats* and *dplyr* libraries. The number of experimental repeats used for analysis is summarised in Table 7.

6.3 Analysis of detergent-resistant membranes

6.3.1 DRM isolation

The method development is described in detail in chapter 2 and modified based on (Takeda, Kawate, and Chang 2004). The final protocol used for this study is described

briefly here, more details can be found in chapter 2.3.1. Exponentially growing cells were isolated by centrifugation at 3000 rpm for 10 min in a Sorvall RC-B5 centrifuge with 500 ml conical centrifuge tubes (CORNING) in 1 litre buckets with the according cushions (CORNING). The cell slurry was shock frozen by dropping into liquid nitrogen and stored at -80° C. It was ground in liquid nitrogen with a motorized mortar grinder (Retsch RM 100), first for 8 min with the pistil pressure set to 0, then 40 min with setting 1 (Givens et al. 2011). The cell powder was stored at -80° C until further use.

During the following steps, samples were always kept on ice. Ca. 45-60 mg cellular material was weighted into 1 ml ice-cold lysis buffer (365 mM sucrose, 20 mM MOPS, pH 7.4) (Takeda, Kawate, and Chang 2004) with protease inhibitors (Promega) and vortexed at 4° C for 5 min. The suspension was spun at 3000x*g* for 5 min at 4° C. 950 µl of the supernatant (S3) were centrifuged at 4°C and 100 000x*g* for 30 min on a Beckman Coulter Optima™ MAX-XP Ultracentrifuge in ultracentrifuge safe microfuge tubes in a TLA100.3 rotor (both Beckmann Coulter). The supernatant (S100) was removed and the pellet (P100) was resuspended in ice-cold 100 µl TNE(5x TNE: 750 mM NaCl, 10 mM EDTA, 250 mM Tris-HCl, pH 7.4) (Schuck et al. 2003) with protease inhibitors using a syringe with a 25 G needle. 81 µl of the suspension were mixed with 9 µl 10% Triton X-100 (Roche, for membrane research) by pipetting up and down 3 times and kept on ice for 30 min. 180 µl 60% Optiprep (Axis Shield) were added to the mixture for a final concentration of 40% Optiprep. 245 µl were placed in a 5 x 41 mm Ultra-Clear ultracentrifuge tube (Beckmann Coulter) and overlaid with 450 µl 35% Optiprep (7 vol. 60% Optiprep : 5 vol. TNE with protease inhibitors) and 35 µl TNE with protease inhibitors. After 2 hours centrifugation at 200 000 x *g* at 4° C, the gradient was fractionated from the top. The floating fraction (ca. 100-120 µl) was reextracted with Triton-X100 for 30 min on ice and re-isolated on a second gradient.

6.3.2 Western blotting

Standard protocols were used to analyse the fractions with Western blotting. Proteins from the gradient fractions were precipitated with 2 vol. 15% TCA on ice, washed with ice-cold ethanol, dried at room temperature, reconstituted in SUMEB buffer (1% SDS, (8 M Urea, 10 mM MOPS, pH6.8, 10 mM EDTA, 0.01% Bromophenol Blue) and loaded on the Western gel (NuPage™ 4-12% Bis-Tris-Gel, invitrogen). Protein concentrations were

measured by a method described by Schaffner and Weissmann (1973). GFP-Tna1 was detected with mouse anti-GFP (Roche) and Ost1-mCherry with rabbit anti-mCherry (Abcam). The used rabbit anti-Pma1 antibody was a kind gift by Hirofumi Aiba (Ito et al. 2010). Secondary anti-mouse and anti-rabbit antibodies (both Promega) and ECL Western blotting substrate (Promega) were used for visualization. Amidoblack staining of Western blots was done using chemicals described by Schaffner and Weissmann (1973).

6.3.3 Sample preparation for mass spectrometry

Screen 1: The TCA precipitated, dried samples were sent for MS analysis.

Screen 2: At room temperature, the TCA precipitated, dried samples were resuspended in 120 µl 1% RapiGest (Synthesised by the Bernd Wollscheid group, kindly provided by Erich Brunner, it is commercially available from Waters) solution in 50 mM ammonium bicarbonate with a syringe with a 27G needle and vortexed. The samples were boiled for 2 min. 1 µl DTT was added to 100 µl resuspended sample to 5 mM final concentration. Afterwards, the samples were incubated at 60° C for 30 min. 1 µl $CaCl_2$ 100 mM and half of the needed amount of Trypsin (in total 2-10 µl, depending on the protein content) were added and the samples were incubated for digestion at 37° C for 1 hour. The second half of Trypsin was added, and the digestion was continued overnight. The peptides were purified on Waters OASIS MCX 1cc (30 mg) extraction cartridges, 300 µg capacity (a kind gift from Erich Brunner). The extraction protocol from Erich Brunner was used. To avoid plastic contamination from pipetting tips, they were changed for every pipetting step. The cartridges were equilibrated with 2 ml methanol then with 2 ml 0.1% TFA. The samples were acidified with TFA (pH≥3) and loaded slowly on the cartridge. To ensure binding, the loading was repeated 3 times. The cartridge was washed with 5 ml 0.1% TFA and 5 ml 80% ACN/ 0.1% TFA and the peptides were eluted with 1 ml 10% NH_4OH/ 90% methanol. The purified peptides were dried/concentrated in a SpeedVac Concentrator.

6.3.4 Mass spectrometry analysis

Samples were analysed by the Functional Genomics Center Zürich (FGCZ) in collaboration with Dr. Peter Hunziker. Samples were dissolved in 20 µl 0.1% formic acid. Subsequently, 4 µl sample were mixed with 16 µl 0.1% formic acid for LC/MS/MS. All samples

were analysed on a Q Exactive Hybrid Quadrupole-Orbitrap mass spectrometry instrument from Thermo Fisher Scientific. Mascot database searches were performed against SwissProt (all species and *S. pombe*). The Scaffold Viewer was used to view the resulting data.

Bibliography

Abenza, Juan F., Anatole Chessel, William G. Raynaud, and Rafael E. Carazo-Salas. 2014. "Dynamics of Cell Shape Inheritance in Fission Yeast." *PLoS ONE* 9 (9). doi:10.1371/journal.pone.0106959.

Arellano, Manuel, Teresa Niccoli, and Paul Nurse. 2002. "Tea3p Is a Cell End Marker Activating Polarized Growth in Schizosaccharomyces Pombe." *Current Biology* 12 (9): 751–56. doi:10.1016/S0960-9822(02)00821-7.

Baek, Guem Hee, Haili Cheng, Vitnary Choe, Xin Bao, Jia Shao, Shiwen Luo, and Hai Rao. 2013. "Cdc48: A Swiss Army Knife of Cell Biology." *Journal of Amino Acids* 2013: 1–12. doi:10.1155/2013/183421.

Bagnat, M, S Keränen, a Shevchenko, and K Simons. 2000. "Lipid Rafts Function in Biosynthetic Delivery of Proteins to the Cell Surface in Yeast." *Proceedings of the National Academy of Sciences of the United States of America* 97 (7): 3254–59. doi:10.1073/pnas.060034697.

Bähler, J, J Q Wu, M S Longtine, N G Shah, A McKenzie, a B Steever, A Wach, P Philippsen, and J R Pringle. 1998. "Heterologous Modules for Efficient and Versatile PCR-Based Gene Targeting in Schizosaccharomyces Pombe." *Yeast (Chichester, England)* 14 (10): 943–51. doi:10.1002/(SICI)1097-0061(199807)14:10<943::AID-YEA292>3.0.CO;2-Y.

Bähler, Jürg, and Paul Nurse. 2001. "Fission Yeast Pom1p Kinase Activity Is Cell Cycle Regulated and Essential for Cellular Symmetry during Growth and Division." *EMBO Journal* 20 (5): 1064–73. doi:10.1093/emboj/20.5.1064.

Beckley, Janel R, Jun-Song Chen, Yanling Yang, Junmin Peng, and Kathleen L Gould. 2015. "A Degenerate Cohort of Yeast Membrane Trafficking DUBs Mediates Cell Polarity and Survival." *Molecular & Cellular Proteomics : MCP* 14 (12): 3132–41. doi:10.1074/mcp.M115.050039.

Beinhauer, Jens D., Iain M. Hagan, Johannes H. Hegemann, and Ursula Fleig. 1997. "Mal3, the Fission Yeast Homologue of the Human APC-Interacting Protein EB-1 Is Required for Microtubule Integrity and the Maintenance of Cell Form." *Journal of Cell Biology* 139 (3): 717–28. doi:10.1083/jcb.139.3.717.

Bendezu, F. O., and S. G. Martin. 2011. "Actin Cables and the Exocyst Form Two Independent Morphogenesis Pathways in the Fission Yeast." *Molecular Biology of the Cell* 22 (1): 44–53. doi:10.1091/mbc.E10-08-0720.

Bendezú, Felipe O, and Sophie G Martin. 2012. "Cdc42 Oscillations in Yeasts." *Science Signaling* 5 (253): pe53. doi:10.1126/scisignal.2003630.

Bendezú, Felipe O, Vincent Vincenzetti, Dimitrios Vavylonis, Romain Wyss, Horst Vogel, and Sophie G Martin. 2015. "Spontaneous Cdc42 Polarization Independent of GDI-Mediated Extraction and Actin-Based Trafficking," 1–30. doi:10.1371/journal.pbio.1002097.

Berg, Jeremy M., John L. Tymoczko, and Lubert Stryer. 2007. *Biochemie*. 6. Auflage. München: Elsevier GmbH, Spektrum Akademischer Verlag.

Bhatia, Payal, Olivier Hachet, Micha Hersch, Sergio A. Rincon, Martine Berthelot-Grosjean, Sascha Dalessi, Laetitia Basterra, Sven Bergmann, Anne Paoletti, and Sophie G. Martin. 2014. "Distinct Levels in Pom1 Gradients Limit Cdr2 Activity and Localization to Time and Position Division." *Cell Cycle* 13 (4): 538–52. doi:10.4161/cc.27411.

Bicho, Claudia C, David a Kelly, Hilary a Snaith, Andrew B Goryachev, and Kenneth E Sawin. 2010. "A Catalytic Role for Mod5 in the Formation of the Tea1 Cell Polarity Landmark." *Current Biology : CB* 20 (19). Elsevier: 1752–57. doi:10.1016/j.cub.2010.08.035.

Bodnar, Nicholas, and Tom Rapoport. 2017. "Toward an Understanding of the Cdc48/P97 ATPase." *F1000Research* 6 (0): 1318. doi:10.12688/f1000research.11683.1.

Bonazzi, Daria, Jean Daniel Julien, Maryse Romao, Rima Seddiki, Matthieu Piel, Arezki Boudaoud, and Nicolas Minc. 2014. "Symmetry Breaking in Spore Germination Relies on an Interplay between Polar Cap Stability and Spore Wall Mechanics (." *Developmental Cell* 28. Elsevier Inc.: 534–46. doi:10.1016/j.devcel.2018.07.018.

Brown, Deborah A., and John K. Rose. 1992. "Sorting of GPI-Anchored Proteins to Glycolipid-Enriched Membrane Subdomains during Transport to the Apical Cell Surface." *Cell* 68 (3): 533–44. doi:10.1016/0092-8674(92)90189-J.

Brunner, D, and P Nurse. 2000. “CLIP170-like Tip1p Spatially Organizes Microtubular Dynamics in Fission Yeast.” *Cell* 102 (5): 695–704. http://www.ncbi.nlm.nih.gov/pubmed/11007487.

Busch, Karl E., and Damian Brunner. 2004. “The Microtubule Plus End-Tracking Proteins Mal3p and Tip1p Cooperate for Cell-End Targeting of Interphase Microtubules.” *Current Biology* 14: 548–59. doi:10.1016/j.

Busch, Karl Emanuel, Jacky Hayles, Paul Nurse, and Damian Brunner. 2004. “Tea2p Kinesin Is Involved in Spatial Microtubule Organization by Transporting Tip1p on Microtubules.” *Developmental Cell* 6 (6): 831–43. doi:10.1016/j.devcel.2004.05.008.

Busto, Jon V, Annegret Elting, Daniel Haase, Felix Spira, Julian Kuhlman, Marco Schäfer-Herte, and Roland Wedlich-Söldner. 2018. “Lateral Plasma Membrane Compartmentalization Links Protein Function and Turnover.” *The EMBO Journal*, e99473. doi:10.15252/embj.201899473.

Cao, Xinwang, Michal a Surma, and Kai Simons. 2012. “Polarized Sorting and Trafficking in Epithelial Cells.” *Cell Research* 22 (5). Nature Publishing Group: 793–805. doi:10.1038/cr.2012.64.

Carrie Miceli, M., Miriana Moran, Chan D. Chung, Viresh P. Patel, T. Low, and W. Zinnanti. 2001. “Co-Stimulation and Counter-Stimulation: Lipid Raft Clustering Controls TCR Signaling and Functional Outcomes.” *Seminars in Immunology* 13 (2): 115–28. doi:10.1006/smim.2000.0303.

Cartagena-Lirola, Hugo, Angel Durán, and M Henar H Valdivieso. 2006. “The Schizosaccharomyces Pombe Cfr1+ Gene Participates in Mating through a New Pathway That Is Independent of Fus1+.” *Yeast (Chichester, England)* 23 (5): 375–88. doi:10.1002/yea.1361.

Chambers, John M, William S Cleveland, Beat Kleiner, and Paul A Tukey. 1983. “Comparing Data Distributions.” In *Graphical Methods for Data Analysis*, 60–63.

Chen, Qian, and Thomas D Pollard. 2013. “Actin Filament Severing by Cofilin Dismantles Actin Patches and Produces Mother Filaments for New Patches.” *Current Biology : CB* 23 (13). Elsevier Ltd: 1154–62. doi:10.1016/j.cub.2013.05.005.

Coll, Pedro M, Yadira Trillo, Amagoia Amatzazurra, and Pilar Perez. 2003. “Gef1p, a New

Guanine Nucleotide Exchange Factor for Cdc42p, Regulates Polarity in Schizosaccharomyces Pombe." *Molecular Biology of the Cell* 14 (January): 313–23. doi:10.1091/mbc.E02.

Cooke, Ira R., Kurt Kremer, and Markus Deserno. 2005. "Tunable Generic Model for Fluid Bilayer Membranes." *Physical Review E* 72 (1): 011506. doi:10.1103/PhysRevE.72.011506.

Cross, Nicholas L. 2004. "Reorganization of Lipid Rafts During Capacitation of Human Sperm1." *Biology of Reproduction* 71 (4): 1367–73. doi:10.1095/biolreprod.104.030502.

Curto, M-Ángeles, Mohammad Reza Sharifmoghadam, Eduardo Calpena, Nagore De León, Marta Hoya, Cristina Doncel, Janet Leatherwood, and M-Henar Valdivieso. 2014. "Membrane Organization and Cell Fusion during Mating in Fission Yeast Requires Multipass Membrane Protein Prm1." *Genetics* 196 (4): 1059–76. doi:10.1534/genetics.113.159558.

Daga, Rafael R., and Fred Chang. 2005. "Dynamic Positioning of the Fission Yeast Cell Division Plane." *Proceedings of the National Academy of Sciences of the United States of America* 102 (23): 8228. doi:10.1073/pnas.0409021102.

Danielsen, E. Michael, and Gert H. Hansen. 2003. "Lipid Rafts in Epithelial Brush Borders: Atypical Membrane Microdomains with Specialized Functions." *Biochimica et Biophysica Acta - Biomembranes* 1617 (1–2): 1–9. doi:10.1016/j.bbamem.2003.09.005.

Das, Akash, Michael S Brown, Donald D Anderson, Joseph L Goldstein, and Arun Radhakrishnan. 2014. "Three Pools of Plasma Membrane Cholesterol and Their Relation to Cholesterol Homeostasis." *ELife*, June, e02882. doi:10.7554/eLife.02882.

Das, Maitreyi, Tyler Drake, David J. Wiley, Peter Buchwald, Dimitrios Vavylonis, and Fulvia Verde. 2012. "Oscillatory Dynamics of Cdc42 GTPase in the Control of Polarized Growth." *Science*. doi:10.1126/science.1218377.

Dickson, Barry J. 2002. "Molecular Mechanisms of Axon Guidance." *Science* 298 (5600): 1959–64. doi:10.1126/science.1072165.

Dimopoulos, Sotiris, Christian E. Mayer, Fabian Rudolf, and Joerg Stelling. 2014.

"Accurate Cell Segmentation in Microscopy Images Using Membrane Patterns." *Bioinformatics* 30 (18): 2644–51. doi:10.1093/bioinformatics/btu302.

Dodgson, James, Anatole Chessel, Miki Yamamoto, Federico Vaggi, Susan Cox, Edward Rosten, David Albrecht, et al. 2013. "Spatial Segregation of Polarity Factors into Distinct Cortical Clusters Is Required for Cell Polarity Control." *Nature Communications* 4 (May). Nature Publishing Group: 1834. doi:10.1038/ncomms2813.

Downing, Kenneth H., and Eva Nogales. 1998. "New Insights into Microtubule Structure and Function from the Atomic Model of Tubulin." *European Biophysics Journal* 27 (5): 431–36. doi:10.1007/s002490050153.

Drake, Tyler, and Dimitrios Vavylonis. 2013. "Model of Fission Yeast Cell Shape Driven by Membrane-Bound Growth Factors and the Cytoskeleton." *PLoS Computational Biology* 9 (10): e1003287. doi:10.1371/journal.pcbi.1003287.

Dujon, Bernard A., and Edward J. Louis. 2017. "Genome Diversity and Evolution in the Budding Yeasts (Saccharomycotina)." *Genetics* 206 (2): 717–50. doi:10.1534/genetics.116.199216.

Eggeling, Christian, Christian Ringemann, Rebecca Medda, Günter Schwarzmann, Konrad Sandhoff, Svetlana Polyakova, Vladimir N. Belov, et al. 2009. "Direct Observation of the Nanoscale Dynamics of Membrane Lipids in a Living Cell." *Nature* 457 (7233): 1159–62. doi:10.1038/nature07596.

Etienne-Manneville, S. 2004. "Cdc42 - the Centre of Polarity." *Journal of Cell Science* 117 (8): 1291–1300. doi:10.1242/jcs.01115.

Etienne-Manneville, Sandrine, and Alan Hall. 2002. "Rho GTPases in Cell Biology." *Nature* 420 (6916): 629–35. doi:10.1038/nature01148.

Feoktistova, Anna, Dannel Mccollum, Ryoma Ohi, and Kathleen L Gould. 1999. "A Gene That Interacts with Mutations in the Arp2 / 3 Complex and Actin."

Finley, Daniel, Engin Özkaynak, and Alexander Varshavsky. 1987. "The Yeast Polyubiquitin Gene Is Essential for Resistance to High Temperatures, Starvation, and Other Stresses." *Cell* 48 (6): 1035–46. doi:10.1016/0092-8674(87)90711-2.

Givens, Robert M, Larry D Mesner, Joyce L Hamlin, Michael J Buck, and Joel a

Huberman. 2011. “Integrity of Chromatin and Replicating DNA in Nuclei Released from Fission Yeast by Semi-Automated Grinding in Liquid Nitrogen.” *BMC Research Notes* 4 (1). BioMed Central Ltd: 499. doi:10.1186/1756-0500-4-499.

Glynn, Jonathan M., Raymond J. Lustig, Ana Berlin, and Fred Chang. 2001. “Role of Bud6p and Tea1p in the Interaction between Actin and Microtubules for the Establishment of Cell Polarity in Fission Yeast.” *Current Biology* 11 (11): 836–45. doi:10.1016/S0960-9822(01)00235-4.

Goñi, Félix M. 2014. “The Basic Structure and Dynamics of Cell Membranes: An Update of the Singer-Nicolson Model.” *Biochimica et Biophysica Acta* 1838 (6). Elsevier B.V.: 1467–76. doi:10.1016/j.bbamem.2014.01.006.

Grider, M. H., D. Park, D. M. Spencer, and H. D. Shine. 2009. “Lipid Raft-Targeted Akt Promotes Axonal Branching and Growth Cone Expansion via MTOR and Rac1, Respectively.” *Journal of Neuroscience Research* 87 (14): 3033–42. doi:10.1002/jnr.22140.

Grossmann, Guido, Miroslava Opekarova, Linda Novakova, Jürgen Stolz, and Widmar Tanner. 2006. “Lipid Raft-Based Membrane Compartmentation of a Plant Transport Protein Expressed in Saccharomyces Cerevisiae.” *Eukaryotic Cell* 5 (6): 945–53. doi:10.1128/EC.00206-05.

Harder, Thomas, Peter Scheiffele, Paul Verkade, and Kai Simons. 1998. “Lipid Domain Structure of the Plasma Membrane Revealed by Patching of Membrane Components” 141 (4): 929–42.

Harmouch, N, J Coulon, and R Bonlay. 1995. “Identification of 24-Methylene-24,25-Dihydrolanosterol as a Precursor of Ergosterol in the Yeasts Schizosaccharomyces Pombe and Schizosaccharomyces Octosporus.” *FEMS Microbiology Letters* 134 (2–3): 147–52.

Harner, Max E., Ann Katrin Unger, Willie J.C. Geerts, Muriel Mari, Toshiaki Izawa, Maria Stenger, Stefan Geimer, Fulvio Reggiori, Benedikt Westermann, and Walter Neupert. 2016. “An Evidence Based Hypothesis on the Existence of Two Pathways of Mitochondrial Crista Formation.” *ELife* 5 (NOVEMBER2016): 1–25. doi:10.7554/eLife.18853.

Hayles, J, and P Nurse. 2001. “A Journey into Space.” *Nature Reviews. Molecular Cell*

Biology 2 (9): 647–56. doi:10.1038/35089520.

Head, Brian P., Jason N. Peart, Mathivadhani Panneerselvam, Takaakira Yokoyama, Matthew L. Pearn, Ingrid R. Niesman, Jacqueline A. Bonds, et al. 2010. "Loss of Caveolin-1 Accelerates Neurodegeneration and Aging." *PLoS ONE* 5 (12): 1–13. doi:10.1371/journal.pone.0015697.

Head, Brian P, Hemal H Patel, and Paul a Insel. 2014. "Interaction of Membrane/Lipid Rafts with the Cytoskeleton: Impact on Signaling and Function: Membrane/Lipid Rafts, Mediators of Cytoskeletal Arrangement and Cell Signaling." *Biochimica et Biophysica Acta* 1838 (2). Elsevier B.V.: 532–45. doi:10.1016/j.bbamem.2013.07.018.

Heerklotz, H. 2002. "Triton Promotes Domain Formation in Lipid Raft Mixtures." *Biophysical Journal* 83 (5). Elsevier: 2693–2701. doi:10.1016/S0006-3495(02)75278-8.

Henderson, Robert M, J Michael Edwardson, Nicholas A Geisse, and David E Saslowsky. 2004. "Lipid Rafts : Feeling Is Believing," no. 10: 39–43.

Hermann, Greg J., John W. Thatcher, John P. Mills, Karen G. Hales, Margaret T. Fuller, Jodi Nunnari, and Janet M. Shaw. 1998. "Mitochondrial Fusion in Yeast Requires the Transmembrane GTPase Fzo1p." *Journal of Cell Biology* 143 (2): 359–73. doi:10.1083/jcb.143.2.359.

Holmes, Kenneth C., D Popp, W Gebhard, and W Kabsch. 1990. "Atomic Model of the Actin Filament." *Nature*. doi:10.1038/347044a0.

Holthuis, Joost C M, and Anant K Menon. 2014. "Lipid Landscapes and Pipelines in Membrane Homeostasis." *Nature* 510 (7503): 48–57. doi:10.1038/nature13474.

Höög, Johanna L., Stephen M. Huisman, Damian Brunner, and Claude Antony. 2013. "Electron Tomography Reveals Novel Microtubule Lattice and Microtubule Organizing Centre Defects in +TIP Mutants." *PLoS ONE* 8 (4): 1–12. doi:10.1371/journal.pone.0061698.

Höög, Johanna L., Cindi Schwartz, Angela T. Noon, Eileen T. O'Toole, David N. Mastronarde, J. Richard McIntosh, and Claude Antony. 2007. "Organization of Interphase Microtubules in Fission Yeast Analyzed by Electron Tomography." *Developmental Cell* 12 (3): 349–61. doi:10.1016/j.devcel.2007.01.020.

Hoya, Marta, Francisco Yanguas, Sandra Moro, Cristina Prescianotto-Baschong, Cristina Doncel, Nagore de León, M. Ángeles Curto, Anne Spang, and M. Henar Valdivieso. 2017. "Traffic through the Trans-Golgi Network and the Endosomal System Requires Collaboration between Exomer and Clathrin Adaptors in Fission Yeast." *Genetics* 205 (2): 673–90. doi:10.1534/genetics.116.193458.

Huang, Cai. 2014. "Roles of E3 Ubiquitin Ligases in Cell Adhesion and Migration." *Cell Adhesion & Migration* 4 (1): 10–18. doi:10.4161/cam.4.1.9834.

Huffaker, Tim C, James H Thomas, and David Botstein. 1988. "Diverse Effects of Beta-Tubulin Mutations on Microtubule Formation and Function." *The Journal of Cell Biology* 106 (6): 1997–2010. doi:10.1083/jcb.106.6.1997.

Hughes, Adam L, Bridget L Todd, and Peter J Espenshade. 2005. "SREBP Pathway Responds to Sterols and Functions as an Oxygen Sensor in Fission Yeast." *Cell* 120 (6): 831–42. doi:10.1016/j.cell.2005.01.012.

Hughes, Bridget T., Christine C. Nwosu, and Peter J. Espenshade. 2009. "Degradation of Sterol Regulatory Element-Binding Protein Precursor Requires the Endoplasmic Reticulum-Associated Degradation Components Ubc7 and Hrd1 in Fission Yeast." *Journal of Biological Chemistry* 284 (31): 20512–21. doi:10.1074/jbc.M109.002436.

Huisman, Stephen M, and Damian Brunner. 2011. "Cell Polarity in Fission Yeast: A Matter of Confining, Positioning, and Switching Growth Zones." *Seminars in Cell & Developmental Biology* 22 (8). Elsevier Ltd: 799–805. doi:10.1016/j.semcdb.2011.07.013.

Hwang, Jiwon, Diedre Ribbens, Sumana Raychaudhuri, Leah Cairns, He Gu, and Adam Frost. 2016. "A Golgi Rhomboid Protease Rbd 2 Recruits Cdc 48 to Cleave Yeast SREBP."

Insenser, María, César Nombela, Gloria Molero, and Concha Gil. 2006. "Proteomic Analysis of Detergent-Resistant Membranes from Candida Albicans." *Proteomics* 6 Suppl 1 (April): S74-81. doi:10.1002/pmic.200500465.

Ishiguro, J. 1998. "Genetic Control of Fission Yeast Cell Wall Synthesis: The Genes Involved in Wall Biogenesis and Their Interactions in Schizosaccharomyces Pombe." *Genes & Genetic Systems* 73 (4): 181–91. doi:10.1266/ggs.73.181.

Islam, Mohammed Shehadul, Aditya Aryasomayajula, and Ponnambalam Ravi Selvaganapathy. 2017. "A Review on Macroscale and Microscale Cell Lysis Methods." *Micromachines* 8 (3). doi:10.3390/mi8030083.

Ito, Hirokazu, Tomoko Oshiro, Yasuyuki Fujita, Sachiko Kubota, Chikako Naito, Hokuto Ohtsuka, Hiroshi Murakami, and Hirofumi Aiba. 2010. "Pma1, a P-Type Proton ATPase, Is a Determinant of Chronological Life Span in Fission Yeast." *The Journal of Biological Chemistry* 285 (45): 34616–20. doi:10.1074/jbc.M110.175562.

Iwaki, Tomoko, Haruyuki Iefuji, Yoshikazu Hiraga, Akira Hosomi, Tomotake Morita, Yuko Giga-Hama, and Kaoru Takegawa. 2008. "Multiple Functions of Ergosterol in the Fission Yeast Schizosaccharomyces Pombe." *Microbiology (Reading, England)* 154 (Pt 3): 830–41. doi:10.1099/mic.0.2007/011155-0.

Johnson, Douglas I. 1999. "Cdc42: An Essential Rho-Type GTPase Controlling Eukaryotic Cell Polarity." *Microbiology and Molecular Biology Reviews : MMBR* 63 (1): 54–105. doi:citeulike-article-id:13113720.

Johnson, Jayme M., Meng Jin, and Daniel J. Lew. 2011. "Symmetry Breaking and the Establishment of Cell Polarity in Budding Yeast." *Current Opinion in Genetics and Development* 21 (6). Elsevier Ltd: 740–46. doi:10.1016/j.gde.2011.09.007.

Kawashima, Shigehiro A., Ai Takemoto, Paul Nurse, and Tarun M. Kapoor. 2012. "Analyzing Fission Yeast Multidrug Resistance Mechanisms to Develop a Genetically Tractable Model System for Chemical Biology." *Chemistry and Biology* 19 (7): 893–901. doi:10.1016/j.chembiol.2012.06.008.

Keating, T. J., and G. G. Borisy. 2000. "Immunostructural Evidence for the Template Mechanism of Microtubule Nucleation." *Nature Cell Biology* 2 (6): 352–57. doi:10.1038/35014045.

Kelly, Felice D., and Paul Nurse. 2011. "De Novo Growth Zone Formation from Fission Yeast Spheroplasts." *PLoS ONE* 6 (12). doi:10.1371/journal.pone.0027977.

Kijowski, Adam Rafal, Michèle Gemünden, David Dreher, Robin W Klemm, and Damian Brunner. n.d. "The Microtubule/Tea1p System Controls Cell Polarisation via Non-Vesicular Lipid Transport." *In Preparation*.

Kim, Dong-Uk, Jacqueline Hayles, Dongsup Kim, Valerie Wood, Han-Oh Park, Misun

Won, Hyang-Sook Yoo, et al. 2010. "Analysis of a Genome-Wide Set of Gene Deletions in the Fission Yeast Schizosaccharomyces Pombe." *Nature Biotechnology* 28 (6): 617–23. doi:10.1038/nbt.1628.

Klose, Christian, Christer S. Ejsing, Ana J. García-Sáez, Hermann Josef Kaiser, Julio L. Sampaio, Michal A. Surma, Andrej Shevchenko, Petra Schwille, and Kai Simons. 2010. "Yeast Lipids Can Phase-Separate into Micrometer-Scale Membrane Domains." *Journal of Biological Chemistry* 285 (39): 30224–32. doi:10.1074/jbc.M110.123554.

Klotzsch, Enrico, and Gerhard J Schütz. 2013. "A Critical Survey of Methods to Detect Plasma Membrane Rafts." *Philosophical Transactions of the Royal Society of London. Series B, Biological Sciences* 368 (1611): 20120033. doi:10.1098/rstb.2012.0033.

Klymchenko, Andrey S, and Rémy Kreder. 2014. "Fluorescent Probes for Lipid Rafts: From Model Membranes to Living Cells." *Chemistry & Biology* 21 (1): 97–113. doi:10.1016/j.chembiol.2013.11.009.

Kokkoris, Kyriakos, Daniela Gallo Castro, and Sophie G Martin. 2014. "The Tea4-PP1 Landmark Promotes Local Growth by Dual Cdc42 GEF Recruitment and GAP Exclusion." *Journal of Cell Science* 127 (Pt 9): 2005–16. doi:10.1242/jcs.142174.

Kono, Keiko, Yasushi Saeki, Satoshi Yoshida, Keiji Tanaka, and David Pellman. 2012. "Proteasomal Degradation Resolves Competition between Cell Polarization and Cellular Wound Healing." *Cell* 150 (1). Elsevier Inc.: 151–64. doi:10.1016/j.cell.2012.05.030.

Kovar, David R., Vladimir Sirotkin, and Matthew Lord. 2011. "Three's Company: The Fission Yeast Actin Cytoskeleton." *Trends in Cell Biology* 21 (3). Elsevier Ltd: 177–87. doi:10.1016/j.tcb.2010.11.001.

Kudo, N., N. Matsumori, H. Taoka, D. Fujiwara, E. P. Schreiner, B. Wolff, M. Yoshida, and S. Horinouchi. 1999. "Leptomycin B Inactivates CRM1/Exportin 1 by Covalent Modification at a Cysteine Residue in the Central Conserved Region." *Proceedings of the National Academy of Sciences* 96 (16): 9112–17. doi:10.1073/pnas.96.16.9112.

Kudo, Nobuaki, Saadi Khochbin, Kazuaki Kitano, Mitsuhiro Yanagida, Minoru Yoshida, and Sueharu Horinouchi. 1997. "CELL BIOLOGY AND METABOLISM : Molecular Cloning and Cell Cycle-Dependent Expression of Mammalian CRM1 , a Protein

Involved in Nuclear Export of Proteins Molecular Cloning and Cell Cycle-Dependent Expression of Mammalian CRM1 , a Protein Involved in Nuclea" 272 (47): 29742–51.

Kurzchalia, Teymuras V., Enno Hartmann, and Paul Dupree. 1995. "Guilty by Insolubility - Does a Protein's Detergent Insolubility Reflect a Caveolar Location?" *Trends in Cell Biology* 5 (5): 187–89. doi:10.1016/S0962-8924(00)88990-4.

Lange, Vinzenz, Paola Picotti, Bruno Domon, and Ruedi Aebersold. 2008. "Selected Reaction Monitoring for Quantitative Proteomics: A Tutorial." *Molecular Systems Biology* 4 (222): 222. doi:10.1038/msb.2008.61.

Laporte, Damien, Fabien Courtout, Benoît Pinson, Jim Dompierre, Bénédicte Salin, Lysiane Brocard, and Isabelle Sagot. 2015. "A Stable Microtubule Array Drives Fission Yeast Polarity Reestablishment upon Quiescence Exit." *Journal of Cell Biology* 210 (1): 99–113. doi:10.1083/jcb.201502025.

Leach, Michelle D., David A. Stead, Evelyn Argo, Donna M. Maccallum, and Alistair J.P. Brown. 2011. "Molecular and Proteomic Analyses Highlight the Importance of Ubiquitination for the Stress Resistance, Metabolic Adaptation, Morphogenetic Regulation and Virulence of Candida Albicans." *Molecular Microbiology* 79 (6): 1574–93. doi:10.1111/j.1365-2958.2011.07542.x.

Lee, Do Hee. 1998. "Proteasome Inhibitors: Valuable New Tools for Cell Biologists." *Trends in Cell Biology* 8 (10): 397–403. doi:10.1016/S0962-8924(98)01346-4.

Li, Cuifang, Ayako Kita, Yuuka Hashimoto, Misako Ihara, Ayaka Kato, Naoya Ogura, Akira Doi, et al. 2014. "Functional Link between Rab GTPase-Mediated Membrane Trafficking and PI4,5P2 Signaling." *Genes to Cells : Devoted to Molecular & Cellular Mechanisms* 19 (3): 177–97. doi:10.1111/gtc.12123.

Li, D, and R Roberts. 2001. "WD-Repeat Proteins: Structure Characteristics, Biological Function, and Their Involvement in Human Diseases." *Cellular and Molecular Life Sciences : CMLS* 58 (14): 2085–97. doi:10.1007/PL00000838.

Lingwood, Daniel, and Kai Simons. 2007. "Detergent Resistance as a Tool in Membrane Research." *Nature Protocols* 2 (9): 2159–65. doi:10.1038/nprot.2007.294.

London, Erwin, and Deborah A. Brown. 2000. "Insolubility of Lipids in Triton X-100:

Physical Origin and Relationship to Sphingolipid/Cholesterol Membrane Domains (Rafts)." *Biochimica et Biophysica Acta - Biomembranes* 1508 (1–2): 182–95. doi:10.1016/S0304-4157(00)00007-1.

Lozano, Monica M, Zhao Liu, Eva Sunnick, Andreas Janshoff, Krishna Kumar, and Steven G Boxer. 2013. "Colocalization of the Ganglioside GM1 and Cholesterol Detected by Secondary Ion Mass Spectrometry." *Journal of the American Chemical Society*.

Makushok, Tatyana, Paulo Alves, Stephen Michiel Huisman, Adam Rafal Kijowski, and Damian Brunner. 2016. "Sterol-Rich Membrane Domains Define Fission Yeast Cell Polarity." *Cell* 165 (5). Elsevier Inc.: 1182–96. doi:10.1016/j.cell.2016.04.037.

Marks, J., I. M. Hagan, and J. S. Hyams. 1986. "Growth Polarity and Cytokinesis in Fission Yeast: The Role of the Cytoskeleton." *Journal of Cell Science* 1986 (Supplement 5): 229–41. doi:10.1242/jcs.1986.Supplement_5.15.

Martín-García, Rebeca, Nagore De León, Mohammad Reza Sharifmoghadam, M. Ángeles Curto, Marta Hoya, Pilar Bustos-Sanmamed, and M. Henar Valdivieso. 2011. "The FN3 and BRCT Motifs in the Exomer Component Chs5p Define a Conserved Module That Is Necessary and Sufficient for Its Function." *Cellular and Molecular Life Sciences* 68 (17): 2907–17. doi:10.1007/s00018-010-0596-z.

Martín-García, Rebeca, and Daniel P Mulvihill. 2009. "Myosin V Spatially Regulates Microtubule Dynamics and Promotes the Ubiquitin-Dependent Degradation of the Fission Yeast CLIP-170 Homologue, Tip1." *Journal of Cell Science* 122 (Pt 21): 3862–72. doi:10.1242/jcs.054460.

Martin, Sophie G., and Martine Berthelot-Grosjean. 2009. "Polar Gradients of the DYRK-Family Kinase Pom1 Couple Cell Length with the Cell Cycle." *Nature* 459 (7248). Nature Publishing Group: 852–56. doi:10.1038/nature08054.

Martin, Sophie G., and Fred Chang. 2006. "Dynamics of the Formin For3p in Actin Cable Assembly." *Current Biology* 16 (12): 1161–70. doi:10.1016/j.cub.2006.04.040.

Martin, Sophie G., W. Hayes McDonald, John R. Yates, and Fred Chang. 2005. "Tea4p Links Microtubule plus Ends with the Formin For3p in the Establishment of Cell Polarity." *Developmental Cell* 8 (4): 479–91. doi:10.1016/j.devcel.2005.02.008.

Martin, Sophie G, and Robert a Arkowitz. 2014. "Cell Polarization in Budding and Fission

Yeasts." *FEMS Microbiology Reviews* 38 (2): 228–53. doi:10.1111/1574-6976.12055.

Mata, Juan, and Paul Nurse. 1997. "Tea1 and the Microtubular Cytoskeleton Are Important for Generating Global Spatial Order within the Fission Yeast Cell" 89: 939–49.

Matsuyama, Akihisa, Ritsuko Arai, Yoko Yashiroda, Atsuko Shirai, Ayako Kamata, Shigeko Sekido, Yumiko Kobayashi, et al. 2006. "ORFeome Cloning and Global Analysis of Protein Localization in the Fission Yeast Schizosaccharomyces Pombe." *Nature Biotechnology* 24 (7): 841–47. doi:10.1038/nbt1222.

Maundrell, Kinsey. 1990. "Nmt1 of Fission Yeast." *Journal of Biological Chemistry* 265 (19): 10857–64.

May, J. W., and J. M. Mitchison. 1986. "Length Growth in Fission Yeast Cells Measured by Two Novel Techniques." *Nature* 322 (6081): 752–54. doi:10.1038/322752a0.

Meinhardt, S., R. L. C. Vink, and F. Schmid. 2013. "Monolayer Curvature Stabilizes Nanoscale Raft Domains in Mixed Lipid Bilayers." *Proceedings of the National Academy of Sciences*, March. doi:10.1073/pnas.1221075110.

Meng, Yunfang, Chao Zhang, Jiu Yi, Zhaojing Zhou, Zhenzong Fa, Jingyu Zhao, Yali Yang, Wei Fang, Yan Wang, and Wan Qing Liao. 2016. "Deubiquitinase Ubp5 Is Required for the Growth and Pathogenicity of Cryptococcus Gattii." *PLoS ONE* 11 (4): 1–16. doi:10.1371/journal.pone.0153219.

Mesmin, Bruno, and Bruno Antonny. 2016. "The Counterflow Transport of Sterols and PI4P." *Biochimica et Biophysica Acta - Molecular and Cell Biology of Lipids* 1861 (8): 940–51. doi:10.1016/j.bbalip.2016.02.024.

Miller, P J, and D I Johnson. 1994. "Cdc42p GTPase Is Involved in Controlling Polarized Cell Growth in Schizosaccharomyces Pombe." *Molecular and Cellular Biology* 14 (2): 1075–83. doi:10.1128/MCB.14.2.1075.

Mitchison, J M, and P Nurse. 1985. "Growth in Cell Length in the Fission Yeast Schizosaccharomyces Pom Be." *J. Cell Sci* 75: 357–76.

Mitchison, Tim, and Marc Kirschner. 1984. "Dynamic Instability of Microtubule Growth." *Nature* 312 (5991): 237–42. doi:10.1038/312237a0.

Molnár, Eszter, Mahima Swamy, Martin Holzer, Katharina Beck-García, Remigiusz

Worch, Christoph Thiele, Gernot Guigas, et al. 2012. “Cholesterol and Sphingomyelin Drive Ligand-Independent T-Cell Antigen Receptor Nanoclustering.” *Journal of Biological Chemistry* 287 (51): 42664–74. doi:10.1074/jbc.M112.386045.

Mooren, Olivia L., Brian J. Galletta, and John A. Cooper. 2012. “Roles for Actin Assembly in Endocytosis.” *Annual Review of Biochemistry* 81 (1): 661–86. doi:10.1146/annurev-biochem-060910-094416.

Moreno, S, Amar Klar, and Paul Nurse. 1991. “Molecular Genetic Analysis of Fission Yeast Schizosaccharomyces Pombe.” *Methods in Enzymology* 194: 795–823. http://www.ncbi.nlm.nih.gov/pubmed/2005825.

Mozdy, Amy D, and Janet M Shaw. 2003. “A Fuzzy Mitochondrial Fusion Apparatus Comes into Focus.” *Nature Reviews. Molecular Cell Biology* 4 (6): 468–78. doi:10.1038/nrm1125.

Nakano, K, R Arai, and I Mabuchi. 1997. “The Small GTP-Binding Protein Rho1 Is a Multifunctional Protein That Regulates Actin Localization, Cell Polarity, and Septum Formation in the Fission Yeast Schizosaccharomyces Pombe.” *Genes to Cells : Devoted to Molecular & Cellular Mechanisms* 2 (11): 679–94.

Nicolson, Garth L. 2014. “The Fluid-Mosaic Model of Membrane Structure: Still Relevant to Understanding the Structure, Function and Dynamics of Biological Membranes after More than 40 Years.” *Biochimica et Biophysica Acta* 1838 (6). Elsevier B.V.: 1451–66. doi:10.1016/j.bbamem.2013.10.019.

Ogiso, Yasunari, Reiko Sugiura, Tsuneyoshi Kamo, Satoshi Yanagiya, Yabin Lu, Koei Okazaki, Hisato Shuntoh, and Takayoshi Kuno. 2004. “Lub1 Participates in Ubiquitin Homeostasis and Stress Response via Maintenance of Cellular Ubiquitin Contents in Fission Yeast.” *Molecular and Cellular Biology* 24 (6): 2324–31. doi:10.1128/MCB.24.6.2324.

Owen, Dylan M, and Katharina Gaus. 2013. “Imaging Lipid Domains in Cell Membranes: The Advent of Super-Resolution Fluorescence Microscopy.” *Frontiers in Plant Science* 4 (December): 503. doi:10.3389/fpls.2013.00503.

Papanayotou, Irene, Beimeng Sun, Amy F. Roth, and Nicholas G. Davis. 2010. “Protein Aggregation Induced during Glass Bead Lysis of Yeast.” *Yeast*. doi:10.1002/yea.1771.

Pardo, Mercedes, and Paul Nurse. 2005. "The Nuclear Rim Protein Amo1 Is Required for Proper Microtubule Cytoskeleton Organisation in Fission Yeast." *Journal of Cell Science* 118 (Pt 8): 1705–14. doi:10.1242/jcs.02305.

Pelham, Robert J., and Fred Chang. 2002. "Actin Dynamics in the Contractile Ring during Cytokinesis in Fission Yeast." *Nature* 419 (6902): 82–86. doi:10.1038/nature00999.

Penney, Mary, Itaru Samejima, Caroline R. Wilkinson, Christopher J. McInerny, Søs G. Mathiassen, Mairi Wallace, Takashi Toda, Rasmus Hartmann-Petersen, and Colin Gordon. 2012. "Fission Yeast 26S Proteasome Mutants Are Multi-Drug Resistant Due to Stabilization of the Pap1 Transcription Factor." *PLoS ONE* 7 (11): 1–8. doi:10.1371/journal.pone.0050796.

Pérez, Pilar, Elvira Portales, and Beatriz Santos. 2015. "Rho4 Interaction with Exocyst and Septins Regulates Cell Separation in Fission Yeast." *Microbiology (United Kingdom)* 161 (2015): 948–59. doi:10.1099/mic.0.000062.

Perez, Pilar, and Sergio a Rincón. 2010. "Rho GTPases: Regulation of Cell Polarity and Growth in Yeasts." *The Biochemical Journal* 426 (3): 243–53. doi:10.1042/BJ20091823.

Picotti, Paola, Bernd Bodenmiller, Lukas N Mueller, Bruno Domon, and Ruedi Aebersold. 2009. "Full Dynamic Range Proteome Analysis of S. Cerevisiae by Targeted Proteomics." *Cell* 138 (4). Elsevier Ltd: 795–806. doi:10.1016/j.cell.2009.05.051.

Pike, Linda J. 2006. "Rafts Defined: A Report on the Keystone Symposium on Lipid Rafts and Cell Function." *Journal of Lipid Research* 47 (7): 1597–98. doi:10.1194/jlr.E600002-JLR200.

Pöhlmann, Jennifer, and Ursula Fleig. 2010. "Asp1, a Conserved 1/3 Inositol Polyphosphate Kinase, Regulates the Dimorphic Switch in Schizosaccharomyces Pombe." *Molecular and Cellular Biology* 30 (18): 4535–47. doi:10.1128/MCB.00472-10.

Pöhlmann, Jennifer, Carmen Risse, Constanze Seidel, Thomas Pohlmann, Visnja Jakopec, Eva Walla, Pascal Ramrath, et al. 2014. "The Vip1 Inositol Polyphosphate Kinase Family Regulates Polarized Growth and Modulates the Microtubule Cytoskeleton in Fungi." *PLoS Genetics* 10 (9). doi:10.1371/journal.pgen.1004586.

Presti, Libera Lo, Fred Chang, and Sophie G Martin. 2012. "Myosin Vs Organize Actin Cables in Fission Yeast." *Molecular Biology of the Cell* 23 (23): 4579–91. doi:10.1091/mbc.E12-07-0499.

Proszynski, Tomasz J, Robin W Klemm, Maike Gravert, Peggy P Hsu, Yvonne Gloor, Jan Wagner, Karol Kozak, et al. 2005. "A Genome-Wide Visual Screen Reveals a Role for Sphingolipids and Ergosterol in Cell Surface Delivery in Yeast." *Proceedings of the National Academy of Sciences of the United States of America* 102 (50): 17981–86. doi:10.1073/pnas.0509107102.

Revilla-Guarinos, M. T., R. Martin-Garcia, M. A. Villar-Tajadura, M. Estravis, P. M. Coll, and P. Perez. 2016. "Rga6 Is a Fission Yeast Rho GAP Involved in Cdc42 Regulation of Polarized Growth." *Molecular Biology of the Cell* 27 (9): 1524–35. doi:10.1091/mbc.E15-12-0818.

Ridley, Anne J., Martin A. Schwartz, Keith Burridge, Richard A. Firtel, Mark H. Ginsberg, Gary Borisy, J. Thomas Parsons, and Alan Rick Horwitz. 2003. "Cell Migration: Integrating Signals from Front to Back." *Science* 302 (5651): 1704–9. doi:10.1126/science.1092053.

Rieder, S E, and S D Emr. 2001. "Overview of Subcellular Fractionation Procedures for the Yeast Saccharomyces Cerevisiae." *Current Protocols in Cell Biology / Editorial Board, Juan S. Bonifacino ... [et Al.]* Chapter 3 (May): Unit 3.7. doi:10.1002/0471143030.cb0307s07.

Rincon, Sergio A., Payal Bhatia, Claudia Bicho, Merc?? Guzman-Vendrell, Vincent Fraisier, Weronika E. Borek, Flavia de Lima Alves, et al. 2014. "Pom1 Regulates the Assembly of Cdr2-Mid1 Cortical Nodes for Robust Spatial Control of Cytokinesis." *Journal of Cell Biology* 206 (1): 61–77. doi:10.1083/jcb.201311097.

Rodrigues, Robim M., Peter Macko, Taina Palosaari, and Maurice P. Whelan. 2011. "Autofluorescence Microscopy: A Non-Destructive Tool to Monitor Mitochondrial Toxicity." *Toxicology Letters* 206 (3). Elsevier Ireland Ltd: 281–88. doi:10.1016/j.toxlet.2011.06.025.

Sandblad, Linda, Karl Emanuel Busch, Peter Tittmann, Heinz Gross, Damian Brunner, and Andreas Hoenger. 2006. "The Schizosaccharomyces Pombe EB1 Homolog Mal3p Binds and Stabilizes the Microtubule Lattice Seam." *Cell* 127 (7): 1415–24.

doi:10.1016/j.cell.2006.11.025.

Santos, Beatriz, Javier Gutie, Teresa M Calonge, and Pilar Pe. 2003. "Novel Rho GTPase Involved in Cytokinesis and Cell Wall Integrity in the Fission Yeast Schizosaccharomyces Pombe." *Society* 2 (3): 521–33. doi:10.1128/EC.2.3.521.

Satoh, Ryosuke, Kanako Hagihara, and Reiko Sugiura. 2018. "Rae1-Mediated Nuclear Export of Rnc1 Is an Important Determinant in Controlling MAPK Signaling." *Current Genetics* 64 (1). Springer Berlin Heidelberg: 103–8. doi:10.1007/s00294-017-0732-5.

Satoh, Ryosuke, Yasuhiro Matsumura, Akitomo Tanaka, Makoto Takada, Yuna Ito, Kanako Hagihara, Masahiro Inari, et al. 2017. "Spatial Regulation of the KH Domain RNA-Binding Protein Rnc1 Mediated by a Crm1-Independent Nuclear Export System in Schizosaccharomyces Pombe." *Molecular Microbiology* 104 (3): 428–48. doi:10.1111/mmi.13636.

Sawin, K E, and P Nurse. 1998. "Regulation of Cell Polarity by Microtubules in Fission Yeast." *The Journal of Cell Biology* 142 (2): 457–71. doi:10.1083/jcb.142.2.457.

Schaffner, W., and C. Weissmann. 1973. "A Rapid, Sensitive, and Specific Method for the Determination of Protein in Dilute Solution." *Analytical Biochemistry*. doi:10.1016/0003-2697(73)90217-0.

Schuck, Sebastian, Masanori Honsho, Kim Ekroos, Andrej Shevchenko, and Kai Simons. 2003. "Resistance of Cell Membranes to Different Detergents." *Proceedings of the National Academy of Sciences of the United States of America* 100 (10): 5795–5800. doi:10.1073/pnas.0631579100.

Schuck, Sebastian, and Kai Simons. 2004. "Polarized Sorting in Epithelial Cells: Raft Clustering and the Biogenesis of the Apical Membrane." *Journal of Cell Science* 117 (Pt 25): 5955–64. doi:10.1242/jcs.01596.

Sesaki, Hiromi, and Robert E. Jensen. 1999. "Division versus Fusion: Dnm1p and Fzo1p Antagonistically Regulate Mitochondrial Shape." *Journal of Cell Biology*. doi:10.1083/jcb.147.4.699.

Siegrist, S E, and C Q Doe. 2007. "Microtubule-Induced Cortical Cell Polarity." *Genes & Development* 21 (5): 483–96. doi:10.1101/gad.1511207.contractile.

Simons, Kai, and Mathias J. Gerl. 2010. "Revitalizing Membrane Rafts: New Tools and Insights." *Nature Reviews Molecular Cell Biology* 11 (10). Nature Publishing Group: 688–99. doi:10.1038/nrm2977.

Simons, Kai, and Elina Ikonen. 1997. "Functional Rafts in Cell Membranes," 569–72.

Simons, Kai, and Julio L Sampaio. 2011. "Membrane Organization and Lipid Rafts." *Cold Spring Harbor Perspectives in Biology* 3 (10): a004697. doi:10.1101/cshperspect.a004697.

Singer, S. J., and Garth L Nicolson. 1972. "The Fluid Mosaic Model of the Structure of Cell Membranes." *Science* 175: 720–31.

Sirotkin, Vladimir, Julien Berro, Keely Macmillan, Lindsey Zhao, and Thomas D. Pollard. 2010. "Quantitative Analysis of the Mechanism of Endocytic Actin Patch Assembly and Disassembly in Fission Yeast." *Molecular Biology of the Cell* 21: 2894–2904. doi:10.1091/mbc.E10.

Slaughter, Brian, and Rong Li. 2006. "Toward a Molecular Interpretation of the Surface Stress Theory for Yeast Morphogenesis." *Current Opinion in Cell Biology* 18 (1): 47–53. doi:10.1016/j.ceb.2005.11.003.

Snaith, Hilary A., and Kenneth E. Sawin. 2003. "Fission Yeast Mod5p Regulates Polarized Growth through Anchoring of Tea1p at Cell Tips." *Nature* 423 (6940): 647–51. doi:10.1038/nature01672.

Sommer, Christoph, Christoph Straehle, Köthe Ullrich, and Fred A. Hamprecht. 2011. "ILASTIK : Interactive Learning and Segmentation Toolkit." *Eighth IEEE International Symposium on Biomedical Imaging (ISBI): From Nano to Macro*, no. 1: 230–33. doi:10.1109/ISBI.2011.5872394.

Stewart, Emerson V., Christine C. Nwosu, Zongtian Tong, Assen Roguev, Timothy D. Cummins, Dong Uk Kim, Jacqueline Hayles, et al. 2011. "Yeast SREBP Cleavage Activation Requires the Golgi Dsc E3 Ligase Complex." *Molecular Cell* 42 (2). Elsevier Inc.: 160–71. doi:10.1016/j.molcel.2011.02.035.

Su, B., L. Gao, F. Meng, L. W. Guo, J. Rothschild, and I. H. Gelman. 2013. "Adhesion-Mediated Cytoskeletal Remodeling Is Controlled by the Direct Scaffolding of Src from FAK Complexes to Lipid Rafts by SSeCKS/AKAP12." *Oncogene* 32 (16): 2016–

26. doi:10.1038/onc.2012.218.

Swamy, Musti J., Laura Ciani, Mingtao Ge, Andrew K. Smith, David Holowka, Barbara Baird, and Jack H. Freed. 2006. "Coexisting Domains in the Plasma Membranes of Live Cells Characterized by Spin-Label ESR Spectroscopy." *Biophysical Journal* 90 (12): 4452–65. doi:10.1529/biophysj.105.070839.

Takeda, Tetsuya, Toshimitsu Kawate, and Fred Chang. 2004. "Organization of a Sterol-Rich Membrane Domain by Cdc15p during Cytokinesis in Fission Yeast." *Nature Cell Biology* 6 (11): 1142–44. doi:10.1038/ncb1189.

Tatebe, Hisashi, Kentaro Nakano, Rachel Maximo, and Kazuhiro Shiozaki. 2008. "Pom1 DYRK Regulates Localization of the Rga4 GAP to Ensure Bipolar Activation of Cdc42 in Fission Yeast." *Current Biology* 18 (5): 322–30. doi:10.1016/j.cub.2008.02.005.

Tatebe, Hisashi, Koichi Shimada, Satoru Uzawa, Susumu Morigasaki, and Kazuhiro Shiozaki. 2005. "Wsh3/Tea4 Is a Novel Cell-End Factor Essential for Bipolar Distribution of Tea1 and Protects Cell Polarity under Environmental Stress in S. Pombe." *Current Biology* 15 (11): 1006–15. doi:10.1016/j.cub.2005.04.061.

Terenna, Courtney R, Tatyana Makushok, Guilhem Velve-Casquillas, Damien Baigl, Yong Chen, Michel Bornens, Anne Paoletti, Matthieu Piel, and Phong T Tran. 2008. "Physical Mechanisms Redirecting Cell Polarity and Cell Shape in Fission Yeast." *Current Biology : CB* 18 (22). Elsevier Ltd: 1748–53. doi:10.1016/j.cub.2008.09.047.

Thompson, T. C., S. A. Tahir, L. Li, M. Watanabe, K. Naruishi, G. Yang, D. Kadmon, et al. 2010. "The Role of Caveolin-1 in Prostate Cancer: Clinical Implications." *Prostate Cancer and Prostatic Diseases* 13 (1): 6–11. doi:10.1038/pcan.2009.29.

Tomassian, T., L. A. Humphries, S. D. Liu, O. Silva, D. G. Brooks, and M. C. Miceli. 2011. "Caveolin-1 Orchestrates TCR Synaptic Polarity, Signal Specificity, and Function in CD8 T Cells." *The Journal of Immunology* 187 (6): 2993–3002. doi:10.4049/jimmunol.1101447.

Topolski, Boris, Visnja Jakopec, and Ursula Fleig. 2016. "Segregation Fidelity and Spindle Function in Schizosaccharomyces Pombe" 36 (24): 3128–40. doi:10.1128/MCB.00330-16.Address.

Tran, P. T., L. Marsh, V. Doye, S. Inoué, and F. Chang. 2001. "A Mechanism for Nuclear Positioning in Fission Yeast Based on Microtubule Pushing." *Journal of Cell Biology* 153 (2): 397–411. doi:10.1083/jcb.153.2.397.

Umesono, Kazuhiko, Takashi Toda, Shigeo Hayashi, and Mitsuhiro Yanagida. 1983. "Two Cell Division Cycle Genes NDA2 and NDA3 of the Fission Yeast Schizosaccharomyces Pombe Control Microtubular Organization and Sensitivity to Anti-Mitotic Benzimidazole Compounds." *Journal of Molecular Biology* 168 (2): 271–84. doi:10.1016/S0022-2836(83)80018-7.

van Meer, Gerrit, Dennis R Voelker, and Gerald W Feigenson. 2008. "Membrane Lipids: Where They Are and How They Behave." *Nature Reviews. Molecular Cell Biology* 9 (2): 112–24. doi:10.1038/nrm2330.

Vega, Leticia R., and Frank Solomon. 1997. "Microtubule Function in Morphological Differentiation: Growth Zones and Growth Cones." *Cell* 89 (6): 825–28. doi:10.1016/S0092-8674(00)80266-4.

Vögtle, F. Nora, Julia M. Burkhart, Humberto Gonczarowska-Jorge, Cansu Kücükköse, Asli Aras Taskin, Dominik Kopczynski, Robert Ahrends, et al. 2017. "Landscape of Submitochondrial Protein Distribution." *Nature Communications* 8 (1). Springer US. doi:10.1038/s41467-017-00359-0.

Von Loeffelholz, Ottilie, Neil A. Venables, Douglas Robert Drummond, Miho Katsuki, Robert Cross, and Carolyn A. Moores. 2017. "Nucleotide- and Mal3-Dependent Changes in Fission Yeast Microtubules Suggest a Structural Plasticity View of Dynamics." *Nature Communications* 8 (1). Springer US: 1–13. doi:10.1038/s41467-017-02241-5.

Wachtler, V. 2003. "Sterol-Rich Plasma Membrane Domains in the Fission Yeast Schizosaccharomyces Pombe." *Journal of Cell Science* 116 (5): 867–74. doi:10.1242/jcs.00299.

Wachtler, Volker, and Mohan K. Balasubramanian. 2006. "Yeast Lipid Rafts? - An Emerging View." *Trends in Cell Biology* 16 (1): 1–4. doi:10.1016/j.tcb.2005.11.008.

Wang, Yuchong, Kathryn S Lilley, and Stephen G Oliver. 2014. "A Protocol for the Subcellular Fractionation of Saccharomyces Cerevisiae Using Nitrogen Cavitation and Density Gradient Centrifugation," no. February: 127–35. doi:10.1002/yea.

Wixon, Jo. 2002. “Featured Organism: Schizosaccharomyces Pombe, the Fission Yeast.” *Comparative and Functional Genomics* 3 (2): 194–204. doi:10.1002/cfg.92.

Wood, Elizabeth, and Paul Nurse. 2013. “Pom1 and Cell Size Homeostasis in Fission Yeast.” *Cell Cycle* 12 (19): 3228–36. doi:10.4161/cc.26462.

Wood, V., R. Gwilliam, M. A. Rajandream, M. Lyne, R. Lyne, A. Stewart, J. Sgouros, et al. 2002. “The Genome Sequence of Schizosaccharomyces Pombe.” *Nature* 415 (6874): 871–80. doi:10.1038/nature724.

Wood, Valerie, Midori A. Harris, Mark D. McDowall, Kim Rutherford, Brendan W. Vaughan, Daniel M. Staines, Martin Aslett, et al. 2012. “PomBase: A Comprehensive Online Resource for Fission Yeast.” *Nucleic Acids Research* 40 (D1): 695–99. doi:10.1093/nar/gkr853.

Xu, Chao, and Jinrong Min. 2011. “Structure and Function of WD40 Domain Proteins.” *Protein and Cell* 2 (3): 202–14. doi:10.1007/s13238-011-1018-1.

Xu, Guoqiang, and Samie R Jaffrey. 2012. “The New Landscape of Protein Ubiquitination.” *Nature Biotechnology* 29 (12): 1098–1100. doi:10.1016/j.chemosphere.2012.12.037.Reactivity.

Yaffe, M. P., N. Stuurman, and R. D. Vale. 2003. “Mitochondrial Positioning in Fission Yeast Is Driven by Association with Dynamic Microtubules and Mitotic Spindle Poles.” *Proceedings of the National Academy of Sciences* 100 (20): 11424–28. doi:10.1073/pnas.1534703100.

Yanagida, Mitsuhiro. 2002. “The Model Unicellular Eukaryote, Schizosaccharomyces Pombe.” *Genome Biology* 3 (3): COMMENT2003. doi:10.1186/gb-2002-3-3-comment2003.

Yeaman, Charles, Kent K Grindstaff, and W James Nelson. 1999. “New Perspectives on Mechanisms Involved in Generating Epithelial Cell Polarity” 79 (1): 73–98.

Zaitsevskaya-Carter, T, and J A Cooper. 1997. “Spm1, a Stress Activated MAP Kinase That Regulates Morphogenisis in S.Pombe.” *Embo* 16 (6): 1318–31.

Zhang, Dan, Aleksandar Vjestica, and Snezhana Oliferenko. 2012. “Plasma Membrane Tethering of the Cortical ER Necessitates Its Finely Reticulated Architecture.” *Current Biology : CB* 22 (21). Elsevier Ltd: 2048–52. doi:10.1016/j.cub.2012.08.047.

Zheng, Hongli, Jilong Yin, Zhen Gao, He Huang, Xiaojun Ji, and Chang Dou. 2011. "Disruption of Chlorella Vulgaris Cells for the Release of Biodiesel-Producing Lipids: A Comparison of Grinding, Ultrasonication, Bead Milling, Enzymatic Lysis, and Microwaves." *Applied Biochemistry and Biotechnology* 164 (7): 1215–24. doi:10.1007/s12010-011-9207-1.

Appendix

Strain no.	Genotype	Source	Adapted from
DB558	h-		
DB1886	h- Pnmt1-GFP-tna1::KanMX6	(Makushok et al. 2016), Lab collection	
DB1930	h- Pnmt1-GFP-tna1::KanMX6 tea1Δ::ura4+ ura4-D18	(Makushok et al. 2016), Lab collection	
DB3685	h+ scd1-3GFP::KanMX6	(Kelly and Nurse 2011)	
DB4020	h+ cdc42-3::KanMX6	Lab collection	(Tatebe et al. 2008)
DB4148	h- (SPAC23H4.01c)Δ::KanMX6	Lab collection	(Kim et al. 2010) Bioneer deletion library (V4-P07-29)
DB4207	h+ ura4-294::[shk1 promoter:ScGIC2 CRIB:3xGFP:ura4+]	Lab collection	(Tatebe et al. 2008)
DB4424	h+ cdc42-mCherry-SW-term::KanMX6-3'UTR CRIB-3GFP::ura4+		(Bendezú et al. 2015)
DB4482	h? (SPAC4H3.01)Δ::KanMX6 Pnmt1-GFP-tna1::KanMX6	This study	(Kim et al. 2010), Bioneer deletion library (V5-P22-05)
DB4516	h? (SPCPB16A4.05c)Δ::KanMX6 Pnmt1-GFP-tna1::KanMX6	This study	(Kim et al. 2010), Bioneer deletion library (V5-P28-41)
DB4709	h? fzo1Δ::KanMX6 Pnmt1-GFP-tna1::KanMX6	This study	(Kim et al. 2010), Bioneer deletion library (V5-P25-56)
DB4722	h? mfs3Δ::KanMX6 Pnmt1-GFP-tna1::KanMX6	This study	(Kim et al. 2010), Bioneer deletion library (V5-P34-64)
DB4737	h? cfr1Δ::KanMX6 Pnmt1-GFP-tna1::KanMX6	This study	(Kim et al. 2010), Bioneer deletion library (V5-P24-47)
DB4749	h? cfr1Δ::KanMX6 tea1Δ::ura4+ ura4-D18 Pnmt1-GFP-tna1::KanMX6	This study	(Kim et al. 2010), Bioneer deletion library (V5-P24-47)
DB4755	h? mfs3Δ::KanMX6 tea1::ura4+ ura4-D18 Pnmt1-GFP-na1::KanMX6	This study	(Kim et al. 2010), Bioneer deletion library (V5-P34-64)

DB4769	h? fzo1Δ::KanMX6 tea1::ura4+ ura4-D18 Pnmt1-GFP-tna1::KanMX6	This study	(Kim et al. 2010), Bioneer deletion library (V5-P25-56)
DB4822	h+ kes1Δ::KanMX6	Kijowski et al. (in preparation)	(Kim et al. 2010), Bioneer deletion library (V4-P14-96)
DB4826	h+ (SPCC23B6.01c)Δ::KanMX6	Kijowski et al. (in preparation)	(Kim et al. 2010), Bioneer deletion library (V4-P26-80)
DB5046	h? cdc42-3::KanMX6 tea1::ura4+ ura4-D18	This study	
DB5071	h? kes1Δ::KanMX6 Pnmt1-GFP-tna1::KanMX6	This study	
DB5085	h? osh7(SPCC23B6.01c)Δ::KanMX6 Pnmt1-GFP-tna1::KanMX6	This study	
DB5117	h? scs2Δ::ura4+ scs22Δ::ura4+ ura4-D18	This study	(Zhang, Vjestica, and Oliferenko 2012)
DB5164	h+ leu1::sec9-10 sec9::ura4 psy1-S1::ura4+ ura4-D18	This study	YGRC/NBRP Japan
DB5173	h? leu1::sec9-10 sec9::ura4 ura4-D18 (?) cdc42-3::KanMX6	This study	
DB5182	h+ Pnmt1-GFP-tna1::hphMX6	This study	
DB5183	h- Pnmt1-GFP-tna1::hphMX6	This study	
DB5225	h+ tea1-HL-tagRFP::KanMX6	This study	(Makushok et al. 2016)
DB5227	h+ pSV40-GFP-atb2::LEU2	This study	(Pardo and Nurse 2005)
DB5232	h- lub1Δ::KanMX6	This study	(Kim et al. 2010), Bioneer deletion library (V5-P09-58)
DB5334	h? rnc1Δ::KanMX6	This study	(Kim et al. 2010), Bioneer deletion library (V5-P14-49)
DB5346	h? asp1Δ::KanMX6	This study	(Kim et al. 2010), Bioneer deletion library (V5-P31-69)
DB5408	h? lub1Δ::KanMX6 Pnmt1-GFP-tna1::hphMX6	This study	(Kim et al. 2010), Bioneer deletion library (V5-P09-58)
DB5435	h? lub1Δ::kanMX6 pSV40-GFP-atb2::LEU2	This study	
DB5436	h? lub1Δ::kanMX6 tea1-HL-tagRFP::kanMX6	This study	
DB5446	h? ccr1Δ::kanMX6 Pnmt1-GFP-tna1::kanMX6	This study	(Kim et al. 2010), Bioneer deletion library (V5-P16-19)

DB5447	h? sre1Δ::kanMX6 Pnmt1-GFP-tna1::hphMX6	This study	(Kim et al. 2010), Bioneer deletion library (V5-P23-54)
DB5474	h? lub1Δ::kanMX6 cdc42-3::kanMX6	This study	
DB5475	h? lub1Δ::kanMX6 kes1Δ::kanMX6	This study	
DB5476	h? lub1Δ::kanMX6 osh7Δ::kanMX6	This study	
DB5477	h? lub1Δ::kanMX6 kes1Δ::kanMX6 osh7(SPCC23B6.01c)Δ::kanMX6	This study	
DB5500	h? lub1Δ::kanMX6 ura4-294::[shk1 promoter:ScGIC2 CRIB:3xGFP:ura4+]	This study	
DB5502	h? lub1Δ::kanMX6 cdc42-mCherry-SW-term::kanMX6-3'UTR	This study	
DB5504	h? lub1Δ::kanMX6 cdc42-mCherry-SW-term::kanMX6-3'UTR CRIB-3GFP::ura4+	This study	
DB5506	h? lub1Δ::kanMX6 scd1-3GFP::kanMX6	This study	
DB5537	h? lub1Δ::kanMX6 bud6-3GFP::kanMX6	This study	
DB5538	h? bud6-3GFP::kanMX6	This study	(Martin and Chang 2006)
DB5578	h? crm1-1	This study	(Penney et al. 2012)
DB5594	h? cdc48-ts	This study	YGRC/NBRP Japan
DB5598	h+ cdc48-353	This study	YGRC/NBRP Japan
DB5605	h? Rpap1::ura4+ crm1-1 ura4-D18	This study	YGRC/NBRP Japan
DB5602	h? Rpap1::ura4+ ura4-D18	This study	YGRC/NBRP Japan
DB5632	h? lub1Δ::KanMX6 cdc48-353	This study	
DB5634	h? lub1Δ::KanMX6 cdc48-ts	This study	
DB5635	h? crm1-809	This study	YGRC/NBRP Japan
DB5646	h- Pnmt1-lub1(235-718)::hphMX6	This study	
DB5785	h- lub1(1-248)::natMX6	This study	
DB5787	h? Pnmt1-ubi4::hphMX6	This study	
DB5788	h? lub1Δ::kanMX6 Pnmt1-ubi4::hphMX6	This study	

Table 4: Strains used in the study.

Strain	Genotype	Primer and sequence	Plasmid
DB5170	h- Pnmt1-GFP-TNA1(spac1002.16c)::hph	**DPE627** (rev) ATGACTTTTTCACTTTCAT CCGCTTTGGTAAAGATGCTGCCATTGC TCTTATTACTGCTAGTGTGACTTAAAG ACTTCATTTTGTATAGTTCATCCATGC **DPE628** (fw) AATTGTATTTCCTTTCAGAT TTTGGAATTTCGCGGTACCTTTTCTAAT ACTGGTTTTCACTAATTCACCTTCACTT AAGCGAATTCGAGCTCGTTTAAAC (see also Makushok et al. 2016)	DL361 pFA6a-hphMX6-P3nmt1-GFP
DB5650	h- pnmt1-ubi4::hph	**DPE1637** (fw) AAATTTGAGTGCATATGCTT CAATTTCTATACATAAATGTATTTAGAAA AAACTATCGTATTGGAGATTGTATTTAAA TTTTGAGAATTCGAGCTCGTTTAAAC **DPE1638** (rev) GCTCTTTACATTGTCAATGG-TATCGGAAGATCAACTTCCA ATGTAATAGTCTTTCCAGTT AATGTCTTGACGAAAATC TGCATGATTTAACAAAGCG ACTATAAGTC insertion tested with **DPE1641** (fw) CAACGATTACTGGGGAGA GAA **DPE1644** (rev) GAAGACGAAGAACAAGG TGAA	DL361 pFA6a-hphMX6-P3nmt1-GFP
DB 5785	h- lub1(1-248)::NAT	**DPE1632** (fw) TCGTTT-GTATATTCTTTAACTTATATCCACAACC AGCAGCTGATCGCATCTTGTGGTGAGG ATCGTACAATCAGGATTTGGAAATAGC TCTTATTGACCACACCTCTAC **DPE1633** (rev) CGTTTAAAATAAGAGACA TTTAATCGTAAAGTAAGATTTGAAGTAA GCAACGCGTTTCTTTAAAAAAAACCTCC GAATATTATCGATGAATTCGAGCTCGTT T insertion tested with **DPE1639** (fw) GTTTT-GCTTCCTGCTCTAATG **DPE1640** (rev) ggggatgtatgggctaaatgta	DL 390 pFA6a-linker-GFP-natMX6
DB5646	h- pnmt1-lub1(235-718)::hph	**DPE1634** (fw) TGTGAAAGCCTGTTTAACT TCCTTCTGCGAAAAGCAAATATACCTTT ATATTGGCTTCTCATAATCATCCTTAAT AGACTGAAAGAATTCGAGCTCGTTTAA AC **DPE1635** (rev) TGTCGGTAAAGTAATACA TTGTAAGCACTCTTTACCTTTCCAAATC CTGATTGTACGATCCTCACCACAAGAT GCGATCAGCTGCATGATTTAACAAAGC GACTATA insertion tested with	DL361 pFA6a-hphMX6-P3nmt1-GFP

		DPE1641 (fw) CAACGATTACTGGGGAGA-GAA **DPE1642** (rev) CAACTCGAAC-CTTATCCACT	

Table 5: Primers used for PCR based gene editing.

Protein identified by mass spectrometry	Accession Number	Molecular Weight
Uncharacterized acyltransferase C1851.02 OS=Schizosaccharomyces pombe (strain 972 / ATCC 24843) GN=SPAC1851.02 PE=3 SV=1	YLD2_SCHPO	31 kDa
Cytochrome P450 61 OS=Schizosaccharomyces pombe (strain 972 / ATCC 24843) GN=erg5 PE=1 SV=3	ERG5_SCHPO	62 kDa
Coronin-like protein crn1 OS=Schizosaccharomyces pombe (strain 972 / ATCC 24843) GN=crn1 PE=1 SV=1	CORO_SCHPO	67 kDa
Putative phospholipid-transporting ATPase C24B11.12c OS=Schizosaccharomyces pombe (strain 972 / ATCC 24843) GN=SPAC24B11.12c PE=3 SV=1	ATCX_SCHPO	159 kDa
Obg-like ATPase 1 OS=Schizosaccharomyces pombe (strain 972 / ATCC 24843) GN=SPAC27E2.03c PE=1 SV=1	OLA1_SCHPO	44 kDa
ATP-binding cassette transporter abc4 OS=Schizosaccharomyces pombe (strain 972 / ATCC 24843) GN=abc4 PE=3 SV=1	ABC4_SCHPO	165 kDa
Glutathione S-transferase omega-like 2 OS=Schizosaccharomyces pombe (strain 972 / ATCC 24843) GN=gto2 PE=3 SV=1	GTO2_SCHPO	37 kDa
Uncharacterized AAA domain-containing protein C31G5.19 OS=Schizosaccharomyces pombe (strain 972 / ATCC 24843) GN=SPAC31G5.19 PE=3 SV=1	YEJJ_SCHPO	135 kDa
Uncharacterized protein C328.01c OS=Schizosaccharomyces pombe (strain 972 / ATCC 24843) GN=SPAC328.01c PE=4 SV=2	YKX1_SCHPO	140 kDa
Uncharacterized kinase mug58 OS=Schizosaccharomyces pombe (strain 972 / ATCC 24843) GN=mug58 PE=1 SV=1	MUG58_SCHPO	32 kDa
Uncharacterized alpha-1,2-galactosyltransferase C637.06 OS=Schizosaccharomyces pombe (strain 972 / ATCC 24843) GN=SPAC637.06 PE=2 SV=2	YFE6_SCHPO	41 kDa
Uncharacterized RING finger protein C6B12.07c OS=Schizosaccharomyces pombe (strain 972 / ATCC 24843) GN=SPAC6B12.07c PE=3 SV=2	YDT7_SCHPO	53 kDa
Fatty acid synthase subunit beta OS=Schizosaccharomyces pombe (strain 972 / ATCC 24843) GN=fas1 PE=1 SV=1	FAS1_SCHPO	231 kDa
Uncharacterized WD repeat-containing protein C9G1.05 OS=Schizosaccharomyces pombe (strain 972 / ATCC 24843) GN=SPAC9G1.05 PE=3 SV=1	YE85_SCHPO	65 kDa
Uncharacterized protein PYUK71.03c OS=Schizosaccharomyces pombe (strain 972 / ATCC 24843) GN=SPAPYUK71.03c PE=1 SV=1	YKH3_SCHPO	136 kDa
Vesicle-associated membrane protein-associated protein C16G5.05c OS=Schizosaccharomyces pombe (strain 972 / ATCC 24843) GN=SPBC16G5.05c PE=1 SV=1	YH75_SCHPO	41 kDa
Heat shock protein sks2 OS=Schizosaccharomyces pombe (strain 972 / ATCC 24843) GN=sks2 PE=1 SV=2	HSP75_SCHPO	67 kDa
Mannan polymerase II complex anp1 subunit OS=Schizosaccharomyces pombe (strain 972 / ATCC 24843) GN=anp1 PE=3 SV=1	ANP1_SCHPO	49 kDa
Glycerol-3-phosphate dehydrogenase [NAD(+)] 1 OS=Schizosaccharomyces pombe (strain 972 / ATCC 24843) GN=gpd1 PE=1 SV=2	GPD1_SCHPO	42 kDa

Uncharacterized protein C21B10.03c OS=Schizosaccharomyces pombe (strain 972 / ATCC 24843) GN=SPBC21B10.03c PE=4 SV=1	YHZ3_SCHPO	86 kDa
Uncharacterized ABC transporter ATP-binding protein C29A3.09c OS=Schizosaccharomyces pombe (strain 972 / ATCC 24843) GN=SPBC29A3.09c PE=3 SV=1	YB89_SCHPO	84 kDa
Uncharacterized protein C31F10.16 OS=Schizosaccharomyces pombe (strain 972 / ATCC 24843) GN=SPBC31F10.16 PE=4 SV=2	YB2G_SCHPO	74 kDa
Uncharacterized GTP-binding protein C428.15 OS=Schizosaccharomyces pombe (strain 972 / ATCC 24843) GN=SPBC428.15 PE=3 SV=1	YHOF_SCHPO	44 kDa
Protein sds23/moc1 OS=Schizosaccharomyces pombe (strain 972 / ATCC 24843) GN=sds23 PE=1 SV=1	SDS23_SCHPO	44 kDa
1,3-beta-glucan synthase component bgs4 OS=Schizosaccharomyces pombe (strain 972 / ATCC 24843) GN=bgs4 PE=1 SV=1	BGS4_SCHPO	225 kDa
Uncharacterized protein C1919.03c OS=Schizosaccharomyces pombe (strain 972 / ATCC 24843) GN=SPCC1919.03c PE=1 SV=2	YC63_SCHPO	33 kDa
Probable heat shock protein ssa1 OS=Schizosaccharomyces pombe (strain 972 / ATCC 24843) GN=ssa1 PE=1 SV=2	HSP71_SCHPO	70 kDa
Lysophospholipase 1 OS=Schizosaccharomyces pombe (strain 972 / ATCC 24843) GN=plb1 PE=2 SV=2	PLB1_SCHPO	67 kDa
Protein transport protein sec72 OS=Schizosaccharomyces pombe (strain 972 / ATCC 24843) GN=sec72 PE=1 SV=1	SEC7B_SCHPO	207 kDa
Uncharacterized protein C32A11.02c OS=Schizosaccharomyces pombe (strain 972 / ATCC 24843) GN=SPAC32A11.02c PE=4 SV=1	YD72_SCHPO	97 kDa
Myosin-1 OS=Schizosaccharomyces pombe (strain 972 / ATCC 24843) GN=myo1 PE=1 SV=1	MYO1_SCHPO	136 kDa
Non-classical export protein 2 homolog OS=Schizosaccharomyces pombe (strain 972 / ATCC 24843) GN=fhn1 PE=3 SV=1	NCE2_SCHPO	20 kDa
Aminopeptidase 1 OS=Schizosaccharomyces pombe (strain 972 / ATCC 24843) GN=ape1 PE=3 SV=1	APE1_SCHPO	99 kDa
2-oxoglutarate dehydrogenase, mitochondrial OS=Schizosaccharomyces pombe (strain 972 / ATCC 24843) GN=kgd1 PE=3 SV=1	ODO1_SCHPO	114 kDa
Protein kinase kin1 OS=Schizosaccharomyces pombe (strain 972 / ATCC 24843) GN=kin1 PE=1 SV=3	KIN1_SCHPO	99 kDa
Putative hydroxymethylpyrimidine/phosphomethylpyrimidine kinase 2 OS=Schizosaccharomyces pombe (strain 972 / ATCC 24843) GN=SPBP8B7.18c PE=3 SV=1	THI22_SCHPO	61 kDa
Uncharacterized protein C663.15c OS=Schizosaccharomyces pombe (strain 972 / ATCC 24843) GN=SPCC663.15c PE=4 SV=2	YCPF_SCHPO	77 kDa
Probable sterol O-acyltransferase 2 OS=Schizosaccharomyces pombe (strain 972 / ATCC 24843) GN=are2 PE=1 SV=1	AREH2_SCHPO	55 kDa
AP-1 complex subunit gamma-1 OS=Schizosaccharomyces pombe (strain 972 / ATCC 24843) GN=apl4 PE=3 SV=1	AP1G1_SCHPO	96 kDa
Meiotically up-regulated gene 190 protein OS=Schizosaccharomyces pombe (strain 972 / ATCC 24843) GN=mug190 PE=1 SV=1	MU190_SCHPO	134 kDa
ER membrane protein complex subunit 1 OS=Schizosaccharomyces pombe (strain 972 / ATCC 24843) GN=emc1 PE=3 SV=1	EMC1_SCHPO	101 kDa
Uncharacterized protein C3G9.05 OS=Schizosaccharomyces pombe (strain 972 / ATCC 24843) GN=SPAC3G9.05 PE=1 SV=1	YF75_SCHPO	74 kDa
Uncharacterized protein UNK4.17 OS=Schizosaccharomyces pombe (strain 972 / ATCC 24843) GN=SPAC2E11.17 PE=4 SV=2	YEAH_SCHPO	46 kDa
Copper amine oxidase-like protein cao2 OS=Schizosaccharomyces pombe (strain 972 / ATCC 24843) GN=cao2 PE=3 SV=1	CAO2_SCHPO	90 kDa
Uncharacterized protein C16G5.07c OS=Schizosaccharomyces pombe (strain 972 / ATCC 24843) GN=SPBC16G5.07c PE=3 SV=1	YH77_SCHPO	39 kDa
Uncharacterized J domain-containing protein C17A3.05c OS=Schizosaccharomyces pombe (strain 972 / ATCC 24843) GN=pi041 PE=1 SV=1	YNF5_SCHPO	46 kDa

Uncharacterized serine-rich protein C2F12.03c OS=Schizosaccharomyces pombe (strain 972 / ATCC 24843) GN=SPBC2F12.03c PE=1 SV=1	YB33_SCHPO	99 kDa
Uba3-binding protein but2 OS=Schizosaccharomyces pombe (strain 972 / ATCC 24843) GN=but2 PE=1 SV=1	BUT2_SCHPO	44 kDa
Uncharacterized acyltransferase C428.14 OS=Schizosaccharomyces pombe (strain 972 / ATCC 24843) GN=SPBC428.14 PE=3 SV=1	YHOE_SCHPO	41 kDa
Oxysterol-binding protein-like protein 1 OS=Schizosaccharomyces pombe (strain 972 / ATCC 24843) GN=obp1 PE=1 SV=1	OBP1_SCHPO	59 kDa
Meiotically up-regulated gene 33 protein OS=Schizosaccharomyces pombe (strain 972 / ATCC 24843) GN=mug33 PE=1 SV=1	MUG33_SCHPO	37 kDa
Uncharacterized protein C18.17c OS=Schizosaccharomyces pombe (strain 972 / ATCC 24843) GN=SPCC18.17c PE=4 SV=1	YQ9H_SCHPO	55 kDa
Brefeldin A resistance protein OS=Schizosaccharomyces pombe (strain 972 / ATCC 24843) GN=bfr1 PE=1 SV=1	BFR1_SCHPO	172 kDa
mac1		
Probable sterol O-acyltransferase 1 OS=Schizosaccharomyces pombe (strain 972 / ATCC 24843) GN=are1 PE=3 SV=1	AREH1_SCHPO	63 kDa
Uncharacterized TLC domain-containing protein C17A2.02c OS=Schizosaccharomyces pombe (strain 972 / ATCC 24843) GN=SPAC17A2.02c PE=3 SV=1	YF22_SCHPO	33 kDa
SPAC2E12.03c		
Meiotically up-regulated gene 191 protein OS=Schizosaccharomyces pombe (strain 972 / ATCC 24843) GN=mug191 PE=1 SV=1	MU191_SCHPO	50 kDa
Endocytosis protein end4 OS=Schizosaccharomyces pombe (strain 972 / ATCC 24843) GN=end4 PE=1 SV=2	SLA2_SCHPO	124 kDa
Uncharacterized protein C8E11.05c OS=Schizosaccharomyces pombe (strain 972 / ATCC 24843) GN=SPAC8E11.05c PE=4 SV=1	YFQ5_SCHPO	38 kDa
Oxysterol-binding protein homolog C23B6.01c OS=Schizosaccharomyces pombe (strain 972 / ATCC 24843) GN=SPCC23B6.01c PE=1 SV=2	YJX1_SCHPO	55 kDa
Uncharacterized protein C63.14 OS=Schizosaccharomyces pombe (strain 972 / ATCC 24843) GN=SPCC63.14 PE=1 SV=1	YCJE_SCHPO	131 kDa
Glycerol dehydrogenase 1 OS=Schizosaccharomyces pombe (strain 972 / ATCC 24843) GN=gld1 PE=1 SV=1	GLD1_SCHPO	49 kDa
Uncharacterized PH domain-containing protein C19A8.02 OS=Schizosaccharomyces pombe (strain 972 / ATCC 24843) GN=SPAC19A8.02 PE=3 SV=1	YEE2_SCHPO	141 kDa
Vitamin H transporter 1 OS=Schizosaccharomyces pombe (strain 972 / ATCC 24843) GN=vht1 PE=2 SV=1	VHT1_SCHPO	63 kDa
Uncharacterized protein C26H5.07c OS=Schizosaccharomyces pombe (strain 972 / ATCC 24843) GN=SPAC26H5.07c PE=3 SV=2	YEG7_SCHPO	57 kDa
Meiotically up-regulated gene 86 protein OS=Schizosaccharomyces pombe (strain 972 / ATCC 24843) GN=mug86 PE=1 SV=1	MUG86_SCHPO	34 kDa
Spermidine synthase OS=Schizosaccharomyces pombe (strain 972 / ATCC 24843) GN=SPBC12C2.07c PE=3 SV=1	SPEE_SCHPO	33 kDa
Putative uncharacterized oxidoreductase C1773.04 OS=Schizosaccharomyces pombe (strain 972 / ATCC 24843) GN=SPBC1773.04 PE=1 SV=1	YGD4_SCHPO	38 kDa
Uncharacterized membrane protein C20F10.07 OS=Schizosaccharomyces pombe (strain 972 / ATCC 24843) GN=SPBC20F10.07 PE=1 SV=1	YGZ7_SCHPO	85 kDa
Oxysterol-binding protein homolog C354.07c OS=Schizosaccharomyces pombe (strain 972 / ATCC 24843) GN=SPBC354.07c PE=3 SV=4	YGV7_SCHPO	45 kDa
Uncharacterized protein C594.02c OS=Schizosaccharomyces pombe (strain 972 / ATCC 24843) GN=SPCC594.02c PE=1 SV=1	YJD2_SCHPO	55 kDa

Uncharacterized oxidoreductase C736.13 OS=Schizosaccharomyces pombe (strain 972 / ATCC 24843) GN=SPCC736.13 PE=3 SV=1	YJCD_SCHPO	39 kDa
UPF0591 membrane protein C15E1.02c OS=Schizosaccharomyces pombe (strain 972 / ATCC 24843) GN=SPAC15E1.02c PE=3 SV=1	YKZ2_SCHPO	16 kDa
NADPH-dependent 1-acyldihydroxyacetone phosphate reductase OS=Schizosaccharomyces pombe (strain 972 / ATCC 24843) GN=ayr1 PE=3 SV=2	AYR1_SCHPO	33 kDa
Uncharacterized J domain-containing protein C2E1P5.03 OS=Schizosaccharomyces pombe (strain 972 / ATCC 24843) GN=SPAC2E1P5.03 PE=3 SV=1	YKU3_SCHPO	35 kDa
Zinc-type alcohol dehydrogenase-like protein C1198.01 OS=Schizosaccharomyces pombe (strain 972 / ATCC 24843) GN=SPBC1198.01 PE=3 SV=1	YHG1_SCHPO	46 kDa
Uncharacterized oxidoreductase C215.11c OS=Schizosaccharomyces pombe (strain 972 / ATCC 24843) GN=SPBC215.11c PE=3 SV=1	YH5B_SCHPO	34 kDa
Uncharacterized membrane protein C365.16 OS=Schizosaccharomyces pombe (strain 972 / ATCC 24843) GN=SPBC365.16 PE=4 SV=1	YGRG_SCHPO	30 kDa
Sphingolipid C4-hydroxylase sur2 OS=Schizosaccharomyces pombe (strain 972 / ATCC 24843) GN=sur2 PE=3 SV=1	SUR2_SCHPO	34 kDa
Uncharacterized oxidoreductase C162.03 OS=Schizosaccharomyces pombe (strain 972 / ATCC 24843) GN=SPCC162.03 PE=3 SV=1	YQ53_SCHPO	33 kDa
ATPase get3 OS=Schizosaccharomyces pombe (strain 972 / ATCC 24843) GN=get3 PE=1 SV=1	GET3_SCHPO	37 kDa
C-8 sterol isomerase erg2 OS=Schizosaccharomyces pombe (strain 972 / ATCC 24843) GN=erg2 PE=3 SV=1	ERG2_SCHPO	25 kDa
Putative aldehyde dehydrogenase-like protein C9E9.09c OS=Schizosaccharomyces pombe (strain 972 / ATCC 24843) GN=SPAC9E9.09c PE=1 SV=1	YF19_SCHPO	55 kDa
NADPH--cytochrome P450 reductase OS=Schizosaccharomyces pombe (strain 972 / ATCC 24843) GN=ccr1 PE=2 SV=1	NCPR_SCHPO	77 kDa
Glyceraldehyde-3-phosphate dehydrogenase 2 OS=Schizosaccharomyces pombe (strain 972 / ATCC 24843) GN=gpd3 PE=1 SV=1	G3P2_SCHPO	36 kDa
Uncharacterized ubiquitin-like protein C1E8.02 OS=Schizosaccharomyces pombe (strain 972 / ATCC 24843) GN=SPBC1E8.02 PE=1 SV=1	YB92_SCHPO	67 kDa
UPF0674 endoplasmic reticulum membrane protein C2G5.01 OS=Schizosaccharomyces pombe (strain 972 / ATCC 24843) GN=SPBC2G5.01 PE=3 SV=1	YGX1_SCHPO	43 kDa
Plasma membrane proteolipid 31 OS=Schizosaccharomyces pombe (strain 972 / ATCC 24843) GN=pmp31 PE=1 SV=2	PMP31_SCHPO	12 kDa
Uncharacterized protein C13E7.07 OS=Schizosaccharomyces pombe (strain 972 / ATCC 24843) GN=SPBC13E7.07 PE=4 SV=1	YOH7_SCHPO	31 kDa
Seven transmembrane protein 1 OS=Schizosaccharomyces pombe (strain 972 / ATCC 24843) GN=stm1 PE=1 SV=1	STM1_SCHPO	31 kDa
Oxysterol-binding protein homolog C2F12.05c OS=Schizosaccharomyces pombe (strain 972 / ATCC 24843) GN=SPBC2F12.05c PE=1 SV=2	YB35_SCHPO	148 kDa
Uncharacterized transporter C3B8.04c OS=Schizosaccharomyces pombe (strain 972 / ATCC 24843) GN=SPBC3B8.04c PE=3 SV=1	YBH4_SCHPO	97 kDa
Uncharacterized protein C16H5.12c OS=Schizosaccharomyces pombe (strain 972 / ATCC 24843) GN=SPBC16H5.12c PE=1 SV=3	YBPC_SCHPO	83 kDa
Uncharacterized membrane protein C16E9.09c OS=Schizosaccharomyces pombe (strain 972 / ATCC 24843) GN=SPBC16E9.09c PE=3 SV=1	YB79_SCHPO	25 kDa
Ceramide very long chain fatty acid hydroxylase-like protein C19G12.08 OS=Schizosaccharomyces pombe (strain 972 / ATCC 24843) GN=SPAC19G12.08 PE=3 SV=1	SCS7_SCHPO	40 kDa
Uncharacterized protein C1711.08 OS=Schizosaccharomyces pombe (strain 972 / ATCC 24843) GN=SPBC1711.08 PE=2 SV=1	YNY8_SCHPO	37 kDa

Uncharacterized J domain-containing protein C4H3.01 OS=Schizosaccharomyces pombe (strain 972 / ATCC 24843) GN=SPAC4H3.01 PE=1 SV=1	YAY1_SCHPO	45 kDa
Cysteine synthase 1 OS=Schizosaccharomyces pombe (strain 972 / ATCC 24843) GN=cys11 PE=3 SV=1	CYSK1_SCHPO	38 kDa
Heavy metal tolerance protein OS=Schizosaccharomyces pombe (strain 972 / ATCC 24843) GN=hmt1 PE=2 SV=3	HMT1_SCHPO	94 kDa
Uncharacterized HTH La-type RNA-binding protein C1527.03 OS=Schizosaccharomyces pombe (strain 972 / ATCC 24843) GN=SPAC1527.03 PE=1 SV=1	YLA3_SCHPO	53 kDa
Probable mannose-1-phosphate guanyltransferase OS=Schizosaccharomyces pombe (strain 972 / ATCC 24843) GN=SPBC13G1.02 PE=3 SV=1	YBB2_SCHPO	46 kDa
Oxysterol-binding protein homolog C23H4.01c OS=Schizosaccharomyces pombe (strain 972 / ATCC 24843) GN=SPAC23H4.01c PE=1 SV=2	YEH1_SCHPO	107 kDa
Sterol regulatory element-binding protein 1 OS=Schizosaccharomyces pombe (strain 972 / ATCC 24843) GN=sre1 PE=1 SV=1	SREBP_SCHPO	98 kDa
Phospholipid scramblase family protein C343.06c OS=Schizosaccharomyces pombe (strain 972 / ATCC 24843) GN=SPAC343.06c PE=3 SV=1	YIP6_SCHPO	43 kDa
Cell fusion protein cfr1 OS=Schizosaccharomyces pombe (strain 972 / ATCC 24843) GN=cfr1 PE=3 SV=1	CFR1_SCHPO	67 kDa
Probable heat shock protein ssa2 OS=Schizosaccharomyces pombe (strain 972 / ATCC 24843) GN=ssa2 PE=1 SV=3	HSP72_SCHPO	70 kDa
Tetra-spanning protein 1 OS=Schizosaccharomyces pombe (strain 972 / ATCC 24843) GN=tts1 PE=1 SV=1	TTS1_SCHPO	32 kDa
Vacuolar protein sorting-associated protein 1 OS=Schizosaccharomyces pombe (strain 972 / ATCC 24843) GN=vps1 PE=3 SV=2	VPS1_SCHPO	76 kDa
Uncharacterized CDP-alcohol phosphatidyltransferase class-I family protein C22A12.10 OS=Schizosaccharomyces pombe (strain 972 / ATCC 24843) GN=SPAC22A12.10 PE=3 SV=1	YF3A_SCHPO	44 kDa
Transmembrane GTPase fzo1 OS=Schizosaccharomyces pombe (strain 972 / ATCC 24843) GN=fzo1 PE=3 SV=1	FZO1_SCHPO	87 kDa
Stress response protein ish1 OS=Schizosaccharomyces pombe (strain 972 / ATCC 24843) GN=ish1 PE=1 SV=1	ISH1_SCHPO	76 kDa
Vigilin 1 OS=Schizosaccharomyces pombe (strain 972 / ATCC 24843) GN=vgl1 PE=1 SV=2	VGL1_SCHPO	143 kDa
Fimbrin OS=Schizosaccharomyces pombe (strain 972 / ATCC 24843) GN=fim1 PE=1 SV=1	FIMB_SCHPO	69 kDa
Uncharacterized membrane protein C24H6.13 OS=Schizosaccharomyces pombe (strain 972 / ATCC 24843) GN=SPAC24H6.13 PE=1 SV=1	YA7D_SCHPO	98 kDa
Uncharacterized protein C16A3.08c OS=Schizosaccharomyces pombe (strain 972 / ATCC 24843) GN=SPBC16A3.08c PE=1 SV=1	YBI8_SCHPO	31 kDa
HMG box-containing protein C28F2.11 OS=Schizosaccharomyces pombe (strain 972 / ATCC 24843) GN=SPBC28F2.11 PE=1 SV=1	YHHB_SCHPO	34 kDa
Uncharacterized ABC transporter ATP-binding protein C825.01 OS=Schizosaccharomyces pombe (strain 972 / ATCC 24843) GN=SPCC825.01 PE=1 SV=1	YJQ1_SCHPO	93 kDa
Amino acid transporter 1 OS=Schizosaccharomyces pombe (strain 972 / ATCC 24843) GN=aat1 PE=3 SV=1	AAT1_SCHPO	63 kDa
Uncharacterized protein C3D6.13c OS=Schizosaccharomyces pombe (strain 972 / ATCC 24843) GN=SPBC3D6.13c PE=1 SV=1	YB1D_SCHPO	81 kDa
Uncharacterized amino-acid permease C15C4.04c OS=Schizosaccharomyces pombe (strain 972 / ATCC 24843) GN=SPBC15C4.04c PE=3 SV=1	YG64_SCHPO	60 kDa

Importin subunit beta-3 OS=Schizosaccharomyces pombe (strain 972 / ATCC 24843) GN=sal3 PE=3 SV=1	IMB3_SCHPO	122 kDa
Putative monoglyceride lipase OS=Schizosaccharomyces pombe (strain 972 / ATCC 24843) GN=SPCC5E4.05c PE=1 SV=1	MGLL_SCHPO	42 kDa
Uncharacterized urease accessory protein ureG-like OS=Schizosaccharomyces pombe (strain 972 / ATCC 24843) GN=SPCPB16A4.05c PE=3 SV=1	UREG_SCHPO	31 kDa
Uncharacterized protein C1604.12 OS=Schizosaccharomyces pombe (strain 972 / ATCC 24843) GN=SPBC1604.12 PE=1 SV=1	YG0C_SCHPO	93 kDa
Uncharacterized amino-acid permease C794.03 OS=Schizosaccharomyces pombe (strain 972 / ATCC 24843) GN=SPCC794.03 PE=2 SV=1	YCT3_SCHPO	61 kDa
Uncharacterized WD repeat-containing protein C1773.01 OS=Schizosaccharomyces pombe (strain 972 / ATCC 24843) GN=SPBC1773.01 PE=3 SV=1	YGD1_SCHPO	69 kDa
Uncharacterized alpha-1,2-galactosyltransferase C8D2.17 OS=Schizosaccharomyces pombe (strain 972 / ATCC 24843) GN=pi048 PE=3 SV=2	YGWH_SCHPO	37 kDa
Protein transport protein sec71 OS=Schizosaccharomyces pombe (strain 972 / ATCC 24843) GN=sec71 PE=1 SV=1	SEC7A_SCHPO	207 kDa
Delta(24(24(1)))-sterol reductase OS=Schizosaccharomyces pombe (strain 972 / ATCC 24843) GN=sts1 PE=1 SV=2	STS1_SCHPO	53 kDa
Uncharacterized protein C23C11.06c OS=Schizosaccharomyces pombe (strain 972 / ATCC 24843) GN=SPAC23C11.06c PE=4 SV=1	YDW6_SCHPO	60 kDa
ADP,ATP carrier protein OS=Schizosaccharomyces pombe (strain 972 / ATCC 24843) GN=anc1 PE=2 SV=1	ADT_SCHPO	35 kDa
Uncharacterized GTP-binding protein C9.07c OS=Schizosaccharomyces pombe (strain 972 / ATCC 24843) GN=SPAC9.07c PE=2 SV=1	YFY7_SCHPO	40 kDa
Uncharacterized zinc metalloprotease C1259.02c OS=Schizosaccharomyces pombe (strain 972 / ATCC 24843) GN=SPCC1259.02c PE=3 SV=1	YC52_SCHPO	92 kDa
Probable dihydrolipoyllysine-residue succinyltransferase component of 2-oxoglutarate dehydrogenase complex, mitochondrial OS=Schizosaccharomyces pombe (strain 972 / ATCC 24843) GN=kgd2 PE=3 SV=1	ODO2_SCHPO	49 kDa
3-isopropylmalate dehydrogenase OS=Schizosaccharomyces pombe (strain 972 / ATCC 24843) GN=leu1 PE=1 SV=1	LEU3_SCHPO	40 kDa
Putative lysophospholipase C1A6.03c OS=Schizosaccharomyces pombe (strain 972 / ATCC 24843) GN=SPAC1A6.03c PE=3 SV=3	PLB2_SCHPO	74 kDa
Saccharopine dehydrogenase [NAD(+), L-lysine-forming] OS=Schizosaccharomyces pombe (strain 972 / ATCC 24843) GN=lys3 PE=1 SV=2	LYS1_SCHPO	41 kDa
Uncharacterized protein C23H3.15c OS=Schizosaccharomyces pombe (strain 972 / ATCC 24843) GN=SPAC23H3.15c PE=2 SV=4	YEPF_SCHPO	35 kDa
Uncharacterized protein UNK4,15 OS=Schizosaccharomyces pombe (strain 972 / ATCC 24843) GN=SPAC2E11.15 PE=4 SV=1	YEAF_SCHPO	24 kDa
Alpha-glucosidase OS=Schizosaccharomyces pombe (strain 972 / ATCC 24843) GN=agl1 PE=1 SV=2	AGLU_SCHPO	109 kDa
Uncharacterized protein C11C11.06c OS=Schizosaccharomyces pombe (strain 972 / ATCC 24843) GN=SPBC11C11.06c PE=4 SV=1	YBY6_SCHPO	19 kDa
Protein lsd90 OS=Schizosaccharomyces pombe (strain 972 / ATCC 24843) GN=lsd90 PE=1 SV=1	LSD90_SCHPO	82 kDa
Inositol phosphosphingolipids phospholipase C OS=Schizosaccharomyces pombe (strain 972 / ATCC 24843) GN=css1 PE=1 SV=2	CSS1_SCHPO	48 kDa
Uncharacterized transporter C36.03c OS=Schizosaccharomyces pombe (strain 972 / ATCC 24843) GN=SPBC36.03c PE=3 SV=1	YN43_SCHPO	59 kDa
Protein transport protein sec23-2 OS=Schizosaccharomyces pombe (strain 972 / ATCC 24843) GN=sec232 PE=1 SV=1	SC232_SCHPO	85 kDa

Putative inorganic phosphate transporter C8E4.01c OS=Schizosaccharomyces pombe (strain 972 / ATCC 24843) GN=SPBC8E4.01c PE=1 SV=2	YBN1_SCHPO	64 kDa
Pumilio domain-containing protein P35G2.14 OS=Schizosaccharomyces pombe (strain 972 / ATCC 24843) GN=SPBP35G2.14 PE=1 SV=2	YN8E_SCHPO	114 kDa
Uncharacterized protein CC285.14 OS=Schizosaccharomyces pombe (strain 972 / ATCC 24843) GN=SPCC285.14 PE=3 SV=1	YCRE_SCHPO	133 kDa
Uncharacterized J domain-containing protein C63.03 OS=Schizosaccharomyces pombe (strain 972 / ATCC 24843) GN=SPCC63.03 PE=3 SV=2	YCJ3_SCHPO	69 kDa
Vacuolar membrane protein pep3 OS=Schizosaccharomyces pombe (strain 972 / ATCC 24843) GN=pep3 PE=3 SV=1	PEP3_SCHPO	104 kDa
Uncharacterized protein C962.01 OS=Schizosaccharomyces pombe (strain 972 / ATCC 24843) GN=SPCC962.01 PE=2 SV=3	YC31_SCHPO	156 kDa
Uncharacterized protein C19G7.17 OS=Schizosaccharomyces pombe (strain 972 / ATCC 24843) GN=SPBC19G7.17 PE=4 SV=2	YGMH_SCHPO	52 kDa

Table 6: Candidate proteins selected for *in vivo* studies (screen 1)

Experiment	**Repeats**
Figure 10	1
Figure 14	2 (*asp1Δ, rnc1Δ*); 1 (*lub1Δ*)
Figure 15Figure 16	1
Figure 17	1
Figure 18	1
Figure 19	1
Figure 22Figure 26	3
Figure 31Figure 32	1
Figure 33	1
Figure 35	3 (wild-type, *lub1Δ, kes1Δ lub1Δ, osh7Δ lub1Δ*); 2 (*kes1Δ, kes1Δ osh7Δ lub1Δ*); 1(*osh7Δ*)
Figure 37	2
Figure 39Figure 41	2
Figure 42Figure 44	2
Figure 43	1
Figure 45Figure 47	4
Figure 48	1
Figure 49	3
Figure 51Figure 52	1

Table 7: Number of experimental repeats used for quantification.

Mass spectrometry results (screen 2)

Table 8: Mass spectrometry results (screen 2).

Displayed are exclusive unique peptide counts (≥ 1 peptide, 0.1% FDR)

			wild-type samples (MG0212B)				*tea1Δ* samples (MG0212A)			
#	**Protein Accession Number**	**Mol. Weight**	**1**	**2**	**3**	**4**	**1**	**2**	**4**	**3**
1	G3P1_SCHPO [2]	36 kDa	26	22	22	22	20	24	26	22
2	ENO11_SCHPO	47 kDa	20	18	19	20	18	19	18	15
3	EF1A1_SCHPO (+2)	50 kDa	16	16	15	16	15	18	16	13
4	PMA1_SCHPO	100 kDa	30	31	33	29	30	31	30	32
5	ADH_SCHPO	37 kDa	13	14	12	13	13	13	12	11
6	KPYK_SCHPO	56 kDa	26	26	23	24	24	28	27	26
7	METE_SCHPO	85 kDa	39	33	31	37	33	33	35	29
8	ALF_SCHPO	40 kDa	18	15	15	17	16	18	16	15
9	THI4_SCHPO	35 kDa	13	14	12	13	13	13	13	13
10	HSP72_SCHPO [2]	70 kDa	29	29	26	29	26	28	27	24
11	PGK_SCHPO	44 kDa	25	22	21	21	22	25	25	23
12	EF2_SCHPO	93 kDa	21	20	22	22	20	21	21	18
13	HSP90_SCHPO	81 kDa	31	28	28	31	28	29	30	26
14	PDC2_SCHPO	62 kDa	22	17	18	20	18	19	19	15
15	HSP75_SCHPO	67 kDa	24	23	23	23	22	22	24	22
16	EF3_SCHPO	116 kDa	27	25	27	31	26	28	25	24
17	FAS1_SCHPO	231 kDa	36	35	35	44	36	36	35	28
18	ACT_SCHPO	42 kDa	17	14	15	17	15	15	16	14
19	FAS2_SCHPO	202 kDa	40	36	40	43	36	38	42	32
20	PFKA_SCHPO	103 kDa	20	18	18	25	16	20	18	17
21	SAHH_SCHPO	47 kDa	16	15	15	15	14	17	16	14
22	RS27A_SCHPO (+1)	17 kDa	6	7	6	6	7	7	7	7
23	RS3_SCHPO	28 kDa	7	8	8	10	7	7	7	6
24	ILV5_SCHPO	45 kDa	16	16	16	18	15	16	17	16
25	ACAC_SCHPO	257 kDa	38	30	35	41	28	28	34	29
26	RS3A2_SCHPO [2]	29 kDa	15	14	13	13	14	14	15	13
27	GBLP_SCHPO	35 kDa	11	10	10	11	11	11	11	11
28	6PGD_SCHPO	54 kDa	18	15	17	21	16	16	14	14

29	METK_SCHPO	42 kDa	11	12	11	14	11	12	12	9
30	RL4A_SCHPO [2]	40 kDa	20	19	18	21	16	22	21	18
31	ADT_SCHPO	35 kDa	9	10	9	10	8	10	9	7
32	CLH_SCHPO	190 kDa	24	21	29	31	20	23	27	19
33	RL23A_SCHPO (+1)	15 kDa	2	2	3	2	2	2	2	2
34	NMT1_SCHPO	39 kDa	11	9	9	9	8	11	10	7
35	GLYD_SCHPO	52 kDa	14	16	12	17	18	15	10	11
36	MET5_SCHPO	164 kDa	23	16	16	25	13	20	21	12
37	PYR1_SCHPO	248 kDa	35	33	31	31	31	35	31	25
38	TKT_SCHPO	75 kDa	16	11	11	16	12	15	14	12
39	IF4A_SCHPO	44 kDa	10	9	9	10	8	11	10	11
40	PUR9_SCHPO	64 kDa	19	17	17	17	16	19	16	15
41	PUT2_SCHPO	60 kDa	17	17	15	14	17	16	16	12
42	PYC_SCHPO	131 kDa	27	24	22	26	22	24	22	18
43	HSP7F_SCHPO	80 kDa	24	20	21	25	22	23	25	19
44	SERA_SCHPO	51 kDa	13	14	13	14	12	13	13	11
45	FBRL_SCHPO	32 kDa	10	12	10	10	11	9	11	9
46	RS27_SCHPO	9 kDa	3	3	2	3	3	3	3	3
47	RS2_SCHPO	28 kDa	7	6	6	6	6	7	7	5
48	RL3A_SCHPO (+1)	44 kDa	14	11	11	12	10	14	14	13
49	ASNS_SCHPO	63 kDa	14	12	13	16	13	14	14	9
50	MAOX_SCHPO	63 kDa	16	14	12	17	12	14	13	11
51	HSP7M_SCHPO	73 kDa	19	17	17	18	18	16	20	15
52	HOSM_SCHPO	46 kDa	13	13	12	13	12	13	13	10
53	PMGY_SCHPO	24 kDa	15	11	12	14	10	14	15	8
54	ARO1_SCHPO	174 kDa	25	18	20	22	18	22	18	13
55	LEU3_SCHPO	40 kDa	10	8	9	12	9	10	11	7
56	ATPA_SCHPO	59 kDa	13	10	11	12	10	13	12	10
57	RS6A_SCHPO (+1)	27 kDa	10	10	8	9	8	12	11	8
58	MET3_SCHPO	55 kDa	18	13	13	16	13	15	14	9
59	YIZG_SCHPO	55 kDa	5	6	5	6	5	6	6	6
60	G6PI_SCHPO	61 kDa	8	9	11	11	9	8	8	6
61	RS4B_SCHPO [2]	30 kDa	9	8	7	9	9	10	9	8
62	PDX1_SCHPO	31 kDa	13	9	10	12	10	12	11	12
63	TPIS_SCHPO	27 kDa	12	11	12	13	11	12	11	10
64	ATPB_SCHPO	57 kDa	13	13	11	14	11	12	11	9
65	HXK2_SCHPO	51 kDa	10	7	9	13	9	9	10	6
66	ILVB_SCHPO	73 kDa	12	13	13	13	13	12	13	11

67	GRP78_SCHPO	73 kDa	14	12	13	15	9	12	14	13
68	HMT2_SCHPO	52 kDa	12	11	10	13	10	11	11	10
69	BFR1_SCHPO	172 kDa	11	20	17	16	18	13	17	12
70	LYS9_SCHPO	50 kDa	9	9	8	10	6	9	10	6
71	CARB_SCHPO	127 kDa	19	20	18	16	19	20	19	19
72	LYS2_SCHPO	157 kDa	16	13	16	20	15	14	17	10
73	SEC31_SCHPO	133 kDa	20	16	18	17	15	19	23	16
74	RS7_SCHPO	22 kDa	7	7	6	6	6	8	7	4
75	PABP_SCHPO	72 kDa	14	15	13	13	13	15	14	15
76	SYLC_SCHPO	126 kDa	21	16	19	23	19	16	17	14
77	NOP56_SCHPO	55 kDa	10	11	12	12	11	9	11	9
78	CYPH_SCHPO	17 kDa	8	8	7	8	7	7	8	6
79	UGPA1_SCHPO	56 kDa	12	9	10	12	9	11	11	10
80	C1TC_SCHPO	101 kDa	16	13	14	12	13	17	14	9
81	RS18A_SCHPO (+1)	17 kDa	8	5	7	6	5	7	7	5
82	TRP_SCHPO	75 kDa	10	11	8	9	7	8	10	9
83	HSP60_SCHPO	62 kDa	14	15	15	16	13	16	14	17
84	EF1G_SCHPO	46 kDa	10	8	9	10	7	7	9	7
85	RL15A_SCHPO (+1)	24 kDa	4	4	4	4	4	4	4	4
86	ACSA_SCHPO	73 kDa	11	12	12	12	10	11	9	7
87	DED1_SCHPO	70 kDa	14	11	9	9	11	10	9	9
88	RL16A_SCHPO	22 kDa	4	4	4	4	4	4	4	4
89	DHE4_SCHPO	49 kDa	10	10	7	12	9	10	11	6
90	ACO1_SCHPO	54 kDa	8	8	7	7	7	7	7	8
91	RS14A_SCHPO (+1)	15 kDa	5	6	5	5	5	6	7	7
92	RS9B_SCHPO [2]	22 kDa	11	10	10	11	10	10	10	7
93	PLB1_SCHPO	67 kDa	5	5	5	5	5	6	6	6
94	RL8_SCHPO	29 kDa	11	9	10	10	9	8	8	7
95	TBB_SCHPO	49 kDa	6	8	7	6	6	7	7	6
96	EIF3A_SCHPO	107 kDa	12	9	9	11	10	10	11	12
97	YBP8_SCHPO	69 kDa	13	13	12	12	9	13	14	8
98	RL9A_SCHPO [2]	22 kDa	7	6	5	7	6	6	6	4
99	RLA0_SCHPO	34 kDa	2	3	2	4	3	3	3	3
100	TCPG_SCHPO	58 kDa	12	8	12	11	11	11	10	9
101	ECM33_SCHPO	43 kDa	3	3	3	3	3	3	3	3
102	EIF3B_SCHPO	84 kDa	14	13	13	15	13	14	12	10
103	BGS4_SCHPO	225 kDa	9	10	15	16	13	14	15	9

104	TCPE_SCHPO	59 kDa	10	9	10	12	7	11	13	6
105	SYV_SCHPO	111 kDa	14	11	9	16	12	12	15	10
106	GHT5_SCHPO	60 kDa	4	4	4	4	4	4	4	3
107	IF4G_SCHPO	154 kDa	12	12	12	14	12	10	9	12
108	GCN1_SCHPO	297 kDa	9	13	19	19	14	12	12	8
109	ACL1_SCHPO	67 kDa	11	9	11	11	10	8	7	8
110	NOP58_SCHPO	56 kDa	9	10	11	12	10	7	9	9
111	THI6_SCHPO	56 kDa	9	10	8	10	8	9	9	7
112	PROD_SCHPO	56 kDa	7	8	8	8	8	8	7	6
113	RL1B_SCHPO [2]	24 kDa	5	5	5	6	4	6	4	3
114	YF19_SCHPO	55 kDa	10	9	7	8	7	7	9	6
115	YL8C_SCHPO	34 kDa	6	5	6	6	5	6	6	3
116	TAL1_SCHPO	35 kDa	11	10	11	12	12	13	13	8
117	BUT2_SCHPO	44 kDa	4	5	4	3	5	6	5	4
118	LYS1_SCHPO	41 kDa	8	7	10	10	9	8	8	9
119	IPYR_SCHPO	32 kDa	7	8	7	8	7	8	8	6
120	RL5A_SCHPO (+1)	33 kDa	7	5	5	7	5	7	6	7
121	GLT1_SCHPO	233 kDa	18	11	12	16	9	12	14	9
122	YNY8_SCHPO	37 kDa	7	7	8	6	7	8	9	6
123	ATC4_SCHPO	136 kDa	18	12	12	15	11	14	14	11
124	GHT8_SCHPO	60 kDa	4	4	4	4	4	4	4	4
125	TOM70_SCHPO	70 kDa	11	11	11	12	11	11	12	10
126	G6PD_SCHPO	57 kDa	12	11	9	11	9	9	9	9
127	OSTB_SCHPO	49 kDa	8	10	11	15	9	8	7	7
128	RS11A_SCHPO (+1)	18 kDa	6	7	6	6	5	6	7	4
129	EIF3C_SCHPO	104 kDa	11	11	8	12	10	9	10	8
130	PRS1_SCHPO	79 kDa	7	10	11	10	10	9	8	10
131	RL17A_SCHPO [2]	21 kDa	7	5	10	8	7	8	5	5
132	ARF1_SCHPO	21 kDa	6	5	6	7	5	6	6	4
133	CDC48_SCHPO	90 kDa	12	9	9	10	9	9	10	10
134	RAD25_SCHPO	30 kDa	9	7	8	8	6	8	7	5
135	TCPQ_SCHPO	60 kDa	9	11	10	12	9	8	9	8
136	THI22_SCHPO	61 kDa	9	9	6	11	10	9	10	7
137	APE1_SCHPO	99 kDa	8	13	12	11	11	14	10	9
138	PUR2_SCHPO	85 kDa	12	9	8	14	9	11	11	8
139	PUR8_SCHPO	54 kDa	8	7	11	14	10	13	10	9
140	VGL1_SCHPO	143 kDa	12	13	13	13	9	11	12	10

141	CP51_SCHPO	56 kDa	9	8	10	11	11	9	8	8
142	MET10_SCHPO	111 kDa	10	8	9	11	9	9	10	10
143	THIL_SCHPO	41 kDa	10	11	10	10	10	10	10	7
144	PYRD_SCHPO	48 kDa	7	7	7	9	8	7	5	5
145	RHO1_SCHPO	23 kDa	4	4	4	4	3	4	4	4
146	CHO2_SCHPO	103 kDa	10	8	8	10	8	8	7	6
147	IMDH_SCHPO	57 kDa	7	7	8	7	7	5	7	6
148	RL2A_SCHPO (+2)	27 kDa	3	3	3	3	3	3	3	3
149	SDHA_SCHPO	70 kDa	10	9	5	9	6	10	9	8
150	VATB_SCHPO	56 kDa	11	8	10	10	10	11	7	9
151	AATR1_SCHPO	53 kDa	10	8	8	8	8	10	7	5
152	COPA_SCHPO	136 kDa	9	9	10	12	8	10	10	8
153	RL11A_SCHPO (+1)	20 kDa	4	4	4	4	3	5	4	1
154	THDH_SCHPO	67 kDa	11	11	10	8	9	12	11	12
155	TSA1_SCHPO	21 kDa	7	6	4	7	4	7	7	4
156	LCF1_SCHPO	76 kDa	8	9	6	10	5	7	6	5
157	RL10A_SCHPO [2]	25 kDa	3	4	3	4	4	4	3	3
158	PIL1_SCHPO	40 kDa	6	5	6	5	6	5	5	3
159	SYIC_SCHPO	123 kDa	12	8	7	11	8	11	14	10
160	MPG1_SCHPO	40 kDa	7	5	5	7	6	6	6	5
161	SYTC_SCHPO	80 kDa	10	9	12	10	11	8	10	5
162	TCPD_SCHPO	57 kDa	11	10	11	13	10	10	12	6
163	YDMC_SCHPO	61 kDa	11	8	10	11	9	10	10	8
164	RPN1_SCHPO	98 kDa	9	6	7	11	5	7	8	7
165	UBA1_SCHPO	113 kDa	10	10	10	12	10	11	11	8
166	H2A2_SCHPO [2]	14 kDa	2	3	3	0	2	2	2	1
167	BCA1_SCHPO	48 kDa	8	6	7	9	9	7	8	4
168	OAT_SCHPO	48 kDa	9	8	9	9	8	8	8	8
169	RL20A_SCHPO (+1)	21 kDa	5	5	5	5	5	6	5	6
170	VDAC_SCHPO	30 kDa	7	6	6	7	6	7	5	5
171	NCB5R_SCHPO	34 kDa	9	9	9	10	9	8	9	8
172	RL33B_SCHPO	12 kDa	3	3	3	3	3	3	3	2
173	VATA_SCHPO	69 kDa	11	8	7	10	8	9	9	4
174	MYO1_SCHPO	136 kDa	10	10	9	10	10	9	11	5
175	RS8A_SCHPO (+1)	23 kDa	5	5	4	4	4	5	5	5
176	RS13_SCHPO	17 kDa	7	7	7	8	7	6	5	5
177	ACL2_SCHPO	54 kDa	7	7	6	10	7	7	9	5

178	EIF3I_SCHPO	37 kDa	8	7	7	8	7	6	9	10
179	IMB3_SCHPO	122 kDa	7	8	11	10	8	6	9	6
180	RL6_SCHPO	21 kDa	4	6	4	4	4	6	5	5
181	YH75_SCHPO	41 kDa	7	9	9	10	8	8	7	7
182	CBF5_SCHPO	53 kDa	5	4	3	4	6	4	4	4
183	CYSD_SCHPO	46 kDa	8	7	7	7	7	8	8	7
184	HMCS_SCHPO	49 kDa	7	8	7	6	6	6	7	8
185	TCPB_SCHPO	57 kDa	7	10	12	8	8	8	10	7
186	RS5B_SCHPO	22 kDa	6	6	5	6	5	6	5	3
187	COPG_SCHPO	101 kDa	10	10	8	10	10	8	9	7
188	DBP5_SCHPO	56 kDa	9	12	10	11	9	8	12	10
189	FIMB_SCHPO	69 kDa	9	8	6	9	6	7	8	5
190	ILV3_SCHPO	64 kDa	7	7	7	7	7	6	8	5
191	SYA_SCHPO	107 kDa	9	9	8	9	9	10	9	5
192	TCPA_SCHPO	60 kDa	6	9	9	10	6	9	10	7
193	GPD1_SCHPO	42 kDa	6	5	6	7	5	6	5	4
194	SYEC_SCHPO	81 kDa	9	8	8	10	8	10	7	7
195	EIF3D_SCHPO	63 kDa	8	9	8	7	8	10	8	6
196	NOT1_SCHPO	237 kDa	8	9	13	12	11	5	10	4
197	RL19B_SCHPO [2]	23 kDa	6	8	6	5	6	6	6	10
198	RS16A_SCHPO (+1)	15 kDa	4	4	4	4	4	4	4	4
199	THRC_SCHPO	58 kDa	7	5	7	5	4	6	6	6
200	AK_SCHPO	57 kDa	8	6	7	8	6	8	9	8
201	ARGD_SCHPO	48 kDa	6	5	5	7	5	8	7	6
202	ELF1_SCHPO	117 kDa	11	11	12	10	9	8	11	9
203	NDH1_SCHPO	62 kDa	6	9	9	9	9	4	6	5
204	VTC2_SCHPO	85 kDa	6	7	7	10	5	9	8	6
205	YA7D_SCHPO	98 kDa	8	9	10	9	9	7	7	6
206	IDHP_SCHPO	49 kDa	6	3	4	6	6	8	5	6
207	COPB2_SCHPO	90 kDa	9	8	8	11	7	9	7	7
208	QCR2_SCHPO	46 kDa	13	8	8	13	10	10	10	6
209	YC31_SCHPO	156 kDa	11	11	9	11	5	9	8	5
210	Q9HGN1-DECOY	?	2	0	0	0	1	1	1	2
211	ASSY_SCHPO	46 kDa	7	5	6	6	6	7	7	5
212	LEUC_SCHPO	83 kDa	9	6	4	11	5	7	8	5
213	YG23_SCHPO	69 kDa	7	8	7	8	9	6	8	6
214	ACON_SCHPO	86 kDa	7	7	7	8	7	6	7	6
215	DLDH_SCHPO	55 kDa	10	10	9	12	8	11	11	8

216	SPEE_SCHPO	33 kDa	5	3	3	4	3	5	4	2
217	YB0G_SCHPO	59 kDa	7	7	9	10	7	7	10	5
218	IF2P_SCHPO	120 kDa	9	8	10	12	10	10	11	7
219	PUR4_SCHPO	145 kDa	7	7	9	9	7	5	5	7
220	HS104_SCHPO	101 kDa	12	8	9	11	8	8	9	8
221	LYS12_SCHPO	39 kDa	5	6	7	6	5	5	6	4
222	RAD24_SCHPO	30 kDa	9	7	6	9	5	8	6	5
223	SEC18_SCHPO	88 kDa	11	9	9	11	9	6	10	8
224	PRS4_SCHPO	50 kDa	7	7	7	8	6	4	8	6
225	ACON2_SCHPO	100 kDa	9	6	8	7	6	7	9	5
226	COPB_SCHPO	105 kDa	7	7	7	9	7	7	6	6
227	HMDH_SCHPO	115 kDa	6	7	8	7	4	6	6	5
228	RL7C_SCHPO	29 kDa	4	3	6	6	3	5	4	3
229	YN67_SCHPO	35 kDa	3	7	6	5	5	3	5	4
230	AROG_SCHPO	41 kDa	5	5	4	5	5	5	5	4
231	SYDC_SCHPO	67 kDa	7	6	8	10	8	6	6	6
232	DBP3_SCHPO	64 kDa	7	7	7	7	7	7	7	4
233	DHOM_SCHPO	40 kDa	8	4	6	9	4	7	6	5
234	PRS6A_SCHPO	49 kDa	8	6	7	11	4	6	9	4
235	GUAA_SCHPO	60 kDa	6	6	6	6	5	5	6	5
236	MPCP_SCHPO	34 kDa	6	5	8	7	8	3	4	3
237	DHAS_SCHPO	39 kDa	7	4	5	5	5	6	6	5
238	PRS7_SCHPO	49 kDa	8	9	9	7	8	6	8	8
239	RRP5_SCHPO	188 kDa	6	9	7	6	8	9	6	7
240	SC231_SCHPO	85 kDa	7	7	7	6	5	4	7	6
241	SYNC_SCHPO	64 kDa	8	6	8	6	7	7	5	5
242	YQ52_SCHPO	110 kDa	6	8	10	8	9	6	6	7
243	ABC2_SCHPO	167 kDa	7	9	8	7	9	8	8	7
244	HIS1_SCHPO	34 kDa	7	5	5	5	4	5	5	4
245	ERF3_SCHPO	73 kDa	8	4	6	8	5	6	9	6
246	ERG5_SCHPO	62 kDa	5	6	6	8	8	6	4	5
247	IMB4_SCHPO	118 kDa	7	5	7	10	2	4	6	3
248	ODPA_SCHPO	45 kDa	7	7	6	10	7	7	6	6
249	SAR1_SCHPO	21 kDa	8	6	6	7	6	6	8	5
250	UTP10_SCHPO	186 kDa	7	8	8	9	7	8	8	7
251	VPS1_SCHPO	76 kDa	8	8	9	7	8	4	7	6
252	EFTU_SCHPO	48 kDa	9	8	8	8	5	5	6	1

253	HISX_SCHPO	48 kDa	8	5	6	6	6	5	4	4
254	SND1_SCHPO	98 kDa	9	7	6	10	6	8	9	3
255	YIW2_SCHPO	195 kDa	8	9	9	8	8	6	7	3
256	RTN1_SCHPO	34 kDa	3	3	3	3	3	3	3	3
257	SLA2_SCHPO	124 kDa	8	7	7	10	7	9	7	7
258	YN43_SCHPO	59 kDa	5	6	7	6	5	6	8	4
259	SPI1_SCHPO	25 kDa	3	3	4	3	3	4	3	2
260	SYKC_SCHPO	67 kDa	8	7	7	8	5	5	6	5
261	SYMC_SCHPO	89 kDa	7	7	7	5	5	7	5	9
262	FSF1_SCHPO	35 kDa	7	4	4	6	4	5	5	5
263	LCB2_SCHPO	68 kDa	7	7	7	6	9	4	5	6
264	RL7B_SCHPO	28 kDa	6	3	5	7	4	6	5	4
265	SYG_SCHPO	74 kDa	7	6	7	8	5	9	5	7
266	SYYC_SCHPO	45 kDa	4	5	5	6	5	3	3	3
267	YBN1_SCHPO	64 kDa	6	4	6	5	3	4	5	3
268	FAT2_SCHPO	56 kDa	5	5	5	5	4	5	3	4
269	LEU1_SCHPO	64 kDa	6	5	6	10	7	6	7	3
270	PRS8_SCHPO	45 kDa	8	5	6	8	5	6	6	3
271	ARG56_SCHPO	98 kDa	7	5	2	3	2	6	5	5
272	FPPS_SCHPO	40 kDa	8	8	8	8	8	7	7	2
273	GLNA_SCHPO	40 kDa	6	4	4	7	4	5	5	3
274	ARC1_SCHPO	51 kDa	8	7	6	6	5	7	6	7
275	NOG2_SCHPO	60 kDa	7	7	9	7	7	4	6	6
276	ODP2_SCHPO	52 kDa	5	5	4	7	4	5	5	4
277	OST1_SCHPO	52 kDa	5	5	4	6	4	4	5	4
278	RS19B_SCHPO	16 kDa	4	4	3	4	4	4	4	3
279	IDH1_SCHPO	39 kDa	7	8	9	7	6	5	5	4
280	YI7E_SCHPO	40 kDa	8	5	5	4	5	7	5	5
281	CORO_SCHPO	67 kDa	7	3	5	6	5	5	4	4
282	EIF3G_SCHPO	31 kDa	6	5	4	5	5	4	5	4
283	IF2A_SCHPO	35 kDa	6	5	4	6	3	6	5	4
284	RL14_SCHPO	15 kDa	3	3	3	4	3	4	3	3
285	RS22A_SCHPO (+1)	15 kDa	4	2	3	4	3	4	4	2
286	RS23A_SCHPO (+1)	16 kDa	3	3	2	3	2	4	4	1
287	SEY1_SCHPO	88 kDa	6	8	6	6	7	7	7	5
288	YCT3_SCHPO	61 kDa	4	3	4	3	5	4	3	3
289	YJD2_SCHPO	55 kDa	5	6	5	5	5	5	5	6
290	EIF3F_SCHPO	33 kDa	5	5	5	6	5	4	5	5
291	HXK1_SCHPO	54 kDa	5	5	4	4	4	4	4	4
292	SPO15_SCHPO	223 kDa	7	7	7	8	6	6	9	8

293	YEG9_SCHPO	41 kDa	5	3	3	9	4	2	4	2
294	GPD2_SCHPO	41 kDa	5	5	5	6	6	4	5	4
295	MAP2_SCHPO	47 kDa	5	4	5	6	3	3	6	3
296	OLA1_SCHPO	44 kDa	6	5	6	8	6	5	6	2
297	DHX15_SCHPO	84 kDa	5	7	6	9	7	8	7	4
298	DYR_SCHPO	52 kDa	4	3	4	5	4	3	2	3
299	ODPB_SCHPO	40 kDa	4	6	5	4	5	6	6	6
300	RL32B_SCHPO [2]	14 kDa	3	3	3	2	2	3	3	2
301	GHT2_SCHPO	59 kDa	4	5	5	3	4	5	5	4
302	STT3_SCHPO	85 kDa	4	4	4	5	4	3	4	4
303	VHT1_SCHPO	63 kDa	6	7	5	6	7	6	7	6
304	AROF_SCHPO	40 kDa	4	5	3	6	6	6	7	5
305	EIF3M_SCHPO	45 kDa	3	4	4	3	3	3	4	2
306	PURA_SCHPO	48 kDa	5	4	4	3	4	4	3	4
307	YEAA_SCHPO	37 kDa	6	4	4	7	4	6	6	5
308	RL38B_SCHPO [2]	8 kDa	3	3	2	3	2	4	3	2
309	RS15B_SCHPO [2]	18 kDa	3	2	3	3	3	3	3	3
310	AATC_SCHPO	46 kDa	5	4	4	3	5	5	5	5
311	HOB3_SCHPO	30 kDa	5	5	5	7	6	4	6	4
312	RL27B_SCHPO [2]	15 kDa	6	5	5	5	5	6	5	5
313	RUVB2_SCHPO	52 kDa	3	5	5	6	4	5	7	5
314	TCPH_SCHPO	61 kDa	6	5	4	6	6	4	6	4
315	2AAA_SCHPO	67 kDa	3	3	4	3	3	3	4	2
316	CDB4_SCHPO	42 kDa	7	5	5	6	6	5	5	5
317	ERG6_SCHPO	43 kDa	5	3	3	3	3	4	4	3
318	GCSP_SCHPO	114 kDa	7	6	6	9	8	5	7	2
319	TCPZ_SCHPO	59 kDa	5	6	7	4	7	4	4	6
320	UTP21_SCHPO	101 kDa	4	7	6	5	8	3	6	6
321	YHHB_SCHPO	34 kDa	4	8	5	5	4	4	5	3
322	ABC4_SCHPO	165 kDa	5	6	5	5	5	5	5	6
323	RL13_SCHPO	24 kDa	4	4	4	4	3	4	4	5
324	SYRC_SCHPO	71 kDa	9	3	5	10	6	7	4	2
325	VP13B_SCHPO	354 kDa	6	8	8	6	4	2	5	1
326	VTC4_SCHPO	84 kDa	6	4	5	7	5	6	7	3
327	YPT1_SCHPO	23 kDa	4	5	6	7	5	5	4	4
328	RL22_SCHPO	13 kDa	3	3	3	3	3	3	3	3
329	TPSX_SCHPO	107 kDa	5	4	2	5	2	5	4	3
330	CY1_SCHPO	34 kDa	3	2	3	3	3	3	3	2

331	NG06_SCHPO	148 kDa	5	4	6	3	3	4	3	2
332	RPN5_SCHPO	52 kDa	5	4	6	5	5	4	4	4
333	ARLZ_SCHPO	52 kDa	3	3	3	7	1	8	6	3
334	DAK1_SCHPO	62 kDa	5	5	3	6	3	4	5	3
335	FMO1_SCHPO	50 kDa	4	3	3	6	4	4	4	3
336	GCS1_SCHPO	93 kDa	6	4	4	9	3	6	5	4
337	GET3_SCHPO	37 kDa	3	3	3	3	3	3	3	3
338	LCF2_SCHPO	76 kDa	5	5	5	7	4	3	4	3
339	LYS4_SCHPO	78 kDa	7	5	6	8	8	6	4	0
340	MAS5_SCHPO	45 kDa	3	3	3	3	2	3	4	1
341	RL18B_SCHPO	21 kDa	2	2	2	2	2	2	2	3
342	CARA_SCHPO	46 kDa	5	4	4	5	5	5	3	4
343	H4_SCHPO	11 kDa	4	4	4	4	4	3	3	2
344	MMF1_SCHPO	18 kDa	4	4	4	3	4	4	4	5
345	PRS10_SCHPO	44 kDa	4	3	3	5	4	4	4	5
346	YGMH_SCHPO	52 kDa	3	1	3	3	2	2	2	2
347	RL18A_SCHPO	21 kDa	2	2	2	2	2	2	2	2
348	YIL5_SCHPO	87 kDa	4	4	5	5	4	3	5	3
349	AGS1_SCHPO	272 kDa	5	5	6	5	7	7	4	4
350	PUR6_SCHPO	60 kDa	4	5	5	6	4	4	4	4
351	RL21A_SCHPO [2]	18 kDa	4	2	2	2	2	3	3	2
352	CYSK1_SCHPO	38 kDa	5	4	3	5	3	6	4	1
353	PRS6B_SCHPO	44 kDa	4	4	4	6	3	5	5	3
354	SEC7B_SCHPO	207 kDa	4	4	5	9	3	4	5	4
355	YFG5_SCHPO	32 kDa	2	1	3	3	3	1	1	1
356	ADK_SCHPO	37 kDa	4	4	4	4	4	4	4	3
357	CKI3_SCHPO	50 kDa	5	4	4	4	3	5	4	3
358	EIF3H_SCHPO	40 kDa	6	6	3	5	3	5	6	3
359	FDFT_SCHPO	53 kDa	5	5	5	4	4	3	4	2
360	FFT3_SCHPO	105 kDa	5	5	6	6	3	4	5	3
361	HMT1_SCHPO	94 kDa	5	5	5	6	5	4	4	3
362	P25_SCHPO	22 kDa	4	4	4	4	4	4	4	4
363	SYFB_SCHPO	67 kDa	7	5	6	7	5	5	5	2
364	GCST_SCHPO	42 kDa	4	5	5	4	5	4	5	2
365	KCAB_SCHPO	38 kDa	5	4	3	4	4	4	4	4
366	RL26_SCHPO	14 kDa	4	4	4	4	4	4	4	2
367	RPN3_SCHPO	57 kDa	3	2	2	3	2	3	4	3
368	AP1G1_SCHPO	96 kDa	4	3	4	4	3	4	6	5
369	ARGI2_SCHPO	36 kDa	4	4	4	3	3	4	4	3
370	CALX_SCHPO	63 kDa	4	4	4	5	3	3	4	1

371	SDS23_SCHPO	44 kDa	4	6	4	7	4	3	3	3
372	THI9_SCHPO	65 kDa	5	5	3	3	4	4	4	2
373	TOM20_SCHPO	18 kDa	4	3	4	4	4	4	4	2
374	VPH1_SCHPO	94 kDa	4	5	5	6	4	4	4	2
375	CAO1_SCHPO	81 kDa	4	4	3	4	4	3	2	2
376	MDHM_SCHPO	36 kDa	5	5	4	7	5	5	4	2
377	MDN1_SCHPO	538 kDa	3	2	6	6	2	4	4	3
378	PDI1_SCHPO	55 kDa	5	4	6	4	5	4	4	2
379	RUVB1_SCHPO	50 kDa	3	3	3	7	3	3	3	2
380	SC61A_SCHPO	53 kDa	1	1	1	1	1	1	1	1
381	PLR1_SCHPO	37 kDa	5	3	4	4	3	3	4	1
382	RL28E_SCHPO	15 kDa	3	3	3	3	3	2	2	1
383	RLI1_SCHPO	67 kDa	3	5	3	4	4	5	6	1
384	SEC7A_SCHPO	207 kDa	4	4	6	6	3	2	4	1
385	YG58_SCHPO	73 kDa	4	3	4	4	3	3	3	4
386	YN27_SCHPO	28 kDa	4	2	3	4	2	4	3	3
387	BIOB_SCHPO	41 kDa	3	2	2	2	1	3	3	0
388	NOG1_SCHPO	73 kDa	4	3	3	4	2	3	4	4
389	RL12A_SCHPO (+1)	18 kDa	3	3	2	3	4	2	3	2
390	TCD_SCHPO	54 kDa	5	4	4	5	5	5	3	2
391	TOM40_SCHPO	38 kDa	3	4	2	3	0	2	3	3
392	RS20_SCHPO	14 kDa	3	3	3	3	3	3	3	3
393	ARP3_SCHPO	47 kDa	4	4	3	4	3	4	4	4
394	ETFD_SCHPO	69 kDa	4	2	2	3	2	4	4	3
395	IDH2_SCHPO	41 kDa	4	5	4	5	3	2	2	3
396	MNN9_SCHPO	38 kDa	4	3	4	4	4	4	2	2
397	PHB2_SCHPO	32 kDa	4	3	4	3	5	3	3	1
398	PMM_SCHPO	29 kDa	5	5	4	6	5	5	6	1
399	PUR1_SCHPO	60 kDa	4	4	4	6	3	3	5	2
400	RAE1_SCHPO	39 kDa	3	5	3	4	6	6	6	3
401	SAM50_SCHPO	52 kDa	6	4	3	4	4	5	5	3
402	SYFA_SCHPO	56 kDa	4	4	5	3	5	3	3	4
403	YCO6_SCHPO	44 kDa	4	5	5	4	3	4	6	3
404	H31_SCHPO (+1)	15 kDa	0	0	0	0	0	1	1	0
405	EIF2A_SCHPO	63 kDa	5	4	5	5	3	3	4	4
406	PNU1_SCHPO	36 kDa	5	6	4	4	3	3	4	3
407	RPN11_SCHPO	35 kDa	3	4	4	4	3	4	3	4
408	UBC13_SCHPO	17 kDa	3	3	3	2	3	3	3	3
409	YQD3_SCHPO	64 kDa	2	4	3	3	3	4	3	3
410	BQT4_SCHPO	48 kDa	3	5	5	7	2	3	4	3
411	HEM1_SCHPO	61 kDa	2	4	4	5	4	5	5	4

412	LCB1_SCHPO	57 kDa	5	4	4	6	4	3	3	2
413	SERC_SCHPO	43 kDa	5	5	3	3	3	7	4	5
414	YKH3_SCHPO	136 kDa	4	3	3	4	3	2	2	1
415	GAS1_SCHPO	58 kDa	2	2	2	2	2	2	2	2
416	GSHB_SCHPO	56 kDa	3	2	3	5	4	3	4	2
417	IMA3_SCHPO	116 kDa	4	5	4	5	5	5	5	3
418	MPPB_SCHPO	51 kDa	2	0	2	6	2	2	1	1
419	PMD1_SCHPO	150 kDa	3	4	6	4	2	4	4	4
420	RRP12_SCHPO	131 kDa	4	4	6	4	3	4	4	3
421	RS24B_SCHPO	16 kDa	3	2	2	2	2	3	3	2
422	YKP6_SCHPO	22 kDa	3	3	2	2	2	3	2	3
423	RS17A_SCHPO [2]	16 kDa	3	4	3	4	2	6	4	4
424	2ABA_SCHPO	53 kDa	3	3	1	3	2	2	2	0
425	ARP2_SCHPO	44 kDa	3	2	3	6	2	3	4	4
426	DHH1_SCHPO	55 kDa	4	2	2	4	2	2	4	2
427	ERF1_SCHPO	49 kDa	3	2	3	5	1	3	4	3
428	HIS5_SCHPO	59 kDa	5	3	5	4	4	2	3	3
429	MPI_SCHPO	46 kDa	3	3	4	4	3	3	3	3
430	NAT10_SCHPO	116 kDa	3	3	6	4	2	2	4	2
431	PMP20_SCHPO	17 kDa	3	4	3	3	4	4	3	5
432	RIR1_SCHPO	92 kDa	5	2	2	6	2	3	2	1
433	YA03_SCHPO	25 kDa	3	3	3	2	3	3	2	2
434	YA55_SCHPO	56 kDa	4	3	4	6	4	4	2	2
435	YBL3_SCHPO	40 kDa	4	3	4	4	4	2	2	1
436	YBY6_SCHPO	19 kDa	3	3	3	4	3	3	2	3
437	ALG11_SCHPO	53 kDa	3	3	3	5	3	3	3	2
438	ATC2_SCHPO	142 kDa	4	5	6	4	2	4	4	1
439	CAN_SCHPO	37 kDa	3	2	2	3	2	2	2	2
440	GLY1_SCHPO	41 kDa	3	4	5	4	5	4	3	3
441	MGLL_SCHPO	42 kDa	4	3	4	4	2	4	3	5
442	MS116_SCHPO	59 kDa	3	3	4	4	4	5	4	2
443	PSA1_SCHPO	27 kDa	5	4	3	4	3	6	5	3
444	RGA7_SCHPO	77 kDa	4	1	1	4	1	4	4	1
445	YE0C_SCHPO	29 kDa	3	3	4	4	3	3	3	1
446	YGWH_SCHPO	37 kDa	2	3	5	2	3	2	2	3
447	YJX1_SCHPO	55 kDa	3	2	3	4	2	4	3	2
448	YOSF_SCHPO	58 kDa	4	3	4	4	3	3	2	2
449	CAP_SCHPO	60 kDa	2	2	3	4	4	3	4	1
450	ERG1_SCHPO	50 kDa	3	3	4	5	2	3	2	2

451	H2B1_SCHPO	14 kDa	2	2	3	2	2	1	2	1
452	HEM6_SCHPO	36 kDa	6	2	2	5	3	7	6	2
453	HOB1_SCHPO	51 kDa	4	3	4	4	2	2	2	2
454	RL36A_SCHPO (+1)	11 kDa	4	3	4	3	4	3	3	3
455	SULH2_SCHPO	94 kDa	5	3	0	6	4	2	3	3
456	YB45_SCHPO	27 kDa	4	3	5	5	2	5	4	1
457	YLD2_SCHPO	31 kDa	5	4	4	3	3	6	6	1
458	YNY5_SCHPO	47 kDa	2	4	3	3	4	2	3	3
459	RL24A_SCHPO (+1)	17 kDa	1	1	1	1	1	2	1	1
460	TBA2_SCHPO	51 kDa	2	2	2	2	2	2	2	2
461	BAG1B_SCHPO	23 kDa	2	1	1	3	1	3	3	1
462	COPD_SCHPO	27 kDa	2	2	2	3	2	2	1	2
463	EMC1_SCHPO	101 kDa	4	4	3	6	3	4	4	2
464	GRN1_SCHPO	52 kDa	5	5	4	4	2	4	5	2
465	PDI2_SCHPO	41 kDa	4	3	6	6	1	4	1	4
466	PPIB_SCHPO	22 kDa	2	2	2	2	1	5	4	2
467	RL31_SCHPO	13 kDa	3	3	3	3	3	3	3	3
468	RPA1_SCHPO	189 kDa	1	3	3	4	4	4	4	3
469	SAP1_SCHPO	29 kDa	2	3	2	1	3	2	1	3
470	YBB2_SCHPO	46 kDa	4	3	2	3	2	1	3	3
471	YI13_SCHPO	28 kDa	3	4	2	5	3	4	5	1
472	RS10A_SCHPO	16 kDa	2	2	2	2	2	2	2	2
473	BGS1_SCHPO	200 kDa	2	4	5	4	5	2	3	1
474	CBPY_SCHPO	114 kDa	2	3	2	2	2	3	3	2
475	CISY_SCHPO	54 kDa	3	1	2	6	2	3	1	1
476	IF2G_SCHPO	49 kDa	3	2	2	5	2	4	1	2
477	KPR2_SCHPO	35 kDa	4	3	4	3	4	4	4	3
478	SYH_SCHPO	63 kDa	5	2	3	4	1	4	4	1
479	YJB6_SCHPO	29 kDa	1	2	2	3	2	2	2	1
480	GAR1_SCHPO	20 kDa	2	2	2	2	2	2	2	1
481	RS21_SCHPO	10 kDa	2	2	2	2	2	2	2	2
482	ALG2_SCHPO	57 kDa	3	3	3	2	2	2	3	2
483	ASPG2_SCHPO	38 kDa	4	3	4	5	4	3	3	4
484	PMT1_SCHPO	101 kDa	4	3	2	3	1	4	2	1
485	SRP68_SCHPO	68 kDa	4	3	4	7	2	2	3	2
486	SUB2_SCHPO	49 kDa	2	1	2	4	2	1	2	1
487	TBA1_SCHPO	51 kDa	4	2	2	4	2	3	4	3
488	USO1_SCHPO	122 kDa	3	2	3	3	2	1	2	2
489	YB64_SCHPO	43 kDa	3	4	3	3	3	4	3	3

490	YF14_SCHPO	21 kDa	3	3	3	3	3	3	3	3
491	CAPZB_SCHPO	30 kDa	3	3	3	2	3	3	3	3
492	DBP2_SCHPO	62 kDa	4	2	4	2	2	3	3	2
493	NCPR_SCHPO	77 kDa	2	3	3	3	3	3	3	2
494	ODPX_SCHPO	51 kDa	3	1	2	3	2	3	4	2
495	PGM_SCHPO	61 kDa	3	4	5	3	2	3	2	2
496	PO152_SCHPO	140 kDa	1	6	3	4	2	4	4	1
497	TIM44_SCHPO	49 kDa	3	3	6	2	2	2	2	2
498	TRX1_SCHPO	11 kDa	4	3	4	4	3	4	4	2
499	YDG7_SCHPO	36 kDa	2	2	3	5	2	4	2	3
500	YFM8_SCHPO	26 kDa	4	3	3	2	3	2	4	2
501	YIW4_SCHPO	37 kDa	3	2	2	3	3	3	2	2
502	YKT6_SCHPO	23 kDa	3	2	2	4	2	3	3	2
503	YN8E_SCHPO	114 kDa	2	2	2	5	3	2	3	2
504	RS26B_SCHPO	14 kDa	2	2	2	2	2	3	3	3
505	AROC_SCHPO	42 kDa	3	1	3	3	2	2	3	2
506	DHYS_SCHPO	39 kDa	4	1	3	3	3	2	2	0
507	NAT1_SCHPO	84 kDa	3	3	2	4	0	3	3	1
508	SC232_SCHPO	85 kDa	4	3	2	5	2	4	3	3
509	UTP17_SCHPO	89 kDa	2	3	3	4	4	5	4	2
510	YD1K_SCHPO	33 kDa	4	1	1	4	0	4	3	2
511	YG04_SCHPO	31 kDa	3	1	3	3	2	2	2	1
512	ANP1_SCHPO	49 kDa	2	3	2	3	2	2	3	2
513	AP1M1_SCHPO	49 kDa	3	4	4	4	3	3	2	3
514	DNM1_SCHPO	87 kDa	5	2	2	5	1	2	5	1
515	DPM1_SCHPO	27 kDa	2	2	2	2	2	3	3	2
516	EI2BG_SCHPO	50 kDa	2	2	3	5	3	2	1	3
517	PMT2_SCHPO	85 kDa	2	3	3	3	3	2	2	2
518	RENT1_SCHPO	105 kDa	2	3	4	2	3	4	2	2
519	RL28A_SCHPO [2]	17 kDa	3	3	3	4	3	3	3	3
520	SEC62_SCHPO	32 kDa	4	3	3	3	2	3	3	3
521	YCP9_SCHPO	28 kDa	4	3	3	2	4	2	2	3
522	YDFC_SCHPO	34 kDa	3	3	3	3	4	3	0	2
523	YE48_SCHPO	67 kDa	4	2	2	3	3	3	3	1
524	RSSA2_SCHPO	31 kDa	1	1	1	1	1	1	1	1
525	PIS_SCHPO	28 kDa	1	1	1	1	1	1	1	1
526	ATCX_SCHPO	159 kDa	2	3	6	4	3	1	3	3
527	AVT3_SCHPO	73 kDa	2	3	2	3	2	3	3	1
528	EIF3E_SCHPO	57 kDa	3	2	2	3	2	3	3	1
529	GDH2_SCHPO	126 kDa	3	3	3	4	2	3	2	2

530	MVD1_SCHPO	43 kDa	4	0	2	4	1	3	6	3
531	NDH2_SCHPO	61 kDa	4	0	4	6	2	4	3	1
532	PNPP_SCHPO	33 kDa	2	2	2	4	2	4	4	2
533	RPN2_SCHPO	107 kDa	3	3	2	5	2	3	3	1
534	YAA1_SCHPO	67 kDa	4	4	4	4	3	2	3	2
535	CHO1_SCHPO	25 kDa	2	2	2	3	2	2	2	1
536	FUMH_SCHPO	56 kDa	2	3	3	1	3	4	4	1
537	IPI3_SCHPO	50 kDa	3	3	2	1	3	3	2	2
538	RHO3_SCHPO	23 kDa	1	2	2	1	2	3	3	3
539	SEC24_SCHPO	102 kDa	3	1	3	6	1	3	1	0
540	SRP54_SCHPO	57 kDa	4	1	2	3	4	4	4	3
541	SRPR_SCHPO	61 kDa	2	4	3	5	3	2	3	2
542	TRXB_SCHPO	35 kDa	4	2	2	3	3	3	4	2
543	UTP5_SCHPO	74 kDa	3	3	2	3	3	3	4	2
544	HOG1_SCHPO	40 kDa	1	2	3	1	3	1	1	3
545	RNC1_SCHPO	43 kDa	2	1	1	1	2	2	3	1
546	GAS5_SCHPO	54 kDa	2	1	2	1	1	2	2	1
547	RL25B_SCHPO	16 kDa	2	2	2	2	2	2	2	2
548	BRR2_SCHPO	249 kDa	3	4	3	3	2	1	5	1
549	ISN1_SCHPO	46 kDa	1	3	1	4	3	3	4	1
550	MCS4_SCHPO	57 kDa	3	4	4	2	2	2	4	2
551	SEC72_SCHPO	22 kDa	3	3	2	3	2	3	3	2
552	SNF1_SCHPO	66 kDa	2	2	1	3	3	2	1	1
553	STT4_SCHPO	214 kDa	2	4	4	4	3	2	2	1
554	SYSC_SCHPO	52 kDa	2	2	2	2	2	3	3	2
555	WIS1_SCHPO	65 kDa	2	2	3	3	2	1	0	1
556	YAOF_SCHPO	144 kDa	3	4	3	2	5	1	2	2
557	MKAR_SCHPO	37 kDa	0	2	3	3	3	3	3	2
558	PPA4_SCHPO	52 kDa	1	2	2	2	1	2	2	2
559	SXA1_SCHPO	57 kDa	1	1	1	1	1	1	1	1
560	AATM_SCHPO	48 kDa	2	2	3	4	2	3	2	2
561	ALAT_SCHPO	57 kDa	2	2	3	3	3	3	3	2
562	ATC9_SCHPO	149 kDa	3	3	2	3	1	1	4	3
563	DCTD_SCHPO	36 kDa	2	1	3	2	1	1	1	1
564	G3BP_SCHPO	48 kDa	4	2	3	3	2	3	3	1
565	HIS2_SCHPO	46 kDa	2	3	3	3	3	3	3	2
566	MMS19_SCHPO	115 kDa	3	3	3	2	3	3	3	2
567	PRP1_SCHPO	103 kDa	3	3	3	2	3	2	3	2
568	TPS1_SCHPO	58 kDa	4	3	3	4	1	3	1	3

569	UTP4_SCHPO	79 kDa	1	2	4	1	2	1	3	2
570	VATC_SCHPO	44 kDa	1	5	4	2	3	3	2	1
571	YF38_SCHPO	64 kDa	4	3	2	2	3	3	2	2
572	YJX4_SCHPO	111 kDa	3	4	4	3	2	1	1	4
573	YJ23_SCHPO	74 kDa	2	2	3	2	2	2	1	2
574	UBP2_SCHPO	130 kDa	2	1	2	2	0	1	2	1
575	YHOE_SCHPO	41 kDa	2	2	2	2	2	2	2	1
576	RL30A_SCHPO	12 kDa	1	2	2	2	2	2	2	2
577	ELOH1_SCHPO	38 kDa	2	2	2	2	1	2	2	1
578	APT_SCHPO	21 kDa	3	2	1	3	2	3	2	2
579	CDK1_SCHPO	34 kDa	3	2	3	2	2	2	3	1
580	CYC8_SCHPO	122 kDa	0	1	4	2	1	0	2	0
581	DUG1_SCHPO	53 kDa	4	2	2	4	2	2	3	1
582	ERG26_SCHPO	38 kDa	4	1	3	3	2	2	2	2
583	GLRX4_SCHPO	27 kDa	3	2	4	5	1	1	3	1
584	IF5A1_SCHPO	17 kDa	4	1	1	3	2	4	3	0
585	LNP_SCHPO	37 kDa	2	1	3	3	1	2	3	2
586	LONM_SCHPO	119 kDa	3	3	2	3	2	2	3	3
587	RSSA1_SCHPO	32 kDa	2	1	2	3	2	1	2	1
588	SEC13_SCHPO	33 kDa	3	2	1	3	2	3	2	1
589	TWF1_SCHPO	37 kDa	3	2	3	4	2	2	4	1
590	YKJ7_SCHPO	37 kDa	2	2	1	2	2	3	2	3
591	YN53_SCHPO	58 kDa	4	2	1	3	1	3	1	0
592	YNB3_SCHPO	98 kDa	3	2	5	3	1	2	2	0
593	AP1B1_SCHPO	77 kDa	2	1	3	3	1	2	2	2
594	NHP2_SCHPO	17 kDa	1	2	3	3	2	1	1	0
595	TCTP_SCHPO	19 kDa	2	1	0	2	1	2	2	0
596	YEG7_SCHPO	57 kDa	0	1	1	1	1	1	1	1
597	AMY1_SCHPO	68 kDa	2	2	2	2	4	3	3	1
598	ATC1_SCHPO	98 kDa	3	3	2	3	2	1	2	1
599	LUB1_SCHPO	79 kDa	2	2	2	3	2	1	1	1
600	MAE1_SCHPO	49 kDa	2	1	2	3	1	2	3	1
601	MIC60_SCHPO	63 kDa	4	4	3	3	2	1	3	0
602	OTU1_SCHPO	36 kDa	3	3	3	3	2	2	3	2
603	PEX11_SCHPO	26 kDa	2	3	2	2	2	2	2	2
604	PHB1_SCHPO	31 kDa	3	2	1	4	1	3	2	1
605	PUR7_SCHPO	34 kDa	2	2	3	4	3	3	2	2
606	RGA8_SCHPO	88 kDa	1	1	1	4	1	1	2	2
607	RL35_SCHPO	14 kDa	1	1	1	3	2	2	2	2
608	RPIA_SCHPO	29 kDa	4	2	1	3	2	4	3	1
609	YE85_SCHPO	65 kDa	2	2	2	3	1	3	4	2

610	YJE9_SCHPO	33 kDa	3	2	3	4	2	2	2	0
611	YTA12_SCHPO	85 kDa	2	5	1	4	0	2	2	2
612	CYB52_SCHPO	14 kDa	2	2	2	3	0	2	3	3
613	FAL1_SCHPO	45 kDa	2	3	2	3	1	2	3	1
614	RPN12_SCHPO	31 kDa	3	2	2	3	2	2	0	3
615	YJL2_SCHPO	179 kDa	2	2	2	0	1	2	3	2
616	SDHB_SCHPO	31 kDa	2	1	3	2	2	2	2	2
617	CDC42_SCHPO	21 kDa	1	1	1	1	1	1	1	1
618	CCQ1_SCHPO	83 kDa	2	2	3	2	2	2	2	3
619	CCR4_SCHPO	76 kDa	3	2	4	3	0	3	2	2
620	CYM1_SCHPO	99 kDa	2	1	0	2	2	4	2	1
621	ERMP1_SCHPO	92 kDa	2	4	4	2	3	1	3	1
622	NFS1_SCHPO	56 kDa	2	2	0	1	0	3	2	2
623	PP2C3_SCHPO	45 kDa	0	3	3	4	0	3	2	2
624	PPB_SCHPO	59 kDa	3	2	3	2	1	1	3	1
625	RS24A_SCHPO	15 kDa	1	1	2	3	3	2	1	2
626	SOU1_SCHPO	27 kDa	2	1	2	3	3	2	2	1
627	STI1_SCHPO	66 kDa	3	2	0	4	2	3	3	1
628	UFD2_SCHPO	115 kDa	3	2	2	1	1	0	3	1
629	VA0D_SCHPO	39 kDa	3	2	3	3	3	2	3	1
630	YB2G_SCHPO	74 kDa	2	2	2	4	2	2	3	2
631	YBS1_SCHPO	38 kDa	2	1	0	1	3	3	2	2
632	YOL4_SCHPO	77 kDa	2	3	3	2	2	1	2	2
633	CFR1_SCHPO	67 kDa	2	2	2	2	2	3	3	3
634	LOA1_SCHPO	33 kDa	1	1	2	1	1	1	1	0
635	YPT2_SCHPO	23 kDa	1	2	1	2	2	1	2	1
636	TAF4_SCHPO	41 kDa	2	2	2	2	1	2	2	2
637	RS25A_SCHPO (+1)	10 kDa	1	0	1	1	1	1	1	0
638	FOL1_SCHPO	82 kDa	2	2	2	4	2	0	2	1
639	GLYM_SCHPO	54 kDa	3	3	2	3	3	1	1	1
640	GSH1_SCHPO	77 kDa	1	3	1	2	2	2	2	3
641	GSHR_SCHPO	50 kDa	2	1	1	3	1	2	2	0
642	HIS8_SCHPO	43 kDa	2	1	1	3	1	2	2	2
643	OBP1_SCHPO	59 kDa	3	1	1	3	2	3	3	1
644	PLB2_SCHPO	74 kDa	2	2	1	1	1	2	3	1
645	RIA1_SCHPO	112 kDa	2	2	2	2	1	2	2	3
646	RNA1_SCHPO	43 kDa	2	1	0	4	1	2	2	2
647	RPAC1_SCHPO	39 kDa	3	1	2	3	2	3	2	2
648	YOW5_SCHPO	81 kDa	2	3	2	2	2	2	2	1
649	YQF8_SCHPO	35 kDa	3	2	1	4	1	1	1	2
650	GAR2_SCHPO	53 kDa	2	2	2	2	1	3	2	3

651	PSY1_SCHPO	33 kDa	2	2	2	3	2	2	2	2
652	SCS7_SCHPO	40 kDa	2	2	1	1	1	2	2	0
653	MUG89_SCHPO	45 kDa	2	2	1	2	0	2	1	2
654	LHS1_SCHPO	95 kDa	2	2	2	2	2	2	2	2
655	OST2_SCHPO	13 kDa	1	1	1	1	1	2	2	1
656	YG1G_SCHPO	63 kDa	1	2	2	2	1	1	2	1
657	CAT1_SCHPO [2]	64 kDa	1	2	2	3	0	2	1	1
658	ATPF_SCHPO	27 kDa	1	3	3	2	3	2	1	2
659	BMS1_SCHPO	128 kDa	1	2	2	2	3	1	3	0
660	EF1B_SCHPO	23 kDa	3	2	2	2	1	3	3	2
661	SYC_SCHPO	86 kDa	2	2	2	3	3	2	2	2
662	UGGG_SCHPO	165 kDa	1	1	0	3	2	1	2	2
663	UTP23_SCHPO	30 kDa	2	2	2	1	3	2	2	1
664	YF75_SCHPO	74 kDa	1	2	1	2	1	2	3	1
665	SYQ_SCHPO	92 kDa	2	2	2	2	3	0	2	0
666	YB79_SCHPO	25 kDa	2	1	2	2	1	2	2	1
667	SLY1_SCHPO	72 kDa	2	2	2	2	2	0	2	2
668	EKC1_SCHPO	95 kDa	1	1	1	2	1	1	1	0
669	PVG1_SCHPO	45 kDa	2	1	1	2	2	1	1	1
670	SPP42_SCHPO	275 kDa	1	1	2	2	1	2	2	2
671	STE24_SCHPO	54 kDa	2	1	2	1	1	2	2	0
672	YP52_SCHPO	26 kDa	1	1	1	1	1	1	1	1
673	ETP1_SCHPO	69 kDa	1	1	1	1	1	1	1	1
674	MSMO_SCHPO	36 kDa	1	1	0	1	1	1	1	0
675	ERG28_SCHPO	15 kDa	1	1	1	1	1	1	1	1
676	ART1A_SCHPO	50 kDa	2	3	2	2	1	2	2	1
677	LTN1_SCHPO	184 kDa	3	2	3	3	0	2	1	2
678	MUG70_SCHPO	79 kDa	1	1	2	3	1	2	3	2
679	PPE1_SCHPO	35 kDa	1	2	2	3	2	1	1	2
680	RHO4_SCHPO	22 kDa	2	2	2	3	2	2	2	2
681	YB35_SCHPO	148 kDa	2	2	3	1	1	2	2	1
682	YDT4_SCHPO	48 kDa	2	2	2	3	3	1	1	0
683	YE04_SCHPO	66 kDa	0	1	4	0	2	2	3	2
684	YOFC_SCHPO	20 kDa	3	2	3	2	2	2	2	0
685	YPT3_SCHPO	24 kDa	3	2	0	4	0	4	0	1
686	YPT5_SCHPO	23 kDa	2	2	3	3	2	2	2	0
687	GSK3_SCHPO	44 kDa	2	0	2	1	1	1	2	0
688	YBI2_SCHPO	38 kDa	2	1	0	2	0	3	1	1
689	SDA1_SCHPO	81 kDa	2	2	2	2	1	0	1	0
690	YAO2_SCHPO	17 kDa	2	2	1	2	2	2	2	2

691	HPRT_SCHPO	24 kDa	2	0	1	2	2	1	2	0
692	VIPI_SCHPO	27 kDa	2	2	2	1	2	2	2	2
693	YEK9_SCHPO	98 kDa	1	1	2	2	1	1	2	1
694	NAA25_SCHPO	92 kDa	1	2	2	2	1	1	1	1
695	PTH2_SCHPO	21 kDa	2	2	2	2	2	1	1	0
696	YAOI_SCHPO	55 kDa	2	1	2	2	1	1	1	1
697	YEZB_SCHPO	37 kDa	1	1	1	1	1	1	1	2
698	SYP1_SCHPO	91 kDa	2	2	2	2	0	2	2	1
699	UTP22_SCHPO	126 kDa	2	0	2	2	2	2	2	2
700	BGS3_SCHPO	211 kDa	1	2	2	3	2	1	1	0
701	DPNP_SCHPO	39 kDa	3	2	2	2	2	2	3	0
702	MET7_SCHPO	69 kDa	2	1	1	3	1	2	2	2
703	PKD2_SCHPO	80 kDa	0	3	3	2	2	0	2	1
704	POB3_SCHPO	57 kDa	2	2	2	3	1	2	1	0
705	RPN6_SCHPO	47 kDa	2	1	2	3	1	2	2	1
706	SPEB2_SCHPO	46 kDa	3	1	1	2	3	3	1	1
707	TREA_SCHPO	85 kDa	2	2	2	3	0	0	0	1
708	VAC8_SCHPO	60 kDa	2	2	3	3	2	1	1	1
709	YBA9_SCHPO	21 kDa	1	1	2	2	2	3	2	0
710	YJQ1_SCHPO	93 kDa	3	1	3	1	2	2	2	1
711	YPT7_SCHPO	23 kDa	2	2	1	3	2	3	1	2
712	EFR3_SCHPO	90 kDa	2	0	1	3	0	2	2	0
713	NMD3_SCHPO	57 kDa	1	2	3	2	2	2	1	0
714	SUCA_SCHPO	35 kDa	2	2	1	1	0	3	1	0
715	SLT1_SCHPO	49 kDa	2	1	3	2	2	3	1	1
716	VPS74_SCHPO	38 kDa	3	2	3	3	1	1	2	0
717	TAF5_SCHPO	72 kDa	2	2	2	2	2	1	2	2
718	ODC_SCHPO	33 kDa	2	2	1	2	1	1	1	0
719	PSB6_SCHPO	25 kDa	2	2	2	2	2	2	2	2
720	SEC65_SCHPO	24 kDa	2	2	2	2	2	2	2	2
721	YAKC_SCHPO	38 kDa	1	1	0	1	1	1	1	1
722	COPE_SCHPO	32 kDa	2	1	1	4	0	2	1	0
723	FES1_SCHPO	33 kDa	0	0	2	1	3	1	1	2
724	HIS7_SCHPO	24 kDa	2	1	2	2	2	2	3	1
725	NMT_SCHPO	54 kDa	1	1	1	3	1	1	0	0
726	NUP82_SCHPO	91 kDa	2	3	2	1	1	1	2	1
727	SUMT_SCHPO	55 kDa	2	2	2	1	2	1	3	2
728	UGE1_SCHPO	39 kDa	2	2	2	2	3	1	2	0
729	VIP1_SCHPO	106 kDa	3	1	1	2	1	0	1	0
730	YHLA_SCHPO	121 kDa	1	1	2	3	0	2	2	2
731	YJD1_SCHPO	89 kDa	0	3	2	2	0	2	1	3

732	ZUO1_SCHPO	50 kDa	2	0	2	3	1	3	3	1
733	FKBP4_SCHPO	39 kDa	3	1	2	1	1	2	2	1
734	TPP2_SCHPO	143 kDa	2	1	2	3	0	1	2	2
735	RAS_SCHPO	25 kDa	2	2	2	1	3	2	2	1
736	YCKF_SCHPO	56 kDa	1	2	3	2	0	1	1	2
737	YOH7_SCHPO	31 kDa	0	2	2	3	2	0	2	2
738	PLPL_SCHPO	73 kDa	0	2	2	1	1	0	1	0
739	UCRI_SCHPO	25 kDa	1	1	3	2	1	2	2	1
740	UTP7_SCHPO	60 kDa	1	1	1	1	2	2	1	2
741	ERO11_SCHPO	55 kDa	2	1	1	2	1	2	1	1
742	YOCE_SCHPO	77 kDa	1	2	2	1	2	1	1	1
743	RS10B_SCHPO	16 kDa	1	1	0	2	1	2	2	0
744	PCNA_SCHPO	29 kDa	1	2	1	1	1	2	1	1
745	IMA2_SCHPO	60 kDa	2	2	2	2	1	2	1	1
746	RFA1_SCHPO	68 kDa	1	1	2	1	2	2	2	1
747	RPN9_SCHPO	43 kDa	2	2	2	2	1	2	2	2
748	YFFL_SCHPO	24 kDa	2	2	2	2	2	1	2	1
749	SNU13_SCHPO	14 kDa	1	1	1	1	1	2	1	0
750	GPI7_SCHPO	86 kDa	1	1	1	1	1	1	1	0
751	ILV6_SCHPO	32 kDa	1	1	1	1	1	1	1	1
752	RL34A_SCHPO	13 kDa	0	0	1	0	1	0	1	0
753	RS29_SCHPO	7 kDa	1	1	1	1	1	1	1	1
754	SODC_SCHPO	16 kDa	1	1	1	1	1	1	1	1
755	CLC1_SCHPO	26 kDa	1	2	4	4	1	1	1	0
756	EI2BD_SCHPO	52 kDa	3	1	1	1	1	2	0	0
757	I3ACR_SCHPO	32 kDa	3	1	2	2	2	1	2	0
758	IF6_SCHPO	26 kDa	2	1	1	1	1	3	3	1
759	PTR1_SCHPO	365 kDa	1	3	3	5	1	0	0	0
760	UBP21_SCHPO	131 kDa	2	1	1	4	0	2	1	0
761	YQ75_SCHPO	20 kDa	1	3	2	1	1	1	2	3
762	NDC1_SCHPO	69 kDa	1	2	3	2	0	0	1	0
763	PSA3_SCHPO	28 kDa	2	2	2	3	0	2	0	0
764	RIR2_SCHPO	45 kDa	2	1	2	1	3	1	2	1
765	RNG2_SCHPO	172 kDa	2	2	2	3	1	1	1	2
766	PNPH_SCHPO	34 kDa	0	1	1	1	2	3	3	1
767	OST3_SCHPO	35 kDa	2	2	3	2	0	2	2	0
768	ERG7_SCHPO	83 kDa	0	2	1	1	2	0	1	0
769	INO80_SCHPO	183 kDa	1	2	1	2	1	2	2	2
770	RL1DB_SCHPO	41 kDa	2	2	2	2	2	1	0	0
771	NOP12_SCHPO	49 kDa	1	1	1	1	1	1	1	2

772	YGX1_SCHPO	43 kDa	2	0	2	2	0	1	0	0
773	TIM21_SCHPO	26 kDa	0	1	2	2	1	1	1	1
774	RPA2_SCHPO	132 kDa	1	2	2	0	2	1	2	1
775	MLO3_SCHPO	22 kDa	1	2	1	1	1	2	2	1
776	OXA11_SCHPO	42 kDa	2	2	1	2	1	1	2	1
777	ARX1_SCHPO	46 kDa	1	1	2	1	1	2	1	0
778	EI2BB_SCHPO	43 kDa	2	1	2	2	1	1	2	1
779	HEM3_SCHPO	37 kDa	2	2	2	1	2	1	2	1
780	KPR1_SCHPO	45 kDa	2	2	2	2	2	1	2	1
781	PYRE_SCHPO	24 kDa	2	1	2	1	1	2	2	1
782	PYRG_SCHPO	67 kDa	2	1	2	2	1	2	1	1
783	YAJB_SCHPO	51 kDa	1	1	1	2	1	1	1	0
784	YKM8_SCHPO	39 kDa	2	2	1	1	2	2	2	1
785	ALO_SCHPO	52 kDa	1	1	1	2	1	1	1	2
786	TIM50_SCHPO	53 kDa	1	2	1	2	0	1	0	0
787	BSU1_SCHPO	58 kDa	1	1	1	1	0	0	1	0
788	ARGJ_SCHPO	47 kDa	1	1	1	0	0	0	1	1
789	NCE2_SCHPO	20 kDa	1	1	1	1	1	1	1	1
790	YA38_SCHPO	10 kDa	1	1	1	1	1	1	1	1
791	VATL_SCHPO	16 kDa	1	1	1	1	1	1	1	0
792	FADH1_SCHPO	40 kDa	1	1	2	3	1	2	2	0
793	ODO1_SCHPO	114 kDa	1	2	1	3	1	1	0	0
794	SNF21_SCHPO	140 kDa	1	1	2	3	1	0	1	0
795	SRP72_SCHPO	63 kDa	1	3	0	2	0	2	2	1
796	TYSY_SCHPO	70 kDa	2	2	2	3	1	0	1	0
797	YG03_SCHPO	37 kDa	0	2	3	2	2	2	1	1
798	YGQ3_SCHPO	75 kDa	2	0	3	2	2	0	2	1
799	OAC1_SCHPO	36 kDa	1	2	3	3	2	1	0	0
800	SKB1_SCHPO	73 kDa	1	2	1	3	0	0	2	2
801	CIP2_SCHPO	62 kDa	2	2	2	3	1	0	1	1
802	YB1C_SCHPO	103 kDa	1	2	2	0	1	2	2	0
803	RPE_SCHPO	25 kDa	1	1	2	2	1	2	1	2
804	6PGL_SCHPO	28 kDa	1	1	2	1	2	1	2	1
805	DOP1_SCHPO	193 kDa	2	2	1	2	2	1	2	1
806	KIN1_SCHPO	99 kDa	2	2	1	1	2	1	1	0
807	MTNA_SCHPO	39 kDa	2	2	2	2	2	0	1	2
808	NOT3_SCHPO	73 kDa	1	0	1	2	0	0	2	0
809	QOR_SCHPO	35 kDa	1	2	1	2	1	2	1	1
810	SEC8_SCHPO	123 kDa	1	1	1	2	1	1	2	2
811	YFY7_SCHPO	40 kDa	2	2	2	1	1	2	1	1

812	YNF5_SCHPO	46 kDa	2	2	1	1	2	2	1	2
813	YQ53_SCHPO	33 kDa	2	1	2	2	2	1	2	1
814	MAK3_SCHPO	267 kDa	0	2	2	1	1	2	1	2
815	RS26A_SCHPO	14 kDa	1	1	2	2	2	2	1	1
816	TAF6_SCHPO	50 kDa	2	2	2	1	0	0	2	0
817	DCA13_SCHPO	50 kDa	1	1	1	0	0	2	1	1
818	QCR8_SCHPO	10 kDa	1	1	1	1	1	1	1	0
819	UBP3_SCHPO	58 kDa	0	0	0	1	0	0	0	0
820	NDK_SCHPO	17 kDa	1	1	1	1	1	1	1	1
821	YEAH_SCHPO	46 kDa	1	1	2	4	1	1	1	0
822	GLU2A_SCHPO	106 kDa	2	1	0	1	0	3	1	1
823	MU157_SCHPO	57 kDa	1	2	2	3	1	1	2	0
824	TYW1_SCHPO	78 kDa	3	1	1	2	2	0	1	1
825	YIE2_SCHPO	46 kDa	1	1	1	1	2	1	1	2
826	GET1_SCHPO	20 kDa	1	1	2	1	1	1	1	2
827	YIFC_SCHPO	110 kDa	1	2	1	1	2	0	1	1
828	YAEC_SCHPO	62 kDa	1	1	0	1	2	2	1	1
829	COQ5_SCHPO	34 kDa	1	1	1	2	1	2	2	1
830	COX5_SCHPO	21 kDa	2	1	2	2	1	1	1	2
831	EI2BE_SCHPO	76 kDa	2	0	0	1	1	2	2	1
832	PP2A2_SCHPO	36 kDa	1	1	1	2	1	1	1	1
833	RT35_SCHPO	36 kDa	2	2	2	1	1	2	2	0
834	SEC1_SCHPO	80 kDa	2	1	1	2	1	2	1	0
835	VPS35_SCHPO	96 kDa	1	2	1	2	2	2	1	1
836	XRN1_SCHPO	153 kDa	2	1	1	2	1	1	1	1
837	YB1D_SCHPO	81 kDa	1	2	1	1	1	2	1	1
838	SPC3_SCHPO	22 kDa	2	1	2	2	2	1	1	0
839	SPO14_SCHPO	45 kDa	1	0	0	1	0	1	1	0
840	YLX4_SCHPO	13 kDa	0	1	1	0	1	1	1	1
841	DNJC7_SCHPO	53 kDa	1	1	1	1	1	1	1	0
842	COG3_SCHPO	86 kDa	1	1	1	0	1	0	1	0
843	YDQ4_SCHPO	50 kDa	1	1	1	1	1	1	1	1
844	DPP1_SCHPO	31 kDa	1	0	1	1	1	0	1	0
845	YEAF_SCHPO	24 kDa	1	1	1	1	0	1	1	0
846	BRO1_SCHPO	87 kDa	1	2	2	2	0	0	3	1
847	ETFB_SCHPO	28 kDa	1	0	0	3	1	3	2	0
848	TRPD_SCHPO	38 kDa	2	1	2	3	2	1	0	0
849	PPID_SCHPO	40 kDa	1	2	1	1	1	2	3	0
850	NU184_SCHPO	177 kDa	1	1	1	3	1	1	1	1
851	PXR1_SCHPO	32 kDa	1	2	2	0	2	0	1	1

852	YE07_SCHPO	13 kDa	0	2	1	1	1	2	2	0
853	PCP1_SCHPO	141 kDa	0	1	2	0	0	2	2	1
854	RFC1_SCHPO	103 kDa	0	1	2	0	0	0	1	1
855	ARP9_SCHPO	59 kDa	1	1	1	1	1	1	2	1
856	COMT1_SCHPO	30 kDa	2	1	1	2	1	1	1	1
857	ELP3_SCHPO	62 kDa	1	2	1	2	0	1	2	2
858	GDI1_SCHPO	50 kDa	2	1	1	2	0	2	2	0
859	HEM2_SCHPO	36 kDa	2	1	1	2	2	0	1	0
860	KCY_SCHPO	22 kDa	2	2	1	1	1	1	2	1
861	NOP9_SCHPO	75 kDa	1	1	1	1	1	2	2	1
862	PAP_SCHPO	64 kDa	2	1	2	2	1	1	0	1
863	PPC89_SCHPO	89 kDa	1	2	2	1	1	0	2	2
864	PSB5_SCHPO	30 kDa	2	1	1	1	1	1	2	2
865	SYWC_SCHPO	45 kDa	2	1	2	1	0	1	2	1
866	YGR4_SCHPO	27 kDa	1	1	1	2	1	2	2	1
867	YHD3_SCHPO	57 kDa	1	1	1	2	1	0	1	0
868	YBQ2_SCHPO	52 kDa	1	2	2	1	0	0	0	0
869	SVP26_SCHPO	26 kDa	1	2	1	1	0	1	1	1
870	YHC3_SCHPO	73 kDa	0	1	1	0	0	1	1	2
871	RCF2_SCHPO	27 kDa	0	2	1	2	0	0	0	2
872	AGM1_SCHPO	56 kDa	1	0	1	2	1	1	1	1
873	PGM3_SCHPO	65 kDa	1	1	1	1	1	1	1	1
874	MCD4_SCHPO	106 kDa	1	1	1	1	1	1	1	1
875	YQK7_SCHPO	171 kDa	1	0	0	1	0	1	0	0
876	PTF1_SCHPO	26 kDa	1	1	1	1	1	1	1	0
877	DSD1_SCHPO	46 kDa	2	0	0	3	0	1	1	0
878	YNZ6_SCHPO	40 kDa	0	2	3	2	0	0	0	0
879	MDJ1_SCHPO	57 kDa	2	0	0	1	0	2	2	0
880	COFI_SCHPO	16 kDa	1	0	0	2	0	2	1	0
881	RPA49_SCHPO	48 kDa	1	0	0	1	2	1	2	1
882	RL30B_SCHPO	12 kDa	2	1	1	2	1	2	1	0
883	ADH4_SCHPO	46 kDa	1	2	2	0	1	1	0	0
884	ALF1_SCHPO	72 kDa	1	1	1	2	1	1	1	1
885	ARPC2_SCHPO	37 kDa	1	2	1	2	0	2	0	0
886	ARPC4_SCHPO	20 kDa	1	1	1	2	2	1	1	0
887	CSX2_SCHPO	99 kDa	2	1	2	0	2	2	1	0
888	DPOD_SCHPO	124 kDa	1	1	1	0	1	1	1	2
889	ECM29_SCHPO	191 kDa	1	1	2	1	1	1	1	1
890	GTP1_SCHPO	41 kDa	2	1	1	2	1	1	1	1
891	MTD1_SCHPO	36 kDa	2	0	1	1	1	2	1	1

892	MUG64_SCHPO	32 kDa	2	2	2	1	0	1	0	1
893	NP106_SCHPO	106 kDa	1	2	1	1	2	1	1	1
894	PPT1_SCHPO	53 kDa	2	1	1	1	1	2	1	1
895	PSA4_SCHPO	28 kDa	1	0	2	2	0	1	1	0
896	PUB1_SCHPO	87 kDa	2	1	1	1	1	1	1	0
897	SEC15_SCHPO	89 kDa	1	1	2	2	1	1	1	1
898	YEG5_SCHPO	128 kDa	0	0	1	0	1	1	1	2
899	YOC5_SCHPO	43 kDa	2	2	1	2	2	0	0	0
900	YCPF_SCHPO	77 kDa	2	1	1	1	0	1	1	0
901	TCG1_SCHPO	38 kDa	2	1	1	0	0	1	1	1
902	YI26_SCHPO	64 kDa	2	0	1	2	0	0	1	0
903	SPN2_SCHPO	38 kDa	0	0	0	2	0	2	0	0
904	TIM17_SCHPO	17 kDa	0	2	2	0	1	0	0	0
905	SEC63_SCHPO	70 kDa	1	2	1	1	1	1	1	1
906	YCL3_SCHPO	54 kDa	2	1	1	0	0	0	1	0
907	IF4E1_SCHPO	25 kDa	1	1	1	0	1	1	1	1
908	CBP3_SCHPO	33 kDa	1	1	1	1	1	1	1	1
909	PSA2_SCHPO	26 kDa	1	0	1	0	1	1	1	1
910	RRP6_SCHPO	90 kDa	1	0	0	1	0	1	1	1
911	ODO2_SCHPO	49 kDa	0	1	1	0	0	1	0	0
912	YG64_SCHPO	60 kDa	1	1	1	1	1	1	1	1
913	SIF1_SCHPO	29 kDa	1	1	1	1	1	1	1	1
914	GPX1_SCHPO	18 kDa	1	1	1	1	1	1	1	0
915	DNPEP_SCHPO	52 kDa	1	1	1	0	1	1	1	0
916	TBG_SCHPO	50 kDa	1	1	0	3	0	1	2	1
917	SMC1_SCHPO	141 kDa	0	1	3	0	0	0	1	1
918	MSP1_SCHPO	102 kDa	0	1	1	2	0	1	3	0
919	XPO1_SCHPO	124 kDa	2	2	2	2	0	0	0	0
920	ALG9_SCHPO	66 kDa	2	1	1	1	1	1	1	1
921	DBP6_SCHPO	68 kDa	1	2	1	1	1	0	2	0
922	ENG1_SCHPO	110 kDa	1	2	1	1	1	1	1	1
923	ERG27_SCHPO	39 kDa	1	1	1	1	2	1	1	0
924	ETT1_SCHPO	44 kDa	1	0	1	1	1	1	2	0
925	GNTK_SCHPO	22 kDa	2	1	0	1	1	1	1	1
926	KAD2_SCHPO	24 kDa	2	1	1	2	1	0	2	0
927	MET8_SCHPO	29 kDa	1	0	2	2	1	0	0	0
928	MYO52_SCHPO	175 kDa	1	0	2	1	1	0	1	1
929	NOL10_SCHPO	72 kDa	1	2	1	0	1	1	1	1
930	NOP2_SCHPO	69 kDa	1	2	1	1	1	1	1	0

931	NU146_SCHPO	146 kDa	1	2	2	1	0	1	1	0
932	PHO88_SCHPO	22 kDa	1	1	0	1	0	2	1	2
933	RCC1_SCHPO	58 kDa	1	1	1	1	2	1	1	1
934	SEC14_SCHPO	33 kDa	2	1	1	2	0	1	1	1
935	SMC2_SCHPO	134 kDa	1	1	2	1	2	1	1	0
936	YE38_SCHPO	119 kDa	1	1	1	0	1	1	2	1
937	YKGC_SCHPO	42 kDa	1	0	1	2	0	1	1	0
938	YOOH_SCHPO	69 kDa	0	1	1	0	2	1	1	2
939	YGRG_SCHPO	30 kDa	0	1	2	0	2	1	2	1
940	MSRA_SCHPO	19 kDa	1	1	1	0	2	1	1	0
941	YBH4_SCHPO	97 kDa	2	0	0	0	0	0	2	0
942	MPC1_SCHPO	16 kDa	0	0	0	2	0	2	0	0
943	TRPE_SCHPO	55 kDa	1	0	0	2	0	1	0	0
944	YCVC_SCHPO	27 kDa	0	0	0	0	0	0	0	2
945	SKI2_SCHPO	138 kDa	0	1	1	0	1	0	1	0
946	YG0C_SCHPO	93 kDa	1	1	1	1	0	2	1	0
947	TPP1_SCHPO	94 kDa	1	1	1	1	0	1	1	1
948	RGA6_SCHPO	81 kDa	0	1	1	1	1	1	1	0
949	YIDE_SCHPO	27 kDa	1	1	1	1	0	1	0	0
950	MTAP_SCHPO	34 kDa	1	1	0	0	1	1	0	0
951	CSX1_SCHPO	68 kDa	0	1	1	1	1	0	1	0
952	CSK2A_SCHPO	40 kDa	1	1	1	1	1	1	1	1
953	IMB1_SCHPO	95 kDa	0	0	1	1	1	0	0	0
954	CSE1_SCHPO	109 kDa	0	0	0	0	1	0	0	1
955	KLP2_SCHPO	91 kDa	1	1	1	1	1	1	1	1
956	GSH0_SCHPO	33 kDa	1	1	0	0	1	1	1	1
957	YIP4_SCHPO	25 kDa	1	1	1	1	1	1	1	1
958	YOP1_SCHPO	21 kDa	1	1	1	1	1	1	1	1
959	SLM1_SCHPO	56 kDa	1	1	1	1	1	1	1	1
960	YLM1_SCHPO	94 kDa	1	1	1	1	0	1	1	1
961	ACL4_SCHPO	38 kDa	1	1	1	1	1	1	1	1
962	SC61B_SCHPO	10 kDa	0	1	1	1	1	1	1	1
963	YOSC_SCHPO	14 kDa	1	1	1	1	1	1	1	1
964	RLA6_SCHPO	11 kDa	0	0	0	2	0	3	2	0
964.1	RLA6_SCHPO	11 kDa	0	0	0	1	0	1	1	0
964.2	RLA2_SCHPO	11 kDa	0	0	0	0	0	1	0	0
965	EI2BA_SCHPO	38 kDa	1	1	0	3	0	1	0	0
966	TOP2_SCHPO	168 kDa	0	2	0	2	0	1	1	0
967	OFD1_SCHPO	59 kDa	1	0	1	0	0	2	0	1
968	GLO3_SCHPO	53 kDa	0	1	1	0	2	0	0	0

969	PAT1_SCHPO	84 kDa	2	0	0	2	0	2	1	0
970	STS5_SCHPO	118 kDa	1	0	0	1	0	2	0	0
971	YGV7_SCHPO	45 kDa	2	0	0	0	0	1	1	1
972	2AD1_SCHPO	63 kDa	1	1	1	2	0	1	1	0
973	ASH2_SCHPO	74 kDa	1	1	2	1	0	2	1	0
974	ATU2_SCHPO	98 kDa	1	2	2	0	0	1	1	1
975	CBL_SCHPO	43 kDa	2	0	2	2	1	1	0	0
976	CYB51_SCHPO	14 kDa	1	0	0	1	0	2	1	1
977	GST3_SCHPO	28 kDa	1	1	0	1	1	2	0	0
978	HAS1_SCHPO	65 kDa	0	0	1	0	2	1	1	2
979	HIS4_SCHPO	29 kDa	1	1	1	0	1	0	1	2
980	IF2B_SCHPO	36 kDa	1	1	1	2	1	1	1	0
981	MUG58_SCHPO	32 kDa	2	1	1	1	0	1	1	0
982	NACA_SCHPO	19 kDa	2	0	1	2	0	2	1	0
983	NOT2_SCHPO	34 kDa	1	1	1	2	1	1	1	0
984	PROA_SCHPO	49 kDa	0	0	0	1	0	2	1	2
985	RPAB1_SCHPO	24 kDa	1	1	1	1	2	0	0	1
986	SEC16_SCHPO	218 kDa	1	1	1	1	0	1	1	2
987	SYB1_SCHPO	13 kDa	1	1	1	0	2	1	0	2
988	YBEG_SCHPO	57 kDa	1	2	1	0	2	1	0	1
989	YEW3_SCHPO	27 kDa	1	0	0	2	0	2	1	1
990	YL44_SCHPO	55 kDa	2	1	0	1	1	1	1	1
991	YOD1_SCHPO	51 kDa	1	1	2	0	1	1	0	0
992	YQE2_SCHPO	25 kDa	1	1	1	2	1	1	1	0
993	YEH1_SCHPO	107 kDa	0	0	0	1	0	2	0	2
994	MMS2_SCHPO	16 kDa	1	1	1	0	0	2	2	0
995	CATA_SCHPO	58 kDa	2	1	1	1	1	1	0	1
996	LAC1_SCHPO	45 kDa	1	1	1	2	0	0	2	0
997	PESC_SCHPO	69 kDa	0	1	1	2	0	0	1	0
998	KES1_SCHPO	45 kDa	1	0	0	2	0	1	1	0
999	AFG2_SCHPO	88 kDa	0	1	1	0	1	0	2	1
1000	SNX41_SCHPO	67 kDa	0	2	1	1	0	1	1	0
1001	YEE2_SCHPO	141 kDa	0	2	0	1	0	0	1	1
1002	SSR1_SCHPO	60 kDa	1	1	1	2	0	0	1	0
1003	TSC2_SCHPO	155 kDa	0	1	1	1	0	1	1	0
1004	TXL1_SCHPO	32 kDa	1	1	1	0	1	1	1	1
1005	AAKG_SCHPO	37 kDa	1	1	1	1	1	1	1	0
1006	MUG33_SCHPO	37 kDa	1	1	1	0	1	1	0	1
1007	PPK14_SCHPO	63 kDa	1	1	1	1	0	1	1	1
1008	RM01_SCHPO	28 kDa	1	1	0	1	1	1	1	1

1009	RFC4_SCHPO	38 kDa	0	0	1	0	0	0	0	0
1010	RRP3_SCHPO	52 kDa	1	1	1	1	1	1	1	0
1011	YCTB_SCHPO	52 kDa	1	1	1	1	0	1	1	1
1012	PWP2_SCHPO	95 kDa	1	1	1	1	1	0	1	1
1013	GUAD_SCHPO	58 kDa	0	0	1	1	0	1	1	1
1014	KAPS_SCHPO	23 kDa	1	1	0	1	0	1	1	0
1015	ARD1_SCHPO	20 kDa	1	1	0	1	0	1	1	0
1016	RNA14_SCHPO	84 kDa	1	1	1	1	1	1	1	0
1017	VATE_SCHPO	26 kDa	0	0	1	1	0	0	1	0
1018	IMB2_SCHPO	102 kDa	1	1	1	1	1	1	1	1
1019	CCHL_SCHPO	43 kDa	1	1	1	1	1	1	1	1
1020	DS1PP_SCHPO	47 kDa	1	1	1	0	1	1	1	1
1021	EFGM_SCHPO	86 kDa	1	1	1	1	1	1	1	1
1022	ETFA_SCHPO	36 kDa	1	1	1	1	1	1	1	1
1023	GLO21_SCHPO	28 kDa	1	1	1	1	1	1	1	1
1024	IES2_SCHPO	34 kDa	1	1	1	1	1	1	1	1
1025	IMB5_SCHPO	112 kDa	1	1	1	1	1	1	1	1
1026	MCM2_SCHPO	93 kDa	1	1	1	1	1	1	1	1
1027	MCM6_SCHPO	100 kDa	1	1	1	1	1	1	1	1
1028	MTC1_SCHPO	51 kDa	1	1	1	1	1	1	1	1
1029	NBP35_SCHPO	34 kDa	1	1	1	0	1	1	1	1
1030	PDT1_SCHPO	58 kDa	1	1	1	1	1	1	1	1
1031	PMP31_SCHPO	12 kDa	1	1	1	1	1	1	1	1
1032	PP2C5_SCHPO	50 kDa	1	0	1	1	1	1	1	1
1033	PPX1_SCHPO	43 kDa	1	1	1	1	1	1	1	1
1034	PSB7_SCHPO	29 kDa	1	1	1	1	1	1	1	1
1035	RIB3_SCHPO	23 kDa	1	1	1	1	1	1	1	1
1036	RL1DA_SCHPO	32 kDa	1	1	1	1	1	1	1	1
1037	SC61G_SCHPO	8 kDa	1	1	1	1	1	1	1	1
1038	SED5_SCHPO	35 kDa	1	1	1	1	1	1	1	1
1039	SID2_SCHPO	70 kDa	1	1	1	1	1	1	1	1
1040	TAF10_SCHPO	24 kDa	1	1	1	1	0	1	1	1
1041	TAM14_SCHPO	8 kDa	1	1	1	0	1	0	1	1
1042	TIM23_SCHPO	23 kDa	1	1	1	1	1	0	0	1
1043	UBLH2_SCHPO	34 kDa	1	1	1	1	1	1	1	1
1044	XPOT_SCHPO	110 kDa	1	1	1	1	1	1	1	1
1045	YBB9_SCHPO	51 kDa	1	1	1	1	1	1	1	1
1046	YCV6_SCHPO	34 kDa	1	1	0	1	1	1	1	1
1047	YGW2_SCHPO	19 kDa	1	1	1	1	1	1	1	1
1048	YHZ7_SCHPO	47 kDa	1	1	1	1	1	1	1	1
1049	YLF8_SCHPO	53 kDa	1	1	1	1	1	1	1	1

1050	YNV5_SCHPO	42 kDa	1	1	1	1	1	1	1	1
1051	BEM46_SCHPO	33 kDa	0	1	1	1	1	0	1	0
1052	MET2_SCHPO	54 kDa	1	1	1	1	1	1	1	0
1053	QCR10_SCHPO	9 kDa	1	1	1	1	1	1	1	0
1054	UCP8_SCHPO	91 kDa	0	1	1	1	1	1	1	1
1055	YN8C_SCHPO	23 kDa	1	1	1	1	1	1	1	0
1056	YFHH_SCHPO	171 kDa	1	1	1	1	1	1	1	1
1057	KRI1_SCHPO	70 kDa	0	0	0	0	1	0	3	2
1058	ALG1_SCHPO	49 kDa	1	0	0	1	0	2	1	0
1059	BPL1_SCHPO	71 kDa	0	1	1	2	0	0	1	0
1060	MUG87_SCHPO	98 kDa	1	1	1	1	0	0	2	0
1061	RFC3_SCHPO	38 kDa	0	1	0	2	0	0	2	0
1062	SCD1_SCHPO	99 kDa	2	1	1	1	1	0	1	0
1063	SUCB_SCHPO	47 kDa	0	0	1	0	0	1	0	2
1064	YETC_SCHPO	33 kDa	2	0	2	1	1	0	0	0
1065	YOOC_SCHPO	142 kDa	2	0	0	0	0	0	0	0
1066	ARP4_SCHPO	49 kDa	0	1	1	0	1	1	0	2
1067	YHOF_SCHPO	44 kDa	2	0	0	1	0	0	1	0
1068	MDM28_SCHPO	56 kDa	2	0	0	0	0	0	0	0
1069	YDZ4_SCHPO	30 kDa	2	0	0	0	1	1	1	0
1070	YME2_SCHPO	88 kDa	1	0	1	1	1	0	2	0
1071	YHJ2_SCHPO	62 kDa	1	1	0	0	2	0	1	0
1072	RPN8_SCHPO	36 kDa	1	1	1	1	0	1	2	0
1073	YAS2_SCHPO	51 kDa	1	0	1	1	0	0	1	0
1074	GFA1_SCHPO	77 kDa	1	0	0	1	0	1	1	0
1075	YG1A_SCHPO	22 kDa	0	0	0	0	0	0	1	0
1076	HAL4_SCHPO	69 kDa	1	1	1	0	1	0	0	1
1077	RPC1_SCHPO	158 kDa	1	1	0	0	1	0	0	0
1078	MYO2_SCHPO	176 kDa	1	1	1	1	0	1	1	0
1079	DBP10_SCHPO	95 kDa	0	0	0	0	0	0	1	0
1080	IWS1_SCHPO	49 kDa	0	0	0	1	0	1	0	1
1081	RM19_SCHPO	15 kDa	1	0	1	1	1	1	1	0
1082	SPT6_SCHPO	157 kDa	1	1	1	0	0	1	1	1
1083	YC12_SCHPO	26 kDa	1	1	1	0	1	1	1	1
1084	FT105_SCHPO	105 kDa	0	1	0	1	1	1	1	1
1085	PLB6_SCHPO	71 kDa	0	1	1	0	1	0	0	0
1086	DPH2_SCHPO	56 kDa	0	1	0	0	0	1	0	1
1087	YG1D_SCHPO	32 kDa	1	1	1	1	0	1	1	0
1088	FHP_SCHPO	48 kDa	1	1	1	0	1	1	1	0
1089	O00091-DECOY	?	0	0	0	0	0	0	0	1

1090	SIP1_SCHPO	218 kDa	0	0	1	0	0	0	0	0
1091	PUB3_SCHPO	89 kDa	0	0	0	0	0	0	0	0
1092	ELOH2_SCHPO	42 kDa	0	1	1	1	1	0	1	1
1093	EXG3_SCHPO	54 kDa	1	0	0	1	0	1	1	1
1094	GMS1_SCHPO	39 kDa	0	1	1	1	0	1	1	1
1095	HHP1_SCHPO	42 kDa	1	1	1	1	1	0	1	1
1096	HSP78_SCHPO	90 kDa	1	1	0	1	0	1	1	1
1097	LAG1_SCHPO	46 kDa	1	1	1	1	0	1	1	1
1098	PROF_SCHPO	13 kDa	1	1	1	0	0	1	1	1
1099	RFT1_SCHPO	60 kDa	1	0	1	1	0	0	1	1
1100	SEC22_SCHPO	25 kDa	1	1	1	0	1	1	1	1
1101	SGD1_SCHPO	88 kDa	1	1	1	1	0	1	1	1
1102	SPG1_SCHPO	23 kDa	1	1	1	0	1	1	1	1
1103	STM1_SCHPO	31 kDa	1	0	1	1	1	1	1	1
1104	TIM16_SCHPO	14 kDa	1	1	1	0	1	0	0	1
1105	YAY1_SCHPO	45 kDa	1	0	0	0	0	1	1	1
1106	ATPN_SCHPO	14 kDa	1	1	1	1	1	1	1	0
1107	DGK1_SCHPO	24 kDa	1	1	1	1	1	1	1	0
1108	DNLI1_SCHPO	87 kDa	1	1	1	1	1	0	1	0
1109	OMH5_SCHPO	50 kDa	1	0	1	1	1	1	1	0
1110	TGTL_SCHPO	73 kDa	1	1	1	1	1	1	1	0
1111	VPS17_SCHPO	61 kDa	1	0	1	1	1	1	1	0
1112	YA14_SCHPO	28 kDa	0	1	1	1	0	1	1	1
1113	YGT9_SCHPO	44 kDa	1	1	1	1	1	1	1	0
1114	YIO2_SCHPO	41 kDa	1	1	1	1	1	1	1	0
1115	YJL1_SCHPO	27 kDa	1	1	1	1	1	1	1	0
1116	DPO5_SCHPO	110 kDa	1	1	1	1	1	1	1	0
1117	RT04_SCHPO	29 kDa	0	1	1	1	1	1	1	1
1118	SURF4_SCHPO	34 kDa	1	0	1	1	0	1	0	0
1119	AP3M_SCHPO	48 kDa	1	1	2	1	0	0	1	0
1120	C1TM_SCHPO	106 kDa	2	0	0	0	1	0	0	0
1121	CUE4_SCHPO	24 kDa	2	0	0	1	0	1	2	0
1122	MOT1_SCHPO	218 kDa	1	0	0	2	1	0	1	0
1123	SEC11_SCHPO	21 kDa	2	0	0	1	1	0	2	0
1124	TPSY_SCHPO	101 kDa	1	0	0	2	0	1	0	0
1125	YB7A_SCHPO	86 kDa	0	1	0	0	2	1	1	1
1126	YBN4_SCHPO	37 kDa	1	1	2	0	0	0	1	1
1127	YCKC_SCHPO	96 kDa	1	0	1	1	0	2	1	0
1128	YEE6_SCHPO	45 kDa	0	2	1	1	1	0	0	1
1129	YK66_SCHPO	69 kDa	2	0	1	0	0	1	0	0

1130	KHSE_SCHPO	37 kDa	1	1	0	1	2	1	0	0
1131	PANC_SCHPO	32 kDa	2	0	0	0	0	1	1	1
1132	YD85_SCHPO	57 kDa	0	0	2	2	0	0	1	0
1133	MAN1_SCHPO	122 kDa	0	0	1	2	0	0	0	0
1134	CHR4_SCHPO	70 kDa	2	0	0	1	0	0	1	2
1135	TRPG_SCHPO	83 kDa	1	0	1	0	2	0	0	1
1136	TAF12_SCHPO	49 kDa	1	2	0	1	0	0	1	0
1137	PMT4_SCHPO	90 kDa	0	2	1	1	1	0	0	1
1138	KJ45_SCHPO	86 kDa	0	1	0	2	1	0	1	0
1139	NU120_SCHPO	130 kDa	1	1	1	2	1	0	0	0
1140	VID27_SCHPO	92 kDa	0	0	1	1	0	1	0	0
1141	YBPC_SCHPO	83 kDa	1	0	0	0	0	1	1	0
1142	TMA20_SCHPO	20 kDa	1	1	0	1	0	0	1	0
1143	TUP12_SCHPO	66 kDa	1	1	1	1	1	0	0	0
1144	SN114_SCHPO	111 kDa	0	0	0	0	1	0	1	0
1145	CSS1_SCHPO	48 kDa	0	1	1	0	0	0	0	0
1146	HSE1_SCHPO	42 kDa	0	1	1	0	0	1	1	0
1147	VATH_SCHPO	51 kDa	1	0	0	1	0	0	1	0
1148	YF22_SCHPO	33 kDa	0	0	1	1	1	0	1	1
1149	YB89_SCHPO	84 kDa	1	1	1	1	0	0	1	0
1150	PAN1_SCHPO	193 kDa	0	0	1	0	0	0	1	0
1151	CYS2_SCHPO	56 kDa	0	1	1	1	1	0	0	0
1152	PSA7_SCHPO	28 kDa	0	0	0	1	0	0	0	0
1153	YAI8_SCHPO	44 kDa	0	1	1	0	1	0	1	1
1154	RPB1_SCHPO	194 kDa	1	1	0	1	0	1	1	1
1155	DHSD_SCHPO	18 kDa	1	1	1	1	1	0	0	1
1156	GMH3_SCHPO	38 kDa	0	1	1	0	1	1	1	1
1157	PP2C1_SCHPO	39 kDa	1	1	1	0	0	1	1	1
1158	VTC1_SCHPO	13 kDa	1	1	0	0	0	1	1	1
1159	YE54_SCHPO	31 kDa	0	1	1	0	1	1	1	1
1160	AP3B_SCHPO	84 kDa	0	1	1	1	1	1	1	0
1161	GPN3_SCHPO	32 kDa	1	1	1	0	0	1	1	0
1162	LGUL_SCHPO	34 kDa	1	1	1	1	1	1	0	0
1163	PP11_SCHPO	38 kDa	1	1	1	1	1	0	1	0
1164	RGF1_SCHPO	150 kDa	0	1	1	1	1	1	1	0
1165	TRM1_SCHPO	60 kDa	0	1	1	1	1	1	1	0
1166	TVP23_SCHPO	25 kDa	0	1	1	1	1	1	1	0
1167	UPPS_SCHPO	30 kDa	1	1	1	1	1	0	1	0
1168	VPS54_SCHPO	108 kDa	0	1	1	1	1	1	1	0

1169	YAG9_SCHPO	110 kDa	1	1	1	1	1	0	0	1
1170	YF8B_SCHPO	48 kDa	1	1	1	1	0	1	0	0
1171	ELP2_SCHPO	85 kDa	1	1	0	1	1	0	1	0
1172	PSB1_SCHPO	25 kDa	1	0	0	0	1	1	1	0
1173	YK01_SCHPO	36 kDa	0	1	0	1	0	1	1	0
1174	YL47_SCHPO	59 kDa	1	1	0	1	0	0	1	0
1175	PSU1_SCHPO	42 kDa	1	1	1	1	1	0	0	0
1176	IMP3_SCHPO	22 kDa	0	1	0	0	0	0	1	0
1177	YII1_SCHPO	90 kDa	2	0	2	0	0	0	0	0
1178	PPK21_SCHPO	63 kDa	0	1	0	2	0	0	0	0
1179	ELP1_SCHPO	142 kDa	0	0	0	0	0	2	0	1
1180	GIT7_SCHPO	43 kDa	1	0	0	0	0	1	2	0
1181	NADE_SCHPO	80 kDa	0	1	0	2	0	1	0	0
1182	RCQ1_SCHPO	75 kDa	2	0	0	2	0	0	1	0
1183	UTP20_SCHPO	285 kDa	2	0	1	0	0	0	0	1
1184	VPS4_SCHPO	48 kDa	0	0	1	2	0	0	1	0
1185	YB33_SCHPO	99 kDa	1	1	1	2	0	0	0	0
1186	YBE8_SCHPO	48 kDa	2	1	0	0	0	1	0	1
1187	WIS4_SCHPO	161 kDa	1	0	1	1	0	0	2	0
1188	YGNB_SCHPO	43 kDa	1	0	1	2	0	1	0	0
1189	FZO1_SCHPO	87 kDa	1	1	0	0	2	0	0	1
1190	NCBP1_SCHPO	90 kDa	0	1	0	0	0	0	2	1
1191	YB92_SCHPO	67 kDa	1	1	0	0	0	1	2	0
1192	RIB4_SCHPO	17 kDa	0	0	0	2	0	1	1	0
1193	YOM1_SCHPO	61 kDa	0	0	0	0	2	0	0	0
1194	DBP9_SCHPO	67 kDa	1	0	0	1	0	0	0	1
1195	PPK29_SCHPO	96 kDa	1	0	0	1	0	0	0	0
1196	HIBCH_SCHPO	48 kDa	1	0	0	1	0	1	1	0
1197	RIX1_SCHPO	92 kDa	0	0	0	1	0	1	0	0
1198	FAR11_SCHPO	95 kDa	0	0	0	1	1	0	0	0
1199	YKQC_SCHPO	19 kDa	0	1	1	0	0	0	0	1
1200	LKHA4_SCHPO	70 kDa	0	0	0	1	0	0	1	0
1201	ADRO_SCHPO	53 kDa	0	0	0	1	0	1	1	1
1202	YI14_SCHPO	99 kDa	0	1	1	1	1	0	0	0
1203	UCP12_SCHPO	150 kDa	0	1	1	1	0	0	0	0
1204	YAC5_SCHPO	45 kDa	0	1	1	0	1	0	1	0
1205	MAK5_SCHPO	73 kDa	1	0	0	0	0	0	1	1
1206	YDHE_SCHPO	73 kDa	0	0	1	1	0	1	0	0
1207	CHR2_SCHPO	58 kDa	0	1	0	1	0	1	1	0
1208	YQJ9_SCHPO	30 kDa	1	0	0	0	1	1	1	0

1209	YKY4_SCHPO	81 kDa	0	0	0	1	0	1	1	0
1210	GCH1_SCHPO	26 kDa	0	0	0	0	0	1	1	0
1211	YON1_SCHPO	113 kDa	1	0	1	1	0	0	1	0
1212	NU107_SCHPO	93 kDa	0	0	0	0	0	0	0	0
1213	COX6_SCHPO	16 kDa	0	1	1	0	0	1	1	1
1214	ETR1_SCHPO	41 kDa	0	1	1	0	0	0	0	1
1215	PTR2_SCHPO	69 kDa	1	1	1	0	1	0	0	1
1216	RGA4_SCHPO	104 kDa	0	1	1	0	0	0	1	1
1217	RM03_SCHPO	37 kDa	1	0	0	1	0	1	1	1
1218	RS30A_SCHPO (+1)	7 kDa	1	0	0	1	0	0	1	1
1219	SHY1_SCHPO	33 kDa	1	0	0	1	0	1	1	1
1220	SMD1_SCHPO	13 kDa	1	0	0	0	0	1	1	1
1221	SODM_SCHPO	24 kDa	0	1	1	1	1	0	0	1
1222	SPB1_SCHPO	91 kDa	1	1	1	0	0	0	1	1
1223	US108_SCHPO	36 kDa	1	1	1	0	1	0	0	1
1224	YE31_SCHPO	31 kDa	0	1	0	1	0	1	1	1
1225	YOSE_SCHPO	94 kDa	1	1	0	1	0	0	1	1
1226	SET2_SCHPO	91 kDa	1	0	1	1	0	0	1	1
1227	ALG3_SCHPO	47 kDa	1	1	1	1	0	0	1	0
1228	BPH1_SCHPO	296 kDa	1	1	1	1	0	0	1	0
1229	GGT2_SCHPO	68 kDa	1	1	1	1	1	0	0	0
1230	KEX1_SCHPO	58 kDa	1	1	1	1	0	1	0	0
1231	PAM17_SCHPO	24 kDa	1	1	1	0	0	1	1	0
1232	PANK_SCHPO	45 kDa	1	1	1	0	0	1	0	0
1233	Q10093-DECOY	?	0	0	1	0	1	0	1	0
1234	RS12A_SCHPO (+1)	16 kDa	0	0	1	0	0	1	1	0
1235	SRP2_SCHPO	43 kDa	1	0	1	1	0	1	1	0
1236	YGR1_SCHPO	41 kDa	1	0	1	1	1	1	0	0
1237	YHZ8_SCHPO	22 kDa	0	0	1	0	1	0	0	0
1238	YOUB_SCHPO	20 kDa	1	1	1	0	1	1	0	0
1239	DCUP_SCHPO	40 kDa	1	0	0	1	1	1	1	0
1240	MCP2L_SCHPO	64 kDa	1	0	0	0	1	0	1	1
1241	RPN7_SCHPO	47 kDa	0	0	0	1	0	1	1	0
1242	SPT5_SCHPO	109 kDa	1	0	0	1	1	1	1	0
1243	SREBP_SCHPO	98 kDa	1	0	0	0	1	1	1	0
1244	UTP13_SCHPO	86 kDa	0	0	0	0	1	0	1	0
1245	YCN8_SCHPO	57 kDa	0	0	0	0	1	1	1	0
1246	SVF2_SCHPO	40 kDa	1	0	0	0	0	1	0	1
1247	FOLE_SCHPO	56 kDa	1	0	0	0	0	0	0	0
1248	YE16_SCHPO	32 kDa	1	1	1	1	0	0	0	0

1249	VATD_SCHPO	32 kDa	0	0	0	1	0	0	0	0
1250	YNSG_SCHPO	118 kDa	0	0	0	1	0	0	0	0
1251	O14352-DECOY	?	0	0	0	1	1	1	0	0
1252	CUL3_SCHPO	91 kDa	0	0	2	2	0	0	0	0
1253	FAT1_SCHPO	154 kDa	0	0	1	1	0	0	2	0
1254	TRNL_SCHPO	90 kDa	0	0	1	2	0	0	0	0
1255	ATG11_SCHPO	107 kDa	0	1	2	0	0	0	0	0
1256	IF5_SCHPO	45 kDa	0	0	1	2	0	1	0	0
1257	VPS26_SCHPO	36 kDa	0	1	0	0	0	1	2	0
1258	VPS16_SCHPO	95 kDa	1	0	1	1	0	0	0	0
1259	YGE9_SCHPO	32 kDa	0	0	1	0	0	0	1	1
1260	MPD2_SCHPO	106 kDa	0	0	0	0	0	0	0	1
1261	KRR1_SCHPO	39 kDa	0	0	1	0	0	0	0	0
1262	YLI2_SCHPO	54 kDa	0	0	0	0	0	0	1	0
1263	TIP41_SCHPO	29 kDa	1	0	0	0	0	0	1	0
1264	PCK2_SCHPO	116 kDa	0	0	1	1	0	0	1	0
1265	YKP9_SCHPO	45 kDa	0	1	0	0	1	0	0	1
1266	LCB4_SCHPO	51 kDa	0	0	0	1	0	0	1	0
1267	STS1_SCHPO	53 kDa	0	0	1	0	0	0	0	0
1268	PYRF_SCHPO	29 kDa	0	0	0	0	1	0	0	0
1269	TOR2_SCHPO	266 kDa	1	0	0	1	0	0	1	0
1270	CFD1_SCHPO	68 kDa	1	0	1	0	0	1	0	0
1271	YFE6_SCHPO	41 kDa	0	1	0	1	0	0	0	0
1272	MRD1_SCHPO	94 kDa	0	0	1	0	1	1	0	0
1273	FFT2_SCHPO	144 kDa	1	1	1	0	0	0	0	0
1274	RPAC2_SCHPO	14 kDa	0	0	1	0	1	0	1	0
1275	SNF22_SCHPO	190 kDa	0	1	0	0	0	0	0	0
1276	BST1_SCHPO	129 kDa	1	0	0	1	0	1	0	0
1277	AGM2_SCHPO	59 kDa	0	0	0	1	0	0	0	1
1278	YKX4_SCHPO	82 kDa	0	0	1	0	0	0	0	0
1279	MUG81_SCHPO	219 kDa	1	0	1	1	0	0	1	0
1280	FKBP_SCHPO	12 kDa	1	0	0	0	0	0	1	1
1281	RPA34_SCHPO	28 kDa	0	0	0	0	0	1	1	1
1282	SEB1_SCHPO	66 kDa	1	0	0	1	0	1	0	1
1283	STE20_SCHPO	72 kDa	0	0	1	0	0	0	0	1
1284	UBC1_SCHPO	25 kDa	0	0	0	0	0	1	1	1
1285	ARP8_SCHPO	75 kDa	0	0	1	1	0	0	1	0
1286	AYR1_SCHPO	33 kDa	0	0	1	1	1	1	0	0

1287	EXO70_SCHPO	69 kDa	1	0	1	1	0	0	1	0
1288	HRP1_SCHPO	159 kDa	0	0	1	1	1	0	0	0
1289	IPK1_SCHPO	73 kDa	1	0	1	1	0	0	0	0
1290	MCM3_SCHPO	97 kDa	0	1	1	0	1	0	0	0
1291	PPME1_SCHPO	38 kDa	1	1	1	1	0	0	0	0
1292	SMC4_SCHPO	151 kDa	1	1	1	0	0	0	1	0
1293	TF211_SCHPO (+10)	155 kDa	0	0	1	0	1	1	1	0
1294	UTP11_SCHPO	30 kDa	0	1	1	0	1	1	0	0
1295	UTP15_SCHPO	54 kDa	0	0	1	0	1	0	1	0
1296	YCUD_SCHPO	60 kDa	0	0	1	1	1	0	1	0
1297	YN25_SCHPO	85 kDa	0	1	1	1	0	0	0	0
1298	YTM1_SCHPO	48 kDa	1	0	1	1	0	1	0	0
1299	ATM1_SCHPO	77 kDa	0	1	0	0	1	1	1	0
1300	MAM33_SCHPO	31 kDa	1	1	0	0	0	1	1	0
1301	TGT_SCHPO	45 kDa	1	0	0	1	0	1	1	0
1302	UAP1_SCHPO	53 kDa	1	0	0	0	0	1	1	0
1303	YDT7_SCHPO	53 kDa	1	1	0	0	0	0	1	0
1304	YHD5_SCHPO	63 kDa	0	1	0	0	0	0	1	0
1305	ANM3_SCHPO	62 kDa	0	0	0	1	1	1	0	0
1306	COX1_SCHPO	59 kDa	0	0	0	1	1	1	0	0
1307	ERB1_SCHPO	83 kDa	0	0	0	0	0	1	0	0
1308	GAS2_SCHPO	51 kDa	1	1	0	1	0	1	0	0
1309	IDI1_SCHPO	27 kDa	0	1	0	0	0	1	1	0
1310	KGUA_SCHPO	22 kDa	1	0	0	1	0	1	0	0
1311	OCA3_SCHPO	33 kDa	1	1	0	0	0	1	1	0
1312	RLA1_SCHPO (+1)	11 kDa	1	0	0	0	0	1	1	0
1313	XDJ1_SCHPO	46 kDa	0	0	0	0	0	1	0	1
1314	YH56_SCHPO	21 kDa	1	0	0	0	0	1	1	0
1315	YNTB_SCHPO	58 kDa	1	0	0	0	0	1	0	0
1316	AIM19_SCHPO	13 kDa	1	0	0	1	1	0	0	0
1317	ASL1_SCHPO	54 kDa	1	1	0	0	0	0	0	0
1318	CYAA_SCHPO	190 kDa	1	1	0	1	0	0	0	0
1319	NU132_SCHPO	132 kDa	1	0	0	1	0	0	0	0
1320	VAC14_SCHPO	92 kDa	1	1	1	1	0	0	0	0
1321	YAI5_SCHPO	27 kDa	0	0	0	1	1	0	0	0
1322	TAD2_SCHPO	44 kDa	0	1	0	0	0	0	0	0
1323	UBA4_SCHPO	44 kDa	0	0	0	0	0	1	0	2
1324	AIF1_SCHPO	67 kDa	0	0	0	0	0	2	0	0
1325	YF3A_SCHPO	44 kDa	0	0	0	1	0	0	0	0
1326	QCR9_SCHPO	8 kDa	0	0	0	1	0	0	1	0

1327	YCJE_SCHPO	131 kDa	0	0	1	0	0	0	1	0
1328	AES1_SCHPO	32 kDa	0	0	0	0	0	1	1	0
1329	YQJ8_SCHPO	65 kDa	0	0	0	1	0	0	0	0
1330	CO111_SCHPO (+1)	86 kDa	0	1	0	1	0	0	0	0
1331	PDAT_SCHPO	71 kDa	0	0	0	1	0	0	0	0
1332	YFRD_SCHPO	177 kDa	0	1	0	0	0	0	1	0
1333	YA33_SCHPO	51 kDa	0	0	0	0	1	0	0	1
1334	ANM1_SCHPO	39 kDa	0	0	0	1	0	1	0	0
1335	PEF1_SCHPO	33 kDa	0	0	0	1	1	0	0	1
1336	O60152-DECOY	?	0	0	0	0	1	0	0	0
1337	MTHR1_SCHPO	69 kDa	1	0	0	1	0	0	0	0
1338	BU107_SCHPO	107 kDa	0	0	1	0	0	0	0	1
1339	Q10719-DECOY	?	0	0	0	1	0	0	0	0
1340	PGT1_SCHPO	96 kDa	0	1	0	0	0	0	0	0
1341	GAD8_SCHPO	64 kDa	0	0	0	1	0	0	0	0
1342	CCA2_SCHPO	55 kDa	0	0	1	1	0	0	0	0
1343	AP2A_SCHPO	100 kDa	0	0	0	0	1	0	1	1
1344	DIS1_SCHPO	98 kDa	0	0	1	0	0	0	0	1
1345	PP2C4_SCHPO	44 kDa	0	0	0	1	0	1	0	1
1346	PSS_SCHPO	27 kDa	0	0	1	1	0	0	0	1
1347	RPN10_SCHPO	27 kDa	0	0	1	0	1	0	0	1
1348	RRP42_SCHPO	32 kDa	0	0	1	0	0	1	0	1
1349	RTF1_SCHPO	64 kDa	1	0	0	0	0	1	0	1
1350	TF2B_SCHPO	37 kDa	0	0	0	0	0	0	1	1
1351	TMEDA_SCHPO	24 kDa	0	0	0	0	0	0	0	1
1352	URB2_SCHPO	152 kDa	0	1	0	0	1	0	0	1
1353	UTP6_SCHPO	56 kDa	0	0	0	0	0	1	1	1
1354	YAUB_SCHPO	36 kDa	0	0	0	0	0	0	0	1
1355	YD27_SCHPO	21 kDa	0	0	1	0	1	0	0	1
1356	YDE2_SCHPO	27 kDa	0	0	1	0	0	0	0	1
1357	ZPR1_SCHPO	51 kDa	0	0	0	0	0	0	1	1
1358	AUR1_SCHPO	47 kDa	0	0	1	1	1	0	0	0
1359	CWC22_SCHPO	103 kDa	0	1	1	0	0	1	0	0
1360	KA113_SCHPO	113 kDa	0	0	1	0	0	0	1	0
1361	KAE1_SCHPO	38 kDa	1	0	1	1	0	0	0	0
1362	MAC1_SCHPO	82 kDa	0	1	1	0	1	0	0	0
1363	MAK2_SCHPO	265 kDa	0	0	1	0	0	0	1	0
1364	OXA12_SCHPO	45 kDa	0	0	1	1	1	0	0	0

1365	P5CR_SCHPO	30 kDa	0	1	1	1	0	0	0	0
1366	PHA2_SCHPO	30 kDa	1	0	1	0	0	0	1	0
1367	RT26B_SCHPO	25 kDa	0	0	1	0	0	0	1	0
1368	SPN4_SCHPO	45 kDa	0	1	1	1	0	0	0	0
1369	SSU72_SCHPO	23 kDa	0	1	1	0	0	1	0	0
1370	TAF11_SCHPO	23 kDa	0	0	1	1	0	0	1	0
1371	YORN_SCHPO	76 kDa	0	0	1	1	0	0	0	0
1372	CDR2_SCHPO	86 kDa	1	1	0	0	0	0	1	0
1373	OMH1_SCHPO	47 kDa	0	1	0	1	0	0	1	0
1374	OSM1_SCHPO	55 kDa	1	0	0	0	0	1	1	0
1375	PSA6_SCHPO	30 kDa	0	0	0	0	0	0	1	0
1376	RT26A_SCHPO	31 kDa	1	0	0	0	0	1	1	0
1377	TAM10_SCHPO	19 kDa	0	1	0	0	1	0	1	0
1378	TRM4B_SCHPO	78 kDa	0	0	0	0	1	1	1	0
1379	UREG_SCHPO	31 kDa	1	0	0	1	0	0	1	0
1380	YCS1_SCHPO	55 kDa	0	0	0	1	0	1	1	0
1381	ALG6_SCHPO	59 kDa	1	0	0	0	0	1	1	0
1382	ATPG_SCHPO	34 kDa	0	0	0	0	0	1	0	0
1383	COX9_SCHPO	7 kDa	1	0	0	1	0	1	0	0
1384	IBP1_SCHPO	16 kDa	1	1	0	0	0	1	0	0
1385	TAF73_SCHPO	72 kDa	0	1	0	1	0	1	0	0
1386	TGCE3_SCHPO	53 kDa	0	0	0	1	0	1	1	0
1387	YH77_SCHPO	39 kDa	1	0	0	0	1	1	0	0
1388	YL8H_SCHPO	33 kDa	0	1	0	1	0	1	0	0
1389	YQ72_SCHPO	64 kDa	0	0	0	1	0	1	0	0
1390	NNT1_SCHPO	28 kDa	1	1	0	0	0	0	0	0
1391	UREA_SCHPO	91 kDa	1	1	0	0	0	0	0	0
1392	VATL2_SCHPO	17 kDa	1	0	0	1	0	0	0	0
1393	YAC1_SCHPO	40 kDa	1	0	0	1	0	0	0	0
1394	YAD7_SCHPO	60 kDa	1	0	0	0	0	1	0	0
1395	YB4E_SCHPO	27 kDa	1	0	0	1	1	0	0	0
1396	ABCI_SCHPO	69 kDa	0	1	0	0	1	0	0	0
1397	SEC10_SCHPO	93 kDa	0	1	0	0	0	0	0	0
1398	SYJ1_SCHPO	122 kDa	0	1	0	0	0	0	1	1
1399	TAF14_SCHPO	28 kDa	0	1	0	0	0	0	0	1
1400	YC64_SCHPO	29 kDa	0	1	1	0	0	0	0	0
1401	YPP1_SCHPO	98 kDa	0	1	0	1	0	0	0	0
1402	YNK4_SCHPO	69 kDa	1	0	1	0	0	0	0	0
1403	COQ9_SCHPO	28 kDa	0	0	0	1	0	0	0	0
1404	CYSK2_SCHPO	43 kDa	0	0	0	1	0	0	1	0
1405	YDE9_SCHPO	38 kDa	0	0	0	1	0	0	0	0
1406	YGD1_SCHPO	69 kDa	0	0	0	1	0	0	0	0

1407	YOX2_SCHPO	58 kDa	0	0	1	1	0	0	0	0
1408	YOY4_SCHPO	32 kDa	0	0	0	1	0	0	1	0
1409	O94666-DECOY	?	0	1	0	0	0	0	0	0
1410	PST3_SCHPO	133 kDa	0	0	0	0	0	0	2	0
1411	ALY2_SCHPO	73 kDa	0	0	0	2	0	0	0	0
1412	YD68_SCHPO	31 kDa	0	0	0	0	0	1	0	0
1413	AP3D_SCHPO	93 kDa	0	0	0	0	0	0	0	1
1414	TOP1_SCHPO	94 kDa	0	1	0	0	0	0	0	0
1415	ALM1_SCHPO	198 kDa	0	0	0	0	0	0	1	0
1416	PAN2_SCHPO	124 kDa	0	0	0	1	0	0	0	0
1417	RHB1_SCHPO	21 kDa	0	0	0	1	0	0	0	0
1418	YLOH_SCHPO	72 kDa	0	0	1	0	0	0	0	0
1419	CMB1_SCHPO	26 kDa	0	1	0	0	0	0	0	0
1420	O42924-DECOY	?	1	0	0	0	0	0	0	0
1421	HIR1_SCHPO	104 kDa	0	0	0	1	0	0	0	0
1422	BRL2_SCHPO	78 kDa	0	0	0	1	0	0	0	0
1423	YH51_SCHPO	95 kDa	0	0	0	1	0	0	0	0
1424	DBP8_SCHPO	51 kDa	1	0	1	0	0	0	0	0
1425	AMY3_SCHPO	63 kDa	0	0	0	1	0	0	0	1
1426	EFG1P_SCHPO	22 kDa	0	0	0	0	1	0	0	1
1427	ERV41_SCHPO	38 kDa	0	0	0	0	0	0	1	1
1428	GLU2B_SCHPO	57 kDa	0	0	1	0	0	0	0	1
1429	IF4E2_SCHPO	28 kDa	0	0	0	0	1	0	0	1
1430	MTHR2_SCHPO	72 kDa	1	0	0	0	0	0	0	1
1431	MTR4_SCHPO	126 kDa	0	0	0	0	0	0	0	1
1432	PPK38_SCHPO	72 kDa	0	0	1	0	0	0	0	1
1433	RRB1_SCHPO	54 kDa	1	0	0	0	0	0	0	1
1434	UFD1_SCHPO	38 kDa	0	0	0	1	0	0	0	1
1435	VPS53_SCHPO	88 kDa	0	0	0	0	0	0	1	1
1436	YAGB_SCHPO	42 kDa	0	0	0	0	0	0	0	1
1437	YE19_SCHPO	61 kDa	0	0	0	0	0	0	0	1
1438	YJ7O_SCHPO	8 kDa	0	0	0	0	0	1	0	1
1439	YNW6_SCHPO	55 kDa	0	0	0	0	1	0	0	1
1440	DSC2_SCHPO	42 kDa	0	0	0	0	0	1	0	1
1441	ALP14_SCHPO	89 kDa	0	0	1	0	1	0	0	0
1442	APP1_SCHPO	91 kDa	0	0	1	0	0	0	1	0
1443	ATP7_SCHPO	19 kDa	0	1	1	0	0	0	0	0
1444	EBP2_SCHPO	38 kDa	0	0	1	0	1	0	0	0
1445	NAM9_SCHPO	38 kDa	0	0	1	0	1	0	0	0
1446	NU189_SCHPO	190 kDa	0	1	1	0	0	0	0	0

1447	O94308-DECOY	?	1	0	1	0	0	0	0	0
1448	PAC2_SCHPO	26 kDa	0	0	1	0	0	0	0	0
1449	PSB3_SCHPO	23 kDa	0	0	1	0	1	0	0	0
1450	RGA9_SCHPO	77 kDa	0	0	1	0	0	0	0	0
1451	UGO1_SCHPO	47 kDa	0	0	1	1	0	0	0	0
1452	UTP18_SCHPO	58 kDa	0	0	1	0	1	0	0	0
1453	YGWC_SCHPO	33 kDa	0	0	1	0	1	0	0	0
1454	YJH4_SCHPO	32 kDa	0	0	1	0	1	0	0	0
1455	PEX16_SCHPO	43 kDa	0	0	0	1	0	0	1	0
1456	PLD1_SCHPO	158 kDa	0	0	0	1	0	0	1	0
1457	YJ48_SCHPO	30 kDa	0	0	0	0	0	0	1	0
1458	YNG5_SCHPO	77 kDa	0	1	0	0	0	0	1	0
1459	ARPC3_SCHPO	20 kDa	0	0	0	1	0	1	0	0
1460	ATPO_SCHPO	24 kDa	0	0	0	0	0	1	1	0
1461	CDA1_SCHPO	36 kDa	1	0	0	0	0	1	0	0
1462	DIM1_SCHPO	35 kDa	0	0	0	0	0	1	0	0
1463	FIP1_SCHPO	44 kDa	1	0	0	0	0	1	0	0
1464	MTND_SCHPO	21 kDa	0	0	0	0	0	1	0	0
1465	NIT2_SCHPO	30 kDa	0	0	0	0	0	1	0	0
1466	PUS1_SCHPO	60 kDa	1	0	0	0	0	1	0	0
1467	SEH1_SCHPO	39 kDa	0	0	0	1	0	1	0	0
1468	SPN3_SCHPO	47 kDa	1	0	0	0	0	1	0	0
1469	STR1_SCHPO	68 kDa	0	0	0	0	0	1	0	0
1470	TAF2_SCHPO	134 kDa	0	0	0	0	0	1	0	0
1471	VCX1_SCHPO	45 kDa	0	0	0	1	0	1	0	0
1472	YAQ1_SCHPO	30 kDa	0	0	0	0	0	1	0	0
1473	YGL3_SCHPO	27 kDa	0	0	0	0	0	1	0	0
1474	YHLE_SCHPO	18 kDa	0	1	0	0	0	1	0	0
1475	YLWB_SCHPO	46 kDa	0	0	0	0	0	1	0	0
1476	HACD_SCHPO	24 kDa	1	0	0	1	0	0	0	0
1477	SCK2_SCHPO	72 kDa	1	0	0	1	0	0	0	0
1478	VPS10_SCHPO	165 kDa	1	0	0	0	1	0	0	0
1479	YGI2_SCHPO	32 kDa	1	0	0	0	0	0	0	0
1480	YKX1_SCHPO	140 kDa	1	0	0	1	0	0	0	0
1481	DOA10_SCHPO	142 kDa	0	1	0	0	1	0	0	0
1482	FNX1_SCHPO	58 kDa	0	1	0	0	0	0	0	0
1483	HNT1_SCHPO	15 kDa	0	1	0	1	0	0	0	0
1484	MAP1_SCHPO	42 kDa	0	1	0	0	1	0	0	0
1485	RPB2_SCHPO	138 kDa	0	1	0	0	0	0	0	0
1486	TF3B_SCHPO	56 kDa	0	1	0	1	0	0	0	0

1487	YC63_SCHPO	33 kDa	0	1	0	1	0	0	0	0
1488	YE98_SCHPO	24 kDa	0	1	0	1	0	0	0	0
1489	YH93_SCHPO	48 kDa	0	1	0	0	0	1	0	0
1490	OYEB_SCHPO	45 kDa	0	0	0	1	1	0	0	0
1491	TVP18_SCHPO	18 kDa	0	0	0	0	1	0	0	0
1492	WIN1_SCHPO	163 kDa	0	0	0	0	1	0	0	0
1493	CLD1_SCHPO	49 kDa	0	0	0	1	0	0	0	0
1494	NIF1_SCHPO	75 kDa	0	0	0	1	0	1	0	0
1495	YFQ5_SCHPO	38 kDa	0	0	0	1	0	0	0	0
1496	YG41_SCHPO	52 kDa	0	0	0	1	0	0	0	0
1497	YHJ4_SCHPO	43 kDa	0	0	0	1	0	0	1	0
1498	INVX_SCHPO	58 kDa	0	0	1	0	1	0	0	0
1499	IF1A_SCHPO	16 kDa	0	0	0	0	0	1	0	0
1500	SCE3_SCHPO	43 kDa	0	0	0	0	0	0	1	0
1501	YA99_SCHPO	31 kDa	0	0	1	0	0	0	0	0
1502	YO53_SCHPO	49 kDa	0	1	0	0	0	0	0	0
1503	CTBL1_SCHPO	65 kDa	0	0	0	1	0	0	0	0
1504	KLP9_SCHPO	71 kDa	0	0	0	0	0	0	0	1
1505	ORC4_SCHPO	109 kDa	0	0	0	0	0	0	0	1
1506	RM22_SCHPO	29 kDa	0	0	0	0	0	0	0	1
1507	SMI1_SCHPO	56 kDa	0	0	0	0	0	0	0	1
1508	YCRE_SCHPO	133 kDa	0	0	0	0	0	0	0	1
1509	YIP5_SCHPO	28 kDa	0	0	0	0	0	0	0	1
1510	YL8B_SCHPO	75 kDa	0	0	0	0	0	0	0	1
1511	YQO5_SCHPO	64 kDa	0	0	0	0	0	0	0	1
1512	CYB_SCHPO	44 kDa	0	0	1	0	0	0	0	0
1513	MET16_SCHPO	31 kDa	0	0	1	0	0	0	0	0
1514	NUP44_SCHPO	44 kDa	0	0	1	0	0	0	0	0
1515	OTC_SCHPO	36 kDa	0	0	1	0	0	0	0	0
1516	PUN1_SCHPO	31 kDa	0	0	1	0	0	0	0	0
1517	RFC2_SCHPO	38 kDa	0	0	1	0	0	0	0	0
1518	RGA5_SCHPO	41 kDa	0	0	1	0	0	0	0	0
1519	SPM1_SCHPO	48 kDa	0	0	1	0	0	0	0	0
1520	SULH3_SCHPO	73 kDa	0	0	1	0	0	0	0	0
1521	YD1E_SCHPO	25 kDa	0	0	1	0	0	0	0	0
1522	YDY2_SCHPO	143 kDa	0	0	1	0	0	0	0	0
1523	YIF1_SCHPO	33 kDa	0	0	1	0	0	0	0	0
1524	YL87_SCHPO	13 kDa	0	0	1	0	0	0	0	0
1525	NOP14_SCHPO	95 kDa	0	0	0	0	0	0	1	0
1526	NSA1_SCHPO	44 kDa	0	0	0	0	0	0	1	0
1527	RPA43_SCHPO	19 kDa	0	0	0	0	0	0	1	0

1528	T2EA_SCHPO	49 kDa	0	0	0	0	0	0	1	0
1529	TAF9_SCHPO	18 kDa	0	0	0	0	0	0	1	0
1530	XKS1_SCHPO	62 kDa	0	0	0	0	0	0	1	0
1531	YAI7_SCHPO	62 kDa	0	0	0	0	0	0	1	0
1532	YF9E_SCHPO	62 kDa	0	0	0	0	0	0	1	0
1533	YFK5_SCHPO	66 kDa	0	0	0	0	0	0	1	0
1534	CFT2_SCHPO	89 kDa	0	0	0	0	0	1	0	0
1535	DAP1_SCHPO	19 kDa	0	0	0	0	0	1	0	0
1536	DIS3_SCHPO	110 kDa	0	0	0	0	0	1	0	0
1537	GAP1_SCHPO	88 kDa	0	0	0	0	0	1	0	0
1538	MPPA_SCHPO	56 kDa	0	0	0	0	0	1	0	0
1539	SPT16_SCHPO	116 kDa	0	0	0	0	0	1	0	0
1540	SUM2_SCHPO	46 kDa	0	0	0	0	0	1	0	0
1541	THTM_SCHPO	33 kDa	0	0	0	0	0	1	0	0
1542	TIM14_SCHPO	15 kDa	0	0	0	0	0	1	0	0
1543	YE02_SCHPO	118 kDa	0	0	0	0	0	1	0	0
1544	YF07_SCHPO	27 kDa	0	0	0	0	0	1	0	0
1545	YQL5_SCHPO	31 kDa	0	0	0	0	0	1	0	0
1546	ARP42_SCHPO	47 kDa	1	0	0	0	0	0	0	0
1547	MIP1_SCHPO	149 kDa	1	0	0	0	0	0	0	0
1548	Q9UQY2-DECOY	?	1	0	0	0	0	0	0	0
1549	SERB_SCHPO	32 kDa	1	0	0	0	0	0	0	0
1550	SSR3_SCHPO	50 kDa	1	0	0	0	0	0	0	0
1551	SSR4_SCHPO	44 kDa	1	0	0	0	0	0	0	0
1552	WDR59_SCHPO	149 kDa	1	0	0	0	0	0	0	0
1553	YA3B_SCHPO	149 kDa	1	0	0	0	0	0	0	0
1554	YH2X_SCHPO	76 kDa	1	0	0	0	0	0	0	0
1555	YOS3_SCHPO	79 kDa	1	0	0	0	0	0	0	0
1556	ERG2_SCHPO	25 kDa	0	1	0	0	0	0	0	0
1557	GYP51_SCHPO	116 kDa	0	1	0	0	0	0	0	0
1558	PIK1_SCHPO	97 kDa	0	1	0	0	0	0	0	0
1559	RT28_SCHPO	34 kDa	0	1	0	0	0	0	0	0
1560	SUR2_SCHPO	34 kDa	0	1	0	0	0	0	0	0
1561	UPP1_SCHPO	24 kDa	0	1	0	0	0	0	0	0
1562	VPS27_SCHPO	68 kDa	0	1	0	0	0	0	0	0
1563	YBQ3_SCHPO	41 kDa	0	1	0	0	0	0	0	0
1564	YGK4_SCHPO	62 kDa	0	1	0	0	0	0	0	0
1565	ARP5_SCHPO	82 kDa	0	0	0	0	1	0	0	0
1566	GHT6_SCHPO	59 kDa	0	0	0	0	1	0	0	0

1567	HIS9_SCHPO	35 kDa	0	0	0	0	1	0	0	0
1568	IVN1_SCHPO	42 kDa	0	0	0	0	1	0	0	0
1569	NOP10_SCHPO	8 kDa	0	0	0	0	1	0	0	0
1570	NUP61_SCHPO	59 kDa	0	0	0	0	1	0	0	0
1571	VTI1_SCHPO	25 kDa	0	0	0	0	1	0	0	0
1572	YQFB_SCHPO	20 kDa	0	0	0	0	1	0	0	0
1573	CLP1_SCHPO	50 kDa	0	0	0	1	0	0	0	0
1574	CYK3_SCHPO	98 kDa	0	0	0	1	0	0	0	0
1575	FNX2_SCHPO	63 kDa	0	0	0	1	0	0	0	0
1576	GDE1_SCHPO	118 kDa	0	0	0	1	0	0	0	0
1577	HCS1_SCHPO	75 kDa	0	0	0	1	0	0	0	0
1578	ING1_SCHPO	31 kDa	0	0	0	1	0	0	0	0
1579	MSH1_SCHPO	107 kDa	0	0	0	1	0	0	0	0
1580	NPT1_SCHPO	47 kDa	0	0	0	1	0	0	0	0
1581	PFD3_SCHPO	19 kDa	0	0	0	1	0	0	0	0
1582	POM1_SCHPO	121 kDa	0	0	0	1	0	0	0	0
1583	PRR1_SCHPO	60 kDa	0	0	0	1	0	0	0	0
1584	PRW1_SCHPO	48 kDa	0	0	0	1	0	0	0	0
1585	PSB2_SCHPO	29 kDa	0	0	0	1	0	0	0	0
1586	RM15_SCHPO	24 kDa	0	0	0	1	0	0	0	0
1587	SMC3_SCHPO	137 kDa	0	0	0	1	0	0	0	0
1588	UBP9_SCHPO	67 kDa	0	0	0	1	0	0	0	0
1589	VPS52_SCHPO	58 kDa	0	0	0	1	0	0	0	0
1590	WOS2_SCHPO	21 kDa	0	0	0	1	0	0	0	0
1591	YAGC_SCHPO	36 kDa	0	0	0	1	0	0	0	0
1592	YF51_SCHPO	71 kDa	0	0	0	1	0	0	0	0
1593	YGD4_SCHPO	38 kDa	0	0	0	1	0	0	0	0
1594	YIQ9_SCHPO	35 kDa	0	0	0	1	0	0	0	0
1595	YIVG_SCHPO	20 kDa	0	0	0	1	0	0	0	0
1596	YKQ9_SCHPO	40 kDa	0	0	0	1	0	0	0	0
1597	YL8A_SCHPO	29 kDa	0	0	0	1	0	0	0	0
1598	YOM2_SCHPO	82 kDa	0	0	0	1	0	0	0	0
1599	FIP1X_SCHPO	37 kDa	0	0	0	1	0	0	0	0
1600	SF3B1_SCHPO	137 kDa	0	0	0	0	1	0	0	0
1601	WRIP1_SCHPO	56 kDa	0	0	1	0	0	0	0	0
1602	TLG1_SCHPO	25 kDa	0	1	0	0	0	0	0	0
1603	MNS1_SCHPO	61 kDa	0	0	0	0	0	0	1	0
1604	YME1_SCHPO	78 kDa	0	0	0	0	1	0	0	0
1605	YAMB_SCHPO	421 kDa	0	0	0	0	0	1	0	0
1606	HGH1_SCHPO	41 kDa	0	0	0	0	0	0	0	1

1607	YNQA_SCHPO	57 kDa	1	0	0	0	0	0	0	0
1608	SIF2_SCHPO	45 kDa	0	0	1	0	0	0	0	0
1609	ACEB_SCHPO	59 kDa	0	1	0	0	0	0	0	0
1610	RAD21_SCHPO	68 kDa	0	0	0	0	0	0	0	1
1611	YKU5_SCHPO	59 kDa	0	0	0	0	0	1	0	0
1612	O59814-DECOY	?	1	0	0	0	0	0	0	0
1613	YOW4_SCHPO	118 kDa	0	1	0	0	0	0	0	0
1614	PTA1_SCHPO	76 kDa	0	0	0	0	0	0	0	1
1615	RSC58_SCHPO	45 kDa	0	0	0	1	0	0	0	0
1616	SULH1_SCHPO	96 kDa	0	0	0	1	0	0	0	0
1617	O14040-DECOY	?	0	0	0	1	0	0	0	0
1618	PEP3_SCHPO	104 kDa	0	0	0	1	0	0	0	0
1619	PAN3_SCHPO	67 kDa	0	0	0	0	1	0	0	0
1620	HAT2_SCHPO	48 kDa	0	0	0	0	0	0	1	0
1621	RFC5_SCHPO	40 kDa	0	0	1	0	0	0	0	0